The evolution and dynamic behaviour of the Northern Uummannaq Ice Stream System, West Greenland

TIMOTHY PATRICK LANE

The evolution and dynamic behaviour of the Northern Uummannaq Ice Stream System, West Greenland

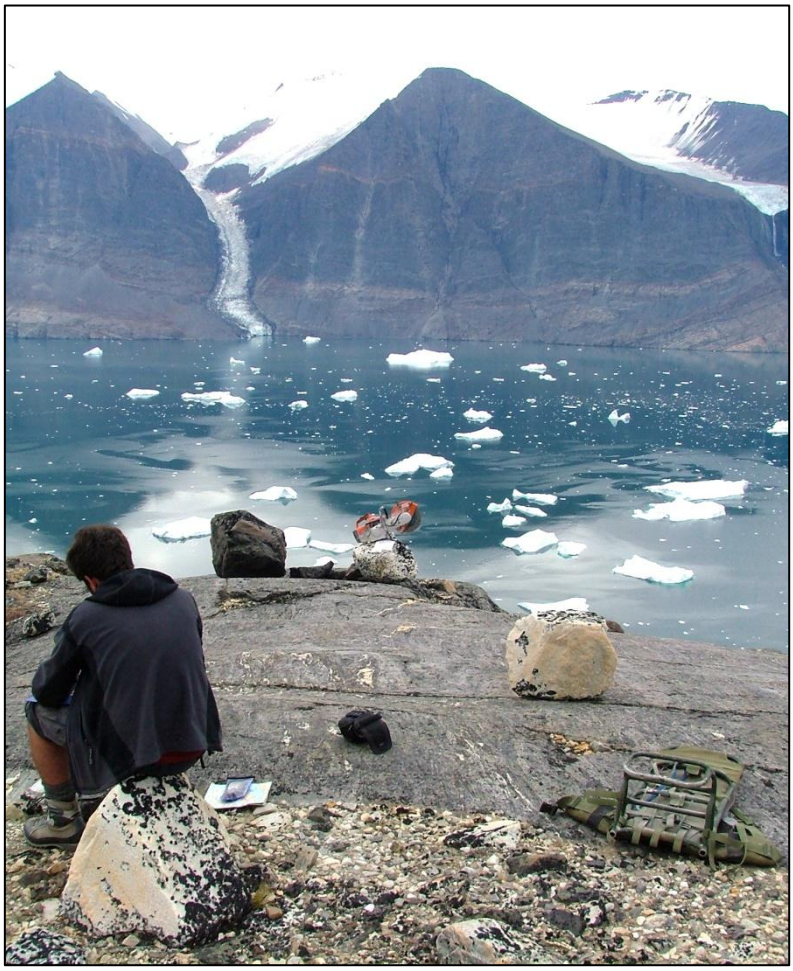

Timothy Patrick Lane

Submitted for the degree of Doctor of Philosophy

Department of Geography

Durham University

February 2013

Timothy Patrick Lane

The evolution and dynamic behaviour of the Northern Uummannaq Ice Stream System, West Greenland

This thesis considers the evolution and dynamic behaviour of the northern Uummannaq Ice Stream System (UISS), a large ice stream which extended to the Greenland shelf edge during the Last Glacial Maximum (LGM). The Uummannaq region has been shown to be dominated by areas of selective linear erosion (SLE) and areal scour. Over multiple glacial cycles, enhanced by favourable geology and uplift, SLE controlled the formation of a confluent fjord system which triggered the onset and development of the UISS. At the LGM, northern UISS ice thicknesses reached 1400-1968 m a.s.l., comparable to data from the southern UISS. However, in the north, thicknesses were not sufficient to overtop fjord confines, with ice flow remaining topographically controlled.

The presence of thick, fast ice flowing ice in the onset zone suggests that subglacial conditions within the study area were characterised by intense basal sliding. The evolution of bedforms (roches moutonnées and whalebacks) was influenced by basal ice dynamics, but bedrock type, joints and bedding were also critical controls on bedform morphometry.

Deglaciation following the LGM began on the outer shelf by 14.9 kyr, with increased air temperature, rising relative sea-level and bathymetric over-deepening driving the UISS to the outer edge of coastal fjords by 11.4-11.0 kyr. Geochronological data demonstrate that the retreat rate of the northern and southern UISS became highly asynchronous during the early-Holocene. In the south, topographic constrictions stabilised the ice from 11.0-9.3 kyr, before it retreated beyond its present ice margin at 8.7 kyr. Ice in the north became pinned at the mouth of Rink-Karrat Isfjord between 11.6-6.9 kyr, remaining stable through the Holocene Thermal Maximum, demonstrating the ability of topography to override climate and sea-level drivers.

Geomorphological and sedimentological evidence has demonstrated that the Svartenhuk Peninsula in the northern Uummannaq region, previously cited as an LGM ice-free enclave, was overrun by ice during the LGM. Ice was sourced from the Svartenhuk interior, and expanded radially to the present coastline. This is contrary to existing work, and suggests there may be a need to reassess the evidence for interstadial, high sea-level conditions throughout Greenland.

TABLE OF CONTENTS

Table of contents i

List of figures vii

List of tables xiv

Declaration and statement of copyright xv

Acknowledgements xvi

CHAPTER ONE

Introduction

1.1. Introduction 1

1.2. The Uummannaq study region 4

1.2.1. Regional geography 4

1.2.2. Geological setting 7

1.2.3. Glaciological setting 8

1.2.4. Glacial history – Last Glacial Maximum to present 11

1.2.5. Central West Greenland relative sea-level history – Last Glacial Maximum to present 13

1.3. Research aims and objectives 16

1.4. Thesis structure 17

CHAPTER TWO

Literature Review: Ice streams and their importance to the Greenland Ice Sheet; past and present

2.1. The Greenland Ice Sheet 20

2.1.1. Present ice sheet dynamics 20

2.1.2. Late-Quaternary glacial history of the West Greenland Ice Sheet 25

2.1.2.1. Saalian glaciation 26

2.1.2.2. Last Glacial Maximum ice sheet extent 27

2.1.2.3. Last Glacial Maximum deglaciation: timing and behaviour 30

2.1.2.4. Ice stream history 35

2.2. Ice streams and their importance in Greenland 37

2.2.1. Palaeo-ice stream reconstruction 39
2.2.1.1. Ice streams with soft beds 39
2.2.1.2. Ice streams with rigid beds 39
2.3. Summary 44

CHAPTER THREE

Glacial landscape evolution in the Uummannaq region, West Greenland

Abstract 46
3.1. Introduction 47
3.2. Background 49
3.2.1. West Greenland landscape evolution 49
3.2.2 The Uummannaq region 52
3.3. Methods 53
3.4. Results 54
3.4.1. Selective Linear Erosion 55
3.4.2. Dissected and non-dissected plateau 56
3.4.3. Areal Scour 58
3.4.4. Mountain Valley and Cirque Glaciers 59
3.4.5. Lowland Terrestrial Deposition 61
3.4.6. Areas dominated by non-glacial landform development 63
3.4.7. Comparison to previous mapping 64
3.5. Discussion 65
3.5.1 Glacial landscape distribution in the Uummannaq region 65
3.5.1.1. Distribution of glaciated landscapes 66
3.5.1.2. Distribution of non-glaciated landscapes 69
3.5.2. Geological control upon fjord formation and ice stream onset 70
3.5.3 The influence of pre-Quaternary landscape processes in glacial landscape evolution 72
3.6. Conclusion 78

CHAPTER FOUR

Ice stream dynamics of the northern sector of the Uummannaq Ice Stream System, West Greenland

Abstract 80

4.1. Introduction and rationale 81
4.2. The Uummannaq Region 83
4.2.1. Topography and geology 83
4.2.2. Current palaeo-glaciological understanding of the Uummannaq system 85
4.2.3. Northern Uummannaq region 87
4.3. Methods 88
4.3.1. Geomorphological Mapping 88
4.3.2. Terrestrial cosmogenic nuclide dating 89
4.3.2.1. Rock sampling for terrestrial cosmogenic nuclide dating 89
4.3.2.2. Terrestrial cosmogenic nuclide sample preparation 90
4.3.2.3. ^{10}Be and ^{26}Al measurements and exposure age calculation 90
4.3.3. Lake coring 91
4.3.4. Radiocarbon dating 92
4.3.5. Bayesian analysis of deglacial chronology 92
4.4. Results 93
4.4.1. Rink-Karrat Fjord: inner fjord 93
4.4.1.1. Geomorphology 93
4.4.1.2. Chronology 96
4.4.2. Qeqertarssuaq 100
4.4.2.1. East Qeqertarssuaq: geomorphology 100
4.4.2.2. Nuugaatsiaq, southwest Qeqertarssuaq 102
4.4.3. Karrat Island 105
4.4.3.1. Geomorphology 105
4.4.3.2. Chronology 106
4.4.4. Ingia Fjord 109
4.4.4.1. Geomorphology 109
4.4.4.2. Chronology 109
4.4.5. Lake sediments 109
4.4.5.1. Karrat Lake 111
4.4.5.2. Ingia Lake 112
4.5. Discussion 114
4.5.1. Configuration of the northern UISS during the LGM 114
4.5.2. Deglaciation of the northern UISS; timing, retreat style, and controls 115

4.5.2.1. LGM limit to Ubekendt Ejland 115
4.5.2.2. Ubekendt Ejland to the fjord margins 118
4.5.2.3. Outer fjord to present ice margin 119
4.5.4. Implications for LGM ice stream history of the West Greenland Ice Sheet 122
4.6. Conclusion 124

CHAPTER FIVE

Controls upon bedrock bedform development in the Uummannaq Ice Stream System, West Greenland.

Abstract 126
5.1. Introduction 127
5.1.1. Importance of glacial bedforms 127
5.1.2. Glacial erosion and bedrock bedforms 128
5.2. Study site 131
5.2.1. Field sites 131
5.2.2. Geology 132
5.2.3. Palaeo-glaciological background 134
5.3. Methods 134
5.4. Results 135
5.4.1. Karrat sub-area 1 (KA1) 135
5.4.2. Karrat sub-area 2 (KA2) 137
5.4.3. Ingia sub-area 1 (IN1) 139
5.4.4. Ingia sub-area 2 (IN2) 140
5.5. Discussion 141
5.5.1. Bedform relationship to ice flow 141
5.5.2. Bedform relationship to geological structure 144
5.5.3. Relationship to other studies – importance of understanding bedrock structure 148
5.5.4. Importance of bedding plane dip relative to ice flow direction 152
5.6. Conclusion 154

CHAPTER SIX

Last Glacial Maximum glaciation of the Svartenhuk Peninsula, an area peripheral to the Uummannaq Ice Stream System

Abstract 156

6.1. Introduction 157

6.2. Previous work on the glacial history of the Svartenhuk Peninsula 160

6.2.1 Geomorphological context 160

6.2.2 Sedimentology and biostratigraphy 162

6.2.3. Chronology 166

6.3. Methods 168

6.3.1. Geomorphological mapping 168

6.3.2. Sedimentology 168

6.3.3. Radiocarbon dating 169

6.4. Results 170

6.4.1. Geomorphological descriptions 170

6.4.1.1. Arfertuarssuk and Quagssugarssuit (Logs 1-4) 170

6.4.1.2. Kugssineq and Tasiussaq (Logs 5-9) 177

6.4.1.3. Uligssat (Log 10) 181

6.4.2. Sedimentological descriptions 183

6.4.2.1. LFA1 Results 190

6.4.2.2. LFA1 interpretation 191

6.4.2.3. LFA2 results 191

6.4.2.4. LFA2 interpretation 193

6.4.2.5. LFA3 195

6.4.2.5.1. LF3a results 195

6.4.2.5.2. LF3a interpretation 196

6.4.2.5.3. LF3b results 198

6.4.2.5.4. LF3b interpretation 198

6.4.2.5.5. LF3c results 199

6.4.2.5.6. LF3c interpretation 200

6.4.2.5.7. LFA3 Interpretation 200

6.4.2.6. LFA4 results 201
6.4.2.7. LFA4 interpretation 202
6.4.2.8. LFA5 203
6.4.2.8.1. LF5a results 203
6.4.2.8.2. LF5a interpretation 203
6.4.2.8.3. LF5b Results 204
6.4.2.8.4. LF5b Interpretation 204
6.5. Discussion 205
6.5.1. Geomorphological evidence for glaciation of southern Svartenhuk 205
6.5.2. Sedimentological evidence for glaciation of southern Svartenhuk 207
6.5.2.1. Subglacial sediment 207
6.5.2.2. Proglacial sediment 208
6.5.3. Chronology of southern Svartenhuk deposits 208
6.5.4. Implications for regional ice sheet history 210
6.6. Conclusions 212

CHAPTER SEVEN

Thesis conclusions and wider implications

7.1. Long-term development of the UISS 214
7.2. The geometry and behaviour of the northern UISS during the LGM 215
7.2.1. Northern UISS geometry during the LGM 215
7.2.2. Bedrock bedform development within the UISS 216
7.2.3. Behaviour of the northern UISS during the LGM deglaciation during the Last Glacial Maximum 217
7.3. Geomorphological and sedimentological evidence for the glaciation of the Svartenhuk Peninsula 217

REFERENCES 219

LIST OF FIGURES

CHAPTER ONE

Figure 1.1. Map of Greenland and its immediate vicinity, with key land-masses and water bodies labelled. 2

Figure 1.2. Map of flow speed velocities (in colour) for the winter 2005-2006, displayed overprinted upon a radar mosaic for the same period. 3

Figure 1.3. Topographic and bathymetric overview of the Uummannaq region, with key locations marked. 5

Figure 1.4. Topographic DEM of the Uummannaq region from ASTER data. Note that the boundary between land and ice sheet is not marked 6

Figure 1.5. Map of the Uummannaq region showing dominant bedrock geology. The three distinct geological regions can be seen, separated by north to south trending faults (adapted from Steenfelt et al., 1998). 8

Figure 1.6. Geological map enlargement of the northern Uummannaq region, showing the distinct difference between the Svartenhuk Peninsula in the west, and the fjordic region to the east. 9

Figure 1.7. Estimated maximum (red) and minimum (grey) ice production from glaciers within the Uummannaq Region. 11

Figure 1.8. Map of flow speed velocities (in colour) for the winter 2005-2006, displayed over a 2000-2001 SAR mosaic (from Joughin et al., 2010). 12

Figure 1.9. Map of the regional trends in marine limits from central West Greenland as hypothesised by Weidick (1992). Based upon an incorporation of sea level data and model predictions. 14

Figure 1.10. A series of five relative sea-level curves from the Disko Bugt region, from 0 - 11 cal. ka BP. Curves 1-4 were constructed by Weidick (1996), and 5 by Long et al. (1999). The dashed line represents a modelled extension of results from 11 – 16 cal. ka BP, taken from Simpson et al. (2009). 15

Figure 1.11. Map of the regional marine limits from the Uummannaq region. Based upon data collected from this study and Roberts et al. (2013). 16

CHAPTER TWO

Figure 2.1. GRACE monthly mass solutions of the whole of the GIS, from April 2002 to 2006 (from Velicogna and Wahr, 2006). 20

Figure 2.2. Map of central West Greenland, showing generalised offshore bathymetry and large offshore moraines (Roberts et al., 2009). 26

Figure 2.3. Reconstructed LGM ice sheet margin from observational and conceptual data. Dates showing onset of ice sheet break up on the shelf
are marked with data collated by Funder *et al*. (2011). 28

Figure 2.4. Compilation of calibrated ^{14}C dates from the Western margin of the Greenland Ice Sheet, with 1σ error bars. These dates represent minimum ages of ice free conditions (from Clark et al. 2009). 31

Figure 2.5. Time-distance diagram of ice sheet extent in West Greenland from the LGM to early Holocene. 32

Figure 2.6. The NGRIP and GRIP ice-core records from the last 30ka, with data at a 50-year resolution. 34

Figure 2.7. Simplified conceptual model of an ice stream, with ice converging in the onset zone, feeding the main ice-stream channel (adapted from Stokes and Clark, 1999). 38

Figure 2.8. (a) Map of the landscapes of glacial erosion on the ice-free rim of Greenland, as mapped by Sugden (1974). 40

Figure 2.9. Diagram of an idealised bedrock bedform continuum across a hypothetical palaeo-ice stream onset zone. Relationship between bedform morphology, bedform density, and subglacial thermal conditions can be seen (from Bradwell et al., 2008). 42

Figure 2.10. Diagram of bedrock bedform development in areas of banded bedrock of contrasting lithology. 43

Figure 2.11. Diagram showing the relationship between bedrock hardness and joint spacing, and the resultant dominant erosional processes.
See Krabbendam and Glasser (2011) for full details and source of data. 44

CHAPTER THREE

Figure 3.1. Map of the landscapes of glacial erosion on the ice-free rim of Greenland, as mapped by Sugden (1974), with enlargement of the Uummannaq region. 48

Figure 3.2. Topographic overview map of Uummannaq region. Altitudes are taken from ASTER imagery, and bathymetry from GEBCO. 50

Figure 3.3. Bedrock geology from the Uummannaq region. 52

Figure 3.4. New map of glacial and non-glacial landscapes throughout the Uummannaq region. 55

Figure 3.5. Geomorphological map overlain on an aerial photograph showing dissected plateau; and continuum of types of dissected plateau present. 57

Figure 3.6. Aerial photographs and field photographs of areally scoured topography throughout the Uummannaq region. 58

Figure 3.7. Geomorphological maps overlain on aerial photographs showing areas of cirque glaciation and valley glaciation from Svartenhuk. 60

Figure 3.8. Geomorphological maps of the 'lowland terrestrial deposition' landsystem identified in this study. 62

Figure 3.9. Aerial photograph (a) and geomorphological map (b) of south-western Svartenhuk. 63

Figure 3.10. Idealised geological profiles taken north-south through the Nuussuaq Basin in the Uummannaq region, illustrating the development of the UPS and LPS, and the re-exposure of the Precambrian etch surface. 73

Figure 3.11. Schematic diagram illustrating the hypothesised landsurfaces throughout the Uummannaq region. 75

CHAPTER FOUR

Figure 4.1. Topographic and bathymetric overview of the Uummannaq region, with key locations marked. 82

Figure 4.2. Map of the Uummannaq region showing dominant bedrock geology 83

Figure 4.3. Geological map of the northern Uummannaq region, showing Rink, Karrat, and Umiamako Fjord (adapted from Henderson and Pulvertaft, 1987b). 84

Figure 4.4. Aerial photograph of the study area in the northern Uummannaq region 94

Figure 4.5. Plate of photographs from inner Rink-Karrat Fjord. 96

Figure 4.6. Aerial photograph of the spur between Rink and Umiámáko Isbræs. 96

Figure 4.7. Aerial photographs showing the locations of samples taken for dating throughout Rink and Karrat Fjord, and their results. 100

Figure 4.8. Plate of photographs from Qeqertarssuaq. 101

Figure 4.9. Aerial photograph of the Nuugaatsiaq peninsula and fjord wall. Striae data from 1040 m a.s.l. and the high-altitude lateral push moraine are shown. 103

Figure 4.10. Photograph looking northeast of the continuation of the Nuugaatsiaq lateral moraine sequence. 104

Figure 4.11. Sediment sequence from the centre of the Nuugaatsiaq Peninisula, interpreted as deposited in a pro-glacial lacustrine/fluvial setting. 104

Figure 4.12. Plate of photographs from Karrat Island. 107

Figure 4.13. Aerial photograph of eastern Karrat 108

Figure 4.14. (a) Aerial photograph of Ingia Fjord; (b) Photograph of the landscape on the peninsula in Ingia Fjord. 110

Figure 4.15. Photograph and stratigraphic diagram of the lake sediment cores from Karrat and Ingia Lake. Sedimentology is show diagrammatically, as is the location of basal ^{14}C date taken. 113

Figure 4.16. Sample locations, bathymetric profile, channel width, and deglacial ages from the northern UISS: (a) location of transects used in b and d, through the north and south of the Uummannaq region. 116

Figure 4.17. NGRIP and GRIP δ18O record, relative sea-level curve from Arveprinsens Ejland, and JJA radiation for 70°N. 118

Figure 4.18. Schematic of the deglaciation of the UISS from its shelf-edge position at the LGM. 123

CHAPTER FIVE

Figure 5.1. Topographic overview map of Uummannaq region. 131

Figure 5.2. Aerial photographs showing the areas from which bedforms were analysed. Locations of each sub-area are labelled. 132

Figure 5.3. Overview of the bedrock geology of the Uummannaq region, with enlargements of Karrat and Ingia. 133

Figure 5.4. Photographs of bedforms from each of the sub-areas in this study. 136

Figure 5.5. Bedding data from KA1 and KA2, including strike and joint dip orientation, plot of width against length, and elongation ratio against length. 138

Figure 5.6. Striae data from the sub-areas studied, plotted in rose diagrams. 138

Figure 5.7. Aerial photograph with rose diagrams superimposed, showing striae measurements across Karrat Island, and bedform long axes and secondary axes. 139

Figure 5.8. Bedding data from IN1 and IN2, including strike and joint dip orientation plot of width against length, and elongation ratio against length. 139

Figure 5.9. Idealised schematic diagrams of bedforms from KA1, KA2, IN1 and IN2. 145

Figure 5.10. Photographs and sketches of a large, abraded whaleback bedform From IN1, in side-profile view. 147

Figure 5.11. Schematic diagram showing the idealised development of bedforms in each sub-area, showing a simplified version of the joint and bedding systems. 150

Figure 5.12. Model of bedform formation in regions of different relative up- or down-ice bedding plane dip, and hypothesised resultant bedforms. 153

CHAPTER SIX

Figure 6.1. Map of the landscapes of glacial erosion on the ice-free rim of Greenland. 158

Figure 6.2. Topographic overview map of Uummannaq region. Altitudes are taken from ASTER imagery, and bathymetry from GEBCO. 159

Figure 6.3. Enlargement of the Svartenhuk Peninsula, with sites and valleys discussed in the text labelled. In addition, surficial deposits of glaciofluvial/fluvial and marine sediment are mapped. 160

Figure 6.4. Geology map of the Svartenhuk peninsula showing bedrock geology, and surficial deposits. Reproduced from (Henderson and Pulvertaft, 1987b). 162

Figure 6.5. Geomorphological map of the Arfertuarssuk Fjord and Quagssugarssuit valley region, showing logs referred to in the text. 172

Figure 6.6. Photographs from Arfertuarssuk Fjord showing the geomorphology 173

Figure 6.7. Photographs of the general morphology of the Quagssugarssuit region 175

Figure 6.8. Two examples of deeply incised overspill channels in the Quagssugarssuit region. 176

Figure 6.9. Photographs from the Kugssineq and Tasiussaq valleys 178

Figure 6.10. Geomorphological map of the Kugssineq valley and Tasiussaq region showing deposits and landforms mapped during this study. 179

Figure 6.11. Photographs from Tasiussaq valley. 180

Figure 6.12. Erratic boulders found resting upon the upper surface of the 36-24 m a.s.l. delta. 181

Figure 6.13. Plate of photographs from the Uligssat Valley 182

Figure 6.14. Sedimentary Logs 1-4, recorded from Arfertuarssuk Fjord. 184

Figure 6.15. Sedimentary Logs 5-8 from Tasiussaq Valley. 185

Figure 6.16. Sedimentary log of Log 9, from the mouth of Tasiussaq. 186

Figure 6.17. Sedimentary log and sediment photographs of Log 10. 187

Figure 6.18. Clast form (triangle plots) and clast roundness (histograms) from samples throughout the study. 188

Figure 6.19. Plot of clast form data from this study, showing RA values against C40 values for all samples, with lithofacies codes labelled 189

Figure 6.20.Cumulative distribution graphs showing the particle size of matrix samples taken from this study 189

Figure 6.21. (a) clast fabric triangle of samples from LFA2 and LF5a taken during this study (red circles), superimposed upon known fabric data from previous studies (Benn, 1994). 190

Figure 6.22. Photograph from Logs 5, showing the only exposure of LFA1 192

Figure 6.23. Photograph of the sedimentary exposure 10 m to the north of Log 2. 196

Figure 6.24. Photograph of horizontally stratified silty-clay, silt, and sand, characteristic of LF3b. 197

Figure 6.25. Photographs from the delta section recorded in Log 8. 199

Figure 6.26. Photograph of horizontally stratified medium sands characteristic of LF3c. Photograph is from Log 6 200

Figure 6.27. (a) photograph of section from Log 3, displaying dipping, planar bedded gravels (LF3b), overlain by LFA4; (b) sedimentary detail of LFA4, with dipping bedding evident 201

LIST OF TABLES

CHAPTER ONE

Table 1.1. Fjord locations, characteristics and outlet glacier ice flux throughout the Uummannaq region. 10

CHAPTER FOUR

Table 4.1. Fjord locations, characteristics and outlet glacier ice flux throughout the Uummannaq region. 87

Table 4.2. TCN sample locations, elevations, type and shielding factors for samples presented in this study. 97

Table 4.3. ^{10}Be TCN exposure ages from the northern UISS 98

Table 4.4. ^{26}Al TCN exposure ages from the northern UISS 99

Table 4.5. ^{14}C ages and calibrated age ranges for the two lake sites in this study. 99

CHAPTER FIVE

Table 5.1. Key features of bedforms mapped and characterised in this study. 137

CHAPTER SIX

Table 6.1. List of locations logged in this study, their log number, and a reference if they studied by previous authors. 163

Table 6.2. Table of present chronological control from the southern and western Svartenhuk Peninsula. All ^{14}C except one returned infinite ages. 164

Table 6.3.Summary of macrofossil biostratigaphic results. 165

Table 6.4. Table of lithofacies associations, lithofacies, a short description of each lithofacies, and the facies/units from each logged section correlated to each lithofacies association. 183

Table 6.5. Table of two new radiocarbon ages produced during this study, from Log 1, Arfertuarssuk. 194

DECLARATION AND STATEMENT OF COPYRIGHT

I confirm that no part of the material presented in this thesis has previously been submitted by me or any other person for a degree in this or any other university. In all cases, where it is relevant, material from the work of others has been acknowledged.

Timothy Patrick Lane

Durham University

February 2013

ACKNOWLEDGEMENTS

First and foremost I would like to thank my supervisors, David Roberts, Colm Ó Cofaigh and Andreas Vieli. They have been an excellent support throughout my PhD, and I always looked forward to our supervisions. Their insightful, probing, and inspiring comments have been of great use to the development of my PhD, and to my wider understanding of the discipline. Special thanks go to David Roberts for the conception of the PhD project, and his (unwavering!) belief in me. He was fantastic in the field, office, and pub, providing sustained ideas, comments, and (sometimes) outrageous hypotheses. Thanks also to other members of Geography staff, and in particular members of the group formerly known as QEC. Their questions and comments during talks, field trips and coffee have been thought provoking.

Fieldwork would have been impossible without help in the field from Harrhy James and Brice Rea. Harrhy was a great help in the field, and his enthusiasm for clast fabric and form measurements did not falter during his month in Greenland. Brice was an invaluable asset during the 2010 field season, and was brilliant fun to work with. Some of his ideas have formed the basis for much of the work presented here. Besides this, his boat hauling skills are second to none.

Much of the field and laboratory work would have been impossible without the funding I received during my PhD. Thanks are due to: Department of Geography, Durham University; Royal Geographical Society (with IBG); the Quaternary Research Association (for multiple grants covering field and laboratory work); Department of Geograph, University of Aberdeen; NERC radiocarbon facility; and NERC cosmogenic isotope analysis facility.

Field work was also made possible by supported by the wonderful Barbara Stroem-Baris and Remy in Nuugaatsiaq, whose 'Martini and philosophy' night was a memorable welcome to Greenland. Further thanks to Alun Hubbard for helicopter support in 2010. That day not only provided us with some brilliant samples, but was also a fantastic experience.

The numerous postgrads and postdocs in the Department of Geography, both past and present, have made my time at Durham highly enjoyable. I've enjoyed sharing drinks, food, and discussions (academic or otherwise) with them all. It should also be said that almost all of this PhD has been written under the influence of caffeine, and I am indebted to Jean and Paul for their coffee brewing skills, and cheap biscuits, and Gary in the library café. Special thanks to Tim, Matthew, Sassi, and Louise for providing a fun (and occasionally productive) office environment!

The technical staff in the labs and workshop have been an enormous help throughout my time here, with special thanks to Merv, Kathryn, Neil, Amanda, Martin, and Alison. Also, Ángel Rodés and Allan Davidson at the NERC CIAF laboratory were a brilliant help during my stays in East Kilbride, and made me feel very welcome.

Throughout my PhD Kathryn Adamson has been a wonderful friend, brilliant company, and great help with everything, academic or otherwise (despite her distaste for the Holocene). Our trips have been amazing fun, and I'm certain that I could not have completed this PhD without her support. Thanks for introducing me to Montenegro, Candy King, Stockport, Hendrick's Gin, Nik, and probably a million other things.

My brother has always been supportive of my studies, and always takes an interest in my studies, despite his anti-climate change tendencies. His passion for architecture, Diet Coke, and his hair has been an inspiration throughout my PhD. Finally I'd like to thank my parents. My dad was fully supportive of everything I did throughout my life, including my undergraduate degree, and I have no doubt that he would have been proud of my work since. My mum has been an amazing help throughout my PhD. Her patience and support has never faltered, even when I have been busy, difficult or withdrawn. Thank you.

CHAPTER ONE

Introduction

1.1. Introduction

The Greenland Ice Sheet (GIS) (Figure 1.1) is the only remaining ice sheet in the northern hemisphere. It contains over 7 m of sea-level equivalent, presently contributing 0.5 mm a^{-1} to global sea-level rise (Shepherd and Wingham, 2007). Under future climate change scenarios, this contribution to average sea-level from the GIS is expected to rise (Rignot *et al.*, 2011). The meltwater produced by the GIS (through surface melting, ocean melting, and iceberg calving) has important effects upon global mean sea-level and ocean circulation in the areas surrounding Greenland, as well as the wider North Atlantic. The potential changes in the amount and intensity of meltwater produced by the GIS are driven through fluctuations in ice sheet mass balance, and increases in calving from outlet glacier termini. Recent analysis has shown a marked increase in GIS mass loss over the past decade (Box *et al.*, 2012). This has been through increases in: surface melting (Mote, 2007, Fettweis et al., 2011); runoff (Box, 2006, Ettema, 2009); dynamic thinning (Krabill et al., 2004, Pritchard et al., 2009); and glacier discharge (Rignot and Kanagaratnam, 2006, Howat et al., 2008). Of this loss, ~50% is thought to be through surface melt, and ~50% is thought to be through dynamic ice sheet effects (van den Broeke et al., 2009). Outlet glaciers in Greenland are particularly susceptible to dynamic changes in a warming climate as they are ocean terminating, meaning they are affected by oceanic warming and relative sea-level rise in addition to atmospheric warming (Nick *et al.*, 2009). However, the processes causing these recent dynamic changes remain poorly constrained, with air temperature, ocean temperature, and relative sea-level likely to be influential forcing mechanisms. As a result of the global ramifications enhanced GIS melt will cause, it is of vital importance that we have a robust understanding of the interactions between climate, oceans, and the GIS.

However, present observational data are limited in their time-scale, and are insufficient for predicting future dynamic changes in GIS behaviour. Thus, in order to provide a robust understanding of the role atmospheric and oceanic changes have upon ice sheet dynamics, we must look to the palaeo-record. Well constrained palaeo-glaciological reconstructions of the GIS allow the factors controlling ice sheet and ice stream retreat behaviour to be analysed. In turn this can inform predictions about the future behaviour of the GIS.

Developments in our knowledge of ice sheet activity has demonstrated that fast-flowing

Figure 1.1. Map of Greenland and its immediate vicinity, with key land-masses and water-bodies labelled. The location of the study area is shown by the red box, and in Figures 1.3 and 1.4.

outlet glaciers drain the majority of the GIS and are the largest source of present mass loss, exerting a strong control upon ice sheet mass balance (Figure 1.2) (Rignot and Kanagaratnam, 2006, Joughin et al., 2010). It is thought that these fast flowing outlet glaciers have been the most dynamic portions of the GIS in the past, and will continue to be in the future. Therefore, the study of past ice streams extent and behaviour will assist in

developing a fuller understanding of how these systems responded to climate change, allowing more robust predictions about their future activity. In areas of favourable topographic settings, over-deepened fjords can converge, acting to enhance ice stream onset, and trigger the formation of large composite ice streams (Lowe and Anderson, 2002, Ó Cofaigh et al., 2002, Angelis and Kleman, 2008, Ottesen et al., 2008, Swift et al., 2008, Roberts et al., 2010, 2013). Large-scale ice streams such as this are likely to have played a

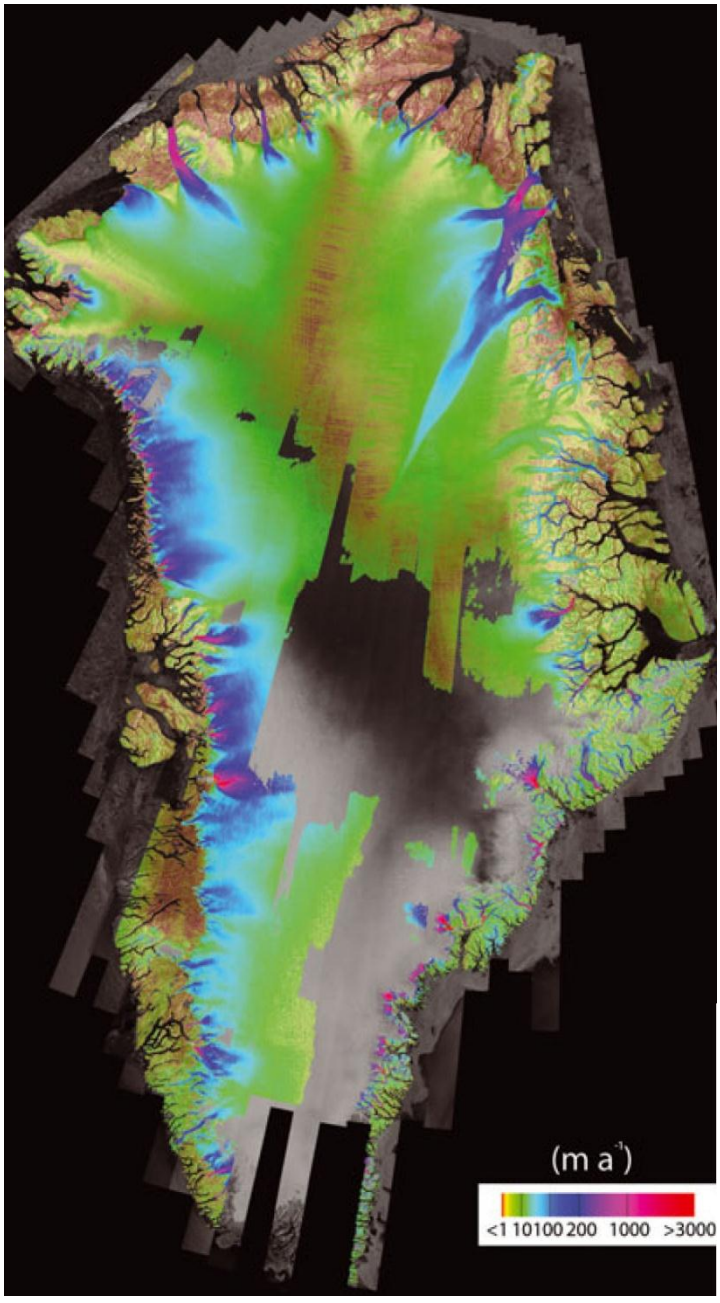

key role in the regulation of GIS mass balance, and the evacuation of ice to the shelf-edge during previous glacial periods. However, there is a widespread

Figure 1.2. Map of flow speed velocities (in colour) for the winter 2005-2006, displayed overprinted upon a radar mosaic for the same period (from Joughin *et al.*, 2010).

paucity of information concerning the location and behaviour of these large ice streams throughout Greenland. The Uummannaq region in central West Greenland is an area of highly convergent fjords, containing a series of high discharging outlet glaciers. Recent research has demonstrated that these outlet glaciers advanced and coalesced during the Last Glacial Maximum (LGM), forming the Uummannaq Ice Stream System (UISS) (Ó Cofaigh et al., 2013b, Roberts et al., 2013). This extended 300 km offshore, reaching its terminal position at the shelf-edge where it formed a trough mouth fan (Ó Cofaigh et al., 2013a, 2013b). During the LGM the UISS is thought to have exerted a major influence upon the dynamics of the West GIS, and is predicted to have drained ~5% of the total GIS (calculated from Rignot and Kanagaratnam, 2006). Work has shown that post-LGM deglaciation of the UISS began by 14.9 cal. kyr BP (Ó Cofaigh et al., 2013b), with outlet glaciers in the south of the region reaching present fjord heads by 8.7 kyr (Roberts *et al.*, 2013). Despite development in our understanding of UISS behaviour from its LGM margin to present both offshore (McCarthy, 2011, Ó Cofaigh et al., 2013b) and in the south of the system (Roberts *et al.*, 2013), the dynamic behaviour of the northern UISS is unknown. Therefore, producing a record of the extent and behaviour of the entire system is a key step in understanding the process that control large ice stream behaviour during deglaciation.

As well as their contribution to relative sea-level and oceanic circulation, ice sheets have played an important role in landscape evolution throughout the Quaternary. Ice streams, the most active portions of ice sheets, are particularly important in the development of the landscape in previously glaciated regions. Understanding the way ice sheets are organised is therefore important for analysing their impact upon landscapes. The extensive partitioning which they cause determines ice sheet-landscape interaction, and the resultant imprint upon the landscape (Kleman, 1994, Kleman and Borgström, 1994, Hughes, 1995, Kleman and Glasser, 2007, Kleman et al., 2008, Stroeven and Swift, 2008, Angelis and Kleman, 2008, Winsborrow et al., 2010). These landscapes of extreme contrast can develop over timescales of 100 ka to 1 Ma through positive feedbacks of selective linear erosion, flow convergence, and subglacial thermal organisation (Kessler et al., 2008, Jamieson et al., 2008, Kleman and Glasser, 2007).

1.2. Study area: the Uummannaq region

1.2.1. Regional geography

The Uummannaq region is a mountainous area of West Greenland, with peaks reaching >2000 m a.s.l. It lies between 70.33°N and 72.00°N and covers ~40,000 km^2. The region is in the Low to High-Arctic transition with mean annual air temperatures of -3°C to -7°C (Box, 2006). At present, the West Greenland Current (WGC) operates offshore, bringing warm subsurface water close to the present fjords (Holland et al., 2008a). The area is characterised by a series of deep, fjords, running northeast – southwest in the north, and

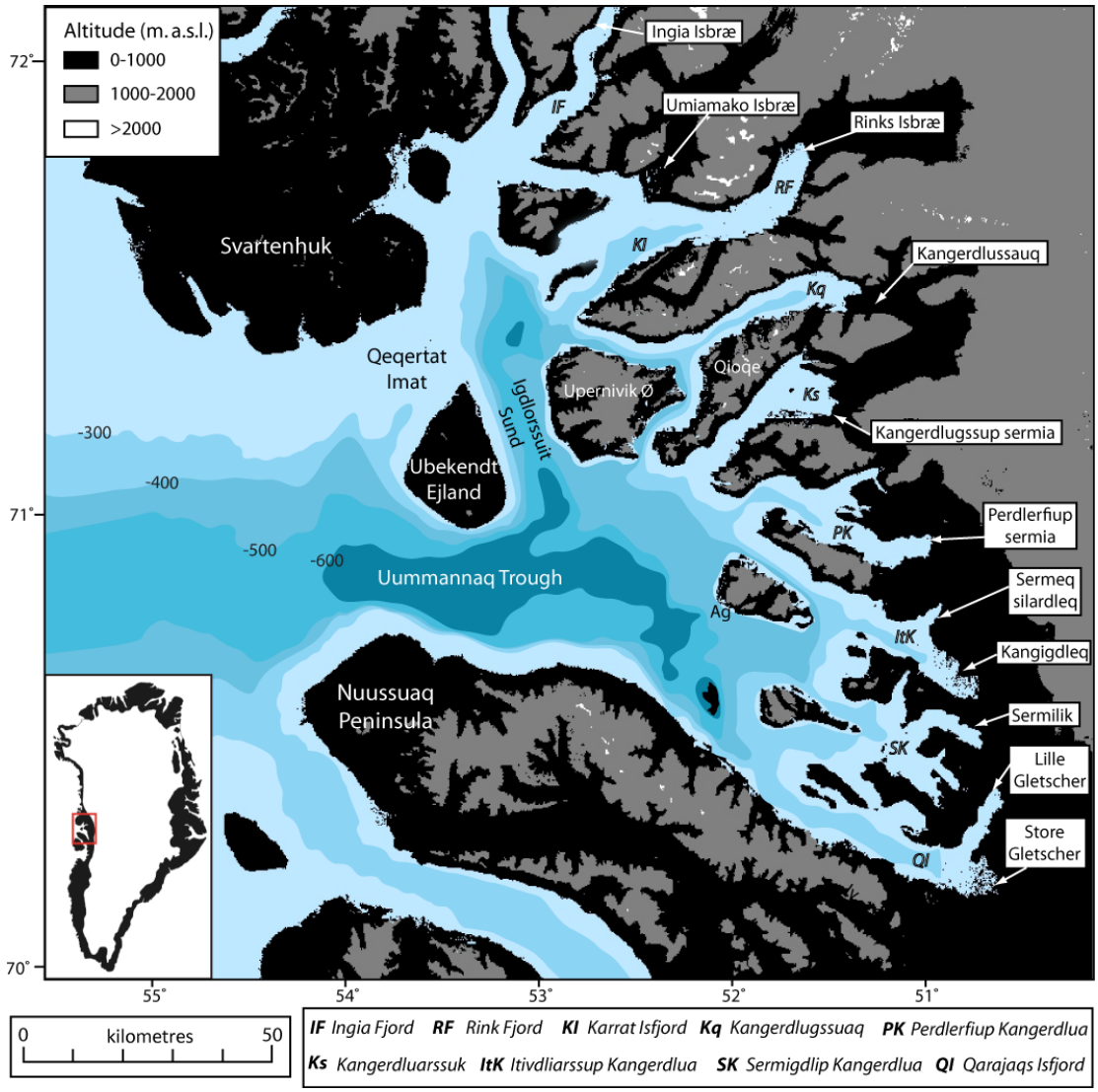

Figure 1.3. Topographic and bathymetric overview of the Uummannaq region, with key locations marked. Bathymetric depths are from GEBCO data, and topography from ASTER data.

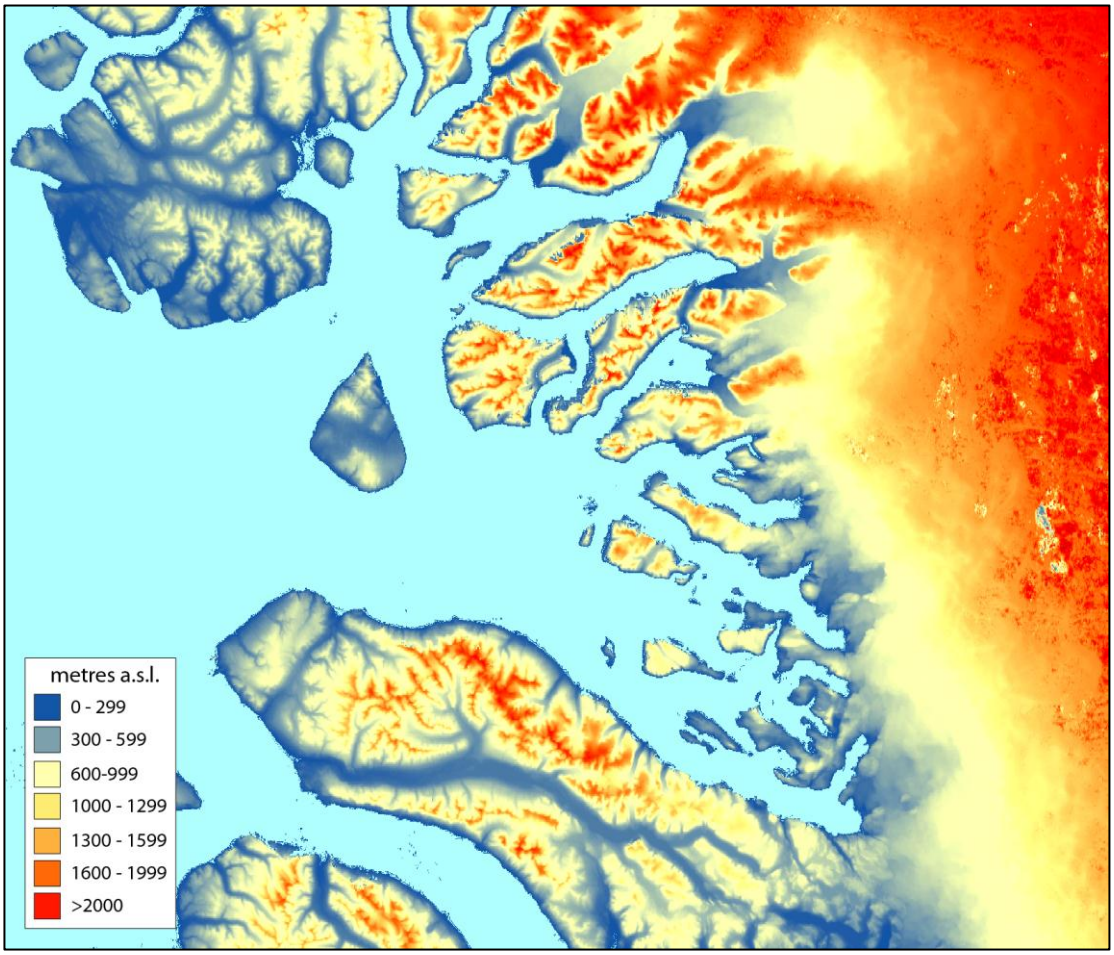

Figure 1.4. Topographic DEM of the Uummannaq region from ASTER data. Note that the boundary between land and ice sheet is not marked.

southeast to northwest in the south, producing a convergent pattern (Figure 1.3 and 1.4). These are currently occupied by marine terminating outlet glaciers which drain the central West Greenland Ice Sheet. The majority of fjords are at least 500 m deep, and become confluent in Igdlorssuit Sund, and the Uummannaq Trough, the latter of which extends to the shelf edge. It is the highly convergent fjord configuration, and deep cross-shelf trough has led to the hypothesis that the region fostered a large ice stream system during the LGM (Ó Cofaigh et al., 2013b, Roberts et al., 2013). The Uummannaq trough (Figure 1.3) is more than 800 m deep, although several areas of shallow topography have been identified from multibeam data (in places < 300 m depth) (Harff, 2007, Ó Cofaigh, 2009). The bathymetry of this region shows an underwater sill to the north of Ubekendt Ejland, through Qeqertat Imat, with water depths of <200 m a.s.l., significantly less than the surrounding waters.

1.2.2. Geological setting

The Uummannaq region is characterised by three distinct geological regions, separated by a series of north-south running faults (Figure 1.5). The eastern most and oldest of these regions is formed of Precambrian basement rock. This forms the convergent inner fjord system (Figures 1.3, 1.4, and 1.5). This basement is comprised of Archean orthogneisses (~2800 Ma) (Garde and Steenfelt, 1999), overlain by Palaeoproterozoic sediments (Kalsbeek et al., 1998, Bonow et al., 2007). These sediments are part of the Nûkavsak, Qeqertarssuaq and Marmorilik Formations, which together form the Karrat Group, part of the extensive Rinkian mobile belt of west Greenland (Kalsbeek et al., 1998). The Nûkavsak Formation is the most extensive of these, and comprises the majority of surficial outcropping bedrock in the northern half of the Uummannaq region. It is comprised of interlayered granular semipelite (metagreywacke) and politic schist, interpreted as turbidites, and shows little lithological variation through its vertical and horizontal extent (Kalsbeek et al., 1998, Henderson and Pulvertaft, 1987a). The metagreywacke exhibits multiple sub-vertical and sub-horizontal joints, and thin beds (c.10cm). In the field, infrequent outcrops of sub-horizontally bedded quartzite bands were found. To the south of these, lithologies from the Karrat Group are not found, and the Archean gneiss forms the surficial bedrock.

To the west, lying between the outer margin of the fjord system and Ubekendt Ejland, in the Nuussuaq Basin, is a unit of Cretaceous-Tertiary marine mudstones and sandstones, deposited in a fluvial and wave dominated environment (Pedersen and Pulvertaft, 1992, Dam et al., 2000). They are bounded to the east by an extensional fault system, though the deposits are likely to have extended further in the past, and are now either eroded or overlain (Henriksen et al., 2000).

West of this are a series of basalts, laid down during major eruptions at the continental edge during the initial phases of seafloor spreading in the Tertiary (Henriksen et al., 2000). The volcanics contain high levels of picrites and olivine basalts, and are iron-bearing (Clarke and Pedersen, 1976). The basalts reach thicknesses of 10km, as seen on Ubekendt, and were initially lain down between 61 and 59 Ma, with a period of later eruptions at 52.5 Ma on Ubekendt, Svartenhuk and Nuussuaq (Henriksen et al., 2000).

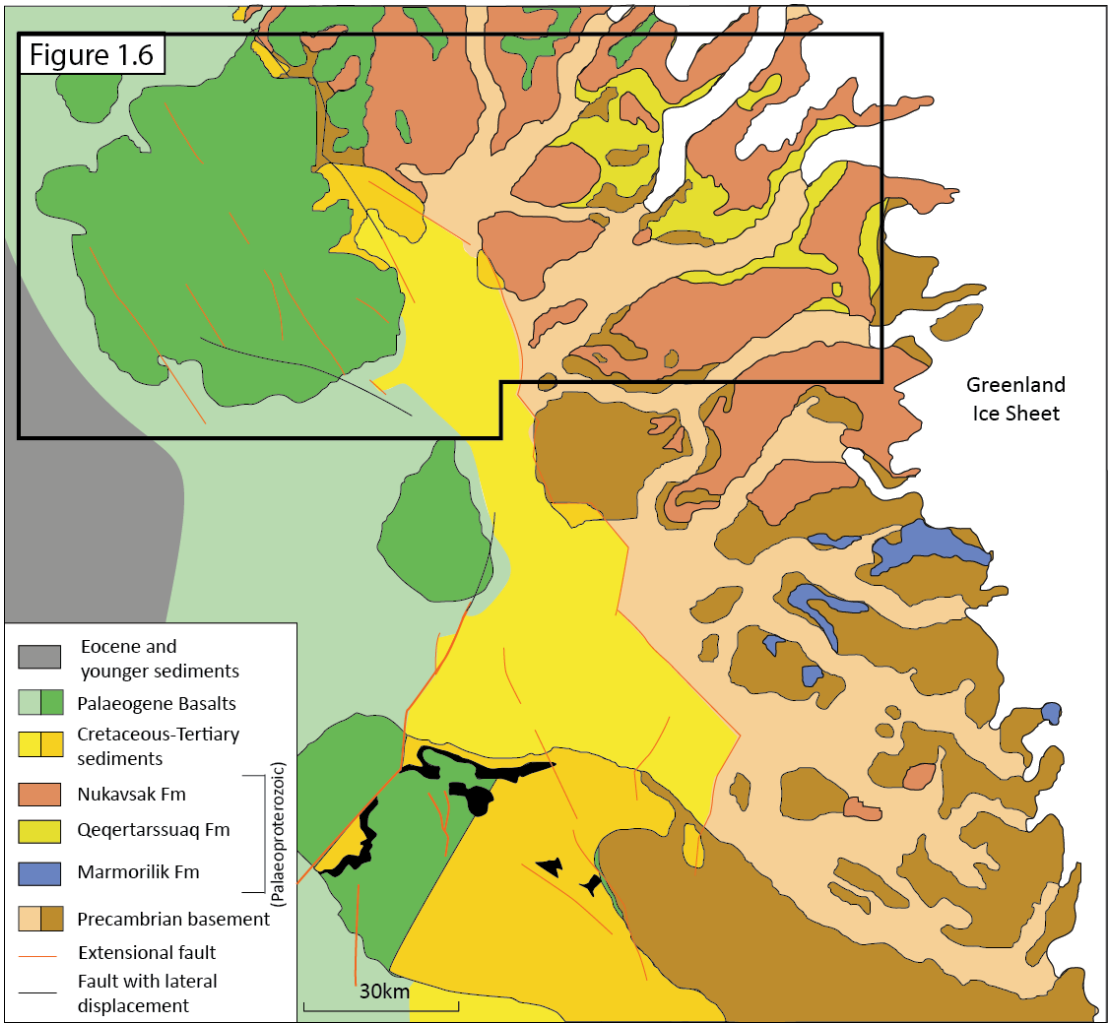

Figure 1.5. Map of the Uummannaq region showing dominant bedrock geology. The three distinct geological regions can be seen, separated by north to south trending faults (adapted from Steenfelt et al., 1998).

1.2.3. Glaciological setting

Central West Greenland has the highest concentration of outlet glaciers in Greenland (Reeh, 1985). The Uummannaq region contains 11 major outlet glaciers of varying size and discharge, the largest of which are Rink Isbræ and Store Gletscher, which produces 10.5-16.7km^3 a^{-1} and 13.2-17.5km^3 a^{-1} ice that calves into the ocean (Table 2.1) (Figure 1.7) (Bauer et al., 1968, Carbonnell and Bauer, 1968, Rignot and Kanagaratnam, 2006). Between 2000 and 2010 these outlets have experienced a combined net area loss of 51km^2 (Box and Decker, 2011). Umiámáko glacier experienced the most change during this period, with a large 15km^2 loss between 2005 – 2006 (Box and Decker, 2011). Rink Isbræ and Store Gletscher both maintained relatively stable ice front positions between 2000 and 2010. Due to variations in subglacial bed topography and ice sheet glaciology, outlet glacier drainage basin varies widely throughout the Uummannaq region (Figure 1.8). An extensive subglacial

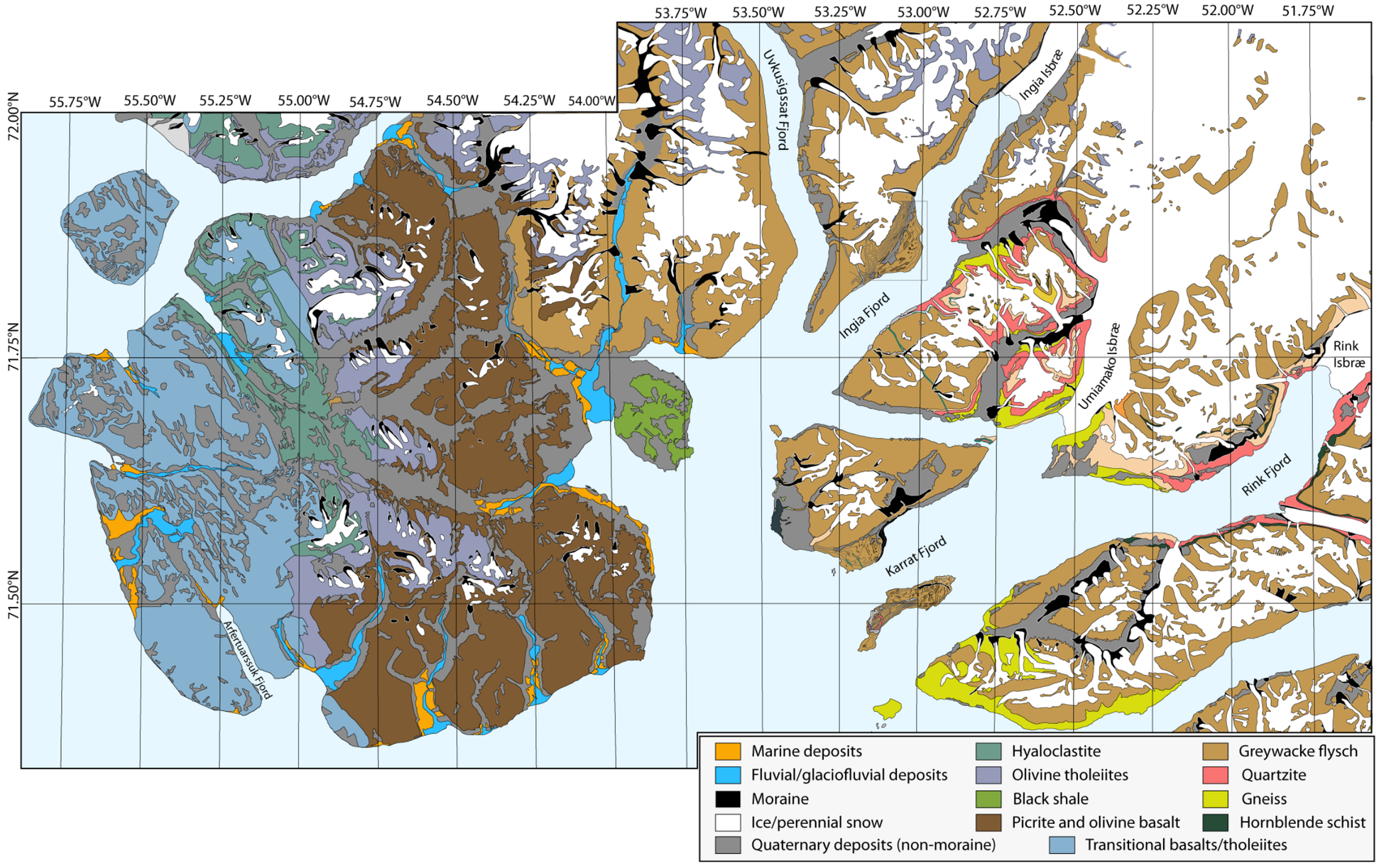

Figure 1.6. Geological map enlargement of the northern Uummannaq region, showing the distinct difference between the Svartenhuk Peninsula in the West, and the fjordic region to the East. Previously identified Quaternary deposits are also shown (adapted from Henderson and Pulvertaft, 1987b).

Fjord Name	Outlet Glaciers	Mouth location	Snout location	Orient. (°)	Length (km)	Width at SL (km)	Plateau height (m a.s.l.)	Max. water depth (m)[a]	Max ice flux (km^3 yr^{-1})[b]
Northern Fjords									
Ingia Fjord	Ingia Isbræ	71.73°N 53.32°W	72.00°N 52.70°W	213.43	38.5	4.5	1444	-	1.1
Rink-Karrat Fjord	Umiámáko Isbræ,Rink Isbræ	71.40°N 53.07°W	71.73°N 53.65°W	238.12	63.6	6.2	1791	1108	11.8
Kangerdlug.	Kangerlussuup Sermersua	71.38°N 53.00°W	71.45°N 51.83°W	263.22	61.7	4.2	1894	570	2.4
Southern Fjords									
Kangerdluar	Kangerluarsuup Sermia	71.13°N 52.30°W	71.25°N 51.52°W	244.96	34.9	5.7	1671	770	0.3
Perdlerjiup Kangerdlua	Perlerfiup Sermia	71.05°N 52.00°W	70.98°N 50.95°W	282.01	42.5	5.5	1388	1246	1
Itivdliarssup Kangerdlua	Sermeq Silarleq, Kangigdleq	70.98°N 51.97°W	70.80°N 51.00°W	302.1	42.5	5.56	1332	844	7.6
Sermigdlip Kangerdlua	Sermilik	70.7°N 51.52°W	70.62°N 50.63°W	291.5	38.2	4.4	1180	1287	2.6
Qarajaqs Isfjord	Lille Gletscher, Store Gletscher	70.68°N 52.28°W	70.37°N 50.60°W	302.7	75.4	6. 9	1308	956	17.8

[a]Data from GEBCO_08 Grid and Hareø-Prøven bathymetric charts

[b]Data from (Bauer, 1968, Carbonell and Bauer, 1968, Rignot and Kanagaratnam, 2006)

Table 2.1. Fjord names, locations, characteristics and outlet glacier ice flux throughout the Uummannaq region. The outlet glaciers found within each fjord are named, and their locations are identified in Figure 1.3.

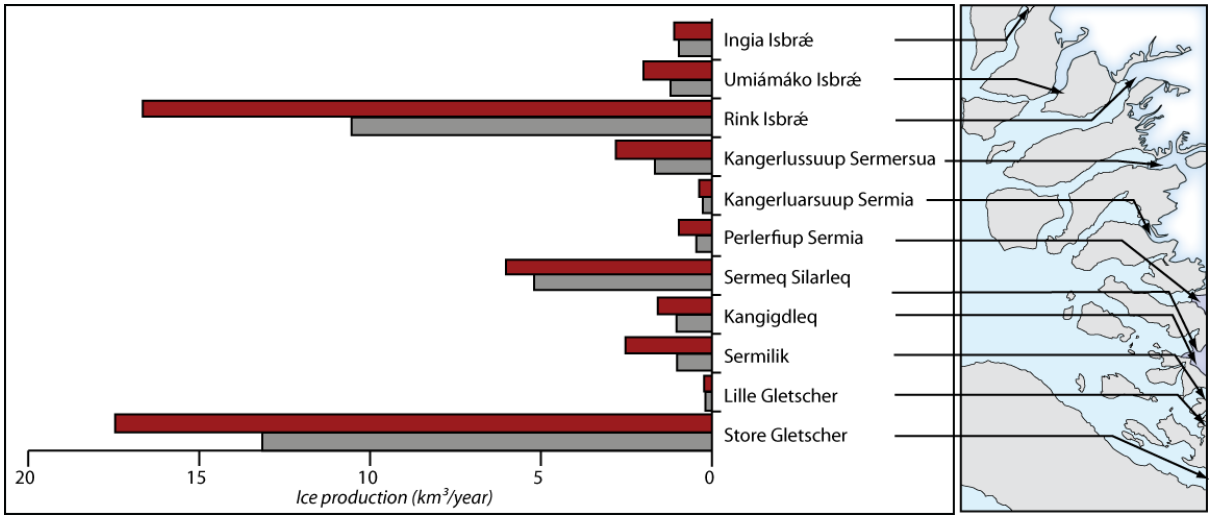

Figure 1.7. Estimated maximum (red) and minimum (grey) ice production from glaciers within the Uummannaq Region. Modified from Weidick and Bennike (2007) (data from Bauer, 1968, Carbonell and Bauer, 1968).

mountain range exists to the north of the Uummannaq region, at 72°N. The subglacial topography of this area is >900m asl, persisting for at least 200km inland (Bamber et al., 2001). This has acted to block ice from the north, and restrict the drainage basin size of outlet glaciers in the north of the Uummannaq region.

1.2.4. Glacial history – Last Glacial Maximum to present

During its LGM maximum extent the UISS extended to a shelf-edge position, depositing sediment at the trough mouth fan at the edge of the Uummannaq Trough (Ó Cofaigh et al., 2013b). Recent offshore studies have provided evidence of ice out to the shelf-edge at the LGM, and have provided a minimum age of deglaciation of 14.9 cal. kyr BP. Dates from organic material in the area (Patorfik and Svartenhuk) have placed deglaciation to the present coastline as between 10.5-9.5 kyr BP (Kelly, 1985). Geomorphological and terrestrial cosmogenic nuclide dates from the south of Ubekendt Ejland suggests a relatively rapid initial retreat after the local LGM (Roberts *et al.*, 2013). Following this retreat from the continental shelf, the south of the UISS is thought to have deglaciated rapidly back into its fjord confines by 11.4 kyr in the south (Roberts *et al.*, 2013). Here, the outlet glaciers became pinned by topography, inducing slowdowns and standstills. After this, early Holocene retreat back to the present ice margin took place, driven by surface thinning (Roberts *et al.*, 2013). These dates are in agreement with a radiocarbon date from the northern coast of Nuussuaq (10800 cal. yrs BP - Simonarson, 1981). Despite this extensive

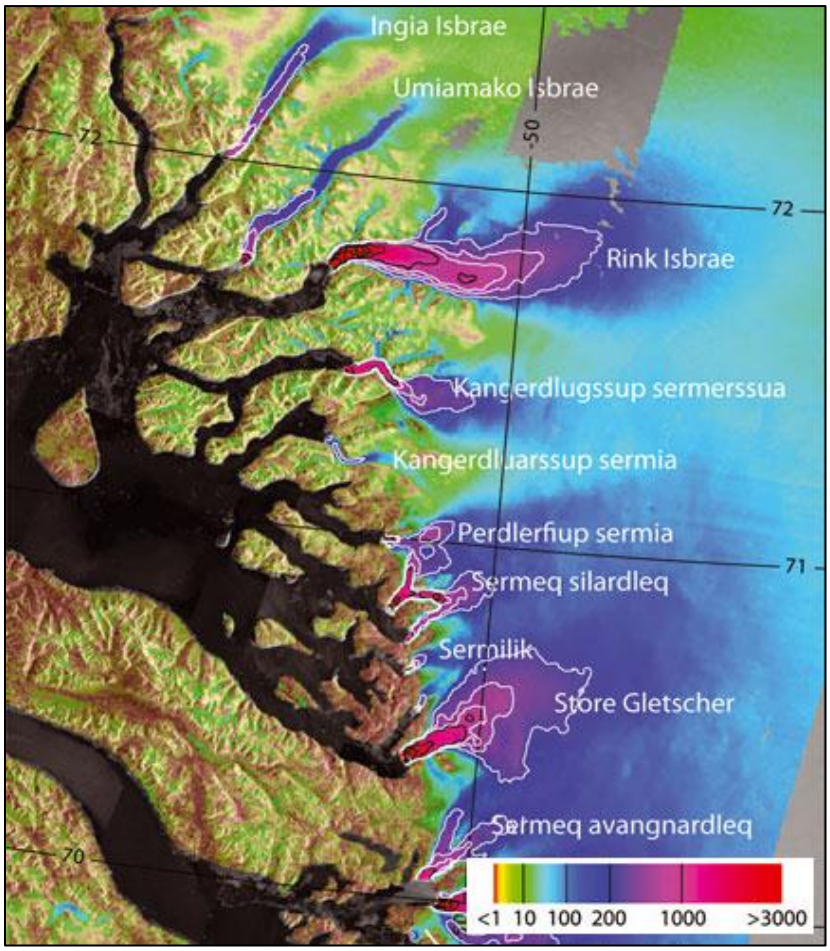

Figure 1.8. Map of flow speed velocities (in colour) for the winter 2005-2006, displayed over a 2000-2001 SAR mosaic, with contours at every 250 m a^{-1} (from Joughin *et al.*, 2010). Note the variability in the width of the fast ice flow corridor (> 50 m a^{-1}) across outlet glaciers in the Uummannaq region. Outlet glaciers in the far north of the region (Ingia and Umiámáko Isbræ) appear very narrow, and topographically confined, whereas those in the south show less topographic confinement.

chronology from the southern UISS, the glacial history of the north of the region remains unknown, with deglaciation constrained by a single radiocarbon date from eastern Svartenhuk (10500 cal. yrs. BP – Bennike, 2000). As a result, the behaviour of the northern half of the UISS, and its synchroneity or asynchroneity with the southern sector of the UISS is not understood. The factors which have controlled the retreat also remain unknown, and are currently poorly constrained. However, as mentioned above, topography, as well as post-glacial relative sea-level rise, Holocene air temperature increased, and ocean warming are likely to have played important roles.

The glacial history of the region has been characterised by extensive selective linear erosion, plateau formation, and areal scour, throughout the Quaternary. This has led to the

development of a series of high relief fjords and extensive relict plateau surfaces (Sugden, 1974; This Study, Chapter Three). These fjords are highly confluent to the east and south of Ubekendt Ejland, and contain contemporary outlet glaciers (Figure 1.3 and 1.7). Recent research has demonstrated that these outlet glaciers advanced and coalesced during the Last Glacial Maximum (LGM), forming the Uummannaq Ice Stream System (UISS) (Roberts et al., 2013, Ó Cofaigh et al., 2013b). Areas to the north (Svartenhuk) and south (Nuussuaq) of the Uummannaq region represent large topographic barriers, and would have assisted in confining ice flow into the Uummannaq Trough. The Svartenhuk Peninsula is of particular interest as it is relatively low lying, and previous work has reported that it has experienced little to no glacial erosion (Sugden, 1974), with sedimentological studies displaying extensive raised marine deposits, and no evidence for glaciation (Rink, 1853, Steenstrup, 1883, Laursen, 1944, Funder, 1989b, Bennike et al., 1994). It is instead thought that the peninsula was occupied by local mountain and plateau glaciers (Bennike *et al.*, 1994). It is possible that the conditions on Svartenhuk were aided by the positive feedback links, through the intense drawdown of ice through the Uummannaq Trough. This would have starved peripheral areas, such as the Svartenhuk Peninsula, of ice sheet ice, allowing the growth of localised mountain valley glaciers.

During the LGM the UISS would have exerted a major influence upon the dynamics of the West GIS, and is predicted to have drained 5-6% of the total GIS (calculated from Rignot and Kanagaratnam, 2006). Work has shown that post-LGM deglaciation of the UISS began by 14.9 cal. kyr BP (Ó Cofaigh et al., 2013b), with outlet glaciers in the south of the region reached present fjord heads by 8.7 kyr (Roberts *et al.*, 2013). Despite development in our understanding of UISS behaviour from its LGM margin to present both offshore (McCarthy, 2011, Ó Cofaigh et al., 2013b) and in the south of the system (Roberts *et al.*, 2013), knowledge of the north of the UISS is absent. The Uummannaq region represents a seemingly unique example of large-scale fjord confluence a palaeo-ice stream onset. As a result, producing a record of the extent and behaviour of the entire system is a key step in understanding the process that control large ice stream behaviour during deglaciation.

1.2.5. Central West Greenland relative sea-level history – Last Glacial Maximum to present

Patterns of relative sea-level (RSL) change through West Greenland have been relatively well documented, and prior to sea-floor bathymetric study were one of the principle

sources of dating ice sheet retreat (Weidick, 1968, Funder and Hansen, 1996). In West Greenland these RSL records have been constructed through an amalgamation of: radiocarbon dates of shells from raised marine deposits (Weidick, 1972, Weidick, 1976, Donner and JUNGNER, 1975, Kelly, 1985, Funder, 1989b); dates from mammalian bones, driftwood, and archaeological remains; and ages on lake sediment from isolation basins (Foged, 1977, Bennike, 1995, Long et al., 1999).

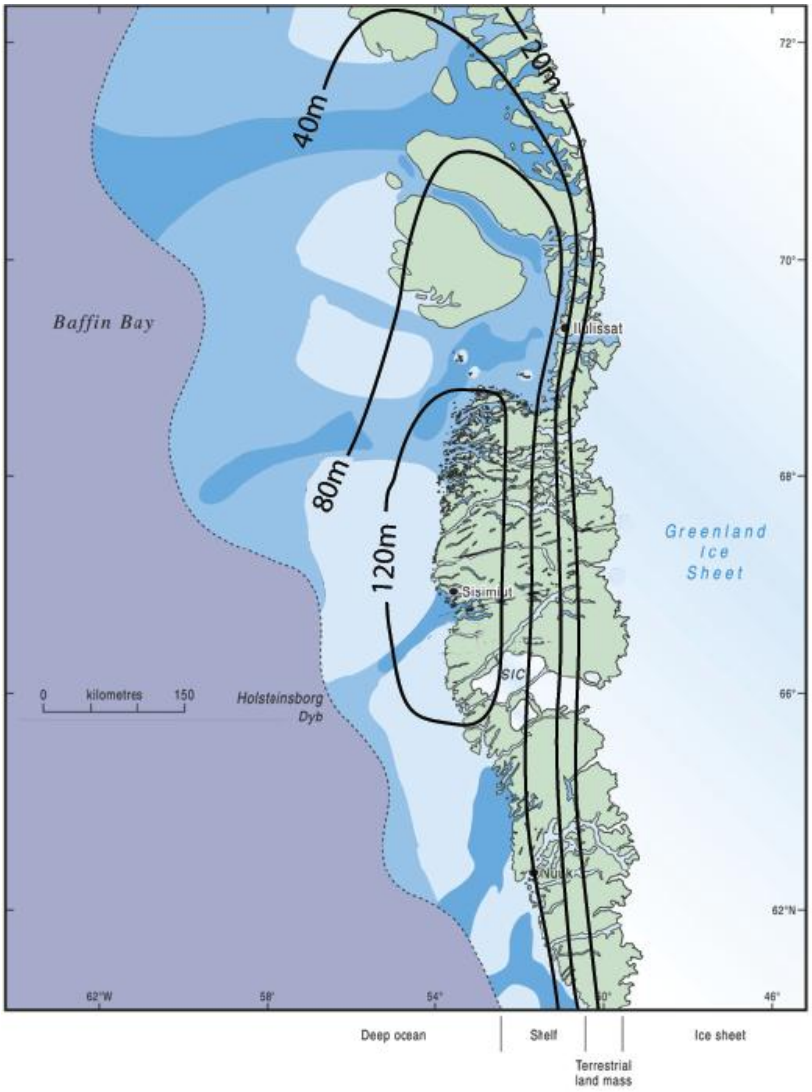

Figure 1.9. Map of the regional trends in marine limits from central West Greenland as hypothesised by Weidick (1992). Based upon sea level data and model predictions.

Following ice expansion at the Last Glacial Maximum, widespread ice sheet break-up led to large amounts of ice sheet melt, and a subsequent global eustatic RSL rise. This eustatic RSL rise is likely to have begun at ~16 cal. kyr BP and reached its peak (expressed as the local marine limit) at ~11 cal. kyr BP (Simpson *et al.*, 2009). Though the marine limit varies, dependent upon the local ice loading and unloading history, the regional marine limit trend in Disko Bugt is shown in Figure 1.9. After reaching the marine limit, RSL fell as glacio-

isostatic rebound was able to out-pace continuing eustatic RSL rise (Long et al., 1999). This RSL fall continued until 4.4-3.2 cal. kyr BP, when submergence then occurred (Rasch and Nielsen, 1994, Rasch and Nielsen, 1995, Rasch and Jensen, 1997, Rasch et al., 1997, Long et al., 1999), thought to be due to renewed ice sheet advance and crustal re-loading during the Neoglacial (Kelly, 1980, Weidick, 1993, Weidick, 1996). The Disko Bugt region is the most studied region of West Greenland, and therefore has the best resolved RSL history. This is based upon raised marine deposits and isolation basin stratigraphy, and has a regional record to 11 cal. kyr BP (Figure 1.10) (Long et al., 1999). This record has been since extended to ~16 cal. kyr BP using glaciological model predictions (Simpson et al. 2009). In Disko Bugt the RSL record is highly spatially variable, with marine limits ranging from ~40 to 120 m (Figure 1.9) due to the timing of ice sheet unloading (Long et al., 1999).

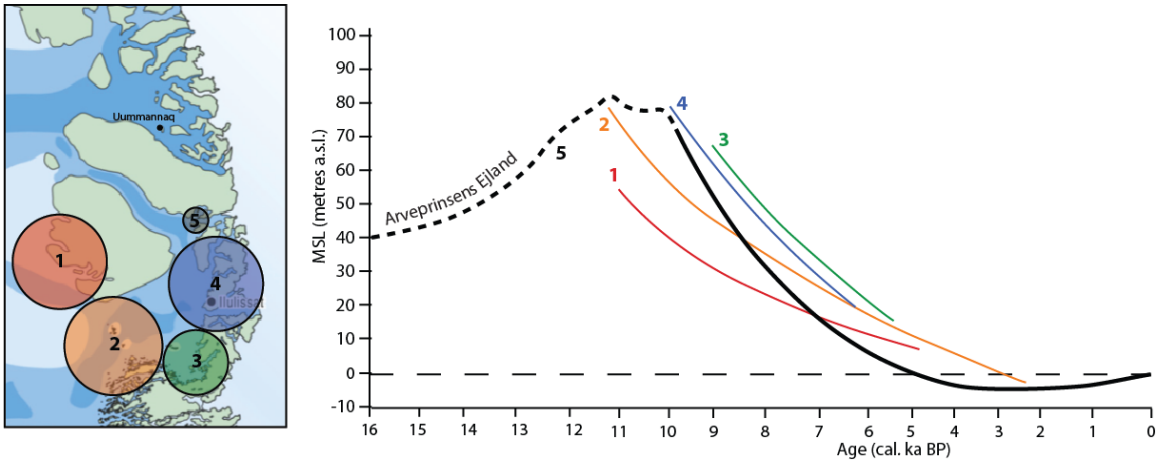

Figure 1.10. A series of five relative sea-level curves from the Disko Bugt region, from 0 - 11 cal. ka BP. Curves 1-4 were constructed by Weidick (1996), and 5 by Long et al. (1999). The dashed line represents a modelled extension of results from 11 – 16 cal. ka BP, taken from Simpson et al. (2009).

The marine limit in the Uummannaq region is currently poorly constrained as a result of limited marine indicators (perched boulders and raised marine deposits) (see Figure 1.11). Based upon a series of undated marine sediments, the marine limit in southern Svartenhuk has been ascribed to ~35 m a.s.l. (Kelly, 1985). However, evidence of a marine limit of at least 70 m a.s.l. has been found in southwestern Svartenhuk (see Chapter Six). Other investigations from the Uummannaq region place the marine limit on northern Ubekendt Eljand at 65 m a.s.l. (Roberts, pers. comm) and at ~35 m a.s.l close to Store Gletscher present margin (Roberts *et al.*, 2013) (Figure 1.11).

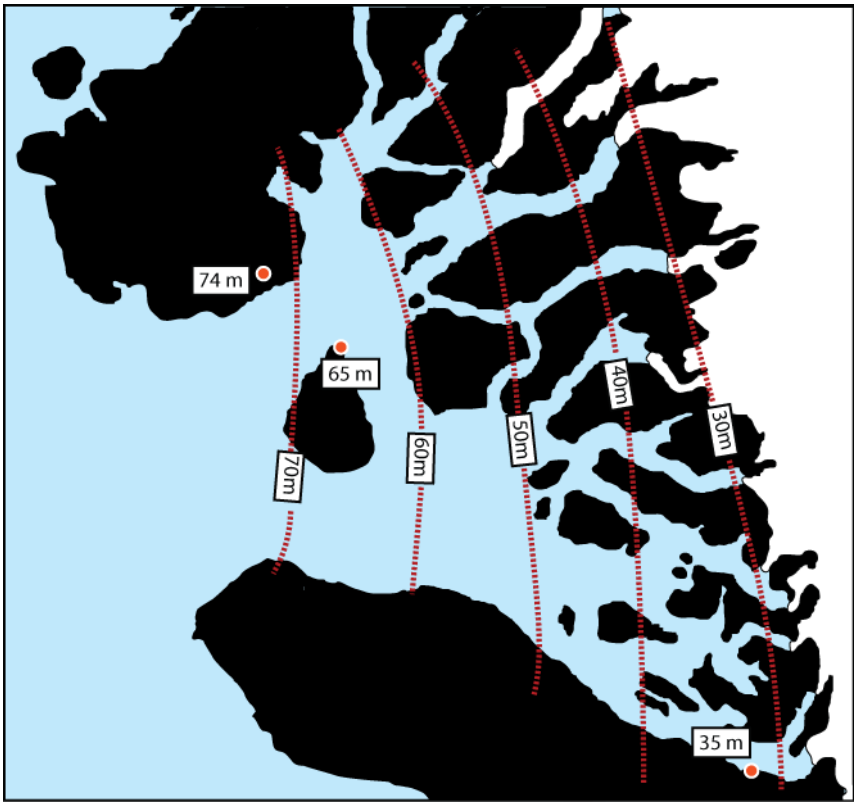

Figure 1.11. Map of the regional marine limits from the Uummannaq region. The marine limit contours are an estimate based upon the data collected from this study and Roberts et al. (2013).

1.3. Research aims and objectives

This thesis broadly aims to investigate the long-term dynamics of the Uummannaq Ice Stream System, West Greenland, with a focused placed upon its northern sector. During the Last Glacial Maximum and previous Pleistocene glaciations, outlet glaciers throughout the Uummannaq region coalesced to form the Uummannaq Ice Stream System, advancing to the shelf-edge (Ó Cofaigh et al., 2013b, Roberts et al., 2013). The identification of this system is recent, and its northern sector has received little research attention. As a result, it represents an important, unstudied location in which to analyse ice stream dynamic retreat behaviour, landscape development in an area of intense glacial activity, and the evolution of areas peripheral to ice streams. These broad aims will be investigated using the following objectives:

1. To describe and evaluate the regional-scale distribution of glacial landsystems throughout the Uummannaq region, and investigate the factors controlling their distribution throughout the Quaternary.

2. To understand the Last Glacial Maximum dynamic behaviour of the Uummannaq Ice Stream System
3. To evaluate and understand the subglacial conditions controlling bedrock bedform development in an area of rapid palaeo-ice flow
4. To investigate the controls which have governed the evolution and glaciation of areas peripheral to large ice stream system

1.4. Thesis structure

Beyond the introduction, this thesis contains six chapters:

Chapter Two provides a synopsis of published material deemed relevant to this study. It outlines the current theoretical and observed knowledge of ice streams, and their importance in ice sheet mass balance and regulation. Methods of palaeo-ice stream reconstruction are discussed, with a focus upon evidence from palaeo-ice streams on rigid (bedrock) beds. Following this, the present state of outlet glaciers throughout Greenland is discussed, and their relationship with climatic and oceanic forcing (air temperature, ocean temperature, and relative sea-level) is analysed. A short review of the glacial history of West Greenland is provided, detailing known information of terminal ice extent during both MIS 6 and MIS 4-2 (LGM), and current understanding of deglaciation of West Greenland and Baffin Bay. Following this, a review focusing on West Greenland ice stream history is presented. Finally the regional geography, geology, current glacial setting, and previous research undertaken in the study site (the Uummannaq region) are presented.

Chapter Three addresses Research Objective 1, aiming to understand glacial and non-glacial landscape distribution throughout the Uummannaq region. This is achieved through new high-resolution remote and field geomorphological mapping, which delimited areas of selective linear erosion, area scour, dissected plateau, mountain valley and cirque glaciers, lowland terrestrial deposition, and no – little evidence of glacial erosion. These results are combined with the known geological structure of the region, and its Neogene and Quaternary uplift history. This provides a model of long-term landscape development, varying with altitude and time.

Chapter Four addresses Research Objective 2, understanding the extent, thickness, and deglacial behaviour of the northern UISS. Investigation of geomorphology in combination

with surface exposure dating (^{10}Be and ^{26}Al cosmogenic isotopes) allows the upper limit of the most recent (LGM) glaciation to be identified. This dual approach prevents the possibility of mis-interpretation of geomorphological data, and allows robust reconstruction of LGM ice thickness in the northern UISS. In addition, geochronological data allow the retreat of the northern UISS to be constrained, and processes causing this retreat to be identified. Initial retreat to the mid-fjord was shown to be relatively rapid, and synchronous with the southern UISS, driven by increasing air temperature and relative sea-level. However, a major marginal still-stand occurred at 11.5-6.9 kyr, driven by topographic constrictions (shallow bed and narrow fjord walls). This chronology is shown to vary from other published records of ice stream retreat, demonstrating the asynchroneity of ice stream response across West Greenland.

Chapter Five addresses Research Objective 3, presenting new bedrock bedform and structural geology data from as series of four sub-areas within inner fjord margins of the northern UISS. Analysis of the data shows that, though influential, palaeo-ice flow properties (e.g. direction, ice thickness) are not the primary factor controlling bedform morphology within this study. Bedding plane orientation relative to ice flow and dip, joint orientation, dip, and frequency, are shown to play important roles in bedform width, length, type, and elongation. Lateral plucking is also found on a series of bedforms from Ingia Fjord, demonstrating that this mechanism is not exclusive to the development of negative landforms (see Krabbendam and Bradwell, 2011).

Chapter Six addresses Research Objective 4, investigating the Late-Quaternary history of the Svartenhuk Peninsula. This is carried out using geomorphological and sedimentological analysis of both new and previously studied sites along the southern Svartenhuk coastline. Results provide strong evidence for extensive glaciation during the Late-Quaternary, radiating from the inner mountainous massifs of the peninsula. Results are integrated to form a process-based model for sediment deposition throughout the region. This region appears unique throughout Greenland, and its investigation is important in order to develop a regional-scale understanding of ice activity in close proximity to a large ice stream.

Following these substantive chapters, Chapter Seven provides a synthesis of results and interpretations from the preceding chapters, with respect to the main aims of the thesis. It then brings these results together and discusses the wider importance of the study.

It should be noted that this thesis does not contain a standalone methods or study site chapter. Instead, relevant study site and methodological information is contained within each of the substantive results and interpretations chapters (Chapters Three - Seven). This has been done in order to provide the reader with relevant information when needed and for publication purposes.

CHAPTER TWO

Literature Review: Ice streams and their importance to the Greenland Ice Sheet; past and present

2.1. The Greenland Ice Sheet

2.1.1. Present ice sheet dynamics

Recent research into large tidewater outlet glaciers and ice streams in the high-latitudes has shown an almost universal signature of increased ice discharge into the oceans since the 1990s (Bindschadler, 2006). Greenland Ice Sheet (GIS) is the only ice sheet in the Northern Hemisphere, and is extremely vulnerable to rising temperatures in this area. Recent studies from GRACE data have shown that melting of the GIS is responsible for 15% - 30% of global sea-level rise since 2003 (Figure 2.1) (Velicogna, 2009, Velicogna and Wahr, 2006, Chen et al., 2006, van den Broeke et al., 2009, Khan et al., 2010). Of this loss, ~50% is thought to be loss through surface melt, and ~50% is thought to be loss through dynamic ice sheet effects (van den Broeke et al., 2009). Including the contribution made by dynamic discharge by ocean-terminating outlet glaciers, it is now thought that Greenland could add 0.16-0.54 m to global sea-level rise by 2100 AD (Pfeffer et al., 2008), with Greenland's contribution to

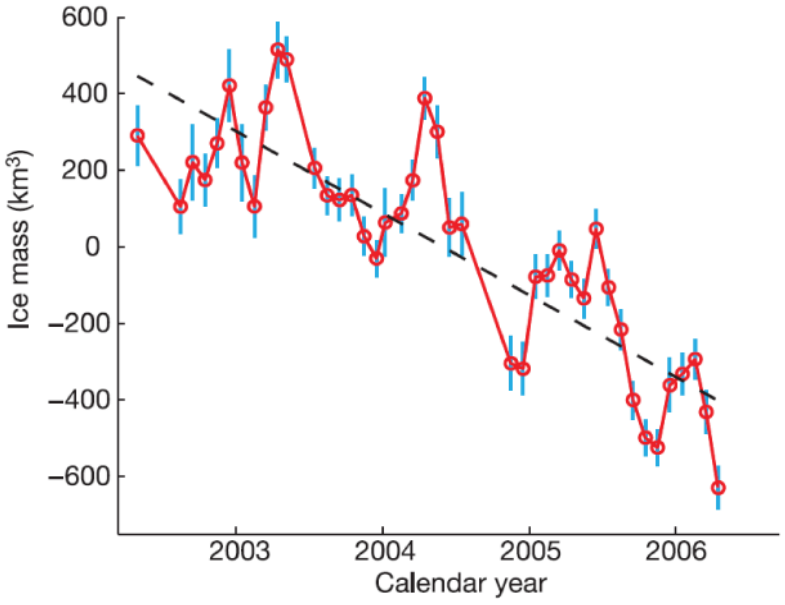

Figure 2.1. GRACE monthly mass solutions of the whole of the GIS, from April 2002 to 2006 (from Velicogna and Wahr, 2006).

global sea-level between 2002 and 2006 estimated at 0.5±0.1mm a^{-1} (Velicogna and Wahr, 2006). Clearly this is of concern, as is the notion that the mechanisms behind this current and future ice mass loss are not fully understood. Hence, associated predictions can have inherently large errors associated.

The past two decades has seen rapid increases in the flow speed of a number of tidewater outlet glaciers in Greenland (Rignot and Kanagaratnam, 2006, Howat et al., 2007), accompanied by surface thinning (Abdalati et al., 2001, Krabill et al., 2004, Thomas et al., 2009). These changes are now acknowledged to be too rapid to be solely explained by increases in summer melting of the ice surface (Abdalati et al., 2001, Thomas et al., 2009). Investigation has demonstrated widespread acceleration in glaciers, concentrated in particular south of ~69-70^{o}N (Krabill et al., 2004, Chen et al., 2006, Rignot and Kanagaratnam, 2006, Velicogna and Wahr, 2006, Moon et al., 2012, Bjorck et al., 2012), with an average ice front retreat of 2.3km between 2001 and 2005 (Seale *et al.*, 2011). North of this, little significant ice front retreat was recorded over the period (Seale *et al.*, 2011).

This acceleration has occurred in both East and West Greenland, but due to their unparalleled ice mass loss over the past two decades, the majority of research has focused upon three of Greenland's outlet. Major changes have occurred at Jakobshavn Isbræ, Helheim Glacier and Kangerdlugssuaq Glacier, with dramatic thinning (15m a^{-1}, 40m a^{-1}, and 25m a^{-1} since 2003 respectively), marked terminus retreat, and doubling of ice flow velocities (Joughin et al., 2004, Bindschadler, 2006, Howat et al., 2005, 2011, 2008b, 2008c, Krabill et al., 1999). More recently it has been shown that the ice loss trend originally documented in southern Greenland can now be found in northwest Greenland, with the majority of marine terminating outlet glaciers displaying marked thinning and retreat between 2005 and 2009 (Khan et al., 2010, McFadden et al., 2011, Bjorck et al., 2012, Kjær et al., 2012). The synchroneity of fluctuations, between Jakobshavn, Helheim and Kangerdlugssuaq, as well as the entire west coast is striking, suggesting that their fluctuations are controlled by a regional forcing factor, and that this factor is intimately linked to dynamic ice stream response (Luckman *et al.*, 2006).

These newly recognised, rapid changes in ice discharge have caused a paradigm shift in our view of the way glaciers respond to climatic change. Originally, the response of marine terminating ice sheets to climatic forcing was thought to be relatively slow (10 – 100 yrs), with the inherent potential for rapid retreat (Meier and Post, 1987). This has been

highlighted by recent work, demonstrating that the marine terminating portions of ice sheets can respond on sub-decadal to seasonal time-scales, often presenting an immediate response to climatic or oceanic forcing (Joughin et al., 2004, Truffer and Fahnestock, 2007, Nick et al., 2009).

Thomas *et al.,* (2009) propose the existence of four types of outlet glacier response type in Greenland today:

1. Glaciers with thinning rates which have been increasing since 1998. The changes in thinning rate are small, and explicable by precipitation driven mass balance changes
2. Similar to the first category but with more rapid thinning and retreat, concentrated about the glacier terminus. Thinning rates are too high to be mass balance driven. Areas thinning are beneath present sea-level, suggesting that thinning is due to ungrounding of ice near the grounding line, which reduces the buttressing effect.
3. Glaciers characterised by rapid thinning (>10m a^{-1}) within several tens of kilometres of the terminus, with increasing rates since 1998-99. The area of thinning is thought to be below sea-level. The outlets of Helheim, Jakobshavn and Kangerdlussuaq all fall into this category. Thinning and retreat in these examples appears driven by a deep bed close to the present grounding line.
4. Glaciers in the recovery stage of a typical surge cycle, showing near coastal thinning, and upstream thickening, too high to be explainable by mass balance changes.

Thomas *et al.,* (2009) also demonstrated that glaciers with shallow gradient beds have far lower thinning rates than those with steep gradient beds. Thus, they suggest that the thinning is primarily a response to bed topography as opposed to surface melt, and propose deep ocean warming as a trigger mechanism. This would first affect outlet glaciers with beds which run into deep fjords, meaning they are more susceptible to warming of deep ocean waters.

Despite the wealth of research undertaken around Greenland, and the clear parallels between recent acceleration, thinning, and retreat of outlet glaciers, and both oceanic and climatic warming, the mechanisms linking these remain poorly understood, and direct links are unclear (Vieli and Nick, 2011). The current changes are typified by marginal thinning and increased discharge via calving (Howat et al., 2007), paralleled by an increase in the length and intensity of the Greenland melt season over the past decade (Hanna *et al.*, 2005). However, it is unlikely that simply enhanced levels of surface melting and therefore changes in mass balance are able to produce thinning of inland areas of the Greenland Ice Sheet

exceeding 1m a^{-1} (Abdalati *et al.*, 2001). Work by Zwally *et al*. (2002), attributed the seasonal acceleration of outlet glaciers to the rapid delivery of increased levels of meltwater to the ice-bed interface, enhancing basal lubrication and glacial sliding. This would lead to a positive feedback in which increases in the ablation area would occur, leading to further surface melt and meltwater delivery (Parizek and Alley, 2004). Though existence of this mechanism has been verified (Shepherd et al., 2009, Das et al., 2008), its impact appears to be confined to land-terminating outlet glaciers, which are normally slow moving (Joughin, 2008), and appear to have minimal impact upon larger outlet glaciers, such as Jakobshavn Isbræ (Joughin et al., 2008c). Studies have shown that the effect of seasonal melting on overall ice velocity is minimal. Van de Wal *et al*. (2008) found that seasonal meltwater only accounted for 10-20% of flow acceleration, and Andersen *et al*. (2011) demonstrated that an increase in melt of 45% caused a velocity change of 2-4%. Similarly, a number of studies have rejected increases in basal lubrication as the cause of increased flow velocities based upon their modelled outputs from outlet glaciers (e.g. Nick *et al.*, 2009).

Instead authors have proposed that dynamic factors affecting outlet glaciers are responsible for the observed changes. However, no dynamic forcing factor with a clear causative link to ice acceleration has been found. Due to this, large scale numerical ice-sheet models remain unable to simulate observed changes accurately (Vieli and Nick, 2011). The vast majority of outlet glaciers in Greenland are tidewater, and therefore terminate in fjords. This means they are extremely sensitive to changes in oceanic properties, even over short times scales (annual to decadal) (Bamber et al., 2007). A number of studies have now shown that marine terminating glaciers are experiencing far more extensive thinning and retreat than their terrestrial counterparts (Moon and Joughin, 2008, Sole et al., 2008, Holland, 2010). Land terminating glaciers have been shown to thin primarily in accordance with rates of surface melt, whereas ocean terminating outlet glaciers appear to thin as a result of changes to their ocean-based termini (Seale *et al.*, 2011). The importance of ocean water upon glacier thinning rates has been strengthened by recent work, which shows a reproducible pattern of thinning commencing at the terminus and moving up-ice, suggesting a trigger mechanism which acts upon the terminus first (Thomas, 2004, Howat et al., 2008, Nick et al., 2009). However, there is a lack of ocean data from glacier calving fronts, meaning that the exact processes by which ocean changes are linked to dynamic changes are still unclear (Holland, 2010, Straneo et al., 2010, Christoffersen et al., 2011). The dynamic changes seen appear to be caused by perturbations to the outlet glacier ice front, in deeply incised fjords, coincidental with the warming waters seen around Greenland. Mapping of the movement

of warm water in both West (Holland et al., 2008b) and East (Seale *et al.*, 2011) Greenland has provided a clear mechanism by which synchronous retreat and acceleration could occur. However – studies have found outlet glacier retreat to be ubiquitous, but asynchronous, and unexplainable by variations in ocean temperature (McFadden et al., 2011). The principal method by which these increased ocean temperatures can cause perturbations at the glacier front is by basal melt. This thins the floating portion of the glacier tongue, or can cause undercutting of grounded calving fronts (Bindschadler, 2006, Benn et al., 2007, Rignot et al., 2010, Straneo et al., 2010). This leads to increased fracturing and calving rates. Alternatively, increased meltwater could enter the fjord as plumes beneath the glacier tongue, mixing warm fjord water towards the glacier (Holland, 2010, Rignot et al., 2010). However, Rignot *et al.,* (2010) showed that large variations in water properties occur between fjords only 30km apart, meaning that any extrapolation based upon oceanic conditions from one fjord is problematic

Changes witnessed as a result of oceanic warming can often be explained by stress perturbations (McFadden et al., 2011). Driving stresses from tidewater glaciers are generally opposed by resistance from basal and lateral shear stresses, as well as longitudinal stresses (Nick *et al.*, 2009). The majority of flow resistance to marine terminating glaciers (as opposed to basal drag on land-terminating glaciers) is provided by shear stresses imposed by fjord walls (McFadden et al., 2011). Thus, a reduction in any of these, via thinning or dramatic calving at the ice front, leads to a reduction in the resistive stresses, and consequent flow acceleration (Thomas, 2004, Luckman et al., 2006, Howat et al., 2007, Nick et al., 2009). The same reduction in stresses can result from the removal of the buttressing effect of ice tongues via increased calving (Joughin et al., 2004). This can then cause further acceleration, due to penetration of water to the grounding zone, reducing basal drag (McFadden et al., 2011). A decrease in sea ice or removal of an ice shelf can also reduce flow resistance in a similar way, reducing the buttressing effect (Luckman *et al.*, 2006). This process has been demonstrated in modelling results from Jakobshavn Isbræ, where enhanced ocean melt has been shown to trigger those changes observed, via increases in calving and consequent terminus retreat and loss of buttressing (Vieli and Nick, 2011, Joughin et al., 2012). However, observations have shown Jakobshavn Isbræ to continue its high flow speeds, whilst retaining a stable terminus. This is in contrast to modelled results, which show a reduction in flow velocity once a stable margin was established (Vieli and Nick, 2011). These studies confirm the suspected sensitivity of tidewater outlet glaciers to marine perturbations, and their ability to adjust rapidly (Nick et

al., 2009, Vieli and Nick, 2011). Despite this knowledge, current published studies have a number of short falls, due to resolution, and the seemingly unique nature of each outlet glacier. Current ice-sheet models are 5-10km in resolution, which is adequate for reconstructions of wide-scale changes, but is not high enough to resolve the narrow, deep outlet glaciers (Vieli and Nick, 2011). Models designed for specific outlet glaciers have had more success in investigating and understanding these dynamic changes (Thomas, 2004, Nick et al., 2009, Vieli and Nick, 2011). However, as every outlet glacier is inherently unique, results concerning the forcing factors important to one glacier cannot be extrapolated to others. Similarly, Seale *et* al. (2011) studies of modern day processes either provide good spatial coverage but limited temporal coverage (Sole et al., 2008, Moon and Joughin, 2008), or good temporal coverage, but poor spatial coverage (Joughin et al., 2004, 2008a, Thomas, 2004, Luckman et al., 2006). Therefore, forcing factors are specific to individual tidewater outlet glaciers, meaning that extrapolation across regions of Greenland, or even between neighbouring outlet glaciers is inherently problematic, and uncertainty over the mechanisms behind dynamic ice loss in Greenland remain.

Understanding the mechanisms and processes which control GIS behaviour is of vital importance for our ability to understand the likely magnitude and speed of future changes it is likely to experience. However, as demonstrated above, our understanding of present day glaciological processes remains complicated. Observations aiming to explain these processes and changes are restricted to short time scales (~ two decades). As a result, these observations are unable to resolve long-term trends in outlet glacier dynamics required for future sea-level predictions (e.g. IPCC). This hinders our ability to produce rigorous predictions for the future behaviour of outlet glaciers throughout Greenland. Thus, in order to improve these predictions we must look to the ancient record. This record provides a longer-term perspective for the dynamic changes witnessed, and can provide information about the magnitude and speed of changes to the GIS in the past. This can then be used to help better understand, and predict, the changes occurring at the present day.

2.1.2. Late-Quaternary glacial history of the West Greenland Ice Sheet

A large amount of research has been undertaken into the glacial history of the GIS, both onshore and offshore. However, as the focus of this study is on central West Greenland, this review of the GIS' glacial history is focused solely upon West Greenland.

2.1.2.1. Saalian glaciation

Funder *et al*. (2011) review the evidence for Saalian glaciation (MIS 6) in West Greenland. It is likely that the majority of onshore evidence recording this glaciation in West Greenland has been removed by erosion during subsequent cold stages (Weichselian; MIS 5d – 1) glaciation. However, as MIS 6 glaciation is thought to have been the most extensive glaciation of the

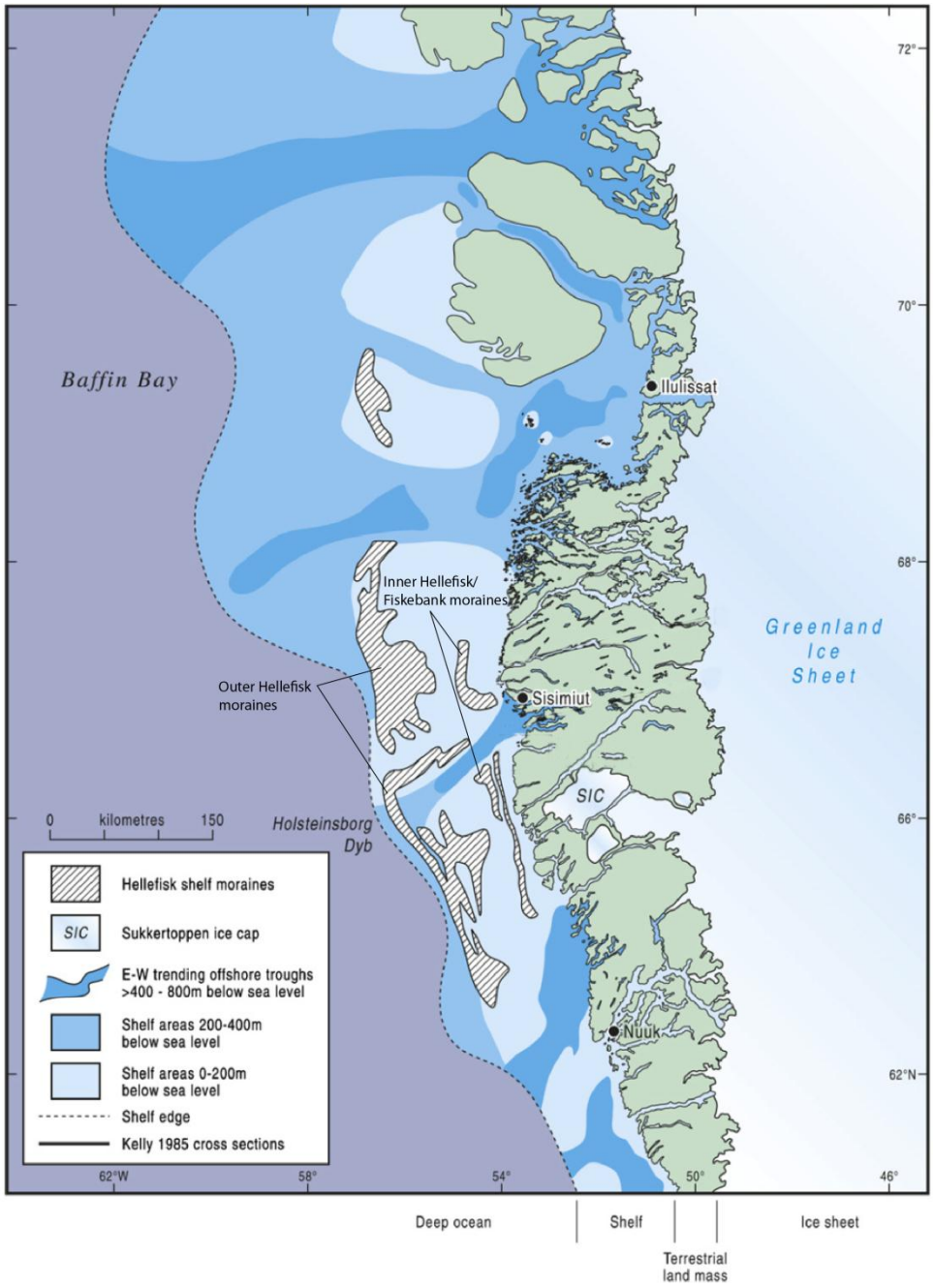

Figure 2.2. Map of central West Greenland, showing generalised offshore bathymetry and large offshore moraines (from Roberts et al., 2010).

past 300 kyr (Funder *et al.*, 2011), it is likely that a large amount of the evidence for it is offshore. Glacial sediments from north-west Greenland have provided evidence for two glaciations predating MIS5e; the Agpat and Narssarsuk glaciations, both of which were more extensive than Weichselian ice advances (Kelly *et al.*, 1999). In addition, recent terrestrial cosmogenic nuclide (TCN) exposure dates from south west Greenland have suggested that mountain summits remained ice free during the LGM, and were last overridden by erosive ice during the Saalian (Rinterknecht et al., 2009, Roberts et al., 2009). However, no evidence of Saalian glacial activity has been recorded from central West Greenland, including in the large cross-shelf troughs of Jakobshavn and Uummannaq.

There are two major moraine systems offshore of the west coast of Greenland: the outer Hellefisk moraines (~100 km offshore, running from 61° - 69° N); and the inner Hellefisk moraines (also named the Fiskebanke moraines) (~40 km offshore) (Figure 2.2) (Brett and Zarudzki, 1979, Zarudzki, 1979). There is some evidence to suggest that the Hellefisk moraines date to Saalian glaciation (Brett and Zarudzki, 1979, Zarudzki, 1979, Kelly, 1985). This age was initially proposed by Kelly (1985), as a result of an ice surface projection produced through the extrapolation of trimlines and deeply weathered till and erratics throughout the coastal mountains of West Greenland. As a result the outer Hellefisk/Fiskebanke moraines, located inside the Hellefisk moraines, were assigned an LGM (Sisimiut glaciation) age. However, the correlation of the Hellefisk moraines to a Saalian glaciation is currently circumstantial, and lacks any robust direct dating control.

2.1.2.2. Last Glacial Maximum ice sheet extent

The local Last Glacial Maximum (LGM) in West Greenland occurred at ~22 kyr BP (the Sisimiut Stade) (Bennike and Bjorck, 2002, Weidick and Bennike, 2007), and is thought to have been characterised by contemporaneous ice expansion onto the continental shelf (Figure 2.3). Ice expansion throughout central and Northwest Greenland is thought to have been relatively restricted, with major ice sheet expansion only occurring in the south.

The expansion across West Greenland is known to have reached at least the Inner Hellefisk moraines (Figure 2.2), and is thought to have reached the shelf edge in places (Funder, 1989b, Bennike and Bjorck, 2002). Recent work from offshore western Greenland has now provided robust evidence that the outer Hellefisk moraines are LGM in age, and the inner

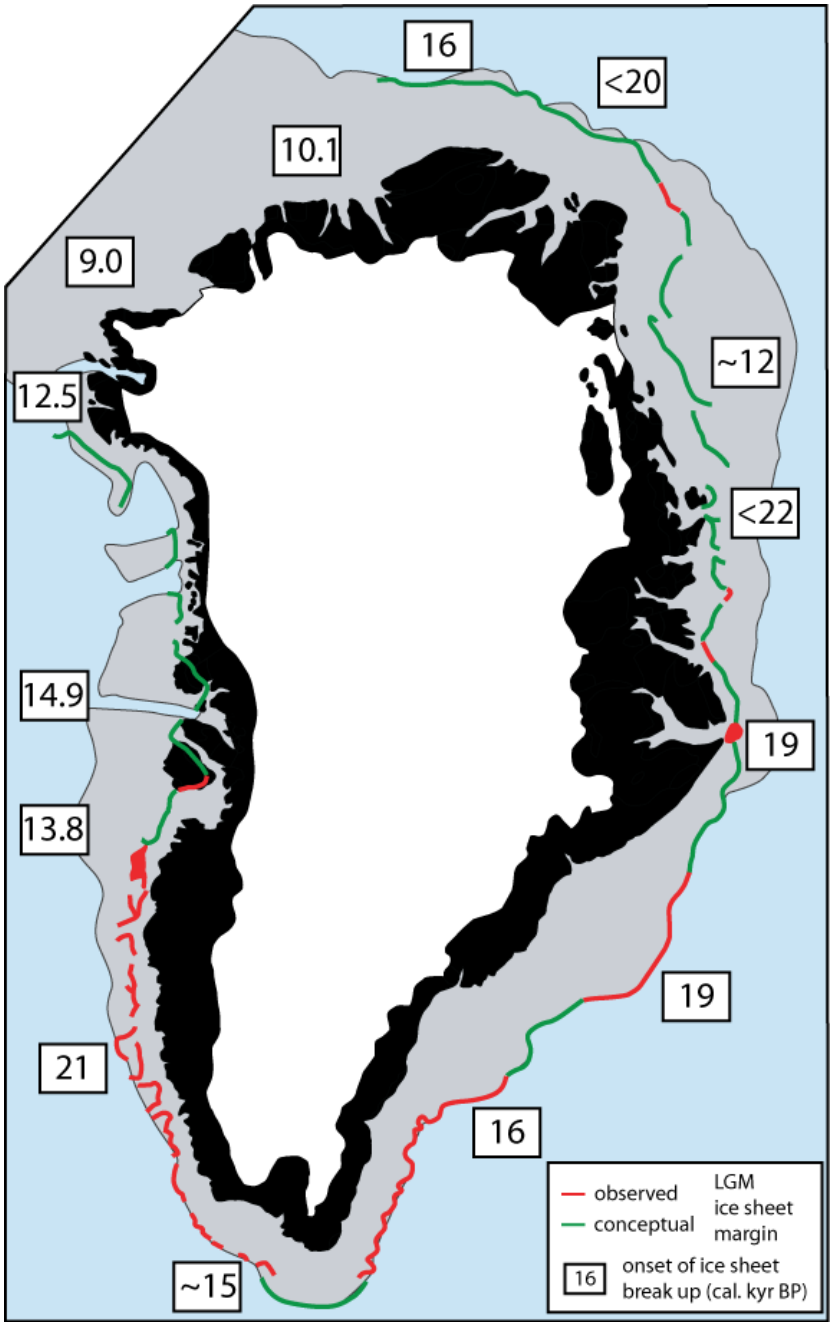

Figure 2.3. Reconstructed LGM ice sheet margin from observational and conceptual data. Dates showing onset of ice sheet break-up on the shelf are marked with data collated by Funder et al. (2011). Additional data has been included from England (England, 1999) and (Ó Cofaigh et al., 2013b).

Fiskebanke date to Greenland Stadial 1 (correlative to the Younger Dryas) (Funder et al., 2011, Ó Cofaigh et al., 2013b). The precise limit of LGM ice sheet extent throughout West Greenland is not known, as it lies offshore, and the number of offshore-studies is limited (Weidick and Bennike, 2007, Ó Cofaigh et al., 2013b). As a result of this, evidence for ice extent was provided by trimline mapping.

Trimlines are the boundaries between zones of differentially weathered material (Dyke, 1977); distinct altitudinal boundaries at the lower boundary of frost-weathered bedrock (Sollid and Sørbel, 1979, Nesje and Sejrup, 1988, Kleman and Borgström, 1994, Ballantyne, 1997). Research into the phenomenon of weathering zones began in Arctic Canada, and has since been used in numerous palaeo-glaciated regions to hypothesis limits of glacial erosion.

Glacial trimlines are usually thought to represent either: (1) the upper limit of erosion by the last ice sheet, with areas above the trimline represent land exposed to periglacial conditions for at least a single glacial cycle; (2) an englacial thermal boundary, representing the point at which the subglacial thermal regime of the ice sheet switched from a higher altitude region of cold-based ice, to a lower region of warm based ice (Stone et al., 1998). However, differentiating between these scenarios can be extremely difficult due to the similar geomorphological imprints left by all three processes. This equifinality has led to intense debate regarding the genesis of these geomorphological indicators, with some supporting trimlines as robust indicators of ice sheet surface (Ballantyne, 1997, Sollid and Sørbel, 1979, Nesje and Sejrup, 1988, Nesje and Dahl, 1990), and other suggesting they reflect englacial thermal boundaries (Sugden, 1978). Recent advances in surface exposure dating have changed the way in which trimlines are interpreted, and led to differentiation between the two hypotheses. However, these only remain useful on a case by case basis due to the likely equifinality of both hypotheses.

Extensive trimlines throughout West Greenland were mapped up to 1100 m a.s.l. by Kelly (1985), and interpreted as the upper limit of glaciation. Kelly (1985) inferred ice thickness in south west Greenland from this trimline evidence, and identified some possible areas of extremely low ice thicknesses (Upernavik and Svartenhuk). Extrapolation of these trimlines offshore allowed an estimate of former ice sheet extent on the shelf, with ice extending at least 30 - 35 km onto the inner shelf throughout West Greenland and forming the inner Fiskebanke moraines (Kelly, 1985, Funder, 1989b).

However, since the advent of cosmogenic nuclide exposure dating, trimline evidence has been questioned. Though still an important geomorphological indicator of palaeo-ice thicknesses, more strength can be put in interpretations made using geomorphological and exposure dating methods, as differentiation between ice surface trimlines, and englacial thermal boundaries can be made (Fabel et al., 2012). Kelly's (1985) hypothesised ice sheet

thicknesses of <1100 m a.s.l. throughout southern West Greenland are supported by exposure ages in the Sisimiut region, which have confirmed that previously identified trimlines do mark the upper limit of erosive LGM ice (Rinterknecht et al., 2009, Roberts et al., 2009). However, the lateral extent of LGM ice in southern West Greenland remains debated, between the inner-shelf Fiskebanke moraines (Kelly, 1985, Funder et al., 2011), and the outer-shelf (Weidick et al., 2004, Roberts et al., 2009). In contrast, research further south suggests that ice up to 1500m thick covered the coastal mountains during the LGM and reached the continental shelf edge (Bennike et al., 2002, Weidick et al., 2004). In Disko Bugt evidence for the offshore limit of Sisimiut Stade ice is, again circumstantial, and remains undated, though workers have again related LGM ice extent to the inner Fiskebanke moraines (Kelly, 1985, Weidick and Bennike, 2007). This would have left coastal mountain summits ice free, as evidenced by weathering limits (Kelly, 1985).

Current ice sheet wide models lack the spatial resolution to accurately resolve individual fjords, ice streams, and their ice thicknesses. However, they remain a useful tool for understanding ice sheet wide processes. Estimates from model reconstructions have placed ice thickness in the Kangerdlussuaq area at 1100-1300m (Tarasov and Peltier, 2002). Simpson et al. (2009) used relative sea-level (RSL) and ice extent field data to constrain a three-dimensional model of the GIS. This model placed the LGM limit at a mid-outer shelf position on the western coast of Greenland, possibly coincident with the Outer Hellefisk moraines (Simpson *et al.*, 2009). Funder and Hansen's (1996) work shows the LGM ice limit as located offshore in most of Greenland, but it is evident that the central- and north-western limits of the ice margin are very poorly constrained. Thus, present knowledge of LGM ice sheet extent and thickness in West Greenland is fragmentary, and relies strongly upon trimline interpretations with little robust chronological control.

2.1.2.3. Last Glacial Maximum deglaciation: timing and behaviour

The response of the extent and thickness of the GIS to post-LGM climatic changes is currently poorly constrained by existing ^{14}C and TCN ages (Clark *et al.*, 2009), and appears to be spatially highly variable. Onset of deglaciation, as recorded in ocean cores, appears highly variable, even in neighbouring ice streams (Figure 2.3). As a result, determining the timing of initial GIS retreat can be problematic. Following the LGM, air temperature rose rapidly until it reached a maximum during Greenland Interstadial 1e (Bølling Interstadial –

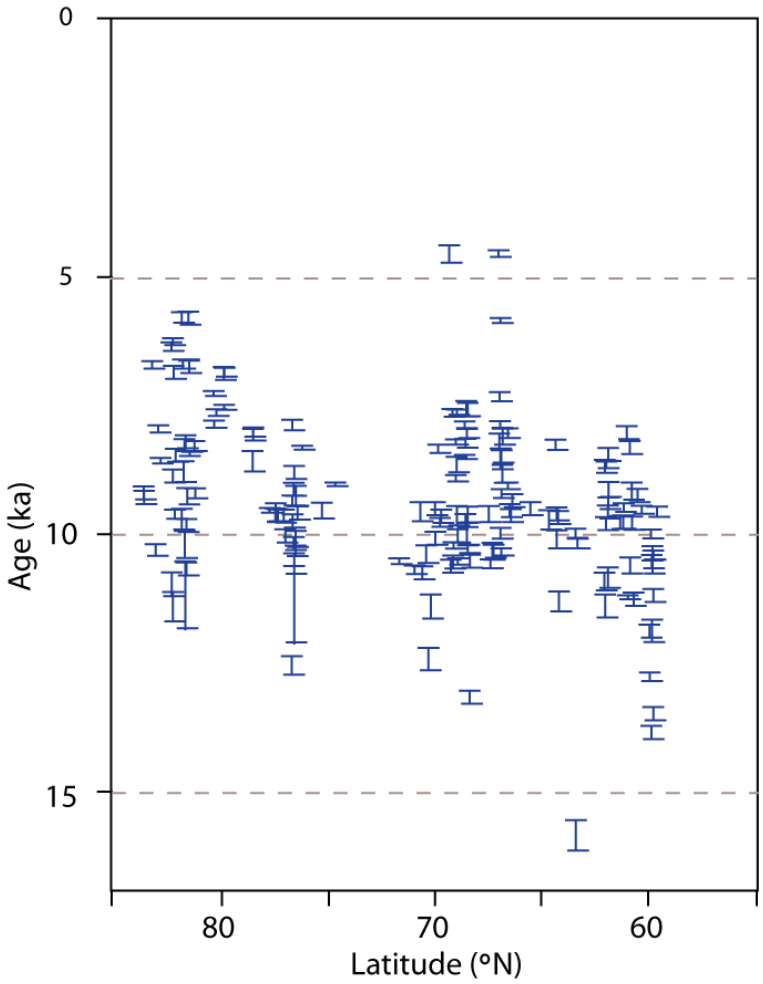

Figure 2.4. Compilation of calibrated ^{14}C dates from the Western margin of the Greenland Ice Sheet, with 1σ error bars. These dates represent minimum ages of ice free conditions (from Clark *et al.*, 2009).

see Figure 2.6). This atmospheric warming would have driven increased rates of surface ablation, causing down-wasting of the ice sheet, and marginal retreat (Roberts et al., 2009).

In West Greenland, it is likely that rising relative sea-level had an important impact upon the deglacial history of the ice sheet. In central western Greenland sea-level is predicted to have risen from 16 cal. kyr BP, reaching its maximum at ~11 cal. kyr BP (Simpson *et al.*, 2009) (see Section 1.2.5). This high sea-level stand at the marine limit (~100 m a.s.l.) would have first destabilised thin ice, grounded in shallow areas, before increasing water depths would have resulted in the destabilisation of thicker ice. Finally, ocean temperature increases would also have an effect upon the retreat of shelf based ice and ice streams. Work has suggested that the West Greenland Current (WGC), a warm subsurface ocean current, first arrived in Baffin Bay at 10.9 kyr (Knudsen *et al.*, 2008), reaching the coast close

to Thule in Northwest Greenland by 10.2 kyr (Funder, 1990b), but only reached the mid-shelf of the Disko trough at ~9.2cal. kyr BP (Lloyd et al., 2005, McCarthy, 2011). The increasing ocean temperatures would have helped to accelerate ice retreat, via enhanced

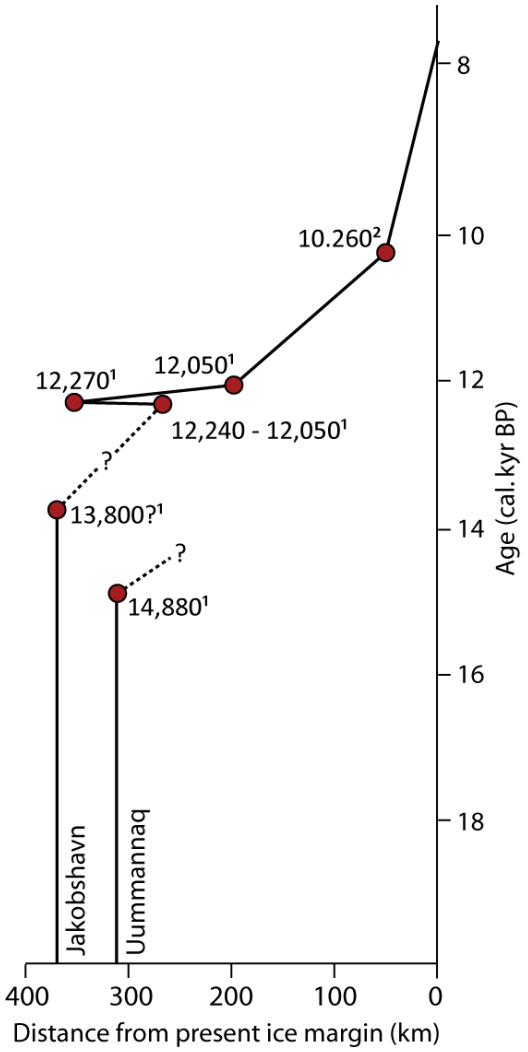

Figure 2.5. Time-distance diagram of present knowledge of ice stream extent in West Greenland from the LGM to early Holocene. Red dots represent radiocarbon ages constraining deglaciation from: [1](Ó Cofaigh et al., 2013b), and [2](Lloyd *et al.*, 2005).

marginal and basal thinning (Holland et al., 2008a). There are a number of reconstructions of the timing of initial retreat of the GIS from the shelf in West Greenland. Some suggest retreat began following warming during the Bølling Allerød warm period (14.7 – 12.6 kyr (Lambeck and Chappell, 2001)); others between 15 and 10 cal. kyr BP (Funder and Hansen, 1996), whereas others suggest the onset of retreat began between 13 and 11.5 cal. kyr BP (Weidick, 1996).

Exposure ages from the Sisimiut region of West Greenland suggest deglacial thinning began between 21 ± 1.9 ^{10}Be kyr and 13.6 ± 1.42 ^{10}Be kyr (Roberts et al., 2009), and 12.3 ± 1.5 ^{10}Be kyr and 8.3 ± 1.2 ^{10}Be kyr further north (Rinterknecht *et al.*, 2009). Offshore work from the central West Greenland shelf has shown that retreat began in the Uummannaq trough by 14.8 cal. kyr BP, and by 13.8 cal. kyr BP in the Disko trough (Ó Cofaigh et al., 2013b). This shows the inherent asynchroneity of GIS outlet glacier response throughout a small region of West Greenland. It should, however, be noted that dates on the onset of deglaciation are presently limited in their number, and thus the difference could be a result of chronological limitations.

Funder and Hansen (1996) proposed a model for the deglaciation of the GrIS following the LGM, featuring two discrete stages. Initially, eustatic sea-level rise caused increased calving, forcing a rapid retreat of the GrIS from the continental shelf by 16 kyr BP. This period of retreat lasted until 10ka, when fjord glaciers began retreat, following a short lived glacier readvance (10.3 - 9.5ka; Taserqat Stade (Funder, 1989b)). Following this, a second, slower land-based retreat took place from ~10.0 kyr BP, characterised by ice sheet surface thinning, driven by increases in air temperature, and continued calving from within fjord confines (Funder and Hansen, 1996). The initial timing of onset appears compatible with the majority of offshore dates around the Greenlandic continental shelf (Figure 2.3), suggesting retreat by 16 ka. Terrestrial radiocarbon ages from the western margin of the GIS are in broad agreement with the second stage of the Funder and Hansen (1996) model, with ages demonstrating land-based retreat between ~14 and 6 cal ka BP. However, study of the ages demonstrates a spread of results, and hints towards a possible drop in the age of deglaciation with increasing latitude (Figure 2.4). However, recent work has challenged this simplistic two stage model of retreat. Simpson *et al.* (2009) have suggested that retreat induced by high sea-level would have only occurred during a relative sea-level peak between 12 and 11ka, not as early as suggested by Funder and Hansen (1996). This stability of thick, topographically confined ice streams into the Holocene is in direct contrast to conventional thinking, in which trough based portions of ice sheets retreat rapidly in response to rising water depths.

Throughout the Disko Bugt region, central West Greenland, a wealth of deglacial landforms and dateable material has allowed the creation of a detailed, if complex, chronology of retreat. This is based upon sediment cores from lakes (Long et al., 1999, Long and Roberts, 2003), marine settings (Lloyd et al., 2005, Ó Cofaigh et al., 2013b, 2013a), and raised marine

deposits (Bennike *et al.*, 1994). Section 1.2.5. provides an overview of the marine limit trends from Disko Bugt and Uummannaq.

Despite the amount of research into the region, the deglacial history remains debated, with reconstructions ranging from rapid to slow stepped retreat. Initial retreat from the continental shelf occurred before 12.3 cal. kyr BP (McCarthy, 2011). This was followed by deglaciation of the western edge of Disko Bugt, which occurred at 11 – 10.2 cal. kyr BP,

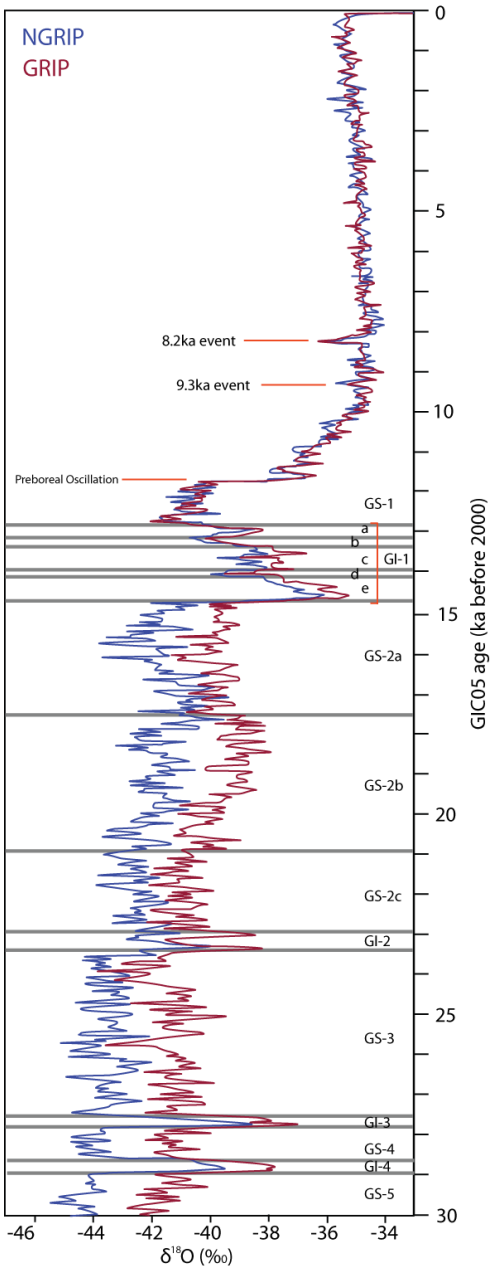

Figure 2.6. The NGRIP and GRIP ice-core records from the last 30 kyr, with data at 50 yr resolution. The GIC05 chronology was developed using a $\delta^{18}O$, continuous flow analysis, electrical conductivity measurement and stratigraphical data (data from Rasmussen et al., 2006, Lowe et al., 2008).

dated using the marine limit (Long and Roberts, 2003). Similar ages are found throughout Disko Bugt, suggesting that deglaciation through the bay was rapid. In the case of the Uummannaq ice stream system, offshore dates from Ó Cofaigh (2013b) demonstrate deglaciation was underway by 14.9 cal. kyr BP. Work from within the fjord system shows retreat into a mid-fjord position buy 10.7 cal. kyr BP in the south of (Simonarson, 1981), and 10.5 cal. kyr BP in the north of the Uummannaq region (Bennike, 2000).

The recent development of terrestrial cosmogenic nuclide dating with improved precision has allowed thinning rates to be constrained. Using vertical transects of cosmogenic nuclide dates, workers have been able to measure post-LGM thinning rates of ice streams in western Greenland. Roberts *et al.* (2009) calculate lowering of 6-12cm a^{-1} between 21±1.9 ^{10}Be kyr BP and 13.6±1.42 ^{10}Be kyr BP, relating to increased temperatures during the Bølling Interstadial. Nearby, Rinterknecht *et al.* (2009) calculate a similar, but slightly lower rate of 4-8cm a^{-1} between 12.3±1.5 ^{10}Be kyr BP and 8.3±1.2 ^{10}Be kyr BP. These rates compare with modern thinning rates of 10-40cm a^{-1} for this sector of the GIS (Krabill *et al.*, 2004). Further North, in the Upernavik region, work has shown deglaciation of ice streams to the present coastline by 12.5 - 11.1 ^{10}Be kyr BP, based upon measurements from erratic-bedrock pairs (Corbett *et al.*, 2009).

2.1.2.4. Ice stream history

Through improvements in cosmogenic dating onshore and the application of marine geophysical techniques offshore, progress has been made in understanding the long-term retreat history of ice stream systems in Greenland. The coupling of offshore and onshore data, in combination with cosmogenic dating (which allows deglacial ages to be determined from rock samples), has allowed for development in our understanding of ice stream processes. Though limited in number, some recent work has used these techniques with high-quality results (Roberts and Long, 2005, Roberts et al., 2008, 2013, Rinterknecht et al., 2009, Evans et al., 2009, Ó Cofaigh et al., 2013a, 2013b). Thus, there remain large areas of Greenland suitable for application of these techniques, which have not been studied. The land in West Greenland is characterised by heavily abraded bedrock, with a sparse cover of Quaternary sediments, due to intense glacial erosion and sediment evacuation (Funder, 1989b). Traditional soft-bedded landforms, used to infer fast ice flow, ice direction, and ice stream presence (Stokes and Clark, 1999) are sparse (Roberts et al., 2010). Though a growing field of research has studies the properties of bedrock bedforms in areas of ice

streaming (Evans, 1996a, Roberts and Long, 2005, Roberts et al., 2010, Krabbendam and Glasser, 2011, Krabbendam and Bradwell, 2011, Hooyer et al., 2012, Iverson, 2012, Eyles, 2012), their use as an indicator of palaeo-ice flow conditions remains underdeveloped (see Chapter Five).

The continental shelf offshore of West Greenland is cut by a minimum of six cross-shelf troughs (Brett and Zarudzki, 1979, Funder and Hansen, 1996, Roberts et al., 2010). These are likely to have acted to focus and route outlet glaciers of the GIS toward the shelf edge during previous periods of glaciations. The size of these troughs means they would have evacuated a large portion of the West GIS, and would have been of vital importance to the mass balance of the ice sheet.

Thus far, the majority of work on LGM ice stream extent in West Greenland has so far focused on two main areas. Firstly, in the Disko Bugt region, the extent, thickness and behaviour of Jakobshavn Isbræ has been studied, with authors reporting an LGM advance of the ice stream onto the continental shelf (Roberts and Long, 2005, Weidick and Bennike, 2007), confirmed by recent marine geophysical investigations (Ó Cofaigh et al., 2013b). Work onshore has dated a series of inset moraines, now shown to represent an ice marginal response of Jakobshavn Isbræ to both the 9.3 and 8.2 kyr events (Long and Roberts, 2002, Long et al., 2006, Briner et al., 2010, Young et al., 2011a, 2011b, 2013). This has demonstrated the high sensitivity of large ice streams to short-lived climatic oscillations. The second area studied is in the Sisimiut region, the largest ice-free area of land in western Greenland. Here, workers found an advance of topographically routed, outlet glaciers which converged into a large ice stream system, and flowed onto the continental shelf. In this region, LGM ice thickness estimates vary from 500 to >1000 m a.s.l. (Roberts et al., 2009, Rinterknecht et al., 2009). These thickness estimates are in accordance with modelled ice sheet profiles, which reconstruct LGM ice thickness to ~900m a.s.l. in these regions (Simpson *et al.*, 2009). The onset of deglaciation through this ice stream system is relatively late compared to ice sheet deglaciation in other areas of Greenland (Roberts et al., 2010). This timing, and variability within other systems along the West Greenland coast (Weidick and Bennike, 2007, Ó Cofaigh et al., 2013a, Roberts et al., 2013) has led to the suggestion that ice stream systems, though vulnerable to rapid deglaciation due to their size, may have had a delayed retreat response to post-LGM warming, meaning that ice stream characteristics promoted stability on the inner continental shelf into the Holocene (Roberts et al., 2010).

2.2. Ice streams and their importance in Greenland

Ice streams are known to exert a considerable influence upon ice sheet dynamics and configuration during their advance and retreat stages, forming fast flowing arteries of ice which rapidly evacuate inland ice to the ice sheet margin (Stokes and Clark, 2001, Bennett, 2003). This is true of the Greenland Ice Sheet both now, and in the past. Ice streams are portions of ice sheets which flow more rapidly than surrounding ice, often by several orders of magnitude (Swithinbank, 1954). They are grounded, and bounded by either slower moving ice sheet ice, or topography (Bentley, 1987, Stokes and Clark, 2001, Bennett, 2003, Truffer and Echelmeyer, 2003). Ice streams can be divided into two broad categories: topographic (or isbræ), where ice flow is heavily controlled by lateral topographic constraints; and pure, where no significant lateral topographic control is exerted upon the ice, and ice streams are bounded by slower moving ice (Stokes and Clark, 1999). Ice streams are typically characterised by a series of tributary glaciers, emanating from an ice sheet. These coalesce to form an ice stream trunk (Figure 2.7) (Stokes and Clark, 1999). Due to their size and velocity (> one order of magnitude faster than ice sheet ice) they are responsible for the majority of ice and sediment discharge from ice sheets. Their potential to discharge much of this into the ocean has global ramifications for ocean currents, including the thermohaline circulation (Bennett, 2003), and the mass balance of the ice sheet they drain (Bennett, 2003, Ó Cofaigh et al., 2003, Sejrup et al., 2003, Roberts et al., 2010). Their instability and variability in response is known to be controlled by both internal and external processes (Bennett, 2003), meaning that their behaviour is affected by global, regional, and local factors. Therefore, understanding their short- and long-term variability, their relationship to the ice sheets they drain, and their impact upon ice sheet stability in the past is of vital importance for predicting ice stream response to current and future climate change.

At present, ice streams flowing at > 100 m yr^{-1} drain the majority of ice from the GIS interior. Observations of present-day ice streams have documented their spatially variable, complex behaviour. See section 2.1.3. for a full discussion of current ice stream behaviour in Greenland. In certain settings of convergent topography, large ice stream systems can develop, formed of multiple individual ice streams (Ottesen et al., 2008, Roberts et al., 2010, Roberts et al., 2013). Convergent ice flow, often into over-deepened troughs formed over

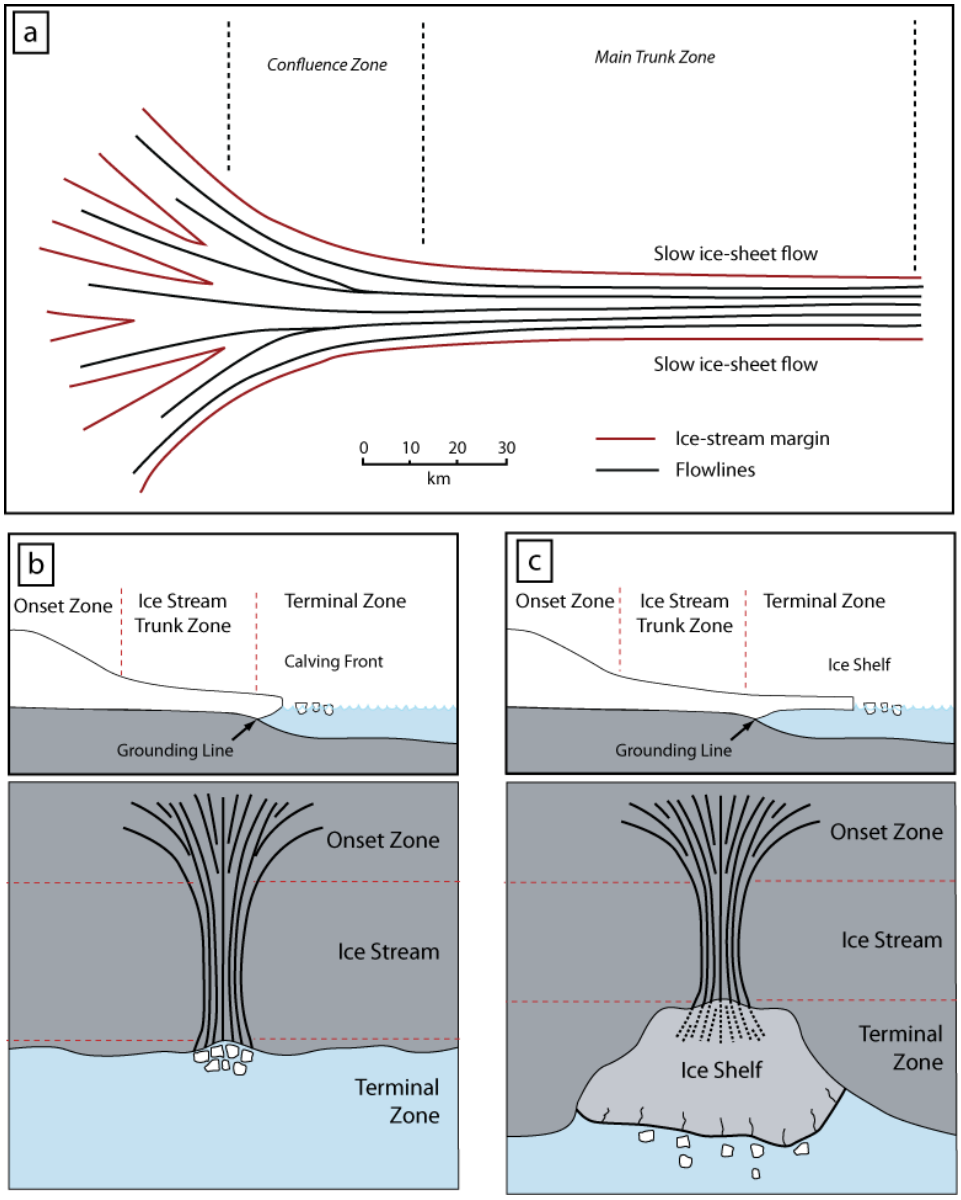

Figure 2.7. (a) Simplified conceptual model of a pure ice stream, with ice converging in the onset zone, feeding the main ice-stream channel (Adapted from Stokes and Clark, 1999); (b & c) Conceptual configurations of marine-based ice streams draining into open water (b), and feeding ice shelves (c) (from Stokes and Clark, 2001).

multiple glacial cycles, allows these ice stream systems to flow at high velocities. Coupled with their large palaeo-drainage basins, these palaeo-ice streams would have been critical to the mass balance of the ice sheet. Therefore, in order to accurately reconstruct any palaeo-ice sheet, it is important to understand the evolution of these large palaeo-ice streams.

2.2.1. Palaeo-ice stream reconstruction

2.2.1.1. Ice streams with soft beds

Alongside investigation into contemporary ice streams through remote and field based observations, much of our present understanding of ice stream processes and activity has been achieved through the study of palaeo-ice stream beds. Specifically, bed accessibility allows the study and

interpretation of glacial landforms (e.g. moraines, drumlins, roches moutonnées, eskers, striations). These can be used to delineate areas of palaeo-ice streaming, and establish the basal conditions of the ice stream at a specific time during its history (Stokes and Clark, 1999, Stokes and Clark, 2001). Initial work by Stokes and Clark (1999) identified and developed a series of geomorphological criteria for identifying the former presence of ice streams in the geological record, including: highly convergent bedform patterns; highly attenuated bedform morphology (length to width ratio of >10:1); sharply delineated shear margins. Following this, Stokes and Clark (2002) then argued that highly attenuated bedforms (including mega-scale glacial lineations), with length to width ratios of >10:1 can be used to infer zones of fast ice flow, and therefore interpret palaeo-ice streams. This has allowed the identification of palaeo-ice streams, and aided in palaeoglaciological reconstructions of ice sheets (Ottesen *et al.*, 2008).

2.2.1.2. Ice streams with rigid beds

West Greenland is known to produce little sediment, the majority of which is rapidly evacuated to the continental shelf (Funder, 1989b). Outlet glaciers throughout West Greenland have been generally constrained to over-deepened fjords and continental shelf troughs, and terrain above sea-level is often high in relief. This leaves relatively few onshore areas in which soft sediment bedforms could develop. As a result, soft-bedded environments do tend to exist offshore, in the base of contemporary fjords and cross-shelf troughs (e.g. Evans et al., 2009, Block and Bell, 2011, Ó Cofaigh et al., 2013b).

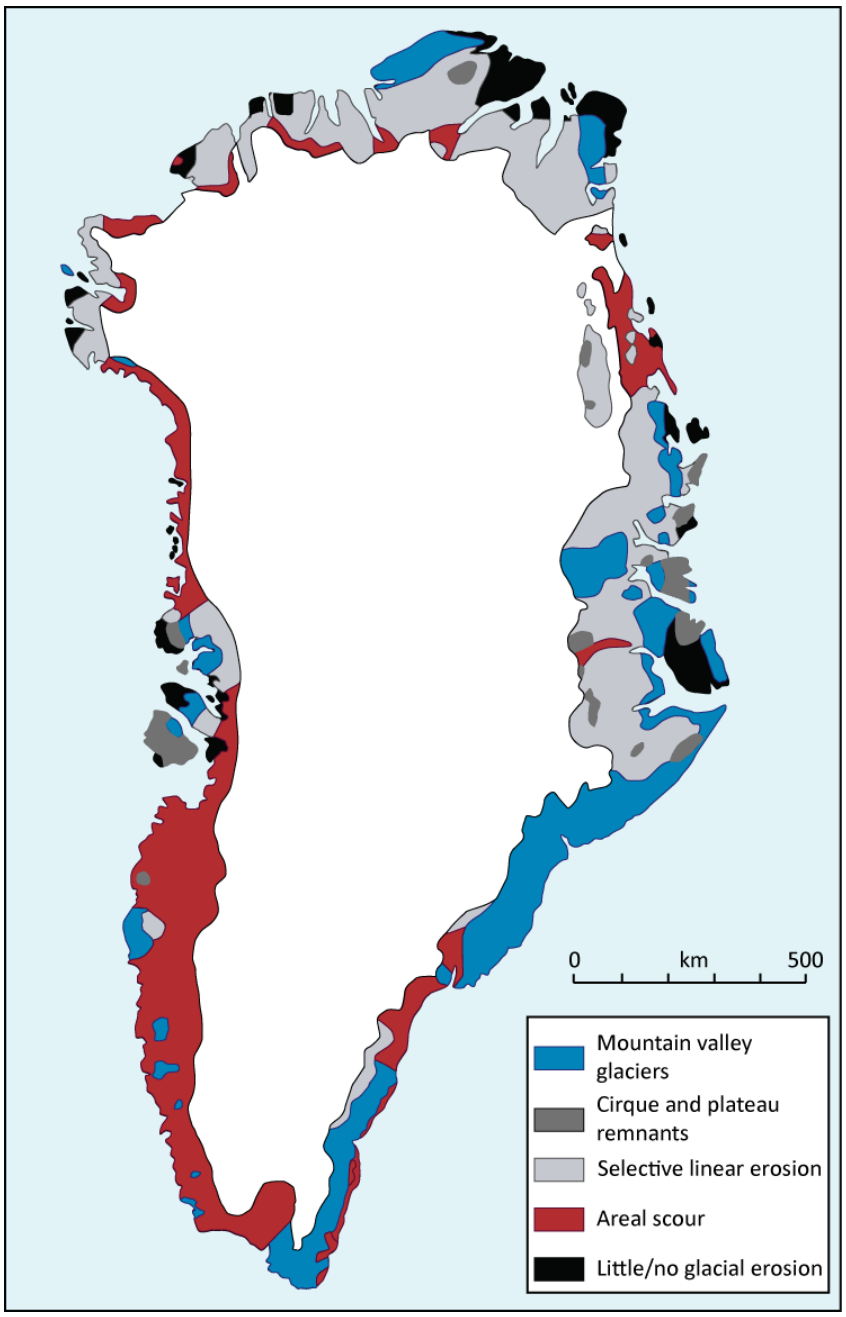

Figure 2.8. (a) Map of the landscapes of glacial erosion on the ice-free rim of Greenland, as mapped by Sugden (1974).

Consequently, the vast majority of glacial landforms reflecting palaeo-ice stream activity across ice-free areas of Greenland are erosional in origin. The majority of recently glaciated, low elevation (<1000 m a.s.l.) terrain in West Greenland displays extensive areal scour (Figure 2.8) (Sugden, 1974). Within these areas, erosional glacial landforms such as roches moutonnées and whalebacks are ubiquitous (e.g. Glasser and Warren, 1990, Roberts and Long, 2005). From study of these bedrock bedforms, reconstructions of basal conditions,

bed-coupling, and relative velocity can be made. More widely, studies of offshore rigid-bed palaeo-ice streams have reported drumlins, crag and tail

features, crudely streamlined forms with blunt stoss sides and tapered lee sides, and p-forms (Lowe and Anderson, 2002, Ó Cofaigh et al., 2002). Throughout both Greenland and northern Europe, onshore investigations have reported: streamlined roches moutonnées and whalebacks (e.g. Gordon, 1981, Sugden et al., 1992b, Roberts and Long, 2005, Roberts et al., 2010, Krabbendam and Glasser, 2011); megadrumlins and large-scale crag-and-tail forms (Jansson et al., 2003, Ottesen et al., 2008), large bedrock ridges and deep mega-grooves (Bradwell et al., 2008).

In comparison to soft-sediment bedforms, bedrock bedforms are often able to record a complex formation history. It is important that these complicating factors are appreciated when reconstructing ice flow histories. The nature of bedrock bedforms makes them more resistant to erosive forces than soft sediments. As a result they can form and endure modification over multiple glacial cycles (Kleman, 1994, Kleman and Borgström, 1996). This complicates the ice flow history which they record. Similarly, bedform development complication can arise from changes in ice thickness, velocity and direction during a single glacial cycle. These changes cause variations in ice-bed coupling and therefore can alter the balance of abrasion and plucking (Roberts and Long, 2005, Roberts et al., 2010, Krabbendam and Glasser, 2011, Hooyer et al., 2012, Iverson, 2012). These factors combine to form complex bedforms, requiring careful interpretation. In addition to external glaciological factors, local geological structure can exert a control upon bedform development. Bedding planes, joint orientation and density, and rock hardness act as key controls upon bedform morphology (Krabbendam and Glasser, 2011, Roberts et al., 2010, Hooyer et al., 2012). Despite these complexities, a number of studies have been able to successfully discriminate between the impacts of geology and those of ice dynamics, and have reconstructed the evolution of bedrock bedforms in areas of ice streaming (Roberts and Long, 2005, Roberts et al., 2009, Bradwell et al., 2008, Krabbendam and Glasser, 2011)

However, in contrast to the study of soft-sediment bedforms, a simple relationship between elongation ratio (ELR) and ice velocity cannot be inferred. Work by Evans (1996a) demonstrated that the differences in bedform type (whalebacks and roches moutonnées) can be used to differentiate between fast and slow ice flow by inferring if ice-bed decoupling and therefore plucking, took place. If so, this is cited as evidence for the

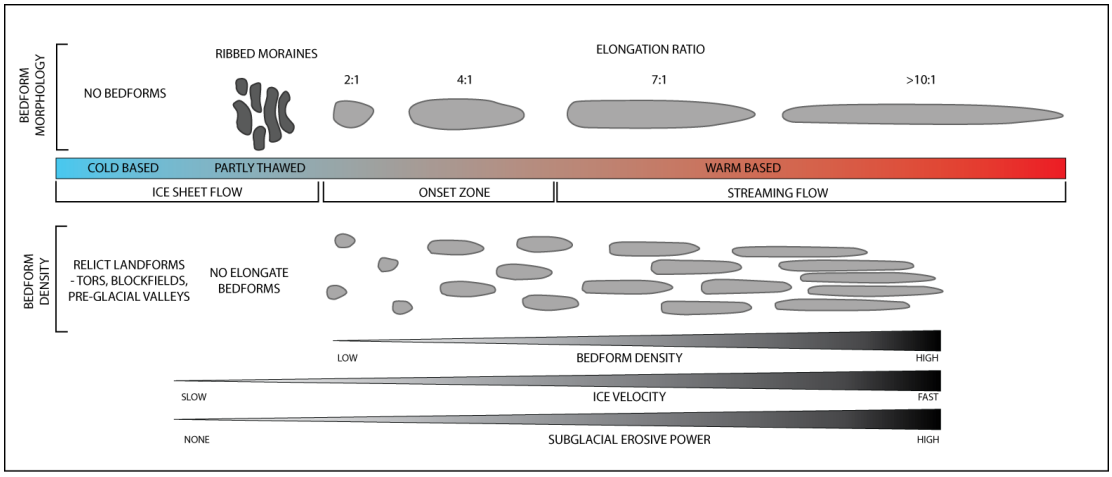

Figure 2.9. Diagram of an idealised bedrock bedform continuum across a hypothetical palaeo-ice stream onset zone. Relationship between bedform morphology, bedform density, and subglacial thermal conditions can be seen (from Bradwell et al., 2008).

presence of slow, thin ice. Bradwell *et al*. (2008) developed an elongation continuum of bedrock bedforms through a palaeo-ice stream onset zone that they related to degrees of erosive power, ice velocity, and subglacial thermal regime (Figure 2.9).

Other workers have used bedrock landform morphology to assist in inferring ice flow velocities and bed conditions, with close association of RMs and undisturbed tors providing evidence for a sharp transition from a cold to warm basal thermal regime (Hall and Glasser, 2003). Analysis of bedforms can allow for the creation of flow sets, based upon the distribution, density, and form of mapped bedrock features (Jansson et al., 2003, Roberts and Long, 2005). For example, Roberts and Long (2005) used spatial differences in WB and RM density and elongation ratio to define the palaeo-margin of Jakobshavn Isbræ, separating fast and slow ice flow, having discounted ice thickness as the controlling factor upon bedform characteristics. In rigid-bedded settings, authors have found that bedform elongation ratios (ELRs) in areas of ice streaming are low (<5:1) (Roberts and Long, 2005). This is in contrast with evidence from former soft-bedded ice streams, where ELRs are often >10:1 (Stokes and Clark, 1999). Some workers have hypothesised that the low ELRs of bedforms found beneath palaeo-ice streams in rigid bed settings are due to fixed basal perturbations, and high bed roughness. These factors prevent the basal ice from forming a stable subsole or path, thus hindering the formation of bedforms with high elongation ratios (Roberts and Long, 2005). Recent work has contested this, finding high ELRs in rigid bed settings (>5 - 25:1), inferring that pathway stability is viable (Bradwell et al., 2008). However, many bedrock bedforms can suffer secondary plucking episodes, either during the deglacial phase, or in consequent glacial episodes (Roberts and Long, 2005).

Other studies have separated the impact of bedrock geology upon bedform development from ice flow dynamics. This has shown that under certain geological settings, changing ice dynamics can have minimal impact upon bedform morphology and type (e.g. Roberts et al., 2010, Krabbendam and Glasser, 2011). A number of other studies undertaken in West Greenland and North-West Scotland have attempted to unravel these complex interactions between bedrock bedforms, ice flow dynamics and bedrock structure. Work by (Gordon, 1981) explored the role which variations in bedding plane orientation, joint orientation, and rock hardness can have upon resultant bedform morphology. Roberts *et al*., (2010) reported bedform data from areas of ice sheet and ice stream flow in West Greenland. Bedforms from areas hypothesised to have experience palaeo-ice sheet flow displayed very high ELRs (>10:1), whereas those from areas of palaeo-ice streaming had lower ELRs of 3.7:1. This is clearly a function of bedrock structure. The elongate bedforms from Sisimiut (Roberts et al., 2010) (which would be suggestive of fast flow in a soft bed setting), are a result of repeated glacial erosion along lines of weakness running sub-parallel to ice flow. The form of the less elongate bedforms is also a result of bedrock structure. Some bedforms display multiple plucked faces, suggesting multiple flow directions affected the region. Roberts *et al*., (2010) related these bedform characteristics to bedrock structure, joint density and joint orientation. In one area ice flow was initially east-west, flowing transverse to bedrock. This created short, wide bedforms. Following this, ice flow became NE-SW, with bedforms and bedrock structure becoming sub-parallel to ice flow. This produced secondary plucked faces, and altered bedform plan form and morphometry (Figure 2.10). In a study from north-west Scotland, Krabbendam and Glasser (2011) analysed bedforms from an area of consistent palaeo-ice flow, but across different bedrock

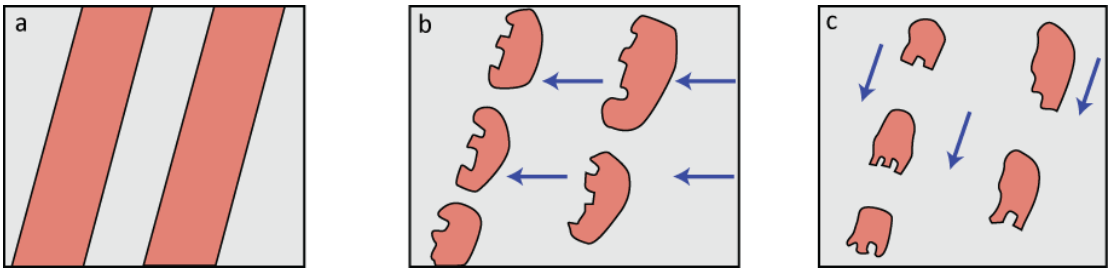

Figure 2.10. Diagram of bedrock bedform development in areas of banded bedrock of contrasting lithology – orange areas represent resistant lithologies: (a) resistant bedrock bands trending NE-SW prior to ice advance; (b) formation of roches moutonnées by plucking on the down ice side of bedforms, along joints running transverse to ice flow; (c) ice flow becomes parallel to the lithological banding, and plucked faces appear down ice of the new ice flow direction (from Roberts et al., 2010).

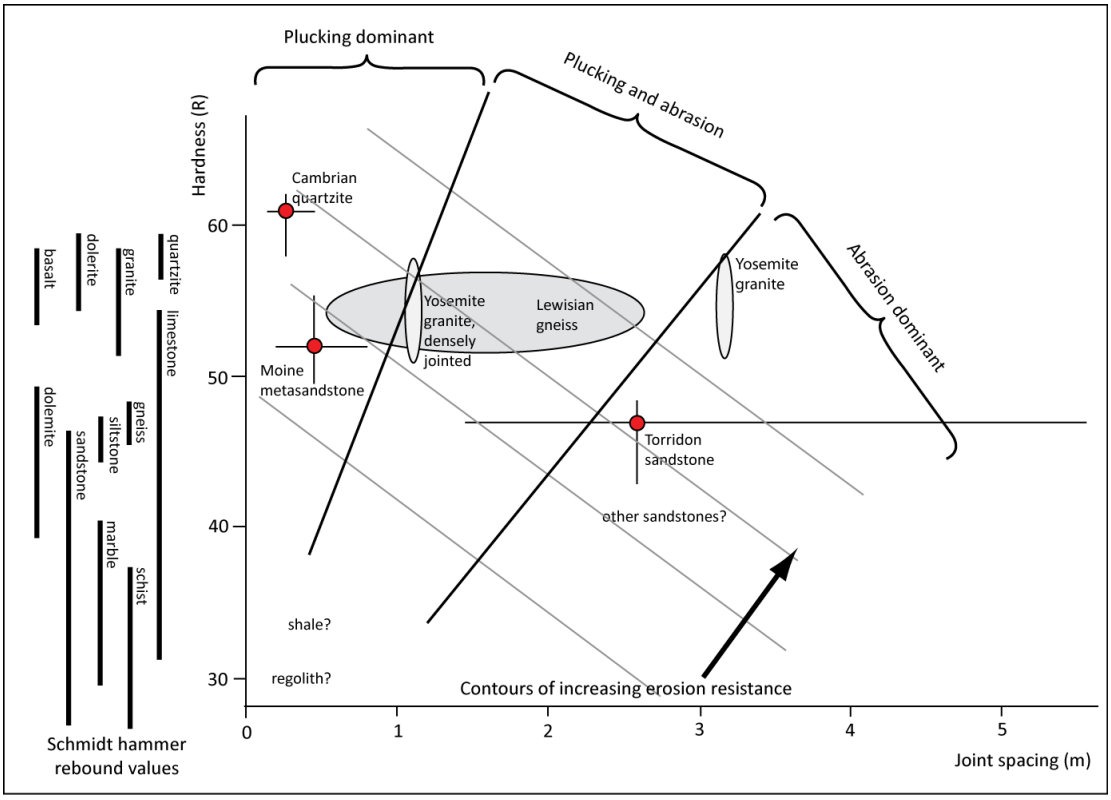

Figure 2.11. Diagram showing the relationship between bedrock hardness and joint spacing, and the resultant dominant erosional processes See Krabbendam and Glasser (2011) for full details and source of data.

lithologies. They suggest that in this instance, changes between the dominance of abrasion and plucking are due to variations in joint spacing and rock hardness, not changes in ice flow dynamics (Figure 2.11).

2.3. Summary

This chapter has provided a summary of the literature relevant to this study. It has outlined the present knowledge of outlet glaciers throughout Greenland, and the processes thought to control their behaviour. In doing this, it is clear that our current understanding is not sufficient to reliably link a forcing factor (either climatic or aclimatic) to outlet glacier behaviour. In addition, the records which are used to interrogate these processes have a low temporal scale, often only producing observed data for the past two decades. As a result, the present day changes are not fully understood and future predictions concerning outlet glacier response and sea-level contributions cannot be made with any certainty. In light of this, looking to the past record of outlet glacier response through Greenland is necessary in order to understand the changes observed both today and in the future. The palaeo record can provide a longer timescale reconstruction of ice sheet behaviour, and

proxies can be used to reconstruct the magnitude of a variety of factors active upon the ice sheet during these times. This allows the relative contribution of a number of forcing factors to be ascertained, and the nature of ice sheet response to be characterised (slow, rapid, retreat, advance etc).

Ice streams are known to be the most active portions of ice sheets. At present they drain the majority of ice from the Greenland Ice Sheet, and are also likely to have in the past. They therefore represent the places in which long-term ice sheet behaviour can be identified and characterised. In addition, due to the size and speed of these ice steams, they are likely to have been of great importance to the mass balance of the Greenland Ice Sheet during the Last Glacial Maximum. Therefore, identifying the location of these ice streams during previous periods of glacial activity is of vital importance to understanding how the ice sheet evolved and functioned. This reconstruction is carried out using the geomorphological footprint left by the ice stream across the landscape. This can be difficult in regions of highly dissected, bedrock bedded terrain, but has been achieved previously. Production of high-resolution studies which record ice stream and ice sheet behaviour over long timescales (thousands of years) are therefore a valuable way to predict the way in which the Greenland Ice Sheet will respond to future changes in atmospheric and oceanic climate.

CHAPTER THREE

Glacial landscape evolution in the Uummannaq region, West Greenland

Abstract

The distribution and development of glaciated and non-glaciated landscapes in the Uummannaq region, West Greenland has been investigated using high resolution remote and field geomorphological mapping. As in other continental ice sheet margins, the Uummannaq region is characterised by a patchwork of glacial landsystems which have developed throughout the Quaternary. Glacial activity over this period had modified a pre-glacial fluvial surface. This pattern is consistent with hypothesised landscape distribution resulting from variations in subglacial thermal regime. The regional landscape is dominated by selective linear erosion which has partitioned the landscape. This has led to the development of deep fjords, bordered by high altitude relict plateaux which foster small poly-thermal ice caps and small valley glaciers. Low altitude areas contain areally scoured terrain, appearing more concentrated in the south. Two areas displaying little glacial erosion were mapped on the Svartenhuk and Nuussuaq peninsulas, in the north and south respectively. It is likely that during glacial conditions these were not engulfed by ice from the Greenland Ice Sheet, due to intense drawdown of ice into the Uummannaq trough. They would have instead been partially covered by locally sourced ice caps. Individual landsystem properties vary throughout the region with altitude and location, as a result of variability in erosion rates and bedrock geology. Erosion rates are controlled by internal glaciological factors such as ice thickness, basal water pressure, and basal sliding. From the onset of glaciation to present, subglacial thermal organisation (and the resulting selective linear erosion it has led to) has been the primary control on landscape development throughout the Uummannaq region. It led to fjord and high-elevation plateaux development, and prevented widespread low-elevation areal scour from developing in the north. This selective linear erosion has created an over-deepened, coalescent fjord system which helped to seed the onset zone of the large cross-continental shelf Uummannaq ice stream system (UISS).

Previous research has suggested that central West Greenland experienced several periods of regional uplift from 33 Ma to present. This uplift has removed surfaces from the impact of widespread warm-based glaciation, leaving them as relict landsurfaces. Because uplift began prior to widespread West Greenland glaciation, the highest surfaces within the

Uummannaq region were above the limit of intense, warm-based glacial erosion once it began to operate. This has created an altitude-dependant continuum of landscapes of glacial modification throughout the Uummannaq region, from relatively unmodified, high-elevation plateaux to highly modified, low-elevation trough floors. Glacial landsystem variability appears inexplicable solely through glaciological activity. Processes of long-term uplift, glacial erosion/protection, and spatial variability in erosion intensity have produced a highly partitioned landscape.

3.1. Introduction

Ice sheets have played a major role in landscape evolution throughout Earth history, especially during the Quaternary Period. Landscapes of glacial erosion are the product of multiple periods of glacial inundation during this time. The differential action of ice sheets and its impact upon landscape evolution has long been known. Across glacially inundated landscapes across the world, early work identified zones of areal scour, selective linear erosion and little to no glacial modification (Sugden, 1974). These differences in ice sheet erosion, driven by variation in subglacial thermal regime have been used to explain the common juxtaposition of over-deepened troughs and relict plateau surfaces (Sugden, 1974, Hall and Glasser, 2003, Swift et al., 2008). In contrast, areas affected by glaciation but located outside the limits of ice sheet influence are characterised by cirque and mountain valley glaciers, or small ice caps (Sugden, 1974). In recent years, the combination of geomorphological mapping and terrestrial cosmogenic nuclide (TCN) exposure dating has highlighted the complex interplay between landscape preservation beneath areas of cold-based ice sheet ice, and extensive erosion beneath warm-based ice (Kleman et al., 2008, Stroeven and Swift, 2008, Swift et al., 2008, Strasky et al., 2009, Di Nicola et al., 2009). More recently the important role of ice streams in controlling ice flux from ice sheets has highlighted how they are able to partition their flow. Their location and areal extent determines the interaction between ice streams, ice sheets, and the landscape (Angelis and Kleman, 2008, Winsborrow et al., 2010). In many cases, highly topographically confined fjords act as tributaries for ice stream onset, forcing convergence and flow acceleration through ice drawdown (Lowe and Anderson, 2002, Ó Cofaigh et al., 2002, Ottesen et al., 2008, Roberts et al., 2013). In Greenland, the majority of palaeo-ice sheet research has focused on developing a robust understanding of ice sheet extent and behaviour at the Last Glacial Maximum (LGM) and during previous glaciations (Funder and Hansen, 1996, Bennike and Bjorck, 2002, Weidick et al., 2004, Hakansson et al., 2007a, 2007b, Roberts et al., 2009,

2010, 2013, Ó Cofaigh et al., 2013b). However, a number of studies have highlighted the effect of regional glacial and non-glacial processes on landscape evolution in Greenland. These include the influence of continental scale geological variability on fjord development (Swift et al., 2008), and the impact of cross-shelf ice streams upon ice sheet flow patterns (Roberts et al., 2010, 2013).

Alongside glaciation over million year timescales, landscapes develop through Cenozoic tectonic uplift, and glacio-isostatic rebound and unloading (Small and Anderson, 1998, Oskin and Burbank, 2005, Egholm et al., 2009, Nielsen et al., 2009). Recent study has led to the generation a series of models which couple uplift and landscape development in glaciated regions, specifically in Scandinavia (Nielsen et al., 2009, Steer et al., 2012) and West Greenland (Japsen et al., 2006, Bonow et al., 2007). These studies provide a number of uplift scenarios for glaciated margins which can then be integrated with hypotheses of landscape development. However, few studies have attempted to integrate ice sheet erosion, geological variability, and long-term uplift.

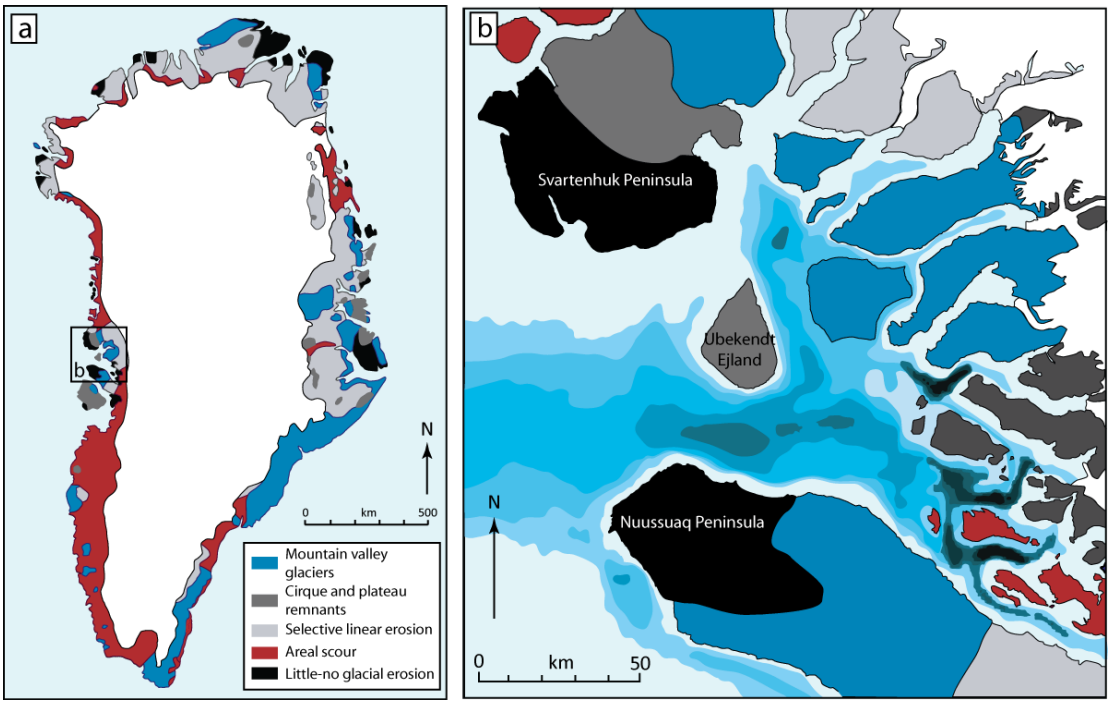

Figure 3.1. (a) Map of the landscapes of glacial erosion found in the ice-free rim of Greenland, as mapped by Sugden (1974); (b) Enlargement of the Uummannaq region, with regional bathymetry from GEBCO (adapted from Sugden, 1974).

This chapter aims to: i) explore the regional scale impact of ice sheet and ice stream erosion upon landscape evolution, by developing a regional map of glacial landscapes in the Uummannaq region, at higher-resolution, and in more detail than previous work; ii) assess the influence of ice sheet evolution on the process of ice stream onset; and iii) evaluate the influence of pre-Quaternary uplift on landscape evolution.

3.2. Background

3.2.1. West Greenland landscape evolution

Previous work has classified the terrestrial glacial and non-glacial landscapes of the entire ice free rim of Greenland, based upon morphological and landform characteristics (Figure 3.1, Sugden, 1974). These classifications included distinct areas pertaining to large-scale warm-based ice sheet erosion (areal scour, selective linear erosion), and small-scale landscapes resulting from erosion by individual glaciers (mountain valley glaciers and cirques) (Figure 3.1). A number of isolated areas displaying either little or no sign of glacial erosion were also mapped.

Areally scoured topography, often referred to as 'knock and lochan' topography (Linton, 1963), describes areas affected by ubiquitous glacial erosion through abrasion and plucking. This topography is formed by abrasive exploitation of structural weaknesses in bedrock by glaciers (Sugden, 1974) and is found in areas of both palaeo- and contemporary ice sheet action (Gordon, 1981, Benn and Evans, 2010). These areas are characterised by depressions and adjacent rock bumps often characterised by the presence of many roches moutonnées and whalebacks (Sugden, 1974). The relief of these features is generally limited to several metres, promoting debate regarding the depth of erosion through scouring. Some relate products of areal scour to strong glacial erosion (Amantov et al., 2011), others suggesting erosion simply "strips" regolith from an older, weathered landscape (Sugden, 1974, Lidmar-Bergström, 1997), thus only removing several tens of metres through erosion. In West Greenland, Bonow (2006b) proposed that the surface morphology of areally scoured regions are strongly controlled by a re-exposed, Late-Cretaceous etch surface on the Archean basement (75-60 Ma), finding preserved remnants of weathered gneiss and smoothed landforms, recently exhumed from the overlying basalt. Mapping demonstrated that the form of these features is strongly controlled by underlying geology, with only slight modification through glacial erosion. That work therefore inferred that the classification of large scale landscapes solely upon the type and intensity of glacial erosion is an

oversimplification. Johansson *et al*., (2001) also suggested this, proposing that etched relief is a prerequisite for the development of classic 'knock and lochan' topography in Sweden.

Selective linear erosion is characterised by the juxtaposition of high-level plateau surfaces, with deep glacially excavated troughs (Sugden, 1968, Sugden, 1974, Sugden, 1978). This highly contrasting landscape is produced through variations in subglacial thermal regime, and resultant changes in glacial erosion intensities (Hall and Glasser, 2003). This acts to focus erosion into narrow bands, forming over-deepened fjords. These dominate many glaciated continental margins (e.g. Norway, New Zealand, and Arctic Canada). In some regions of Greenland, intensely incised landscapes have been shown to have developed prior to the onset of Quaternary glaciation (Swift et al., 2008). Particularly in East

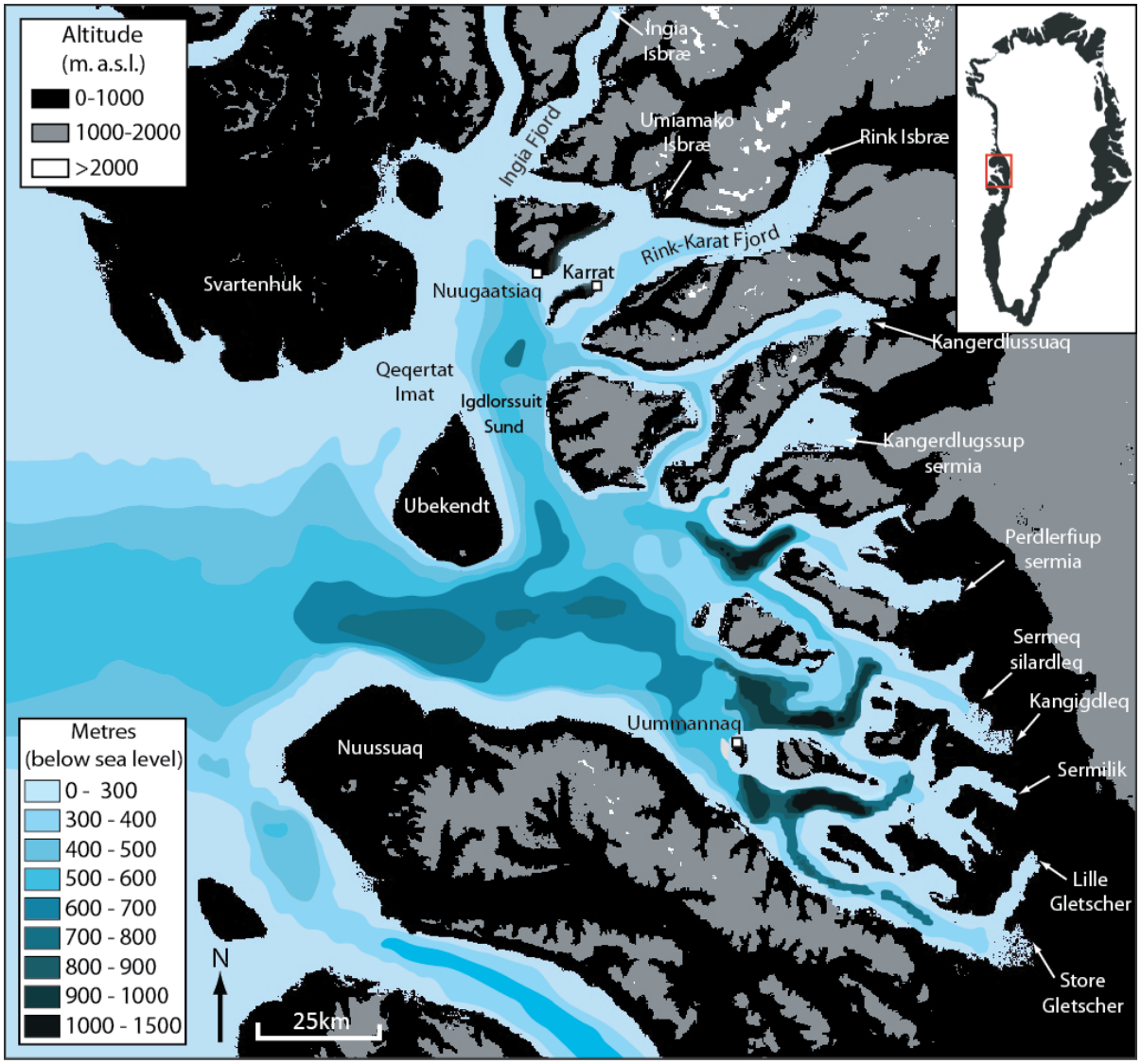

Figure 3.2. Topographic overview map of Uummannaq region. Altitudes are taken from ASTER imagery, and bathymetry from GEBCO. Location and fjord names discussed in the text are identified.

Greenland, Pleistocene ice sheets had little impact upon the landscape as they were predominately cold-based. Quaternary modification has been strongly controlled by pre-existing fluvial valleys (first order topography), and geology (as a function of lithological strength) (Swift et al., 2008). Regions of resistant rock have produced over-deepened fjords and less resistant lithologies producing shallow, wider fjords. Swift *et al.* (2008) cite this geological control upon selective linear erosion as a possible mechanism for the onset of fast ice flow, with wide valleys providing a broader bed over which basal melting can occur. In contrast, recent modelling has suggested that the development of fjord topography comparable to their current state is possible within Quaternary timescales (Kessler et al., 2008). Beyond this, little research has been carried out regarding fjord formation and development in Greenland, although the topographic influence of fjord systems on ice flow may be linked to the onset of large cross-shelf ice stream systems (Evans et al., 2009, Roberts et al., 2009, 2010, 2013). Plateau landscapes are also common in West Greenland, and are synonymous with areas of selective linear erosion (Sugden, 1968, 1974). Preserved plateau land surfaces often contain remnant landforms (tors, blockfields), sediments, and weathering profiles that suggest periods of extensive exposure followed by protection and preservation beneath cold-based ice (Kelly, 1985, Kleman, 1994, Kleman and Borgström, 1994, 1996, Kleman and Glasser, 2007). However, little systematic geomorphological analysis of Greenlandic plateau surfaces has been undertaken compared to other regions in the Arctic (Rea and Evans, 2003).

Parts of West Greenland contain extensive but localised mountain valley glacier systems. These are restricted to isolated mountainous areas, outside the limits of current ice sheet activity. They form in individual, arcuate collecting grounds, coalescing to form trunk valley glaciers, rarely extending further than several tens of kilometres (Sugden, 1974). Cirque glaciers have also been mapped throughout mountainous areas in Greenland (Sugden, 1974).

Finally, a number of lowland regions in Greenland contain areas which display little or no evidence of glacial erosion. Evidence for areal scour and selective linear erosion is absent, and terrain is instead characterised by smooth slopes covered in regolith and incised by fluvial systems (Sugden, 1974). These “non-glaciated” landscapes are likely to have been covered by cold-based ice during Pleistocene maxima, or alternatively, point to limited ice sheet extent during glacial periods of the Late Quaternary, though this is far more unlikely.

3.2.2. The Uummannaq region

The Uummannaq region in West Greenland is mountainous, with plateaux and summits reaching 2000 m a.s.l. (Figure 3.2). This area is ~ 20000 km^2 and contains two large peninsulas, Svartenhuk to the north, and Nuussuaq to the south (Figure 3.2). The area is underlain by three north-south trending geological regions, each bounded laterally by faults (Figure 3.3): Precambrian basement in the east of the region (Archean orthogneisses - ~2800 Ma) (Kalsbeek et al., 1998, Bonow et al., 2007); the Nuussuaq Basin, infilled with Cretaceous-Tertiary marine mudstones and sandstones

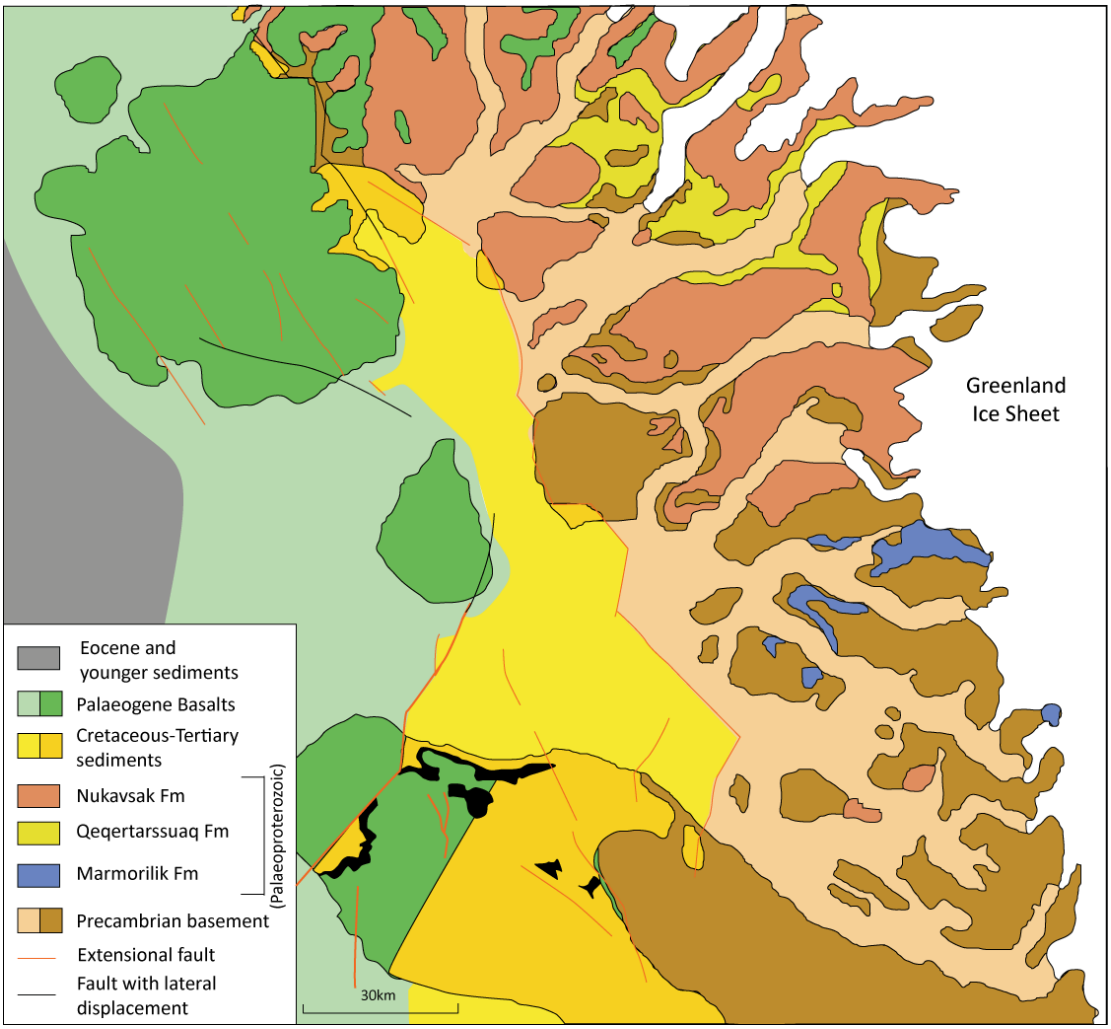

Figure 3.3. Bedrock geology of the Uummannaq region (Henriksen *et al.*, 2009).

Svartenhuk, and the western half of Nuussuaq (Henriksen et al., 2000). The Uummannaq region is (Pedersen and Pulvertaft, 1992, Dam et al., 2000, Henriksen et al., 2000); and Tertiary basalts, which lie offshore and form Ubekendt, dissected by a series of highly entrenched east-west trending fjords which route outlet glaciers to sea-level, and reach

1300 m in depth. They have a convergent configuration, which during periods ofmore extensive ice cover would have acted to cause outlet glacier coalescence. Orientations of the fjords range from south-south-west in the north of the system to north-west in the south of the system. They are occupied by eleven large, ocean terminating outlet glaciers and ice streams: Ingia Isbræ, Umiámáko Isbræ, Rink Isbræ, Kangerlussuup Sermersua, Kangerluarsuup Sermia, Perlerfiup Sermia, Sermeq Silarleq, Kangigdleq, Sermilik, Lille Gletscher, Store Gletscher (see Table 2.1 and Figure 3.2). On average, fjords are 4.20 to 6.94 km wide (at sea level) (See Table 1), and from 34.48 to 75.35 km in length (from current ice snout to fjord mouth). Plateau heights between the troughs range from 1000 to 2300 m a.s.l., and water depths within the fjords vary from ~400 to ~1287 m.

Recent onshore and offshore mapping has reconstructed the onset zone configuration of the Uummannaq Ice Stream System (UISS), with north to south deflection of ice flow from northern fjords, caused by a switch in bedrock geology (Roberts et al., 2013, Ó Cofaigh et al., 2013b). Palaeo-ice flow from the north coalesced with southern fjord outlets to seed onset of the ice stream system's trunk zone in the Uummannaq trough. This flowed westwards, reaching the continental shelf edge at the local LGM (Ó Cofaigh et al., 2013a).

3.3. Methods

Mapping was carried out using: 1:150,000 topographic maps; geological maps (Henderson and Pulvertaft, 1987b); aerial photographs (Kort and Matrikelstyrelsen); and digital elevation models created using ASTER imagery. Ground-truthing was carried out in the Northern Uummannaq region (Figure 4.1), where features of glacial erosion were mapped in order to allow palaeo-ice flow reconstructions (Glasser and Warren, 1990, Roberts and Long, 2005). Erosional forms mapped and noted include small-scale friction cracks, striae (Boulton, 1974b, Benn and Evans, 2010), and p-forms (Dahl, 1965). Measurement of their orientation can be used to interpret former ice-flow directions. Large-scale features of glacial erosion mapped included roches moutonnées (asymmetric bedrock protrusions with abraded stoss faces and plucked lee faces) (Sugden et al., 1992a, Benn and Evans, 2010) and whalebacks (symmetrical bedrock features with abraded stoss and lee faces) (Evans, 1996b, Sugden and John, 1976).

Moraines and trimlines were mapped in order to both constrain glacier geometry. Ice-marginal moraines are depositional features, recording the former margins of glaciers, and are found as end and lateral moraines (Benn and Evans, 2010). End moraines develop at the

glacier snout, representing terminal (the maximum limit of glaciation) and recessional (forming from ice-front stability or readvance during retreat) features. In this study, moraines were identified in the field based upon their position, and arcuate form.

Trimlines are boundaries which mark the maximum altitude to which glacier ice has eroded a hillslope (Ballantyne and Harris, 1994). In the field, trimlines were seen as mountain-side boundaries between glacially scoured bedrock (displaying the small- and large-scale features of glacial erosion mentioned above) and higher-altitude frost weathered detritus. The boundary itself can be distinct (change over several metres), or more gradual (change over several tens of metres), depending upon effectiveness of glacial erosion and mass-movement processes following trimline formation (Ballantyne, 1997). Trimlines have a long history of study (Sollid and Sørbel, 1979, Nesje and Sejrup, 1988, Nesje and Dahl, 1990), and thought to relate to the upper palaeo-ice surface, or an englacial thermal boundaries (Fabel et al., 2012) (see Section 2.1.2.2. for a brief discussion of this).

The geometric resolution of the aerial images (primary tool for landform identification) is ~ 3 m, allowing landforms larger than this to be identified. A selection of the remotely mapped areas and features were ground truthed during field visits between 2008 and 2011 (Svartenhuk, Ingia Fjord, Rink Fjord, Karrat Fjord, and Store Gletscher). Topographic DEMs are derived from ASTER GDEM2 imagery and bathymetric data derived from GEBCO and local bathymetric charts.

3.4. Results

The new map of the glacial and non-glacial landscapes throughout the Uummannaq region is presented below (Figure 3.4). Seven landsystems are displayed on the map, including those glacial (areal scour, dissected plateau, non-dissected plateau, mountain valley and cirque, lowland terrestrial deposition, and selective linear erosion), and non glacial (little or no evidence of glacial erosion) in genesis. A detailed description, and specific examples, of the landsystems is provided below (Sections 3.4.1 to 3.4.5) with focused examples and evidence of each (Figures 3.5 to 3.9).

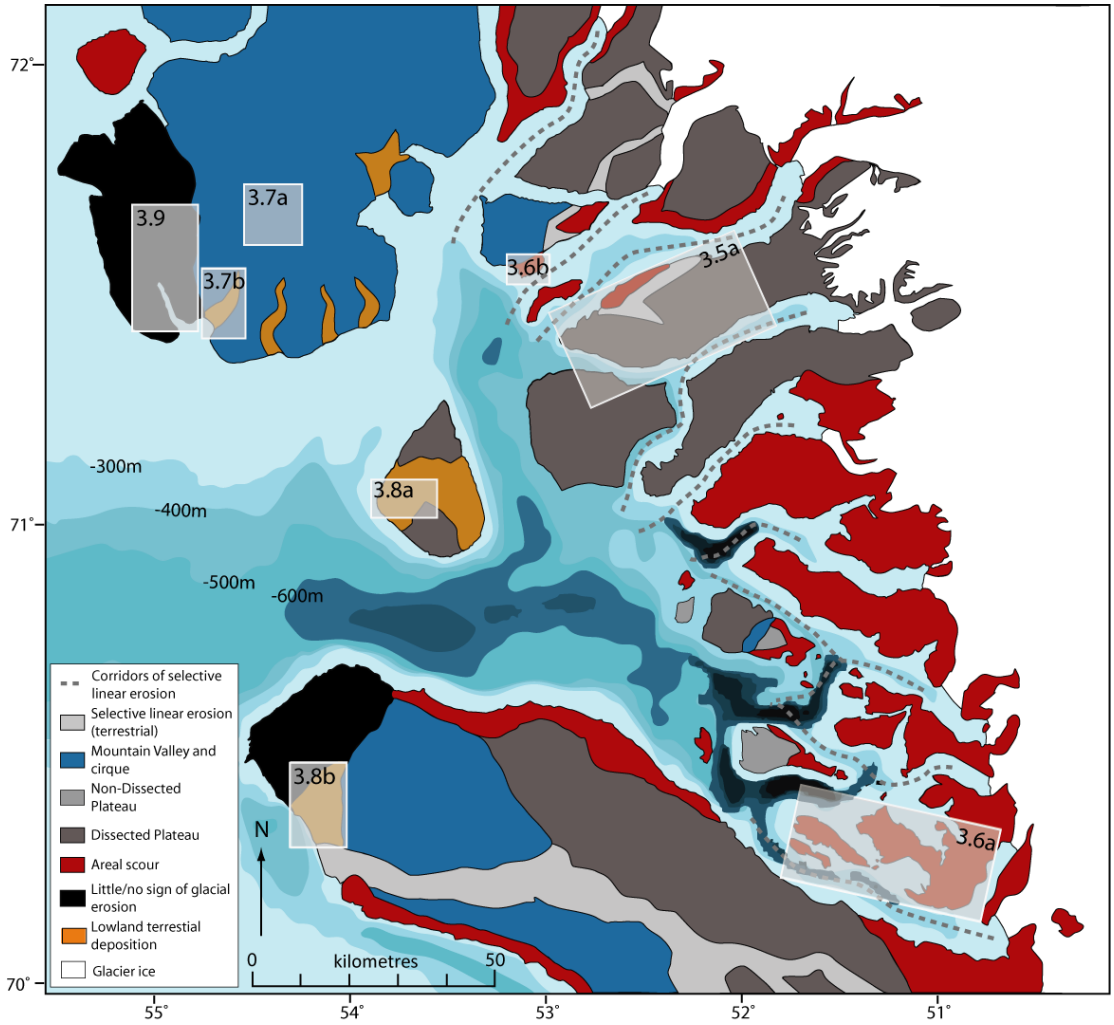

Figure 3.4. New map of glacial and non-glacial landscapes throughout the Uummannaq region. Boxes show the location of subsequent figures. Selective linear erosion is imprinted upon the entire region, and indicated by a dashed line.

3.4.1. Selective Linear Erosion

Selective linear erosion is characterised by the juxtaposition of landscape erosion focused in linear bands, and intervening regions of less erosive plateau ice fields (Sugden, 1978, Sugden, 1974). Selective linear erosion is ubiquitous throughout the Uummannaq region and has been the most influential method of landscape modification at a regional scale, controlling the development of glacially eroded troughs and high-elevation plateaux (Figure 3.4). It is upon the landscape resulting from this method of erosion that other landscapes of glacial erosion and deposition have been preserved. The dominance of this landsystem throughout the region has prevented its inclusion in Figure 3.4, as it would have hindered the presentation of other landsystems. Instead the entire Uummannaq region should be viewed as resulting from the landscape of selective linear erosion. However, landscapes of 'selective linear erosion (terrestrial)' have been identified. These are particular areas in

which the processes of trough development through selective linear erosion are occurring on present landmasses. These highlighted areas (Figure 3.4) are likely to be future fjords. The regional-scale topography is dominated by a series of coalescent fjords, deeply incised into the Precambrian basement, juxtaposed with high-level (>1000 m a.s.l.) plateau surfaces between them. These features are particularly well-developed in the north. The high levels of erosion have formed steep, near vertical fjord walls, up to a maximum relief of ~3000 m. Low elevation, fjord side, lateral moraine systems are common in inner fjord areas (Weidick, 1968), particularly in the north, and tend to be associated with fjord constrictions and pinning points. It is upon this incised fjord topography that other landsystems have developed.

3.4.2. Dissected and non-dissected plateau

Dissected plateaux dominate all high elevation landscapes (>1500 m a.s.l.) throughout the northern Uummannaq system (North of Qioqe – Figure 3.2). Due to the nature of selective linear erosion, these are juxtaposed with the deep fjords which separate them (Figure 3.5a). The level of plateau dissection is highly variable throughout the Uummannaq region (Figure 3.5b-d), with levels of dissection increasing with distance from the present ice sheet margin. The most heavily dissected plateaux underlie a series of cold-based icefields, perched on interior remnants of plateau surfaces (Figure 3.5d), feeding small valley glaciers. In places these individual icefields are separated by glacially eroded arête-like ridges. Where heavy dissection has occurred, deep glacial valleys separate areas of plateau, and in extreme cases the ice masses on dissected plateaux almost represent a series of independent mountain valley glaciers. In these heavily dissected situations, valley floors contain extensive glacial sediments including outwash and controlled moraine (Evans, 2009). In areas closer to the present ice margin, plateaux are far more coherent, with larger ice fields (Figure 3.5b). Small warm-based glaciers emanate from the ice fields, but appear to have achieved minimal erosion. Plateaux in the south appear far less frequently than the north, with only four isolated instances of plateaux mapped. Plateaux appear absent between most fjord troughs in the south, which are instead characterised by areal scour. The plateaux appear similar in morphology to those from the north, although smaller in area, therefore fostering fewer ice caps. In general they are also more coherent and less dissected.

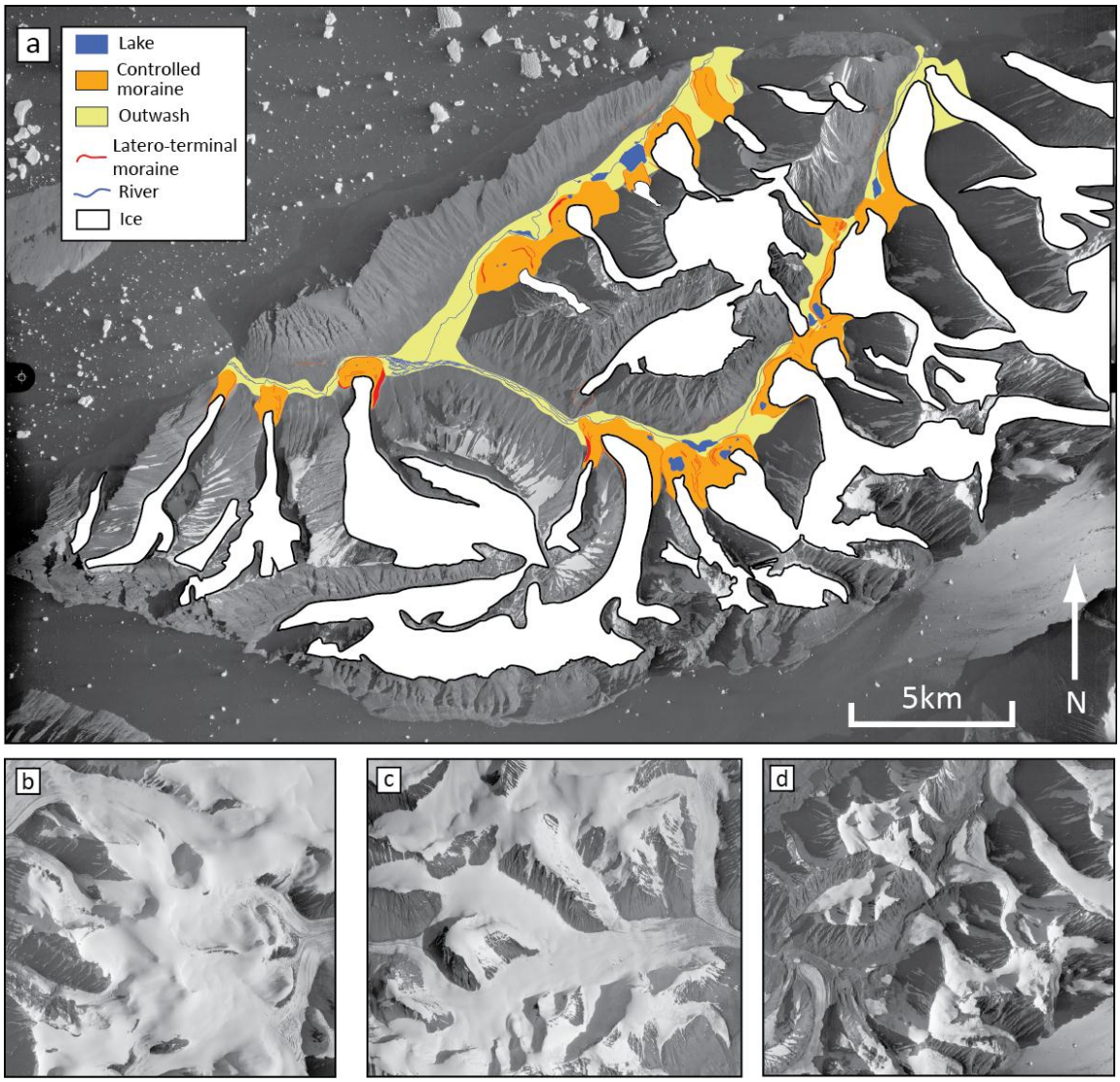

Figure 3.5. (a) Geomorphological map overlain on an aerial photograph, showing an example of a dissected plateau; (b - d) aerial photographs of locations in the northern Uummannaq region (north of Qioqe – see Figure 3.2), showing the continuum of types of dissected plateau. (b) The landsystem still forms a relatively coherent plateau, with some dissection. (c) More dissected, but the majority of the icefields remain connected. (d) Intense dissection has taken place and the icefields appear far more fragmentary, with large inter-plateau valleys present.

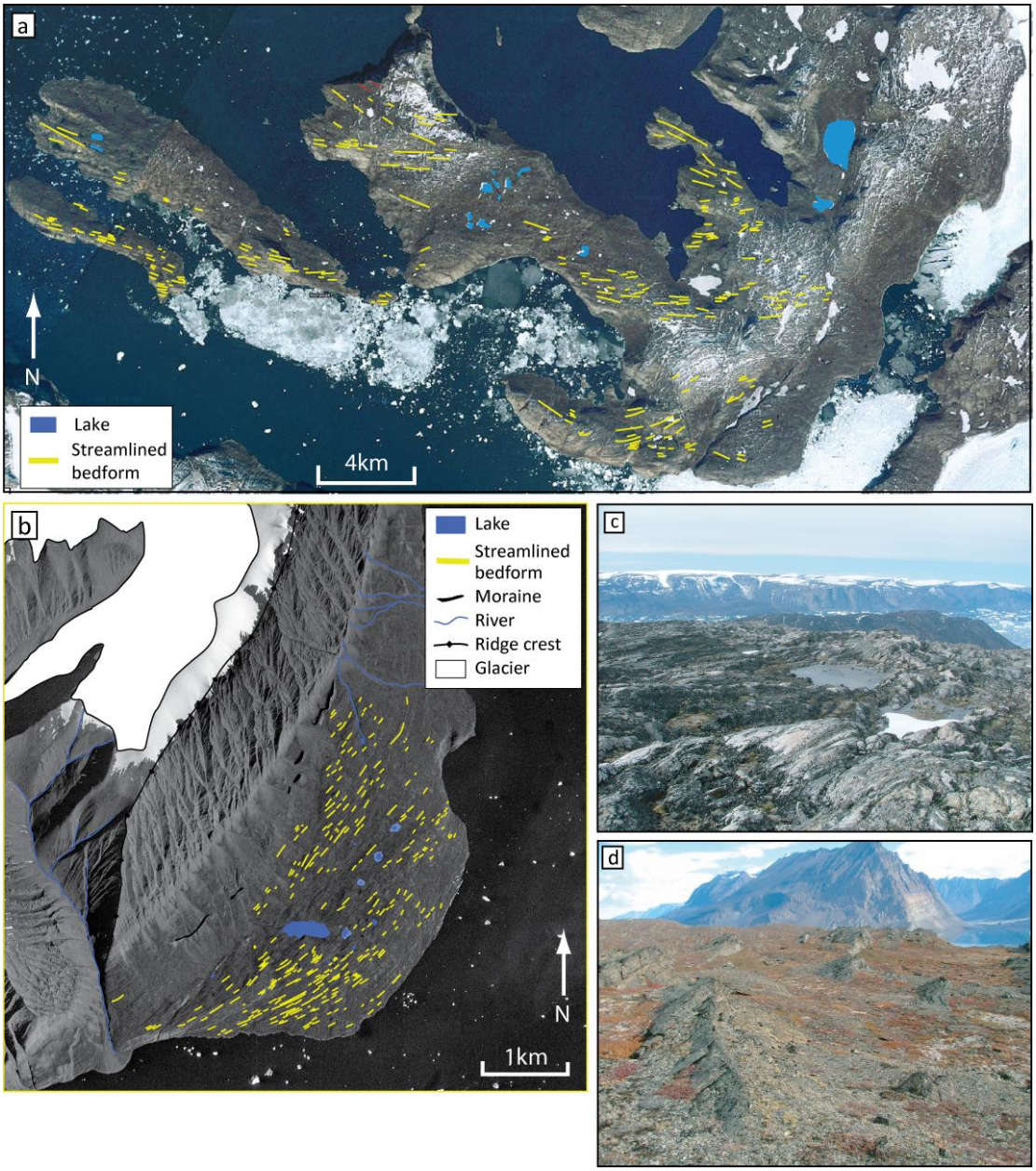

Figure 3.6. (a) Areally scoured topography from the southern Uummannaq region, with large lineations/macro-scale bedforms mapped; (b) Areally scoured terrain from the northern Uummannaq region, with erosional bedforms mapped; (c) Photograph of the areally scoured topography from the south of the Uummannaq region, showing classic knock and lochan topography; (d) Photograph of areally scoured topography in the north of the Uummannaq region, with long, angular bedforms evident.

3.4.3. Areal scour

Areal scour is present throughout much of the Uummannaq region. It covers most fjord walls in the region, up to 300 m a.s.l., but is concentrated in the southern half of the Uummannaq region, south of Kangerdluarssuk Fjord. Here it dominates the landscape up to and above 1000 m a.s.l.; including interfluve areas between fjords (Figure 3.6a and c). It is

found more restrictedly in the northern Uummannaq region, limited to the base of steep fjord walls (below 300 m a.s.l.) in areas otherwise dominated by selective linear erosion (Figure 3.6b and d). In addition to variability in distribution, there is a clear difference in the morphology of areally scoured terrain between the north and south of the Uummannaq region. In the south, areally scoured terrain is stripped of the majority of regolith and has a rounded, ice-smoothed appearance. On this gneissic terrain, it displays classic "knock and lochan" features (Sugden, 1974) with ice moulded bedrock characterised by roches moutonnées and whalebacks, interspersed with small lakes (Figure 3.6c). Conversely, areas in the northern half of the region are characterised by more angular bedforms with higher elongation ratios (Figure 3.6d). The bedform assemblages here are composed of roches moutonnées and whalebacks formed from metagreywacke. This bedrock and its joint and bedding plane properties have exerted a strong control upon bedform morphology (See Chapter Five for a full discussion of these bedforms).

3.4.4. Mountain valley and cirques

The majority of areas expressing mountain valley or cirque landsystems are on the Svartenhuk and Nuussuaq peninsulas which border the North and South Uummannaq region. Some intermittent patches of mountain valley glaciation exist on high altitude on plateaux surfaces between fjords, but these are very restricted (Figure 3.4). Many of the interior valleys on Svartenhuk and Nuussuaq contain isolated valley glaciers which are predominantly north facing. Cirque development in the Uummannaq region is concentrated on the Svartenhuk Peninsula in the North. Areas of cirque development were differentiated from the surrounding landscapes on the basis of topography and landscape development. On the Svartenhuk Peninsula, cirques were found surrounded by areas dominated by non-glacial landform development (see Section 3.4.6. and Figure 3.7a), allowing for clear delineation of the limits of cirque features. These areas appear as a series of cirque basins, cut into upland areas, and are best developed on north facing slopes. Cirque basins are between 0.5 and 1.0 km wide, and several hundred metres deep (from headwall summit to cirque floor). The cirques are isolated, and separated by sharp arêtes on three sides, with narrow plateaux. Small moraines likely to represent Little Ice Age advances are present in several of the cirque floors (Figure 3.7a).

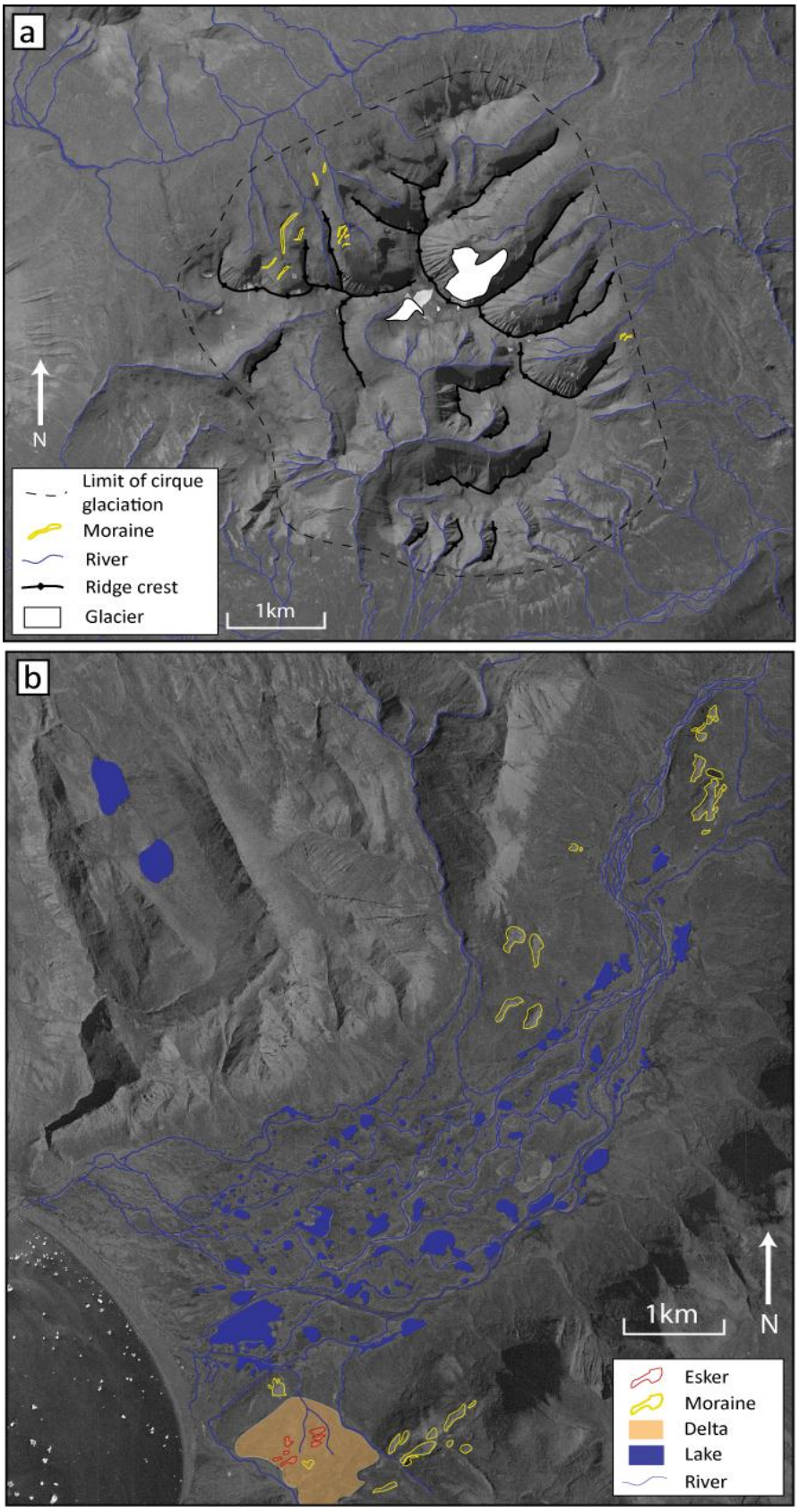

Figure 3.7. Geomorphological maps overlain on aerial photographs showing: (a) areas of cirque glaciation; and (b) valley glaciation from Svartenhuk.

The glaciated valleys that dissect the southern Svartenhuk coast (Figure 3.7b) reflect a very different landsystem signature than the rest of the Svartenhuk, which is dominated by non-glaciated areas and small cirque and mountain glaciers (Figure 3.4). The four valleys are ~3 km wide at their mouth, and 10-20 km in length, emanating from the interior of the Svartenhuk Peninsula. The western most of these valleys, Tasiussaq, exhibits a distinct landform assemblage (Figure 3.7b). The valley comprises a flat valley floor containing an anabranching stream system, with valley walls rising steeply either side to higher elevation ground. There are also a large number of circular small lakes, up to ~500 m wide, connected to a well-developed salt-marsh system. The south-west corner of the valley contains an extensive flat topped delta (14 m a.s.l.), overlain by a series of crude eskers. On higher ground (200 m a.s.l.) there are a series of inset lateral moraines, oriented subparallel to the valley's long axis. This suggests that valley ice was sourced from the interior of the Svartenhuk Peninsula. (See Chapter Six for a full discussion of the glacial history of the Svartenhuk Peninsula).

3.4.5. Lowland Terrestrial Deposition

Two areas of lowland terrestrial deposition were mapped in the Uummannaq Region. The largest of these is found on Ubekendt Ejland (Figure 3.4 and 3.8a). The low lying saddle across the centre of the island (200-350 m a.s.l.) displays a distinct suite of depositional glacial landforms which record ice margin recession and readvance. There are three main components to this landform assemblage. Firstly is a series of subdued low amplitude, lobate moraines deposited in crude arcuate patterns. They are composed of gravelly diamict, are heavily fragmented, and their 'smudged' geomorphology suggests that they have been overrun following deposition (Roberts *et al.*, 2013). The second is a large east-west trending esker ridge, with a series of smaller discontinuous eskers between the subdued moraines. The third component of the landsystem is a series of ice-marginal deltas found to the north of the moraine system. These formed through deposition into ice-marginal lakes during ice down-wasting and retreat. These lakes formed at a terrestrial ice margin, lying above the hypothesised local marine limit.

A second, smaller area of lowland terrestrial deposition is found in the Pingungud kua valley on the southern side of the Nuussuaq Peninsula (Figure 3.8b). The valley appears to be a north-easterly extension of the large Kugssuaq valley, which bisects the Nuussuaq Peninsula. The valley floor is covered by sediment, and has been dissected by a mountain

fed fluvial system. At the northern end of the valley are a series of subdued, hummocky latero-frontal moraines which cluster to form an arcuate ridge (Benn and Evans, 2010). These record the ice marginal position of a glacier from the Kugssuaq valley which was deflected northwards by the presence of thick ice in the Vaigat Fjord.

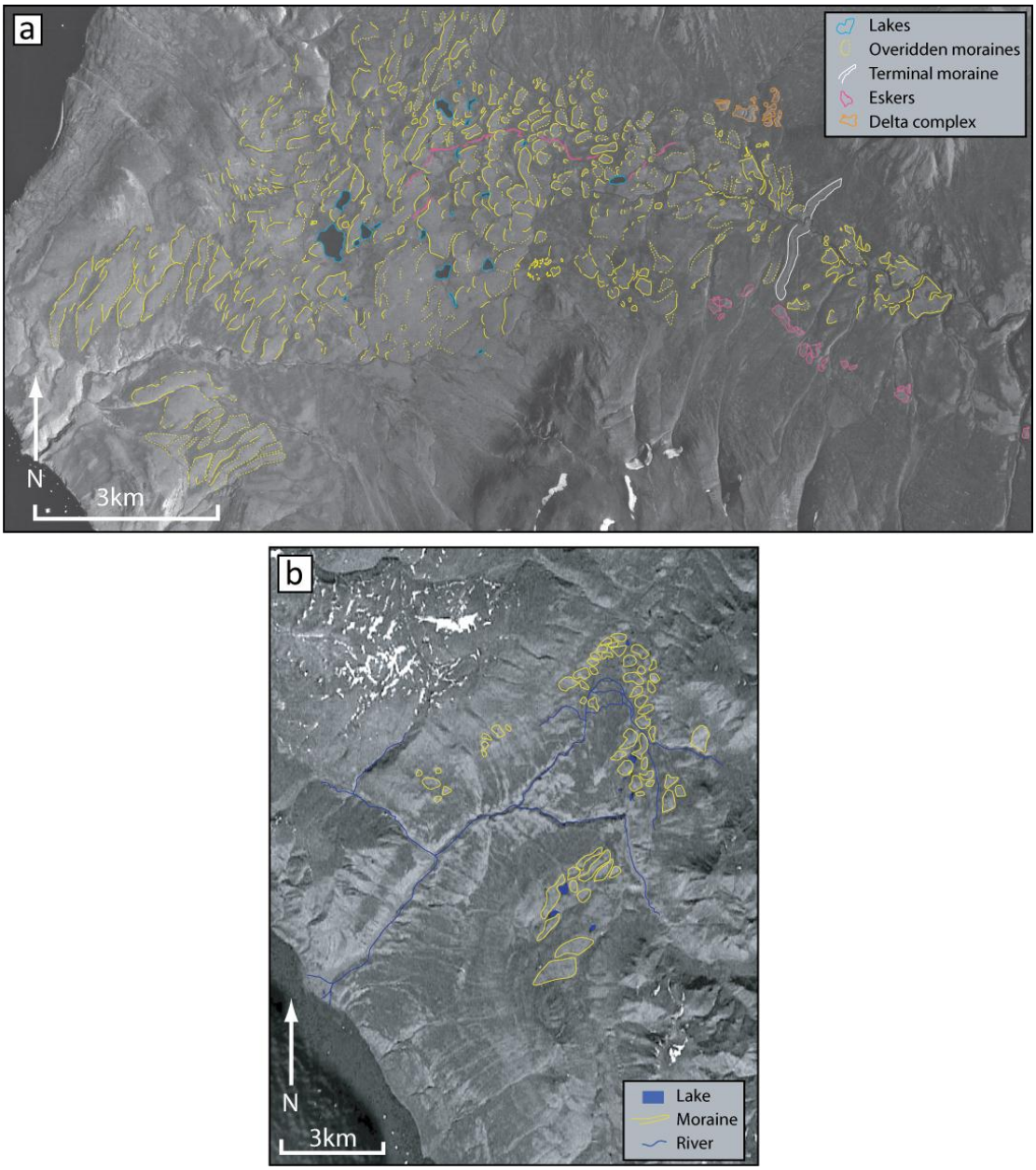

Figure 3.8. Geomorphological maps of the 'lowland terrestrial deposition' landsystem identified in this study. Maps are overlain on aerial photos. These landsystems were limited in abundance, found on (a) Ubekendt and (b) southern Nuussuaq.

3.4.6. Areas dominated by non-glacial landform development

'Non-glaciated' areas were mapped on the western sides of Svartenhuk and Nuussuaq, concordant with those mapped by Sugden (1974). The relief and altitude of the landscape in these areas is considerably lower in elevation than the rest of the Uummannaq region, only reaching ~900 m a.s.l. These areas do not display any clear evidence of areal scour, or glacial overrunning. Instead they are characterised by fluvial valleys incised into widespread sediment deposits, up to 30 m thick (Bennike et al., 1994, Laursen, 1944). The centre of the area mapped as non-glaciated contains a series of elongate, subparallel bedrock ridges, reflecting the NNE-SSW striking bedrock structure (Figure 3.9). They vary in size, from ~ 0.25 to 8 km long, and from 0.06 to 0.76 km in width. Areas between these ridges are infilled with talus and fluvial sediments of unknown depth and age (Figure 3.9), all of which is incised by a shallow fluvial system. Other than these features, the region is largely devoid of any landforms or sediment assemblages that are clearly characteristic of recent

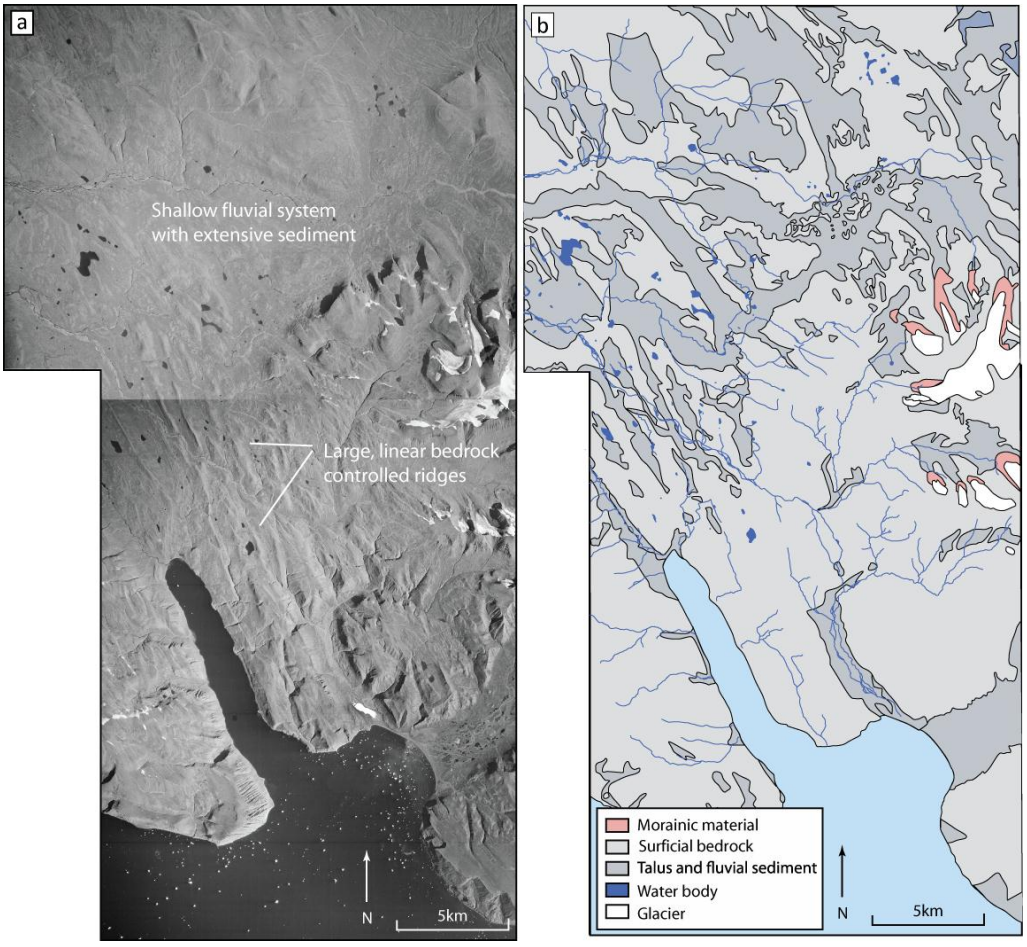

Figure 3.9. (a) Aerial photograph and (b) geomorphological map of southwest Svartenhuk. The well-developed fluvial drainage system and extensive deposits of sediment are evident. Sediment limits are from original geological maps (Henderson and Pulvertaft, 1987b). Little evidence of glacial activity has been recorded (Sudgen, 1974).

glaciation. In some locations channels/gorges cross cut bedrock ridges. These are thought to represent local drainage diversions, caused by the palaeo-damming of the landscape by ice (See Chapter Six for a full discussion of these). The western end of the Nuussuaq Peninsula also contains a similar absence of features of glacial erosion or deposition, instead exhibiting a shallow, anatomising fluvial system, strongly controlled by local bedrock topography. It is a relatively low elevation area (<1000 m a.s.l.), and observations show incised fluvial valleys with a deep mantling of regolith.

3.4.7. Comparison to previous mapping

The regional scale domination of the landscape by selective linear erosion was found both in Sudgen's (1974) mapping (Figure 3.1b) and this study (Figure 3.4). The strong occurrence of areal scour in the south and dissected plateaux in the north was also identified by Sugden (1974), though the boundary between these two landscapes is thought to be situated further north in this study. In contrast to Sudgen's (1974) mapping, this study found areal scour in the north, though restricted to thin strips of low elevation terrain (below 300 m a.s.l.), at the base of steep fjord walls (Figure 3.4).

Areas of lowland terrestrial deposition were not featured in Sugden's mapping of Greenland (Figure 3.1b). These have been identified on central Ubekendt, and southern Nuussuaq, which were previously mapped as 'plateau remnant' and 'little/no glacial erosion' respectively (Figure 3.4). The identification of these landsystems is likely to be the product of higher resolution remote mapping, and ground truthing in the field.

Areas displaying little or no evidence of glaciation mapped in this study are in broadly similar locations to those identified by Sugden (1974), at the western edges of Svartenhuk and Nuussuaq. However, these areas are far smaller than those mapped by Sugden (1974), likely a result of the higher resolution mapping of this study. The original areas included some regions now reclassified as areas of mountain valley and cirque glacier landsystems.

Sudgen's (1974) original classification grouped cirque landscapes and plateau remnants as one landsystem. However, based upon our modern process-based understanding of glacial landsystems (cf. Evans, 2003) it is known that they reflect very different long-term development histories. As a result they have been separated for this study. Thus, a number

of areas were re-classified as mountain valley and cirques. The largest of these regions is on the Svartenhuk Peninsula, an area previously classified as plateau remnant (Sugden, 1974).

3.5. Discussion

Landscapes of glacial erosion, deposition, and those displaying little evidence of erosion have been mapped throughout the Uummannaq region. The factors which have resulted in this distribution and their relationship to the palaeo-UISS are evaluated here. Possible factors such as ice sheet subglacial thermal organisation, bedrock lithology, and longer-term, preglacial landscape processes are discussed below.

3.5.1. Landscape distribution throughout the Uummannaq region

Based upon the described constituent landscape elements, this region is not unique. A number of other currently and formerly glaciated areas demonstrate a similar glacial landsystem assemblage (Stroeven et al., 2002, Kleman et al., 2008, Stroeven and Swift, 2008, Swift et al., 2008). The present regional-scale landscape of the Uummannaq area is chiefly the product of spatial variation in subglacial thermal regime throughout multiple glacial cycles. The glacial and non-glacial landscapes identified in this study are consistent with traditional models of ice sheet subglacial thermal organisation and thermal partitioning (Hughes, 1995, Kleman and Glasser, 2007). This proposes that large ice sheets (both contemporary and those present during the Pleistocene) are composed of a mosaic of areas of warm-based and cold-based ice (Kleman and Glasser, 2007) including: frozen-bed patches; ice streams; ice-stream tributaries; and slower moving ice. The presence (or absence) of these components in varying proportions within an ice sheet has important implications for the landscapes remaining following deglaciation.

Northern Hemispheric glaciation began between 10 and 6 Ma (Wolf-Welling et al., 1995, Maslin et al., 1998), with ice sheet growth centred upon southern Greenland. By 4-3 Ma the expansion of the southern sector of the ice sheet was sufficient to allow coalescence with more restricted ice from northern Greenland (Maslin *et al.*, 1998). This led to the onset of ice sheet growth and glacial erosion inland of the Uummannaq region. Glacial activity has continued and expanded throughout the Quaternary, allowing the domination of selective linear erosion across the Uummannaq region. Initial fjord location is likely to have been dictated by the location of pre-glacial fluvial valleys, or guided by inherent structural

weaknesses within the host bedrock (Bonow et al., 2007). However both hypotheses for fjord development in this area are poorly understood and initial conditions for the onset of glaciation are poorly constrained. The timescales proposed for the incision of the fjords and troughs which dominate the Uummannaq region (~ 4-3 Ma) are in broad agreement with numerical modelling results. Models demonstrate that positive feedbacks between flow convergence, geothermal heat flux, and subglacial thermal regime organisation encourage regional selective linear erosion (Jamieson et al., 2008, Kessler et al., 2008). This leads to the development of fjords over multiple glacial cycles, at timescales of 100 kyr to 1 Ma. Jamieson *et al.* (2008) demonstrated that a fluvial landscape can become recognisably glacial (over-deepened and with increased width towards the terminus) via glacial modification during a single 100 kyr glacial cycle. This occurs as a result of intense focused erosion (up to 3mm yr^{-1}), coupled with high isostatic uplift. Similarly, modelling by Kessler et al. (2008) showed the development of kilometre-deep fjords after ~1 Ma of glacial erosion. They suggest that the dramatically non-uniform distribution of erosion in landscapes which have undergone ice sheet erosion is due to feedbacks between topography, ice flow, and erosion. Valley erosion and subsequent over-deepening provides lines of weakness along which ice flow is channelled during multiple glacial cycles.

3.5.1.1. Distribution of glaciated landscapes

As discussed, the regional-scale topography of the Uummannaq region has been formed through a history of intense selective linear erosion which has produced a distinct, deeply entrenched fjord system (Sugden, 1974) (Figure 3.4). Through erosional feedbacks, this deeply incised fjord system has been able to govern locations in which other glacial landscapes can exist. As a result, high altitude areas throughout the region (>1400 m a.s.l.) are stranded from glacial erosion by focusing of erosion in intervening lower altitude areas. This is most evident in the north of the region, where the majority of high altitude land is occupied by areas of dissected plateau. These areas are today characterised by small poly-thermal plateau ice fields.

In the south of the region, the deeply incised fjords are juxtaposed with zones of high-altitude areal scour as opposed to dissected or non-dissected plateaux. These areas display clear evidence of widespread, warm-based ice operating at high altitudes. It is likely that during initial ice build-up these high altitude areas contained patches of cold-based ice. These would have been progressively engulfed by warm-based ice as ice sheet thicknesses

increased. The heightened erosional ability would have eradicated the geomorphological evidence of initial frozen-bed phases of ice build-up (Kleman and Glasser, 2007). The development of widespread areal scour in the south is the result of two linked factors. Based upon contemporary estimates, the ice flux of the southern Uummannaq region is considerably higher than the north (Table 2.1), allowing widespread inundation and erosion as warm-based ice overwhelmed the topography. In contrast, lower ice flux in northern Uummannaq (again, based upon contemporary estimates) has confined areal scour to the bases of fjord walls. The second factor is the lower average topography in the south of the Uummannaq region compared to the north. Though this is likely to be a long-term product of high ice flux, lower elevation topography allowing more extensive inundation of areas by warm-based ice, and therefore more regions are susceptible to areal scour. Alternative this could simply be a result of a lower inherited topographic surface.

Though the majority of landscape variability is explicable through subglacial thermal organisation, some variability occurs within areas of similar subglacial thermal regime. Areally scoured terrain in the south also shows high variability with altitude. Lower altitude areally scoured areas (<500 m a.s.l.) display well developed, streamlined bedforms. In contrast, areally scoured terrain at higher altitudes (>500 m a.s.l.) displays less streamlined, less well-developed bedforms (e.g. Drygalskis Halvo; Figure 3.6a, c). This variation in scour intensity and bedform production is likely to be a product of variability in ice properties. Driving stresses, governed through ice thicknesses, would have been high over low-elevation areas, encouraging basal strain melting, freeze-on, and melt-out process. In turn, these processes would have led to increased levels of glacial erosion, and increased bedform streamlining. This is, as the level of streamlining and scour intensity is positively correlated to ice thickness, due to increases in driving stresses and therefore erosion. Thus, higher altitude areas in the landscape display evidence of less well developed areal scour.

In addition to altitudinal variations, there is clear intra-landsystem variability in the morphology of areally scoured terrain in the north and south of the Uummannaq region. Bedforms in the north are often highly streamlined (Figure 3.6d), but lack the smooth, abraded surfaces seen in the south. During glacial conditions, areas in the north and south would have been situated within ice stream tributaries, and subject to similar subglacial conditions, ice thicknesses, bed stresses, and ice velocities. Therefore, it appears that spatial variability in the characteristics of areally scoured terrain is a result of variation in bedrock geology rather than ice flow properties. Surficial bedrock in the south is primarily

composed of Archean gneiss (Garde and Steenfelt, 1999). Its crystalline properties, lack of bedding planes and low joint densities means that when eroded by warm-based ice it is able to form "classic" areally scoured terrain, with smoothed surfaces, bedrock bumps, and bedrock bedforms, dominated by abrasion, with some plucking (Sugden, 1974, Rea and Evans, 1996). In contrast, surficial bedrock in the north of the region is characterised by low grade, horizontally bedded metagreywacke. This bedrock contains thin bedding planes and has high joint densities. These inherent structural properties have facilitated preferential exploitation during periods of warm-based ice cover, promoting the development of elongate, blocky bedforms through plucking and abrasion (see Chapter Five for a full discussion of the bedforms in the north of the region).

Thus far, the landsystems discussed have been erosional in nature, formed during periods of ice advance and retreat. Areas of lowland terrestrial deposition, not featured in Sugden's mapping of Greenland have been identified here on central Ubekendt and southern Nuussuaq, previously mapped as 'plateau remnant' and 'little/no glacial erosion' respectively (Figures 3.1 and 3.4). These landscapes, though rare, are with respect to time, the most recent landscape signals throughout the study region, and are ascribed to the most recent deglaciation. These represent preserved records of ice sheet margin retreat and exist in very restricted areas. The geographical setting of the two areas is very different: a large, low altitude saddle (central Ubekendt); and a small valley in the flank of the large Nuussuaq Peninsula. The rarity of these landsystems is a function of the intense regional selective linear erosion. This has left only a few areas of low altitude and relief which are able to preserve these depositional landsystems since the LGM. In contrast, a number of these areas exist on the seafloor. The characteristics of the two areas of lowland terrestrial deposition are very different to one another. The landsystem mapped across the central saddle of Ubekendt Ejland presents evidence for ice retreat, and a subsequent readvance. Retreat, likely to have been from a LGM position, produced a suite of dissected terminal moraines to the west of the island. This retreat is likely to have been coeval with ice stream retreat throughout the Uummannaq region. Following this, an ice marginal readvance over the Ubekendt Ejland saddle overrode the moraine complex, smudging them, whilst also depositing a suite of eskers and allowing delta deposition (Figure 3.8). This readvance could have been a result of GS-1 cooling (12.9 - 11.7 kyr b2k), with a drop in air temperatures encouraging ice margin advance. However, this chronological hypothesis remains untested. Following this readvance, ice retreated towards Igdlorssuit Sund, exposing the saddle and areas of lowland terrestrial deposition. In contrast, the region of terrestrial deposition on

the Nuussuaq Peninsula records a simple valley advance of an ice lobe, depositing a latero-terminal moraine at its maximum extent. It is likely that this was deposited during deglaciation following the regional LGM. Despite their differences, both regions mapped as lowland terrestrial deposition are grouped as a single landsystem, as they represent ice marginal deposition from an ice sheet margin (Benn et al., 2003, Benn and Evans, 2010).

3.5.1.2. Distribution of landscapes dominated by non-glacial landform development

Landscapes of glacial erosion and deposition discussed thus far fit with traditional models of ice sheet organisation and thermal partitioning (Hughes, 1995, Kleman and Glasser, 2007). However, areas identified as displaying 'little/no glacial erosion' by Sugden (1974) were found in this study. These do not directly fit with this model of thermal partitioning. Instead these landsystems developed in close proximity to the Greenland Ice Sheet. The immediacy of these areas to active areas of the Greenland Ice Sheet during glacial periods makes them of interest, as does their relative rarity throughout Greenland. These areas are characterised by fluvial systems and landscapes showing negligible imprint of glacial activity. It is likely that these areas are similar to Greenland's pre-glacial, fluvially dominated topography, but have continued to develop until the present. Similar regions of pervasive ice-free conditions in close proximity to large ice sheets have been reported in areas close to the Fennoscandian palaeo-ice sheet (Kleman and Stroeven, 1997, Hattestrand and Stroeven, 2002), suggesting that though unusual, this is not a unique glaciological situation.

The development of these regions displaying negligible evidence of glaciation is an indirect result of selective linear erosion throughout the Uummannaq region. As well as segregating high altitude areas, the UISS has caused large scale landscape abandonment of these areas close to the trunk zone of the UISS (Roberts *et al.*, 2013). Over multiple glacial cycles, the highly confluent fjord configuration has drawn ice towards the Uummannaq Trough and away from both Svartenhuk and Nuussuaq. This has left these areas removed from the influence of warm-based ice stream or ice sheet ice, leaving them to be colonised by local ice-caps. Though classified as regions dominated by non-glacial landform development, it is highly likely that areas of western Svartenhuk and Nuussuaq were covered by small, polythermal ice caps, emanating from high ground, independent of the Greenland Ice Sheet. Some limited investigation has been carried out into glaciation on the Svartenhuk Peninsula and moraines do record a restricted advance of local valley glaciers and ice caps in the peninsula's interior (Laursen, 1944). More recent research (see this study, Chapter Six) has

shown that individual glaciers advanced radially from the centre of the Svartenhuk Peninsula during the LGM. They are thought to have reached the present coastline in the south, depositing sediment now found in valley floors (Figure 3.7b). It is likely that some LGM advance occurred in the north of the peninsula but the extent of these glaciers is not known. Therefore the present landscape of the Svartenhuk region, though dominated by non-glacial landform development, does contain highly subdued evidence for glacial activity and glacial landform genesis.

As has been shown, the majority of the landscape elements throughout the Uummannaq region fit with classic models of landscape distribution as a result of ice sheet subglacial thermal organisation (Hughes, 1995, Kleman and Glasser, 2007). The region is dominated by the development of troughs and plateaux with sharp lateral boundaries. This has created an area characterised by a mosaic of landscape types, dominated by areas of intense warm-based erosion and less frequent frozen-bed patches. The north and south of the system are flanked by large 'non-glaciated' enclaves that are, likely to have been covered by cold-based ice and individual mountain valley and cirque glaciers during glacial periods. Though the precise configuration varies from examples proposed in Kleman and Glasser's (2007) model, these protected areas are seen as large frozen-bed patches bordering the north and south of the system.

3.5.2. Geological control upon fjord formation and ice stream onset

The distinct geological setting of the Uummannaq region has also played a critical role in determining landsystem distribution and trough morphometry. The triggering of UISS onset is the result of trough development through an interaction between regional first-order geology and selective linear erosion. The relatively sinuous nature of the present inner-fjord regions suggests that the routing of outlet glaciers represents a relatively limited modification of a pre-glacial valley network (Swift et al., 2008) with selective linear erosion causing over-deepening but little lateral erosion or fjord widening.

During full glacial conditions, outlet glaciers throughout the Uummannaq region extended beyond their individual fjord confines, coalescing to the east of Ubekendt Ejland, in Igdlorssuit Sund (Roberts *et al.*, 2013; Chapter Four). This formed the trunk zone of the UISS, which flowed south and then offshore through the Uummannaq Trough. The routing of the northern UISS trunk zone to the south through Igdlorssuit Sund is indicated by

bathymetry to the south of Ubekendt, which display evidence for highly convergent flow from the north and the east (Ó Cofaigh et al., 2013b). Bathymetry north of Ubekendt indicates a shallow submarine sill at Qeqertat Imát (Figure 3.2), at the boundary between the Cretaceous and Tertiary bedrock. In conjunction with Ubekendt Ejland, this represents a considerable topographic obstacle to ice from the outlet glaciers in the northern UISS, and would have forced the majority of the active, fast flowing UISS south, into the Uummannaq Trough. It is likely that a considerable thickness of ice passed through Qeqertat Imat, however, due to a shallow sill running through this region, ice is thought to have been slower flowing and far less erosive than in the Uummannaq Trough.

This major switch in direction of the northern UISS through Igdlorssuit Sund is a result of regional first-order geology. Igdlorssuit Sund is a large, wide north-south trending trough, bounded by the inner fjord system to the east, Ubekendt to the west, and the Svartenhuk and Nuussuaq peninsulas to the north and south respectively. This zone of ice sheet palaeo-convergence contains no landmasses, and is coincident with the mapped extent of the marine mudstones and sandstones (Figure 3.3) (Pedersen and Pulvertaft, 1992, Dam et al., 2000, Henriksen et al., 2000). The Cretaceous-Tertiary mudstones and sandstones are more vulnerable to erosion than the resistant Archean basement to the east, and the Tertiary basalt to the west. This encourages more effective glacial erosion and fjord widening through this region of lithological weakness. Fjord widening through glacial erosion has continued to the boundary with the more resistant Tertiary basalt to the west. The increase in trough cross-sectional area along the flowline of the palaeo-UISS is indicative of a system which develops efficient ice flow (Swift et al., 2008), as ice becomes focused into a single outlet glacier channel. This decrease in lateral confinement and increase in ice flow efficiency (i.e. concentration of flow into a single fjord) encouraged the drawn-down of ice from the inner fjord system, and the establishment of the UISS. The increase in fjord width and accompanying decrease in the number of fjords is a recognised feedback phenomenon indicative of a coalescent, efficient, fast flowing system of ice streams (Augustinus, 1992, Brook et al., 2004, Swift et al., 2008). The focusing of flow into a single, wide fjord as opposed to several narrow, sinuous fjords provides a larger area for basal sliding. Basal sliding encourages basal melting and focuses meltwater, lubricating large areas of the bed. This increases the availability of basal sediment and encourages flow through this region (Swift et al., 2008). This situation is not unique to the Uummannaq region in Greenland. Work from the Scoresby Sund regions of East Greenland shows a similar switch from narrow sinuous fjords within basement geology to few, wider outlets in downstream, less resistant

bedrock. Though not fully studied, fjord convergence is a global phenomenon at present and past ice sheet margins. Though little is known about large scale controls upon fjord convergence and trough development, it appears that in the Uummannaq region this process was facilitated through selective linear erosion and variations in bedrock strength.

In addition to the over-deepened, convergent fjord pattern, Swift et al. (2008) noted a series of low-lying areas adjacent to ice streams in East Greenland which displayed few features indicative of glacial erosion. This supports the model of thin, protective cold-based ice cover close to large ice streams. Though not described in detail by Swift et al. (2008), these areas appear similar in morphology and palaeo-glaciological setting to the 'non-glaciated' regions of Svartenhuk and Nuussuaq described in this study (Section 5.1.2.).

The pattern of first-order geology in the Uummannaq region continues south, to Disko Bugt, into which Jakobshavn Isbræ calves. The long-term landscape response to glacial erosion through this region is very similar to that of the Uummannaq fjords, with narrow, sinuous inner fjords eroded through basement rock, and wider fjords in the less resistant Cretaceous sediment. However, the precise way in which this has, or has not, affected ice stream configuration during glacial periods has not yet been studied. The evidence suggests that lithological variability exerts an important control upon ice stream onset in a number of locations throughout Greenland.

3.5.3. The influence of pre-Quaternary landscape processes in glacial landscape evolution

The glaciation and development of the landscape during the Quaternary has been overprinted upon a complex regional uplift history (Bonow et al., 2006a, 2006b, Japsen et al., 2006). High altitude plateau surfaces throughout the Uummannaq region (continuations of which are present further south) have been identified as remnants of high-level relict plateaux surfaces (Bonow et al., 2006a, 2006b, Japsen et al., 2006). Japsen *et al*. (2005, 2006, 2009) proposed the landscape structure in this area of West Greenland to be the result of three tectonically driven phases, each made of a period of uplift and subsequent erosion to a base level. This uplift of surfaces to high elevations appears to have been an important factor upon long-term landscape development throughout the Uummannaq region. As has been shown, glacial landsystem distribution is dependent upon landsurface altitude, meaning that knowledge of the spatial extent and timing of uplift is essential. The erosional landsurfaces recognised on the Nuussuaq Peninsula and further south in Disko Bugt are erosional remnants of landmasses uplifted during the Neogene (Japsen et al.,

2005). These include an Upper Planation Surface (UPS); a Lower Planation Surface (LPS); and a re-exposed early Late Cretaceous etch surface formed in the Archaen basement (Japsen et al., 2005, 2006, 2009, Green et al., 2011).

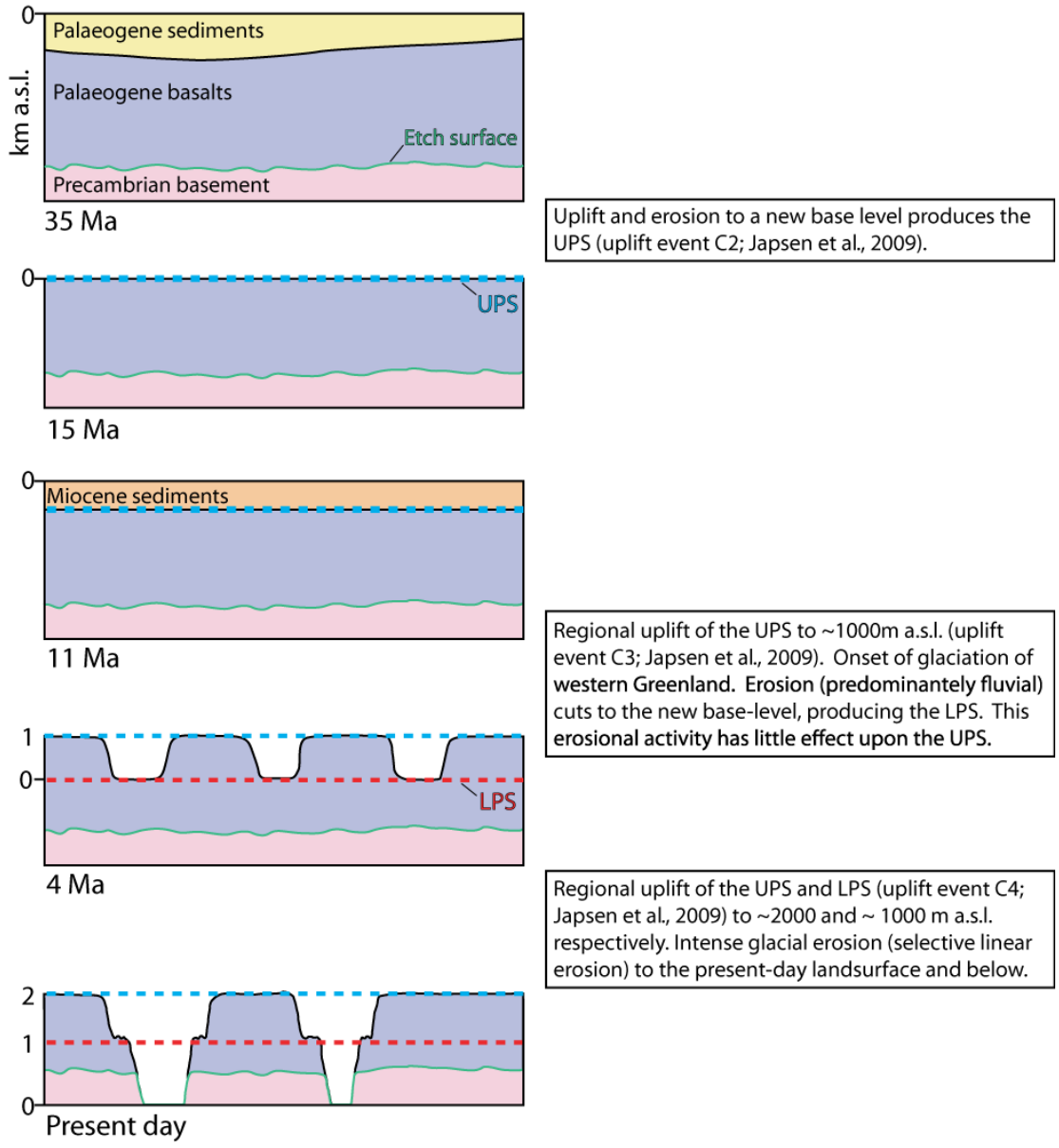

Figure 3.10. Idealised geological profiles taken north to south through the Nuussuaq Basin in the Uummannaq region, illustrating the development of the UPS and LPS, and the re-exposure of the Precambrian etch surface through erosion (adapted from Japsen *et al.*, 2009). The timing of the onset of glaciation and selective linear erosion in the region is shown within the context of uplift. Valleys were incised in two stages as a response to different phases of uplift (C3 and C4). Present day valleys are deeply incised to >1000 m b.s.l.

The highest altitude and oldest surface, the UPS, formed through tectonic uplift beginning at 33±3 Ma. It was uplifted to its current altitude (~2000 m a.s.l.) during two distinct uplift events at 10.5 ± 0.5 Ma and 4.5 ± 2.5 Ma (Figure 3.10) (Japsen *et al.*, 2009). This two-stage uplift allowed the grading of valleys to new base levels. Following initial uplift, the UPS was incised to the present altitude of ~1000 m a.s.l., forming the LPS. Consequent uplifting of the UPS and LPS at 4.5±2.5 Ma raised them to 2000 and 1000 m a.s.l. respectively (Figure 3.10) (Japsen *et al.*, 2009). During their uplift history, fluvial incision of the UPS and LPS was spatially widespread, eroding along, and producing further lines, of structural weakness, therefore preconditioning the landscape for selective linear erosion (Bonow et al., 2006a, Japsen et al., 2006). It should be noted that the age determination of the surfaces used here is reliant upon apatite fission-track analysis (AFTA), the interpretations of which have recently been called into question (Redfield, 2010). Through reanalysis of Japsen's (2005) AFTA data, Redfield (2010) contended that interpretations of uplift occurring in a series of distinct phases, exclusively at 10.5±0.5 Ma and 4.5±2.5 Ma were untenable. Though acknowledging that the land in the north of Disko Bugt, including the Nuussuaq Peninsula, represents a laterally extensive, high-level landsurface, Redfield (2010) argues that data cannot be used to successfully constrain its uplift.

Redfield (2010) instead constrains the uplift of these surfaces to the Late Cretaceous - Palaeocene (following the onset of seafloor spreading through Baffin Bay), suggesting a portion of the regional uplift took place prior to the Neogene. In response, Green et al. (2011) have stated that, despite these issues and differences in data analysis, original interpretations remain accurate. However, if this alternative interpretation of regional uplift history is more viable, and adopted in the future, then slight modifications would be required to this proposed landscape evolution model. In the alternative model (Redfield, 2010), a large areas of the highest landsurfaces would have been above the limit of warm-based glacial activity at the onset of regional glaciation (4 -3 Ma). Though this would have an impact upon the level of landsurface modification through glacial activity, the alternative interpretations of the data do not alter the model of altitudinally dependent variation in Quaternary glacial erosion. Pre-Neogene uplift would have acted to create conditions which allowed this continuum of glacial modification to develop (Figure 3.11).

The influence of these surfaces and their uplift history upon glacial landsystem development and distribution has not been previously investigated. However, the Uummannaq region is dominated by selective linear erosion which acts to spatially and altitudinally partition the

landscape, meaning that landsurface elevation through time is of great importance. Based upon Japsen et al.'s (2009) uplift model, the UPS would have been at a height of at least 1000 m a.s.l. at the onset of glaciation in central West Greenland (4-3 Ma). This would have meant the surface would have been above the local equilibrium line altitude (presently ranging between 400 - 1850 m a.s.l. (Box et al., 2004)), removing it from the full effects of warm-based glaciation during the Late Pliocene/Early Quaternary. With the onset of glaciation and development of selective linear erosion as the main method landscape development, these portions of the UPS would have become rapidly relict. Following their separation from the main GIS, they would have been subject to the development of local, protective, cold-based ice caps. In contrast, elements of the landscape lower than 1000 m a.s.l. at 4 Ma, such as the LPS, would have been subject to warm-based lowland glacial activity, characterised by intense areal scour, focused over low-altitude regions. Through time, the intensity of areal scour acting upon the LPS would have decreased as it was uplifted to ~1000 m a.s.l. by the present day (Figures 3.10 and 3.11). As glaciation progressed areal scour would have eroded new low lying areas. The continuing focusing of areal scour into narrow corridors would have led to the rapid development of glacial troughs, enhancing the abandonment of the high-level UPS during glacial cycles. This would have left it unmodified and effectively relict throughout much of the Quaternary.

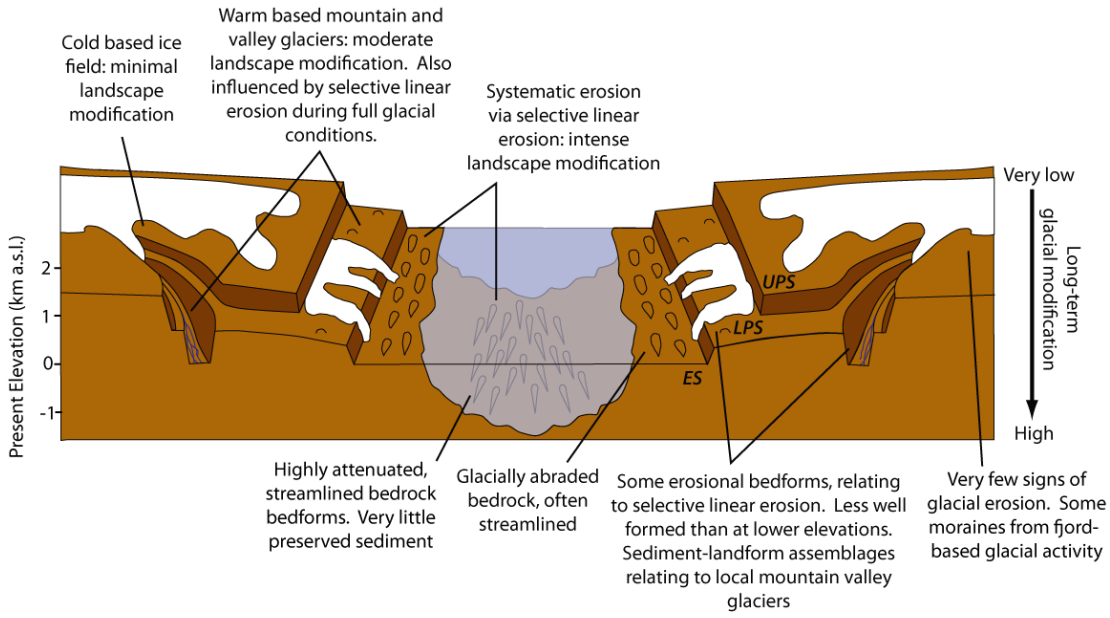

Figure 3.11. Schematic diagram illustrating the hypothesised landsurfaces present throughout the Uummannaq region, their relationship to the region's glacial history, and the resulting landscapes of erosion and deposition. The landsurfaces are the result of the region's uplift history (Bonow et al., 2006a, Japsen et al., 2006, Green et al., 2011).

The uplift of these surfaces, which spans the glacial history of the region, has aided landscape partitioning. Since the onset of uplift of the LPS (4.5±2.5 Ma) and glaciation (4 Ma), fjords of >2000 m have developed (1000 m above sea-level; ~ 1000 m below sea-level). This relates to average incision rates of 0.5 mm yr^{-1} over the period. This value represents an absolute minimum estimate, for a number of reasons: (1) following the onset of glaciation (4 Ma), much of the time has been characterised by warm interglacial conditions. During these periods erosion would have been reduced in comparison to glacials; (2) during glacial periods, only a small proportion of time would have been characterised by widespread warm-based ice conditions (conducive to intense erosion and incision). Much of the time during ice sheet build-up and expansion would have been instead characterised by cold-based ice conditions. Both of these factors are difficult to accurately quantify, but are likely to increase the average incision rate (during warm-based glacial conditions) to >2 mm yr^{-1}. Both of these factors are difficult to accurately quantify, but are likely to increase the average incision rate (during warm-based glacial conditions) to >2 mm yr^{-1}. This compares with modelled results of erosion rates that range from 3 mm yr^{-1} (Jamieson et al., 2008) to 10 mm yr^{-1} (Kessler et al., 2008). It should, however, be noted that the fjord incision in this study has been driven by periods of uplift (Japsen et al., 2006, Bonow et al., 2007) as opposed to the model results.

Recent work from western Scandinavia has investigated the erosional history of the glaciated landscape (Steer *et al.*, 2012). Their analysis of sediment volumes offshore of the Scandinavian coastline demonstrated that only 35-55% of the sediment can be explained by highly focused fjord erosion. The remaining 45-65% of sediment therefore must have been formed through erosion of high-level surfaces now containing plateau ice-fields. This therefore means that these surfaces have experienced extensive glacial processes, with 100 – 400 m of erosion from these surfaces (Steer *et al.*, 2012). This is in contrast to previous work suggesting that selective linear erosion has been the overwhelming landscape modifier in western Scandinavia. This is also in contrast to research from this study, which hypothesised that high-elevation surfaces experienced minimal modification by glacial activity. However, the uncertainties regarding the uplift history of the region makes it difficult to ascertain the full extent of erosional lowering of these higher level surfaces.

As discussed previously, the appearance of areally scoured terrain throughout the Uummannaq region is highly variable, differing with bedrock geology. The areally scoured topography in the south of the Uummannaq region is similar in morphology to the

weathered gneissic etch surface identified in Disko Bugt (Bonow et al., 2006b). This surface is characterised by bedrock roches moutonnées, tors, and clefts which have been exhumed from overlying rocks (Bonow et al., 2006b). It appears likely that the Archean etch surface found in Disko Bugt is also present in the southern half of the Uummannaq region. This has been exposed by fluvial and glacial processes which were triggered by Neogene uplift. In contrast, surficial geology in the northern part of the Uummannaq region is characterised by the Palaeoproterozoic Nukavsak formation (Steenfelt et al., 1998), which overlies the buried etch surface. Some outcrops thought to be an expression of this etch surface were seen on the borders of Rink Fjord, however, their exposure is very limited.

Though clearly glacially modified, Bonow *et al*. (2006b) argue that the landforms developed in the Disko Bugt etch surface have inherited their first-order morphology from the deeply weathered Archean surface, proposing that, once re-exposed, this 'hilly relief' has been only slightly glacially altered to produce areally scoured terrain. This interpretation has important implications for the proposed formation processes of areally scoured terrain both in southern Uummannaq, and in other formerly glaciated areas. Though the presence of a hilly palaeo-surface is unlikely to be a pre-requisite for 'knock and lochan' style terrain, Bonow *et al*.'s (2006b) hypothesis means that bedrock structure is an important control upon bedform development. This is in agreement with work that suggests that bedrock structure exerts a strong control upon bedform morphology in areas of areal scour (Lindstrom, 1988, Roberts et al., 2009, Krabbendam and Glasser, 2011; Chapter Five, this study). This is validated by evidence from this study (see Chapter Five), in which bedrock lithological variability controls bedform morphology (Figures 3.6c and 3.9d). However, though our understanding of the importance of bedrock structure upon bedform morphology is progressing, knowledge of palaeo-surfaces and their impact upon bedform development is lacking.

The preservation of the etch surface throughout the Uummannaq region is a result of differential glacial modification. Areas at low elevations (below 400 m a.s.l.) are more highly modified that those at higher elevations (1000 m a.s.l.) due to the duration of ice cover, ice thicknesses, and the intensity of glacial scour. Low elevation surfaces bordering fjords are ice covered for longer periods, and by thicker ice than those at higher elevations. Therefore erosion is far more intensive, allowing the production of well streamlined bedforms (Roberts and Long, 2005), such as those seen between Store Gletscher and Ikerasak.

Conversely, areas of high elevation areal scour are less frequently subjected to glacial action, and are less heavily scoured as ice cover is thinner.

3.6. Conclusion

New high resolution mapping from remote sensing and field observations has been undertaken throughout the Uummannaq region in order to classify its glacial and non-glacial landscapes. The Uummannaq region is characterised by a patchwork of glacial landsystems, formed over several million years through glacial erosion of contrasting intensity. The broad pattern of landscape distribution fits with accepted models of ice sheet subglacial thermal organisation, and is dominated by corridors of intense selective linear erosion. Through time, over-deepening of a coalescent fjord system has created conditions ideal for the development of the UISS during glacial periods. High-level areas are relict from warm-based glacial activity and have been protected under cold-based ice fields. Due to the intense draw down of coalescent ice into the Uummannaq Trough, areas peripheral to the UISS trunk zone were starved of active ice sheet ice, and instead were protected by cold-based and poly-thermal ice fields during glacial periods.

Switches in first-order geology through the region have led to an increase in fjord width in the outer fjord region, which is indicative of an efficient fjord system. This has encouraged outlet glacier convergence, promoted fast ice flow, and ultimately led to UISS onset. A similar geological control upon ice stream system onset has been reported from other areas of Greenland, suggesting that the transition from resistant to less-resistant geology is a key factor in producing large areas of ice streaming. Through integration of previously developed tectonic uplift models with the known onset of glaciation in West Greenland, it has been possible to develop our understanding of the impact of uplift upon glaciation. Since the onset of glaciation (4-3 Ma), the UPS would have been above the lower limit of warm-based glacial erosion, therefore sustaining minimal glacial modification. The impact of glacial erosion upon the LPS has decreased through time, as further uplift events increased its altitude. Areas lower than 1000 m a.s.l. have remained within the limit of warm-based glacial activity, and display evidence of extensive glacial modification. Combined, these processes of long-term uplift, glacial erosion and protection, and spatial variability in erosion intensity have produced a highly partitioned landscape. As a result of these processes, there exists a modification continuum between highly modified trough floors, and well preserved plateaux surfaces on the UPS. As outlined above, these are

separated by a series of other surfaces (LPS, high-level etch surface, low-level etch surface) which display increasing levels of modification. This study has developed a model to integrate the hypothesised variations subglacial thermal regime, uplift history, and regional first order geology. This provides an important development for explaining glacial landsystem distribution throughout this region.

CHAPTER FOUR

Ice stream dynamics during the last glacial maximum in the northern sector of the Uummannaq Ice Stream System, West Greenland

Abstract

The Uummannaq ice stream system (UISS) was a convergent cross-shelf ice stream system that operated in West Greenland during the Last Glacial Maximum (LGM). This chapter presents new evidence to constrain the geometry and evolution of the northern sector of the UISS and considers the factors controlling its dynamic behaviour. Geomorphological mapping, terrestrial cosmogenic nuclide (TCN) exposure dating, and radiocarbon dating constrain LGM warm-based ice stream activity in the north of the system up to 1400 m a.s.l. Intervening plateaux areas either remained ice free, were covered by cold-based icefields, or by thin ice-sheet ice. Beyond the outer fjords, topography forced ice flow southwards into the Uummannaq Trough, where it coalesced with ice from the south, and formed the trunk zone of the UISS.

Deglaciation of the UISS began at 14.9 cal. kyr BP. Rapid retreat from the LGM limit was forced by an increase in air temperatures and rising sea-level, enhanced by the bathymetric over-deepening of the Uummannaq and Igdlorssuit Sund troughs. Ice reached the present fjord confines in northern Uummannaq area by 11.6 kyr and experienced an ice marginal stabilisation in Rink-Karrat Fjord until 6.9 kyr. It remained stable due to topographic constriction and bathymetric shallowing despite high air temperatures and oceanic warming. In the neighbouring Ingia Fjord, and Store Gletscher to the south, this did not occur. Following this period of stability during the Holocene Thermal Maximum, ice within Rink-Karrat Fjord retreated, reaching approximately the present ice margin after 5 kyr, during the Neoglacial. The presence of a major ice stream within a mid-fjord setting during the mid-Holocene is in direct contrast to records of other ice streams throughout West Greenland, which suggest ice had retreated beyond its present margin by 9-7 kyr. This demonstrates the potential importance of topographic control on calving margin stability, and its ability to override climatic forcing.

4.1. Introduction and rationale

Large ocean terminating outlet glaciers play a vital role in moderating the behaviour of Greenland Ice Sheet (GIS), as indicated by recent rapid changes in outlet glaciers dynamics (e.g. Howat et al., 2007, 2008, 2011, Rignot et al., 2011, Thomas et al., 2009, 2011, Joughin et al., 2012). These current changes are typified by marginal thinning and increased discharge via calving (Howat et al., 2007) and dynamic outlet glacier behaviour has been closely linked to increases in air and ocean temperature, though a widely applicable causative process is yet to be understood (Thomas, 2004, Howat et al., 2008, Nick et al., 2009, Vieli and Nick, 2011). This lack of process understanding, and short record of glacier behaviour (<20 years) makes accurate prediction of outlet glacier response in a changing climate challenging. In order to provide a longer-term record of outlet behaviour, recent work has focussed on understanding of large ice streams and their influence upon the Greenland Ice Sheet (GIS) over thousand year timescales. New constraints upon ice stream extent, thickness, and deglacial behaviour from the Last Glacial Maximum (LGM) to present have been established since the early 2000's both onshore (Bennike and Bjorck, 2002, Hakansson et al., 2007a, 2009, Roberts et al., 2008, 2009, 2010, 2013) and offshore (Ó Cofaigh et al., 2004, 2013a, 2013b, Evans et al., 2009, Bauer, 1968), and these have provided evidence for the existence of large ice streams across the West, Northeast and East Greenland continental shelves throughout the LGM (Lykke-Andersen, 1998, Ó Cofaigh et al., 2004, 2013a, Evans et al., 2009, Bauer, 1968).

In Greenland, it is thought that large ice streams developed through the coalescence of individual outlet glaciers in fjord settings in the coastal zone resulting in convergence and flow onto the continental shelf. These large-scale, coalescent ice streams systems are likely to have dominated drainage from the GIS throughout Quaternary glaciations particularly in favourable topographic or geological settings (Swift et al., 2008, Roberts et al., 2010, 2013). Based upon the presence of cross-shelf submarine troughs, it has been hypothesised that six such palaeo-ice stream systems controlled West GIS behaviour during the LGM and previous glacial periods (Roberts et al., 2010). Despite the increase in research, evidence of ice stream activity from these regions is often fragmentary and thus far few studies have been unable to provide complete on and offshore reconstruction of LGM to present ice stream behaviour. Due to their hypothesised size, ice flux, and number, ice streams of this scale must be understood in order to accurately reconstruct ice sheet configuration during

previous glacial periods and to understand ice sheet interactions with sea-level, climate, and topography.

This paper presents evidence from the northern sector of the Uummannaq Ice Stream System (UISS), central West Greenland. The aims of this paper are: (i) to present new terrestrial geomorphological and geochronological evidence from the northern sector of the UISS, in order to reconstruct its LGM geometry and subsequent evolution; (ii) to use these data in conjunction with evidence from offshore and the southern sector of the UISS to understand shelf-wide ice stream dynamics during deglaciation.

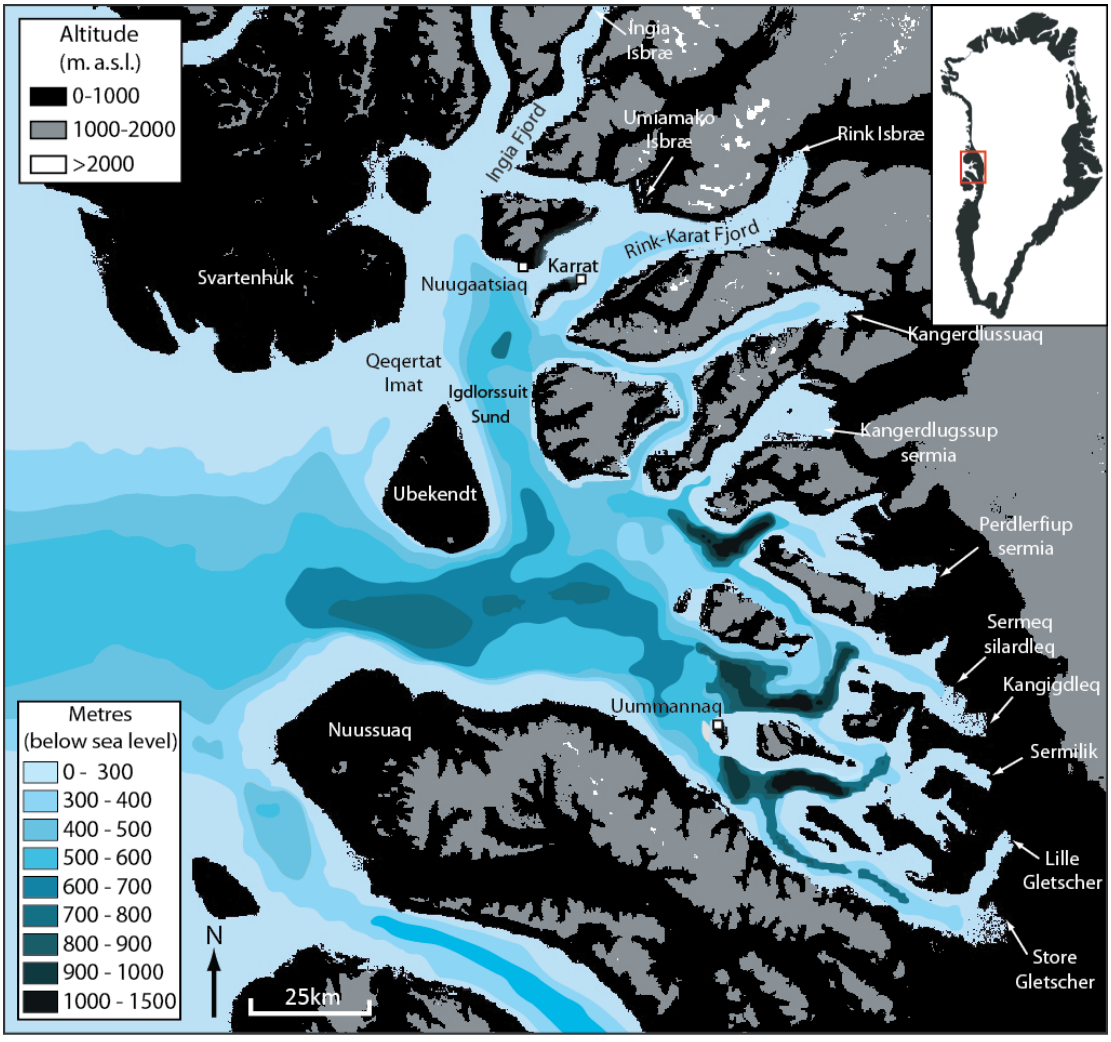

Figure 4.1. Topographic and bathymetric overview of the Uummannaq region, with key locations marked. Note the higher average altitude of land masses in the north of the region, and the shallow Qeqertat Imát north of Ubekendt Ejland, in comparison to the deep Uummannaq Trough. Bathymetric depths are solely from IBCAO data (Jakobsson et al., 2008).

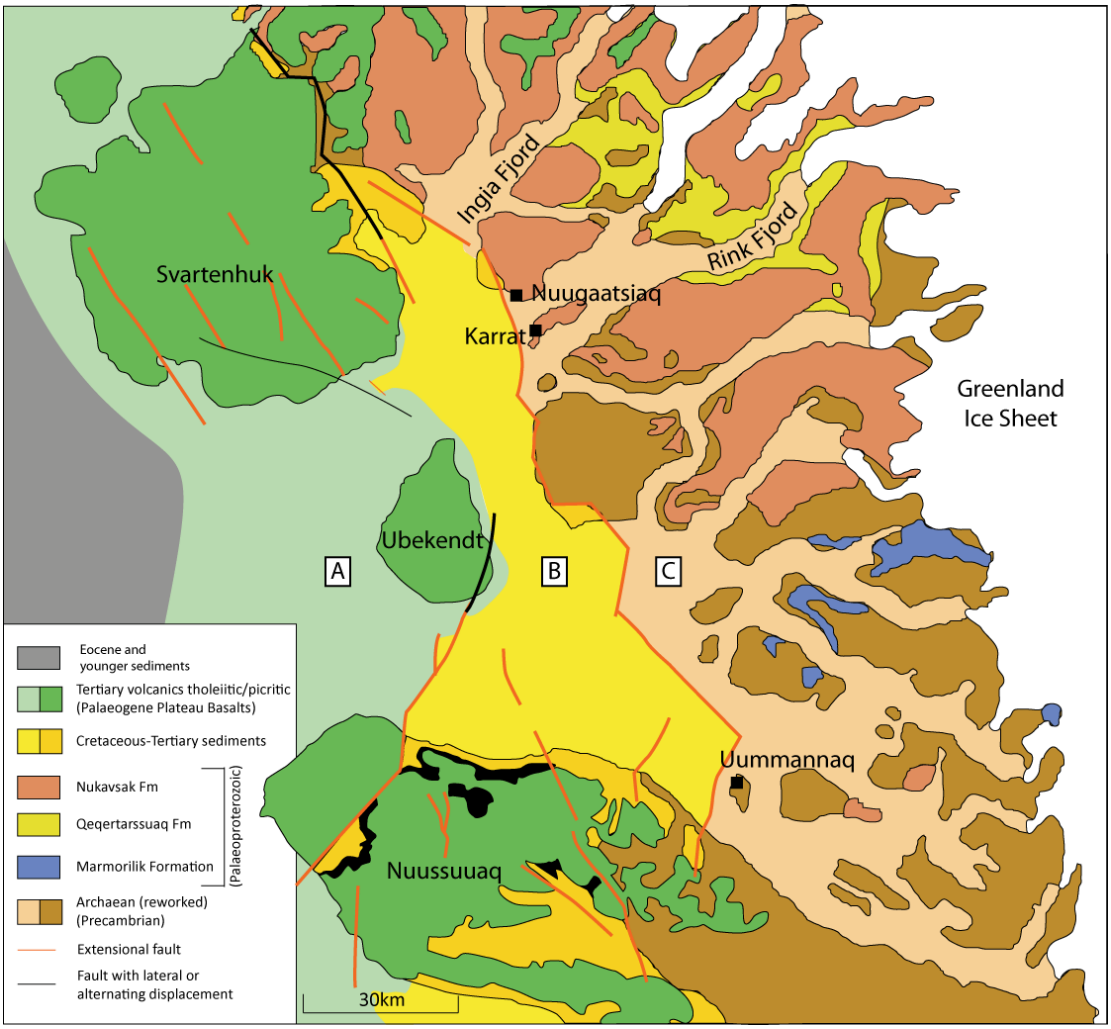

Figure 4.2. Map of the Uummannaq region showing dominant bedrock geology (adapted from Steenfelt et al., 1998. The three distinct geological regions (A, B, and C) can be seen, separated by north to south trending faults (adapted from Steenfelt et al., 1998).

4.2. The Uummannaq Region

4.2.1. Topography and geology

The Uummannaq region covers an area of ~25,000 km^2 and is highly mountainous, with summits reaching >2000 m a.s.l. (Figure 4.1). The region is bounded to the north and south by the peninsulas of Svartenhuk and Nuussuaq respectively (Figure 4.1). These landmasses form large topographic barriers, which confines the flux of ice and water from the inner Uummannaq region through the narrow passages to the north and south of Ubekendt Ejland. Within this landscape, the regional-scale topography is characterised by a series of deep coalescent fjords, broadly running east to west (Figure 4.1). The fjord heads are occupied by marine-terminating outlet glaciers which drain the central west GIS. The fjords

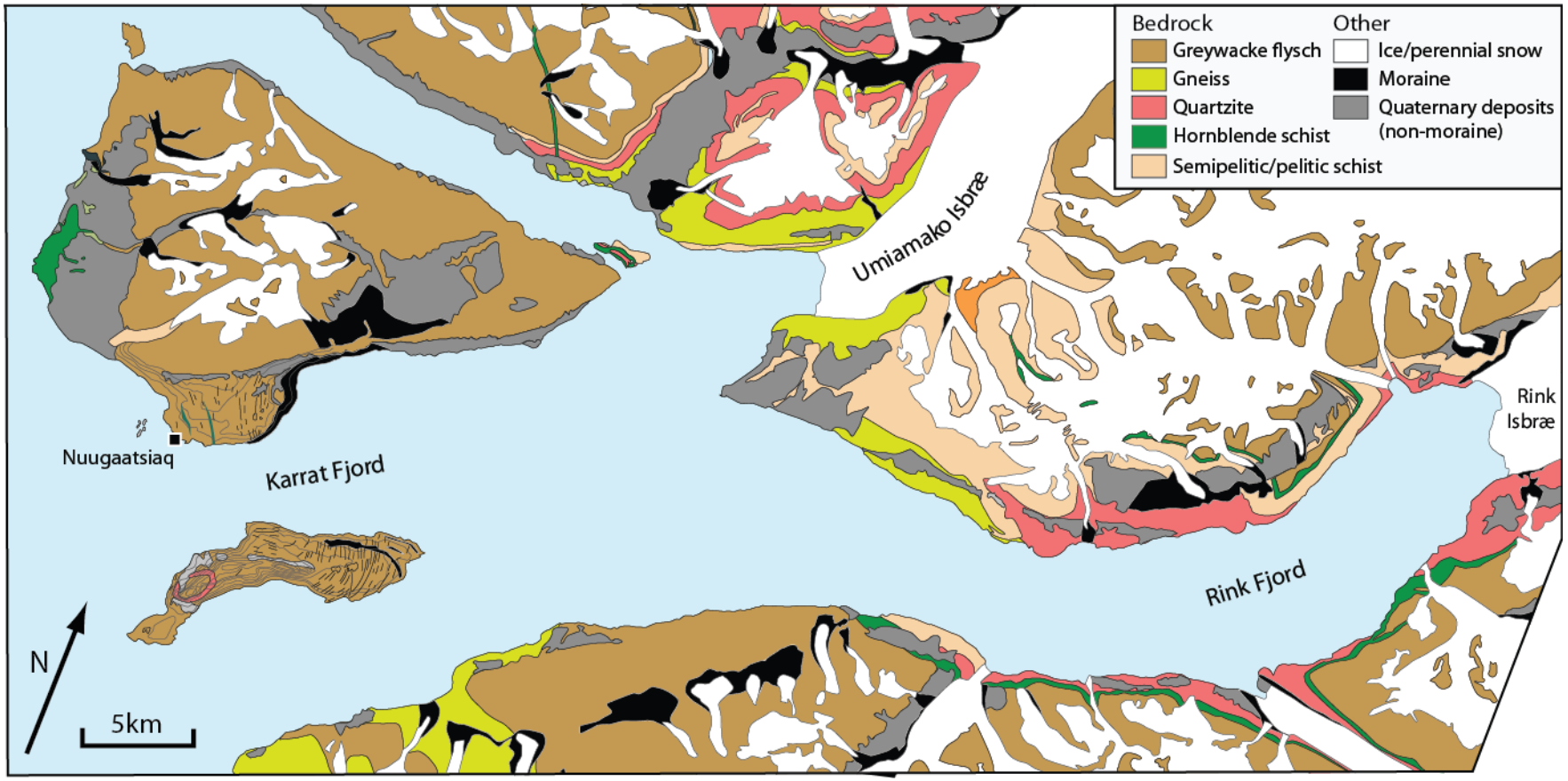

Figure 4.3. Geological map of the northern Uummannaq region, showing Rink, Karrat, and Umiámáko Fjord (Henderson and Pulvertaft, 1987b).

are of variable depth, with the majority reaching at least 500m, and some reaching over 1100 m, and are interspersed with numerous sills and areas of localised shallow bathymetry.

Central West Greenland currently has the highest concentration of outlet glaciers in Greenland (Reeh, 1985, Velicogna and Wahr, 2006). The Uummannaq region contains 11 major outlet glaciers of varying size and discharge, the largest of which are Rink Isbræ in the north and Store Gletscher in the south. Respectively these drain 10.5-16.7 $km^3 a^{-1}$ and 13.2-17.5 $km^3 a^{-1}$ of ice that is calved into the ocean (Table 4.1) (Bauer et al., 1968, Carbonnell and Bauer, 1968, Rignot and Kanagaratnam, 2006). Variability in subglacial topography, width, and drainage basin size is reflected in the variable ice flux they produce. Subglacial ice sheet topography in areas south of Kangerdlugssup Sermia (Figure 4.1) is typically <700 m a.s.l. (Bamber et al., 2001). However, the northern part of the Uummannaq region is bounded by an extensive subglacial mountain range at ~72°N (Bamber et al., 2001). The topography of this area is >900 m a.s.l., and this high terrain persists for at least 200 km inland, partially restricting the influx of ice from the north into the northern Uummannaq region. The geology of the region is characterised by three distinct geological areas, separated by north to south orientated faults (Figure 4.2). The east of the region is underlain by Precambrian gneisses (Archean orthogneisses - ~2800 Ma), and forms the inner fjords (Garde and Steenfelt, 1999) (Figures 4.2 and 4.3). These are overlain by Palaeoproterozoic sediments (~2000 Ma) in the north (Kalsbeek et al., 1998, Bonow et al., 2007). The centre of the region is formed of Cretaceous-Tertiary marine mudstones and sandstones (Pedersen and Pulvertaft, 1992, Dam et al., 2000, Henriksen et al., 2000). Finally, to the west are a series of Palaeocene basalts (61-52.5 Ma), which lie on- and offshore, forming Ubekendt Ejland, Svartenhuk, and the western half of Nuussuaq (Henriksen et al., 2000).

4.2.2. Current palaeo-glaciological understanding of the Uummannaq system

Until recently, the glacial history of much of the Uummannaq region was poorly known, with previous work showing the Uummannaq region to be dominated by intensely focused selective linear erosion and areally scoured terrain, with smaller isolated occurrences of valley glaciers and cold-based ice caps (Sugden, 1974). A number of small, latero-frontal moraines were previously mapped (Henderson and Pulvertaft, 1987b), thought to relate to historical advances of local valley and mountain glaciers. Based upon moraines, trimline

elevations, and blockfields in the Svartenhuk region, a reconstructed LGM ice sheet ice thickness of 450 m a.s.l. was proposed for the northern Uummannaq region (Kelly, 1985), suggesting that ice reached just beyond Ubekendt Ejland. This estimate is considerably lower than reconstructed LGM ice thicknesses in other areas of West Greenland which are >750 m a.s.l. (Rinterknecht et al., 2009, Roberts et al., 2009). Based upon the convergent fjord system, and densely clustered outlet glaciers, it has recently been proposed that the region hosted a large ice stream system (the UISS) during the LGM (Ó Cofaigh et al., 2013a, 2013b, Roberts et al., 2013). The UISS extended to the continental shelf edge at the LGM, depositing sediment on the outer shelf, at a trough mouth fan. This is supported by offshore bathymetry which displays evidence for a deep (>600 m) trough, containing ubiquitous, elongate bedforms indicative of fast flowing ice (Ó Cofaigh et al., 2013b). Roberts et al. (2013) proposed the UISS to be formed of three component parts: (1) a zone of individual outlet glaciers, present within a highly convergent fjord pattern; (2) a confluent onset zone at the head of the Uummannaq Trough (southeast of Ubekendt Ejland), where individual outlet glaciers coalesced, triggering UISS onset; and (3) a single channel ice stream flowing offshore to the shelf edge.

Geomorphological data, surface exposure ages, and modelling have demonstrated that at the LGM the UISS ice reached a minimum of 1266 m a.s.l. in fjord head regions throughout the south of the Uummannaq region (Roberts *et al.*, 2013), at least double that of earlier estimates from the northern Uummannaq region (Kelly, 1985). Initial retreat from the Uummannaq trough mouth fan was underway by 14.9 cal. kyr. BP (Ó Cofaigh et al., 2013b), reaching the outer fjords by 11.4 kyr, and the present southern fjord margins by 8.7 kyr (Roberts *et al*., 2013). This retreat is thought to have been driven by rising eustatic sea-level following the LGM and air temperatures, the influx of warmer oceanic water, and topographic pinning throughout the inner fjords (Ó Cofaigh et al., 2013b, Roberts et al., 2013). Despite this new chronology for the southern UISS, the glacial history of the northern Uummannaq region remains largely constrained by a single radiocarbon date on eastern Svartenhuk, indicating deglaciation at 10.5 cal. kyr BP (Bennike, 2000). As a result, the response of the GIS in the northern Uummannaq region to climate forcing, and its relationship to the southern sector remains unknown.

4.2.3. Northern Uummannaq region

The northern sector of the Uummannaq region includes fjords containing the outlet glaciers Ingia Isbræ, Umiámáko Isbræ, Rink Isbræ, and Kangerdlugssup Sermerssua which discharge ice to the north of Ubekendt Ejland, into Igdlorssuit Sund (Figure 4.1). During the LGM and previous glaciations, these outlet glaciers would have extended beyond their outer fjord confines, becoming confluent to the northeast of Ubekendt Ejland (Roberts *et al.*, 2013). Bathymetric data indicates a shallow sill to the north of Ubekendt Ejland (water depths of <100 m). This would have significantly reduced ice flow between Svartenhuk and Ubekendt Ejland (Roberts *et al.*, 2013), instead forcing ice southwards into Igdlorssuit Sund. Here it would have become coalescent with ice from the southern Uummannaq region, and flowed offshore into the Uummannaq Trough (Roberts *et al.*, 2013).

Fjord Name	Mouth location	Snout location	Orient (°)	Length (km)	Width at SL (km)	Plateau height (m a.s.l.)	Max. water depth (m)[a]	Max ice flux (km^3 yr^{-1})[b]
Northern Fjords								
Ingia Fjord	71.73°N 53.32°W	72.00°N 52.70°W	213.4	38.5	4.5	1444	-	1.1
Rink-Karrat Fjord	71.40°N 53.07°W	71.73°N 53.65°W	238.1	63.6	6.2	1791	1108	11.8
Kangerdlug.	71.38°N 53.00°W	71.45°N 51.83°W	263.2	61.7	4.2	1894	570	2.4
Southern Fjords								
Kangerdlua.	71.13°N 52.30°W	71.25°N 51.52°W	245	34.9	5.7	1671	770	0.3
Perdlerjiup Kangerdlua	71.05°N 52.00°W	70.98°N 50.95°W	282	42.5	5.5	1388	1246	1
Itivdliarssup Kangerdlua	70.98°N 51.97°W	70.80°N 51.00°W	302.1	42.5	5.6	1332	844	7.6
Sermigdlip Kangerdlua	70.7°N 51.52°W	70.62°N 50.63°W	291.5	38.2	4.4	1180	1287	2.6
Qarajaqs Isfjord	70.68°N 52.28°W	70.37°N 50.60°W	302.7	75.4	6.9	1308	956	17.8

[a]Data from GEBCO_08 Grid and Hareø-Prøven bathymetric charts
[b]Data from (Bauer et al., 1968, Carbonnell and Bauer, 1968, Rignot and Kanagaratnam, 2006)

Table 4.1. Fjord locations, characteristics and outlet glacier ice flux throughout the Uummannaq region. Outlet glacier locations are identified in Figure 4.1

This study focuses upon two fjords in the northern Uummannaq region, Rink-Karrat Fjord (including Rink Fjord, Karrat Fjord, and Umiámáko Fjord), and Ingia Fjord (see Figures 4.1 and 4.4). The fast-flowing outlet Rink Isbræ drains into the head of Rink-Karrat Fjord and is

the highest discharging outlet glacier in the northern Uummannaq region. Rink Fjord is joined by Umiámáko Fjord and becomes Karrat Fjord. Rink-Karrat Fjord is a 6-10 km wide, over-deepened glacial trough, with depths reaching 1200 m close to the present ice margin. Water depths decrease to <680 m south of Karrat Island, and reach a shallow sill at <200 m north of Karrat Island. The fjord is bounded to the north and south by mountainous terrain and plateaux up to 2000 m a.s.l., with near-vertical fjord walls. High-level surfaces foster small icecaps, icefields, and individual cirque and valley glaciers. Ingia Fjord is a narrow (3-6 km wide) fjord into which Ingia Isbræ calves, with a discharge of 1.1 km^3 yr^{-1}, an order of magnitude less that Rink Isbræ (10.5-16.7 km3 yr-1; Rignot and Kanagaratnam, 2006). Fjord walls are near vertical, and land surfaces between fjords contain high-level dissected plateaux ice fields up to 2000 m a.s.l. Fjord depths through Ingia Fjord are currently unknown.

4.3. Methods

4.3.1. Geomorphological mapping

Initial geomorphological mapping was carried out using 1:50,000 topographic maps, geological maps (Henderson and Pulvertaft, 1987a, Henderson and Pulvertaft, 1987b), 1:150,000 aerial photographs (Kort and Matrikelstyrelsen) and ASTER GDEMs. Ground-truthing was carried out in the Northern Uummannaq region (Figure 4.1), where features of glacial erosion were mapped in order to allow palaeo-ice flow reconstructions (Glasser and Warren, 1990, Roberts and Long, 2005). Erosional forms mapped and noted include small-scale friction cracks (Harris Jr, 1943), striae (Boulton, 1974a, Iverson, 1991, Benn and Evans, 2010), and p-forms (Dahl, 1965). Measurement of their orientation can be used to interpret former ice-flow directions. Large-scale features of glacial erosion mapped included roches moutonnées (asymmetric bedrock protrusions with abraded stoss faces and plucked lee faces) (Sugden et al., 1992b, Benn and Evans, 2010) and whalebacks (symmetrical bedrock features with abraded stoss and lee faces) (Sugden and John, 1976, Evans, 1996a).

Moraines and trimlines were mapped in order to both constrain glacier geometry. Ice-marginal moraines are depositional features, recording the former margins of glaciers, and are found as end and lateral moraines (Benn and Evans, 2010). End moraines develop at the glacier snout, representing terminal (the maximum limit of glaciation) and recessional

(forming from ice-front stability or readvance during retreat) features. In this study, moraines were identified in the field based upon their position, and arcuate form.

Trimlines are boundaries which mark the maximum altitude to which glacier ice has eroded a hillslope (Ballantyne and Harris, 1994). In the field, trimlines were seen as mountain-side boundaries between glacially scoured bedrock (displaying the small- and large-scale features of glacial erosion mentioned above) and higher-altitude frost weathered detritus. The boundary itself can be distinct (change over several metres), or more gradual (change over several tens of metres), depending upon effectiveness of glacial erosion and mass-movement processes following trimline formation (Thorp, 1981, Ballantyne, 1997). Trimlines have a long history of study (Sollid and Sørbel, 1979, Nesje and Dahl, 1990, Nesje and Sejrup, 1988), and thought to relate to the upper palaeo-ice surface, or an englacial thermal boundaries (Fabel et al., 2012). This geomorphological mapping allowed regional ice thicknesses to be calculated (e.g. Kelly, 1985, Roberts et al., 2009). Glacial, periglacial, and fluvial landforms were mapped using a Garmin GPS 60, to accurately represent their form, length and profile (horizontal error of ±5 m, elevation error of ±5-10 m). Bathymetric estimates are derived from the local Hareø-Prøven bathymetric charts.

4.3.2. Terrestrial cosmogenic nuclide (TCN) dating

4.3.2.1. Rock sampling for terrestrial cosmogenic nuclide dating

Samples were taken for TCN dating from bedrock and erratic boulders at a variety of altitudes in order to constrain LGM ice stream geometry (Fabel et al., 2012). Bedrock samples were taken from areas displaying clear evidence of glacial erosion (e.g. roches moutonnées or whalebacks), or from surfaces displaying striae or glacial polish to minimise the likelihood of cosmogenic inheritance (Gosse and Phillips, 2001). Samples from erratic boulders were taken when the boulder demonstrated clear evidence of subglacial erosion (i.e. edge rounded appearance, with no sharp edges, striated). Samples for surface exposure dating of boulders from moraines can suffer a series of issues, including remobilisation and exhumation (Putkonen and Swanson, 2003). As a result they were largely avoided. Where possible, vertical sample transects were taken at altitudinal intervals of 100 m in order to provide an upper limit on warm-based ice. Samples returning ages younger than the LGM (<24 ka) suggest that erosive warm-based ice was active at that location during the LGM. Ages older than >24 ka would suggest warm-based, erosive ice

was not active at that sample location during the LGM. These ages mean that either: (a) the sample location remained exposed as a nunatak during the LGM; or (b) the sample was covered by unerosive, cold-based ice during the LGM (if dual isotope samples suggest a complex burial-exposure history). A vertical sample transect was achieved on Karrat Island, with samples across the island (KA2, 9, 10, 11, 15, 17, 18, 19), and partially achieved in inner Rink Fjord (KA3, 20, 23). However, though samples were taken, this transect was limited by the number of dates available to process. In order to create a deglacial chronology, samples were also taken in a flow parallel transect from Karrat Island to the present margin of Rink Isbræ. In order to date features indicative of major ice marginal events (e.g. moraines), samples were taken from abraded terrain either side of the feature. Due to the low-relief nature of moraines throughout the fjord, and the absence of crestline boulders, no boulder samples were taken from moraines. Samples were collected using a Stihl TS400 disc cutter and sampling procedures followed Gosse and Phillips (2001) and Roberts *et al*. (2008, 2013).

4.3.2.2. Terrestrial cosmogenic nuclide sample preparation

The sample preparation and $^{10}Be/^{26}Al$ measurement procedures used in this study are described in detail in by both Wilson *et al*. (2008) and Ballantyne *et al*. (2009). A 250 µg Be was added as a carrier to each sample in this study. Inherent Al concentrations in quartz were determined with an ICP-MS at the NERC Cosmogenic Isotope Analysis Facility (CIAF), with a relative standard uncertainty of 3%. An aluminium carrier was added to samples so that 2 mg Al per sample was reached. Samples KA12, KA16 and KA24 did not yield enough quartz to be processed for both ^{10}Be and ^{26}Al measurement. As a result, these are not included.

4.3.2.3. ^{10}Be and ^{26}Al measurements and exposure age calculation

The measurement procedures at the NERC AMS laboratory are described in detail in Maden et al. (2007) and Roberts et al. (2008). $^{10}Be/^{9}Be$ and $^{26}Al/^{27}Al$ ratios were measured with the 5MV NEC Pelletron accelerator mass spectrometer at the SUERC, as part of a routine Be and Al runs. ^{10}Be and ^{26}Al concentrations are based on $2.79 \cdot 10^{-11}$ $^{10}Be/Be$ and $4.11 \cdot 10^{-11}$ $^{26}Al/Al$ ratios for NIST SRM4325 and Purdue Z92-0222 standard respectively (see Dunai and Stuart, 2009). Exposure ages were calculated using the CRONUS-Earth online calculator (Balco et al., 2009, 2008) (Calibration data set name: North-eastern North America. Calibration wrapper version: 2.2-cal-dev. Objective function version: 2.2-dev. Age calculation version:

2.1. Muon calculation version: 1.1. Constants version: 2.2), to get ages based on a sea-level high-latitude production rate of 3.98±0.24 atoms g^{-1} yr^{-1} for the 'St' scaling scheme, according to for Briner et al. (2012). See Roberts *et al*. (2013) for a full description of this procedure. Attenuation correction for sample thickness uses an attenuation length of 160 g cm-2. Topographic shielding correction is determined using the ratio of the production rate at the obstructed site to the production rate at a site at the same location and elevation, but with a flat surface and a clear horizon (Gosse and Phillips, 2001, Balco et al., 2008). The exposure ages are not corrected for past geomagnetic field variations. Including a simple palaeomagnetic correction (Nishiizumi *et al.*, 1989) results in ages ~ 1% older ages than presented for the samples with an exposure age of ~ 10 kyr. Age determinations include a correction for atmospheric pressure related to the altitude, latitude and longitude according to the mean global surface atmospheric pressure field of the NCEP-NCAR re-analysis (www.cdc.noaa.gov/ncep_reanalysis/), but assume the standard atmosphere for geographical scaling of the production rate.

Paired ^{10}Be and ^{26}Al analysis was carried out on several samples (KA1-6) in order to test for complex exposure and shielding histories from high elevations (Gosse and Phillips, 2001). ^{26}Al/^{10}Be concentration ratios are not depleted with respect to surface production rate ratios within a one-sigma, and there is approximate concordance in ^{26}Al and ^{10}Be ages. All TCN ages are given in thousands of years (kyr), meaning thousands of years before sample collection; AD 2010 (Balco *et al.*, 2008). TCN data is presented following the guidelines outlined by Dunai and Stuart (2009), in order to allow the use of this data in the future.

4.3.3. Lake coring

A number of lakes > 2.5 m deep were identified from aerial photographs and chosen as targets for sediment coring. An initial series of cores were taken in order to establish the lake stratigraphy. Core samples to be used for laboratory analysis were taken using Russian-type (50cm) and Eijkelkamp Beeker-type (100cm). A Geotek Multi Sensor Core Logger (MSCL) was then used to record core properties. Linescan images were recorded using the MSCL's line scan camera. Magnetic susceptibility was measured using a Bartington point sensor (MS2E), and gamma density was measured using a Cs137 source.

4.3.4. Radiocarbon dating

Material for radiocarbon dating was sub-sampled from lake cores in Karrat Lake and Ingia Lake. Radiocarbon analysis was carried out by the NERC Radiocarbon facility (samples KAL1 and INL1). Results presented have been corrected to $\delta^{13}C$ VPDB‰ -25 using $\delta^{13}C$ values measured for each sample. The $\delta^{13}C$ values were measured on a dual inlet stable isotope mass spectrometer (Thermo Fisher Delta V) and represent the $\delta^{13}C$ in the original, pre-treated sample material. InL1 was composed of plant macrofossils and KA1 and SV1 of lake gyttja. Samples KAL1 and INL1 were sampled from above the contact with lower minerogenic clays and overlying organic lake gyttja in their respective cores. Radiocarbon ages are presented as a 2σ range of calibrated years before present (cal. yrs BP). Ages were calibrated using OxCal 4.2 and the IntCal09 calibration curve. The lakes samples do not lie within a carbonate catchment, and as such no reservoir correction was applied.

4.3.5. Bayesian analysis of deglacial chronology

In order to rigorously constrain the deglaciation of the northern UISS, Bayesian statistics are applied. This approach allows the integration of multiple pieces of chronological information, combining them in a probabilistic nature (Bronk Ramsey, 2008). This incorporates a series of pieces of chronological data, each with information about the distance from present ice margin (or more conventionally, depth down a sedimentary profile). Through Markov Chain Monte Carlo (MCMC) sampling, this forms a probability distribution of dates through the sequence (Gilks et al., 1995, Bronk Ramsey, 2009), expressed as age cumulative probability functions, representing the likelihood of each sample's age (Bronk Ramsey, 2009). Bayesian analysis of chronological sequences has widely been used to provide coherent frameworks for radiocarbon dates through sedimentary sequences (Gilks et al., 1995, Bronk Ramsey, 2009), however, it is not commonly used for constraining a deglacial chronology (Chiverrell *et al.*, 2013). Despite this, the principles of constraining a deglacial transect are similar to a sedimentary sequence, with distance from present ice margin substituted for depth through a profile. Their age probability distribution can therefore be used with their "stratigraphic" position (i.e. distance from ice margin) to constrain the age model. For this study, a Poisson Sequence has been used, as it allows for flexibility, permitting the depositional/retreat process to be inherently random (Bronk Ramsey, 2008), though with a given position for each age.

4.4. Results

Results are presented by fjord location: Rink-Karrat Fjord; and Ingia Fjord (Figure 4.4). Due to the complexity of the data from Rink-Karrat Fjord, this has been subdivided into four geographically distinct regions within the fjord: Inner Fjord; Qeqertarssuaq; Nuugaatsiaq; and Karrat Island (see Figure 4.4). Chronological results are presented in Figure 4.5.

4.4.1. Rink-Karrat Fjord: inner fjord

4.4.1.1. Geomorphology

In the inner fjord areas below 700-800 m a.s.l. are dominated by intense areally scoured terrain, displaying ubiquitous features of glacial erosion (roches moutonnées, p-forms, striae and glacially abraded surfaces) (Figures 4.4, 4.5a, and 4.5c). A poorly developed moraine was identified at ~740 m a.s.l., formed of sub-angular gravel with abundant erratic quartzite material (Figure 4.5b). Two sets of small (6-10 m in width, 2-4 m high, and at least 500 m in length), poorly developed lateral moraines were mapped on the spur between Rink and Umiámáko Fjords (Figure 4.6). Moraines record ice activity within Rink Fjord (R1 – R3, Figures 4.5d and 4.6), and are found running sub-parallel to one another, between 366 and 235 m a.s.l. The second set (Um1 – Um3) lies directly on the spur between the two fjords, running obliquely downhill from 192 to 137 m a.s.l. (Figure 4.6). All moraines are formed of coarse, sub-angular to sub-rounded diamictic material, comprising both local and erratic lithologies. No continuations of these moraines were observed in Umiámáko Fjord, probably due to the near vertical relief of the fjord walls. Striae mapped from bedrock surfaces below 400 m a.s.l. are sub-parallel to macro-scale fjord topography, recording ice flow northeast to southwest (Figure 4.5a). Striae directions from between Rink and Umiámáko Fjord show evidence for cross cutting flow across the spur, likely reflecting differential response of each margin during deglaciation. Above 800 m a.s.l., areal scour transitioned into heavily weathered and frost shattered bedrock. Surfaces between 1000 and 1400 m a.s.l. are dominated by frost shattering, but a number of small (<10m^2) flat, bedrock outcrops were found, displaying evidence for glacial abrasion (Figure 4.5e). Above 1400 m a.s.l., intact *in-situ* bedrock blocks become very rare, and the land surface characterised by autochonous blockfield (Figure 4.5f).

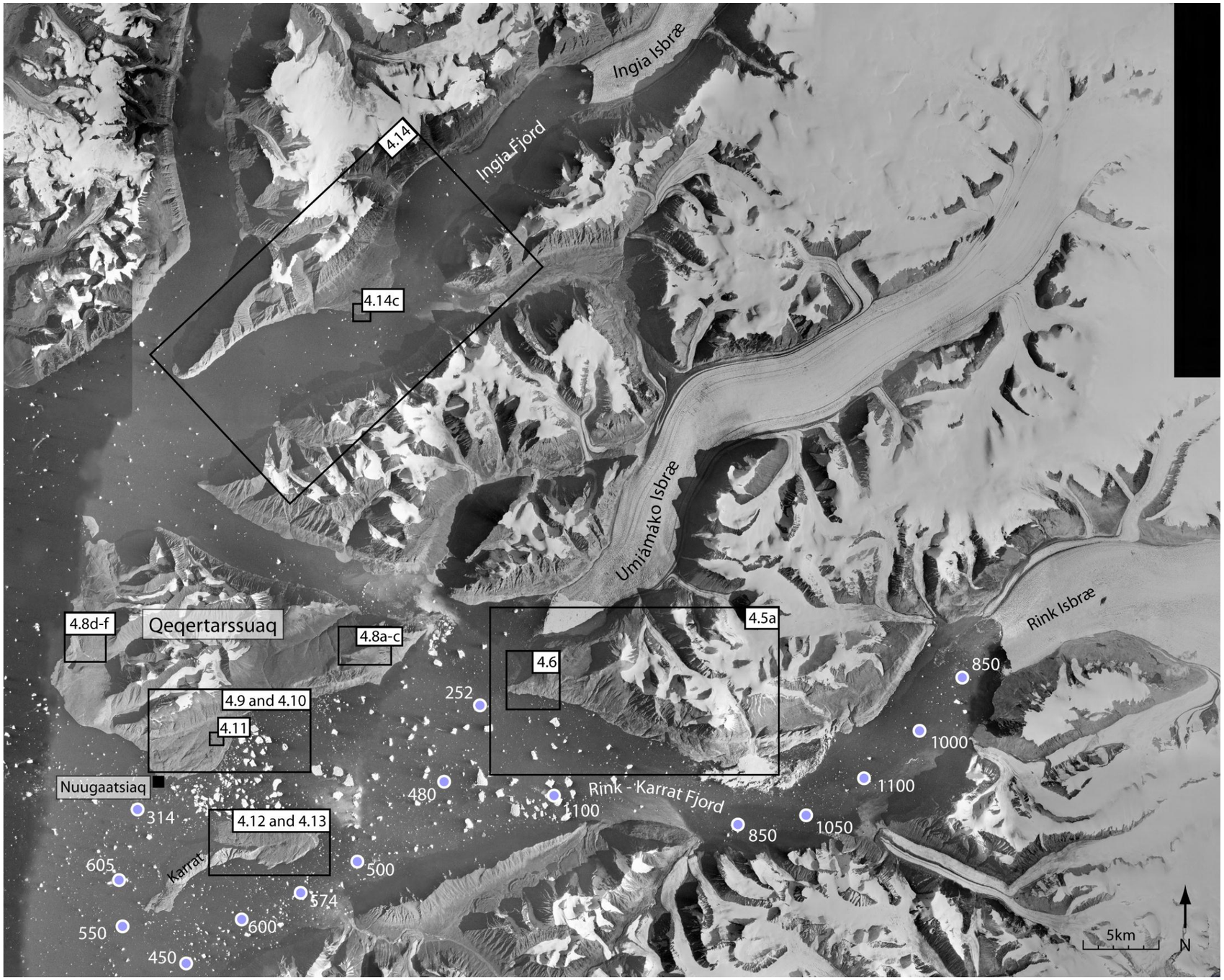

Figure 4.4. Aerial photograph of the study area in the northern Uummannaq region. The focus of this study was Rink – Karrat Fjord and Ingia Fjord, in the south and north of the image respectively. Boxes indicate the locations of other figures. Fjord depths are shown by blue filled circles (from Hareø-Prøven bathymetric charts).

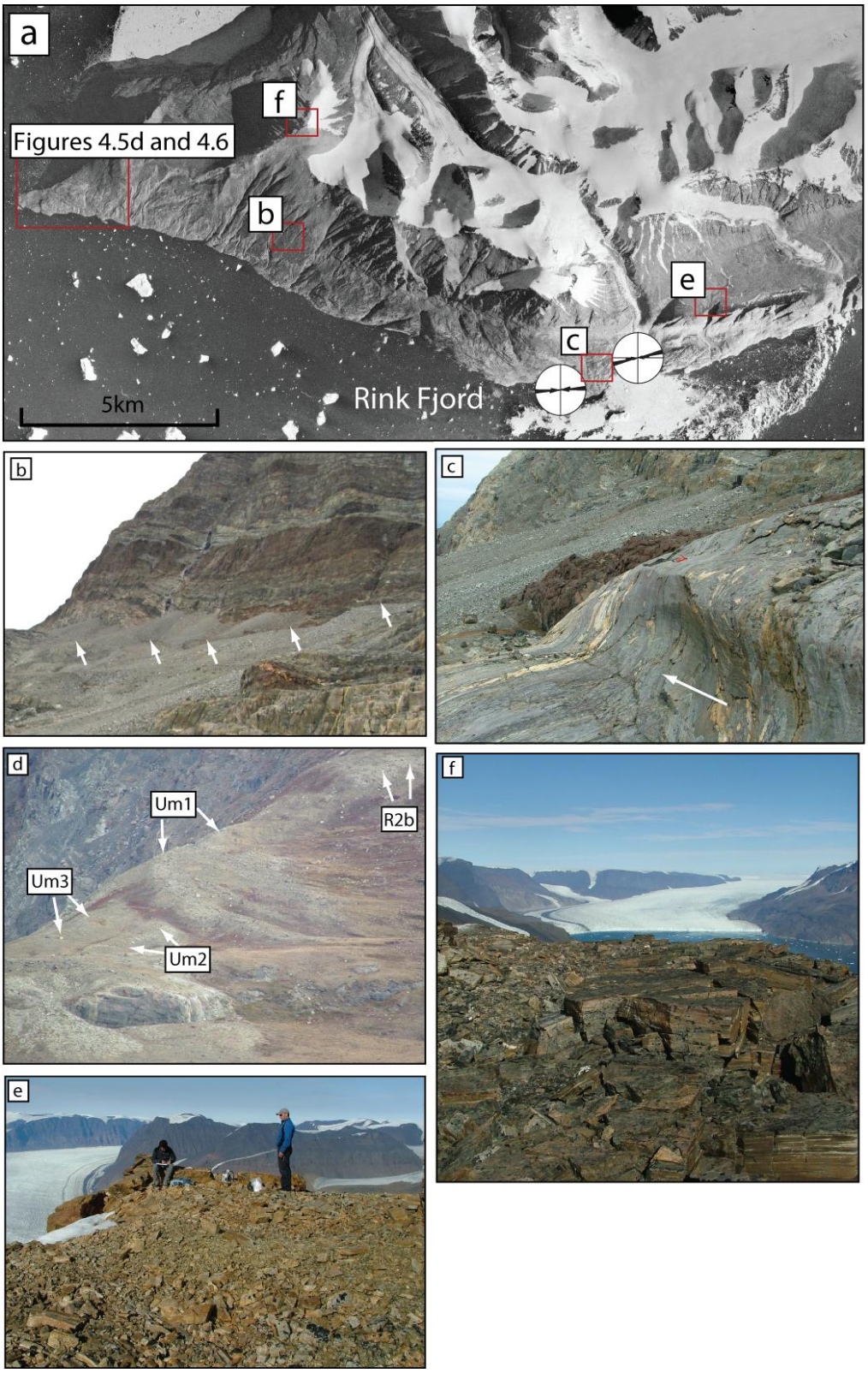

Figure 4.5. Plate of photographs from inner Rink-Karrat Fjord. (a) Aerial photograph showing an overview of inner Rink Fjord, with striae displayed (n=50 per rose diagram) (b) Fragmentary lateral moraine at 740 m a.s.l. in inner Rink Fjord (arrowed); (c) Striated, ice moulded roches moutonnées with lateral p-form arrowed; (d) Moraines Um1-3 and R3 (all arrowed) at the Rink- Umiámáko confluence (see Figure 4.6 for moraine location); (e) Autochonous blockfield at 1400 m a.s.l. in inner Rink Fjord. (f) Autochonous blockfield at 1900 m a.s.l. in inner Rink Fjord (Pyramid Stubben).

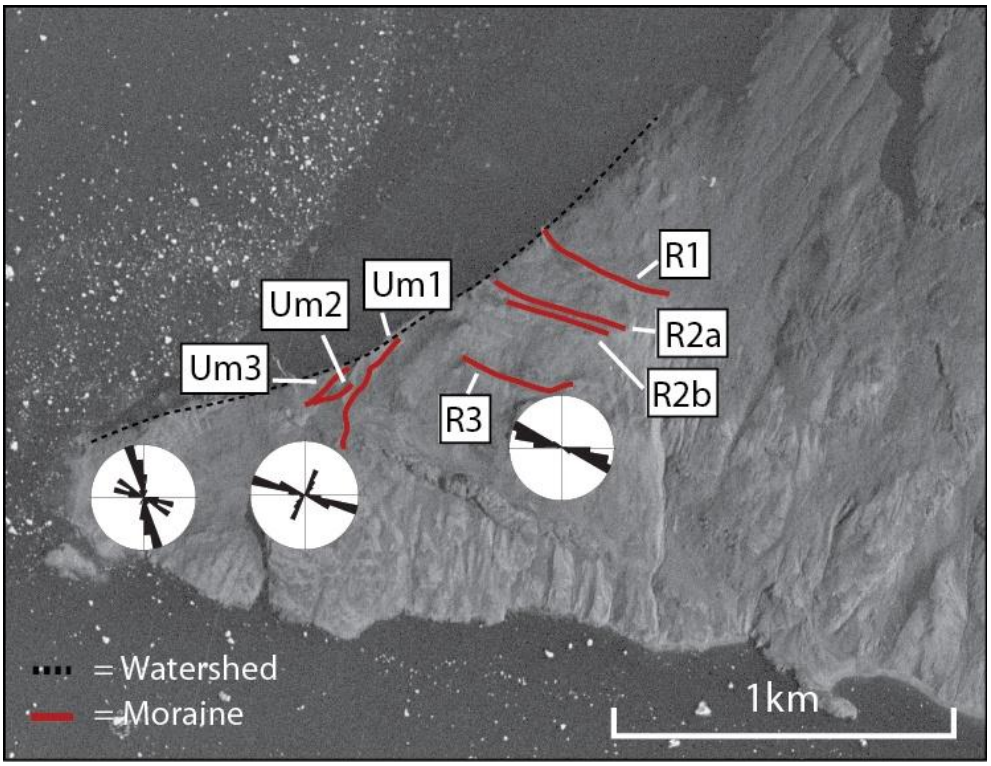

Figure 4.6. Aerial photograph of the spur between Rink and Umiámáko Isbræ (see Figure 4.4 for location). Two discrete sets of moraines were mapped in the field, with on corresponding to ice activity in Rink Fjord (R1-R3), and one to ice in Umiámáko Fjord (Um1-3). Rose diagrams show bedrock striae directions (n=50 per sample site).

4.4.1.2. Chronology

Two samples for TCN dating were taken at high elevations within the inner fjord, KA3 and KA5 (Figure 4.6, Table 4.2). KA3 was a glacially smoothed bedrock surface at 1400 m a.s.l., and returned ages of 18.9±1.9 ^{10}Be kyr (Table 4.3), and 22.5±1.4 ^{26}Al kyr (Table 4.4). KA5 was taken from an *in-situ* bedrock block found within an area of extensive autochonous blockfield at 1964 m a.s.l. This returned an age of 92.0±8.8 ^{10}Be kyr, and 96.1±2.9 ^{26}Al kyr, suggesting the surface had experienced minimal erosion during MIS4-2. Three low elevation TCN samples were taken from the inner fjord, from 110 – 400 m a.s.l. These were two glacially abraded bedrock surfaces (KA23 and KA27) and an erratic boulder (KA20) (Figure 4.7). These returned ages of 5.2±0.7 ^{10}Be kyr (KA20), 6.6±1.1 ^{10}Be kyr (KA27), and 5.0±0.7 ^{10}Be kyr (KA23) (Table 4.3). The geomorphological and chronological data constrain the upper limit of warm-based ice during the LGM to between 1400 and 1964 m a.s.l.

Sample code	Latitude (°N)	Longitude (°W)	Elevation (m a.s.l.)	Sample type	Thickness (cm)[a]	Sample density (g/cm^3)	Shielding factor	Denudation rate (mm a-1)
KA2	71.48291667	53.12581667	720	Bedrock	5	2.6	0.9949	0
KA3	71.65441667	51.99898333	1402	Bedrock	5	2.6	0.9951	0
KA5	71.67086667	52.39133333	1964	Bedrock	5	2.6	1	0
KA9	71.51005	53.0279	482	Bedrock	5	2.6	0.9794	0
KA10	71.51328333	53.02775	380	Bedrock	5	2.6	0.9886	0
KA11	71.51538333	53.02755	286	Bedrock	5	2.6	0.9889	0
KA12	71.5208	52.99253	160	Bedrock	5	2.6	No data	0
KA15	71.52545	52.96826667	76	Bedrock	5	2.6	0.9910	0
KA16	71.52895	52.88033	78	Bedrock	5	2.6	No data	0
KA17	71.5294	52.8801	69	Erratic	5	2.6	0.9977	0
KA18	71.52718333	52.90128333	148	Bedrock	5	2.6	0.9989	0
KA19	71.52696667	52.90623333	148	Erratic	5	2.6	0.9986	0
KA20	71.6293	52.13582	400	Erratic	5	2.6	0.9699	0
KA23	71.6333	52.08198	110	Bedrock	5	2.6	0.9604	0
KA24	71.62132	52.94037	1019	Bedrock	5	2.6	No data	0
KA27	71.64053333	52.56381667	162	Bedrock	5	2.6	0.9934	0

[a] The top faces of all samples were exposed at the surface.

Table 4.2. TCN sample locations, elevations, type and shielding factors for samples presented in this study.

Sample code	^{10}Be conc. (at g^{-1})[abc]	Muon prod. rate (at gr^{-1} yr^{-1})	Spallation prod. rate (at g^{-1} yr^{-1})	^{10}Be Exposure age (yrs)[d,e,f]	Internal uncertainty (yr)	External uncertainty (yr)
KA2	97476 ± 5258	0.236	8.09	11686	632	1198
KA3	284023 ± 13055	0.298	14.71	18932	874	1869
KA5	2119500 ± 72370	0.359	23.1	92027	3216	8789
KA9	79977 ± 3403	0.217	6.36	12146	518	1178
KA10	43476 ± 2895	0.209	5.81	7241	483	596
KA11	49532 ± 4240	0.202	5.28	9055	777	891
KA12	No Data					
KA15	9606 ± 5663	0.187	4.23	2177	1284	1288
KA16	No Data					
KA17	30340 ± 1485	0.187	4.22	6862	336	685
KA18	16276 ± 1287	0.192	4.61	3375	267	397
KA19	31312 ± 1805	0.192	4.61	6529	377	491
KA20	31451 ± 4156	0.210	5.84	5208	689	733
KA23	22171 ± 2271	0.189	4.26	4993	512	566
KA24	No Data					
KA27	32099 ± 5073	0.193	4.66	6624	1049	1096

[a] All beryllium-10 derived from quartz; [b] Uncertainties are reported at the 1σ confidence level; [c] Propagated uncertainties include error in the blank, carrier mass (1 per cent) and counting statistics; [d] Calculation of ages was carried out assuming no erosion; [e] Exposure ages are based upon the constant production rate model, using the scaling scheme for spallation from Lal (1991) and Stone (2000), and the NENA calibration (Balco *et al.*, 2009); [f] Dates were calculated using the CRONUS-Earth online calculator, version 2.2 (Balco *et al.*, 2008).

Table 4.3. ^{10}Be TCN exposure ages from the northern UISS

Sample code	^{26}Al (at g^{-1})[a,b,c]	Muon prod^{n} rate (at gr^{-1} yr^{-1})	Spall^{n} prod^{n} rate (at g^{-1} yr^{-1})	^{26}Al Exposure age (yrs)[d,e,f]	Internal uncertainty (yr)	External uncertainty (yr)	^{26}Al/^{10}Be ratios
KA2	764049 ± 125967	1.971	54.6	13536	2247	2350	7.84±1.45
KA3	2272889 ± 91694	2.496	99.23	22491	917	1433	8.00±0.69
KA5	14630123 ± 428055	3.008	155.85	96084	2948	5693	6.90±0.53
KA9	513851 ± 37179	1.81	42.9	11507	837	1009	6.42±0.70
KA10	338083 ± 34256	1.745	39.17	8297	844	934	7.78 ± 0.94
KA11	425895 ± 52326	1.686	35.63	11479	1418	1523	8.60 ± 1.29
KA24	No Data						

[a] Al aluminium-26 derived from quartz; [b] Uncertainties are reported at the 1σ confidence level; [c] Propagated uncertainties include error in the blank, carrier mass (1 per cent) and counting statistics; [d] Calculation of ages was carried out assuming no erosion; [e] Exposure ages are based upon the constant production rate model, using the scaling scheme for spallation from Lal (1991) and Stone (2000), and the NEMA calibration (Balco *et al.*, 2009); [f] Dates were calculated using the CRONUS-Earth online calculator, version 2.2 (Balco *et al.*, 2008).

Table 4.4. ^{26}Al TCN exposure ages from the northern UISS

Pub. code	Sample code	Lat. (°N)	Long. (°W)	Sample type	$\delta^{13}C_{VPDB}$‰ ± 0.1	Carbon content (% by wt.)	^{14}C Age	Uncertainty 1σ (14C yrs BP)	cal. Min (yr)	cal. Max (yr)	cal. mid (yr)
SUERC-37526	INL1	71.86	53.03	Plant macros	-27.9	27.5	8811	40	9685	9954	9819.5
SUERC-37530	KAL1	71.51	52.95	Bulk lake gyttja	-19.8	4.5	9838	41	11196	11316	11256

Table 4.5. ^{14}C ages and calibrated age ranges for the two lake sites in this study. ^{14}C age is the radiocarbon age corrected for isotopic fractionation, measured and calculated using δ^{13}C. Errors are quoted to 1σ. Ages were calibrated using OxCal 4.2 and the IntCal09 calibration curve, and presented as a range to 2σ.

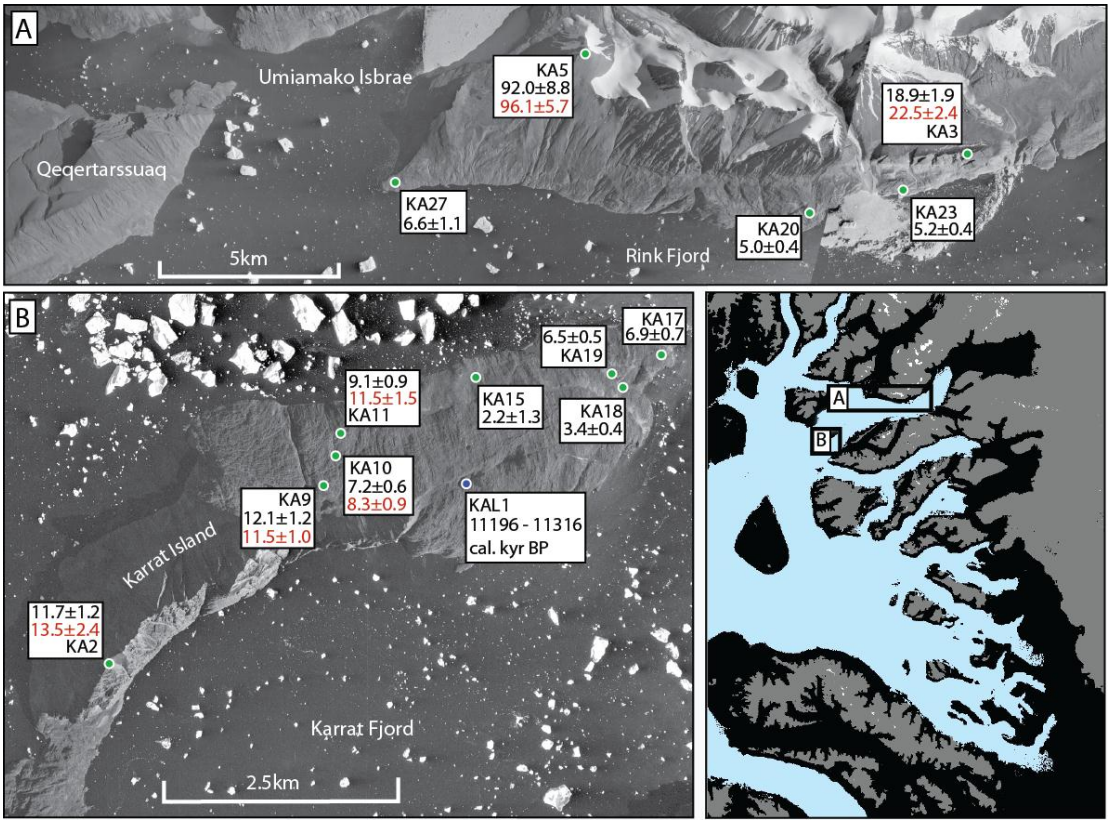

Figure 4.7. Aerial photographs showing the locations of samples taken for dating from Rink-Karrat Fjord, and their results. Successful TCN results are shown by green circles (^{10}Be ages in black, ^{26}Al ages in red). ^{14}C result (KAL1) is indicated by the blue circle (see section 4.4.3.2).

4.4.2. Qeqertarssuaq

4.4.2.1. East Qeqertarssuaq: geomorphology

Qeqertarssuaq is a 165 km^2 island in a mid- to outer-fjord position (Figure 4.4). High altitude areas are characterised by an extensive frost shattered surface, with small valley glaciers found on the northwest of the island. A number of small, infrequent bedrock outcrops were found protruding from this mantling of frost shattered material (Figures 4.8a - 4.8c). In places the upper faces of the bedrock outcrops are glacially abraded, displaying striae. The largest of these bedrock outcrops was found at 1040 m a.s.l. (71.633056°N 52.896389°W), with striae recording ice flow directions of 173˚-353˚ (set 1) and 87˚-267˚ (set 2) (Figure 4.9). Detailed inspection of the striae and their cross cutting relationship was not able to resolve their chronological relationship. However, based upon an increasing degree of topographic control during deglaciation, it is thought that striae set 1 were formed prior to set 2. Regardless of the striae age relationship, this demonstrates warm-based ice above this altitude (1040 m a.s.l.), during the last glaciation. A sample was taken from this location for

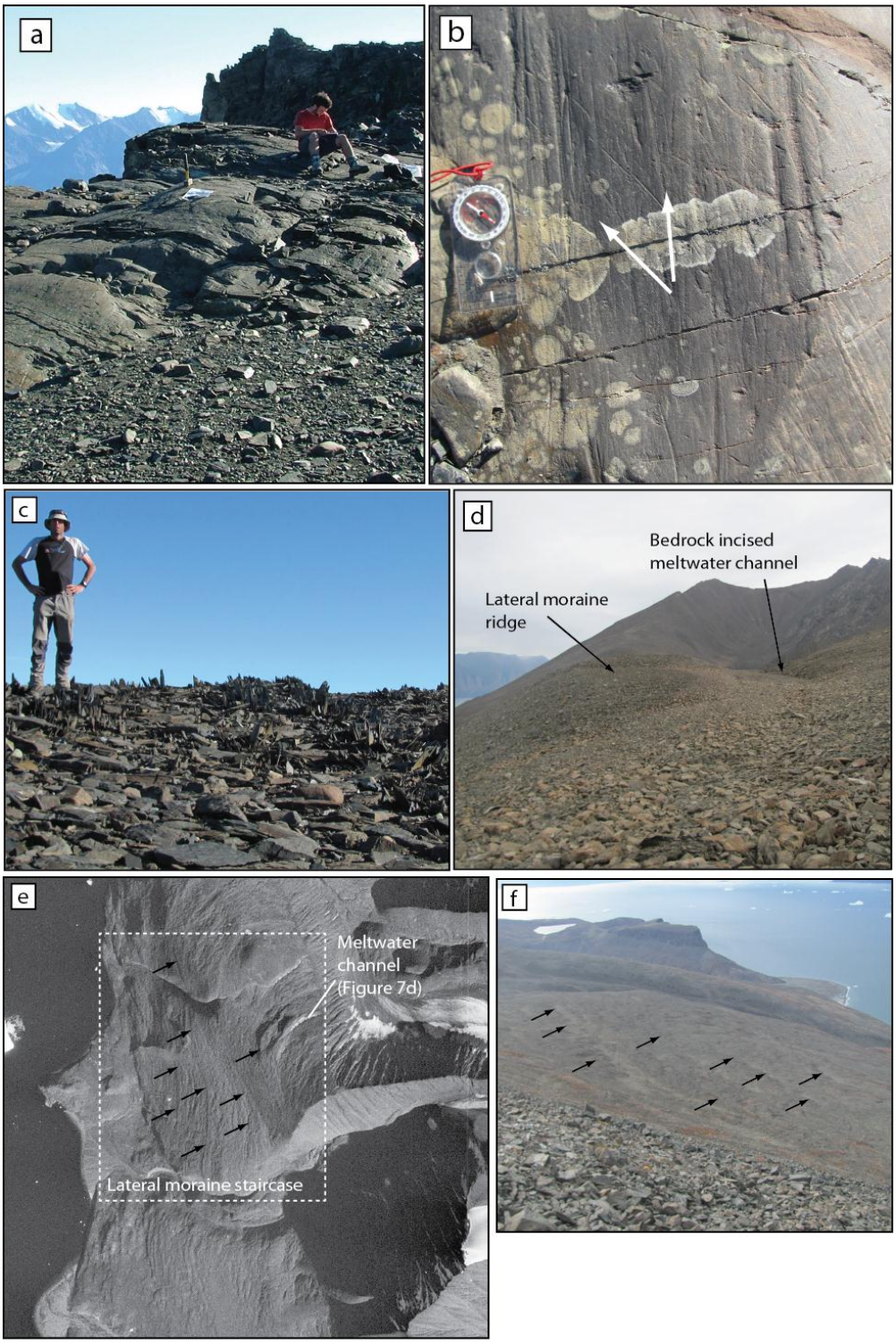

Figure 4.8. Plate of photographs from Qeqertarssuaq. (a) ice-moulded bedrock outcrops at 1040 m a.s.l. on eastern Qeqertarssuaq, (b) enlargement of the striated, ice moulded bedrock surfaces from outcrop in Figure 4.8a, (c) frost shattered and heaved local material at ~1000 m a.s.l., eastern Qeqertarssuaq, (d) large lateral moraine (Q1– 786 m a.s.l.) on western Qeqertarssuaq, abutting a bedrock cut lateral meltwater channel. See person on moraine ridge for scale. (e) Aerial photograph of western Qeqertarssuaq, with the meltwater channel of Figure 4.8d labelled, and the area of lateral moraines boxed, with individual ridges arrowed. (f) Oblique photograph from close to the meltwater channel, looking southwest. Lateral moraines are arrowed.

TCN dating (KA24). However, once processed, there was insufficient quartz in the 125 – 500 µm size fraction to allow etching and successful beryllium recovery. A subdued, poorly developed ridge runs northeast to southwest on the southern edge of the island (Figure 4.9), terminating at the edge of the broad col which covers the centre of the island. The ridge is composed of loose, angular pebbles and cobbles, dominated by local lithologies with occasional erratics and is interpreted as a lateral push moraine, where fjord ice has overtopped the topography.

Above ~800 m a.s.l. the western flank of Qeqertarssuaq is characterised by extensive frost shattered material formed of locally derived angular to sub-angular material. Below this, the lower elevation terrain contains a series of 12 subparallel ridges, with smaller fragmentary ridges between them (Figures 4.8e and 4.8f – and see inset location in Figure 4.4). These are formed of sub-angular to sub-rounded clasts, and are of clearly different lithological composition to the surrounding scree. The highest of the ridges is found at 786 m a.s.l. and is also the most distinct, reaching 6-8 m high (Figure 4.8d). Upslope of Q1 is a large (5 m wide), bedrock incised channel (Figure 4.8d). As a result of these observations, the 12 ridges and fragments between them (found from 786 to 340 m a.s.l.) are interpreted as a lateral moraine staircase, with the highest found in association with a bedrock incised lateral meltwater channel.

4.4.2.2. Nuugaatsiaq, southwest Qeqertarssuaq

Nuugaatsiaq is an 18 km^2 low elevation (<180 m a.s.l.) and low relief peninsula on the southwest side of Qeqertarssuaq (Figure 4.1). The peninsula is bordered to the north by a near vertical wall rising to 1400 m a.s.l. Three ridges of varying preservation were mapped on the eastern side of the peninsula, at 10-30 m a.s.l. (N1), 55-70 m a.s.l. (N2) and 120-133 m a.s.l. (N3) (Figures 4.9 and 4.10). These were formed of diamictic material, dominated by sub-angular to sub-rounded clasts, and interpreted as a series of lateral moraines. A further, more fragmentary moraine was found at the break of slope between the peninsula and fjord wall (N4 – 260 m a.s.l.), displaying evidence of extensive post-depositional rock glacierisation (Figures 4.9 and 4.10). Moraines N1-N3 lie sub-parallel to the present coastline (Figure 4.9). N1-3 continue to the northeast, following the base of the Qeqertarssuaq for 5km (Figure 4.10). Although these slopes are mantled by a thick scree cover, this is clearly discernible from the lighter coloured morainic material (Figures

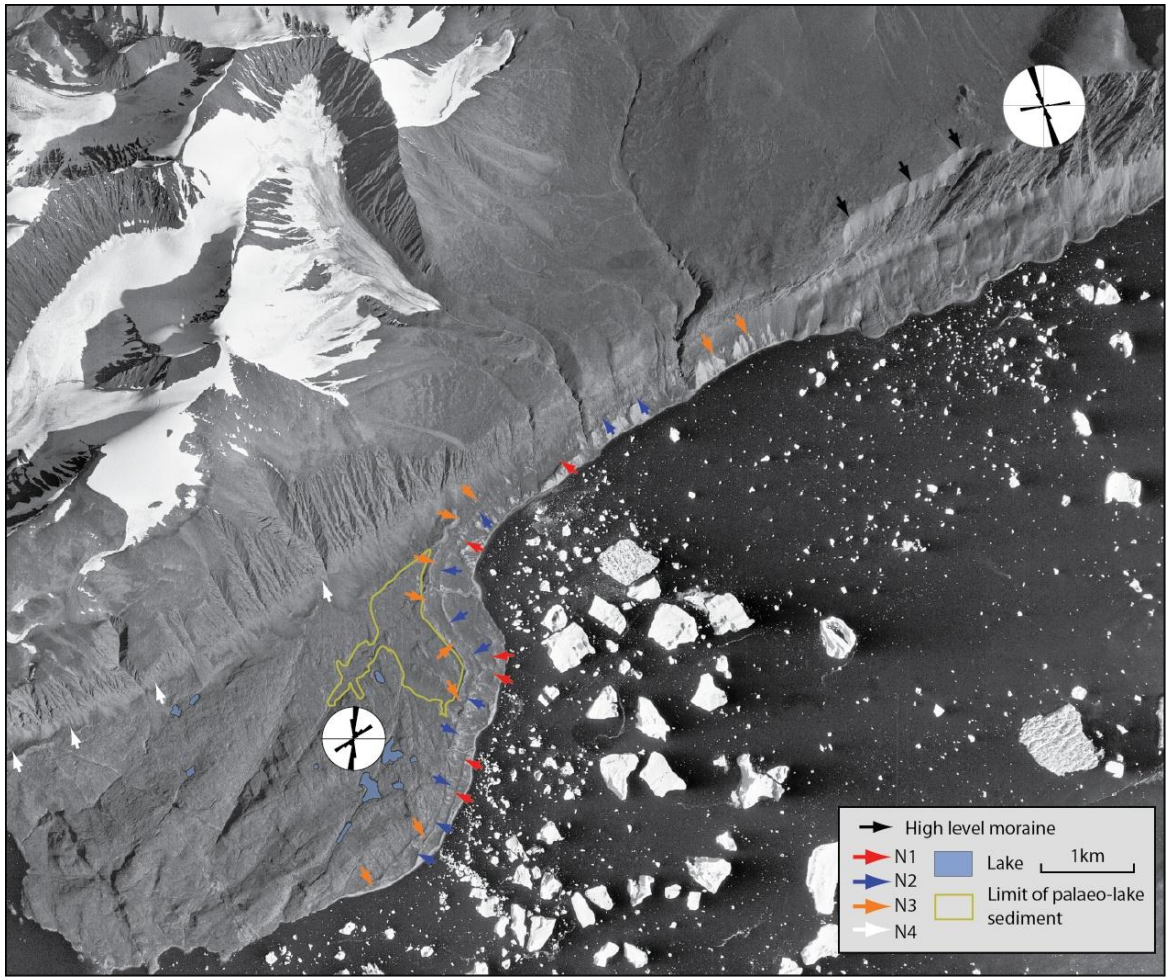

Figure 4.9. Aerial photograph of the Nuugaatsiaq peninsula and fjord wall to the northeast. Striae data from 1040 m a.s.l. are shown at the top right, and the high-altitude lateral push moraine is shown by black arrows. Fragments from each of the four inset lateral moraines (N1-4) are arrowed, and striae shown in a rose diagram (n=50). The hypothesised extent of lake sediment on the peninsula (based upon sediment distribution) is also outlined.

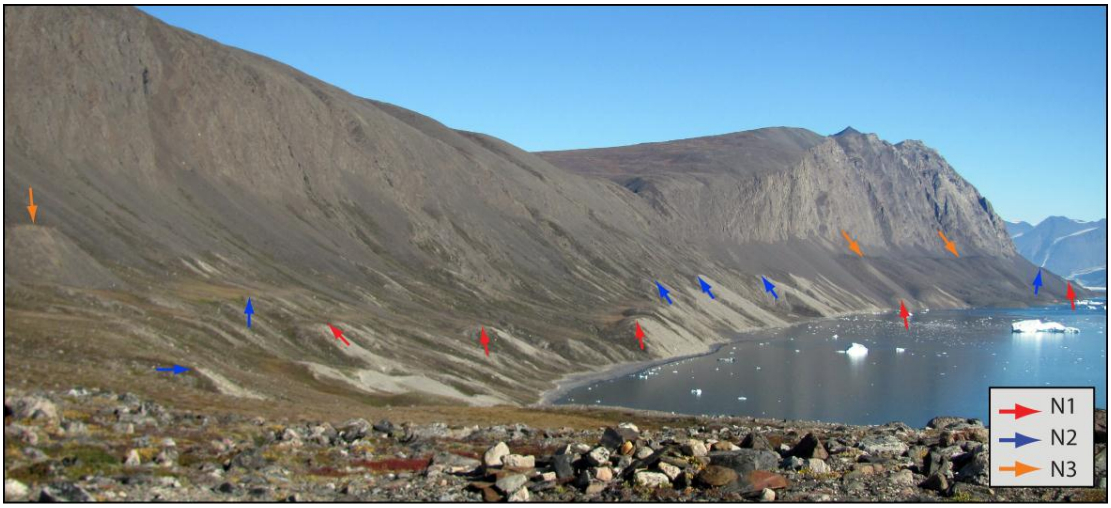

Figure 4.10. Photograph looking northeast at the continuation of the Nuugaatsiaq lateral moraine sequence (arrowed). The moraines are fragmentary, but can be traced for >5km.

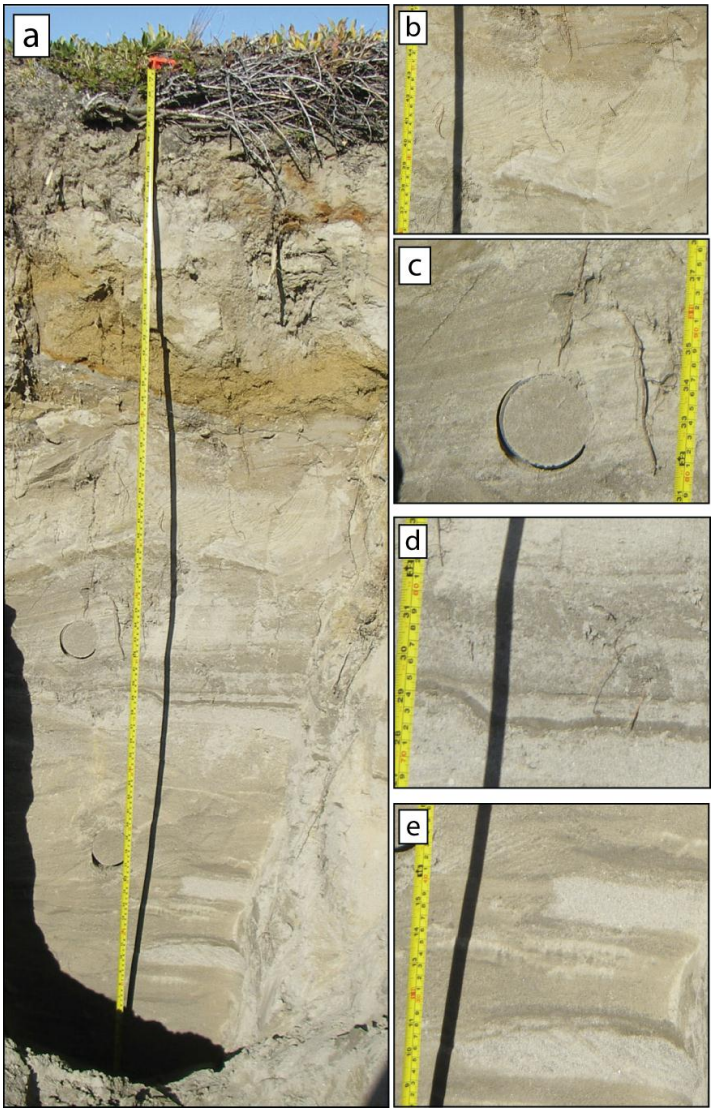

Figure 4.11. (a) sediment sequence from the centre of the Nuugaatsiaq Peninisula, interpreted as being deposited in a pro-glacial lacustrine/fluvial setting; (b) cryoturbated sediment at the top of the section; (c) well sorted, planar stratified sands; (d) large (> 5 mm thick) horizontally continuous massive fine units; (e) ripple cross-stratified sands and fines.

4.9 and 4.10). Striae mapped from bedrock outcrops west of N3 (71.56°N 53.13°W) display cross cutting flow directions of 20°-200° and 58°-238°. The first of these (238°) suggests ice flow concordant with fjord morphology (east-northeast to west-southwest). In contrast, the second set of striae suggests ice overriding the region from a north-eastern source. This is similar to other ice directional indicators found at higher altitude on eastern Qeqertarssuaq.

Land drops in elevation to the west of N3 (Figure 4.10), to a region of low relief bedrock knolls and areas of flat topped sediment infills (at ~90 m a.s.l.). Terrain rises to the north, west and southwest of this depression, enclosing a small shallow basin (~2-4 km^2). At least four flat benches were seen on the terrain to the southwest from ~110 – 140 m a.s.l., though no further analysis of these was undertaken. Extensive sediments at least 2 m thick were found throughout the depression west of the moraine complex on the Nuugaatsiaq Peninsula (Figure 4.11). Some evidence of cryoturbation is present in the upper 30 cm of the sequence, but the majority of sediments are characterised by interbedded fine sand and clayey silt, displaying un-deformed, *in-situ* planar and ripple cross bedding (Figure 4.11). The sediments appear well-sorted, with few granules and no pebbles, suggestive of a relatively low-energy depositional environment. The sediments show no deformation (other than cryoturbation), suggesting deposition following the most recent regional deglaciation. Geomorphological and sedimentological evidence suggests that the sediments were deposited in a glacio-lacustrine setting, in a basin constrained by higher topography to the west of the peninsula, and by the N3 moraine to the east (Figure 4.9). The lake sediments were found above the regional marine limit, meaning that they would have been deposited in a terrestrial, not a marine or glacimarine setting. A series of small breaches were found incised through N3 and are likely to have been caused by a series of lake drainage events, resulting from filling to the level of the moraine crest and subsequent drainage of the lake. The breaches have then been filled by small braided stream systems.

4.4.3. Karrat Island

4.4.3.1. Geomorphology

Karrat is a 56 km^2 island, close to the outer margin of Rink-Karrat Fjord (Figures 4.1 and 4.4). It divides the fjord into two narrow channels, 3.4 km and 5 km wide respectively. The island has a low relief, low elevation eastern end (<300 m a.s.l.), which rises steeply to a 950 m a.s.l. bedrock ridge in the centre (Figure 4.12b). Ridge summits are covered by shattered

bedrock, with a thin cover of autochthonous blockfield and partially shattered bedrock. In some places on the summit, large (~9 m^2) slabs of intact, *in-situ* bedrock were present (Figure 4.12b), though no striae were found. Some of the near vertical ridge walls showed some subtle abrasion and smoothing, suggesting erosion by warm-based ice cover. The low elevation eastern end of Karrat Island is characterised by widespread areally scoured terrain, with glacially smoothed bedrock and roches moutonnées, interspersed with small (100-300 m wide), shallow (3-5 m) lakes (Figure 4.12c). A series of three inset ridges were found on the north and eastern sides of Karrat Island (Figure 4.13). They were formed of coarse (cobble to boulder), angular to sub-rounded material. The ridges are interpreted as a series of inset lateral moraines (K1 – 49m, K2 – 137m, K3 – 210 m a.s.l.) (Figures 4.12d, 4.12e, and 4.13). K3 is the largest and most extensive of the moraines (4m in height, and 15m in width), (Figures 4.12d and 4.12e). These are interpreted as the southern counterpart of the Nuugaatsiaq moraines, representing the lateral portions of a latero-frontal moraine system to the north of Karrat Island.

Glacial bedforms are ubiquitous both inside and outside of the Karrat moraine complex. These are dominated by roches moutonnées, with some whalebacks (7% of the measured bedforms). The majority of bedforms display unidirectional striae (108°-288°), however, a number show evidence for cross cutting ice flow (32°-212° (set 1), 77°-257° (set 2) and 108°-288° (set 3)), and multiple plucked faces (Figures 4.12f and 4.13). Detailed analysis of the striae was not able to robustly constrain their age relationship. However, on the interpretation of a progressive increase in topographic control on ice flow direction during deglaciation, their relative chronology is thought to be set 1 (oldest) to set 3 (youngest).

4.4.3.2. Chronology

The highest elevation TCN sample was KA2 (724 m a.s.l. – see Figure 4.6, Table 4.2), taken from an *in situ* bedrock slab, returning ages of 11.7±1.2 (^{10}Be) (Table 4.3) and 13.5±2.2 (^{26}Al) (Table 4.4). The ^{10}Be and ^{26}Al age determinations are overlapping within error, suggesting a robust age for the sample, and the overriding by erosive ice at this altitude during the LGM. A series of samples were taken across the east of the island. Sample KA9 (482 m a.s.l. – see Figure 4.7) returned a date of 12.1±1.2 kyr (^{10}Be) (Table 4.3) and 11.6±1.0 kyr (^{26}Al) (Table 4.4). Samples KA10 and KA11 also lie outside the moraines (Figure 4.7), and returned ages of 7.2±0.6 ^{10}Be kyr/8.3±0.9 ^{26}Al kyr, and 9.1±0.9 ^{10}Be kyr/11.5±1.5 ^{26}Al kyr respectively (Tables 4.3 and 4.4). These provide a maximum age for moraine formation. Samples KA15,

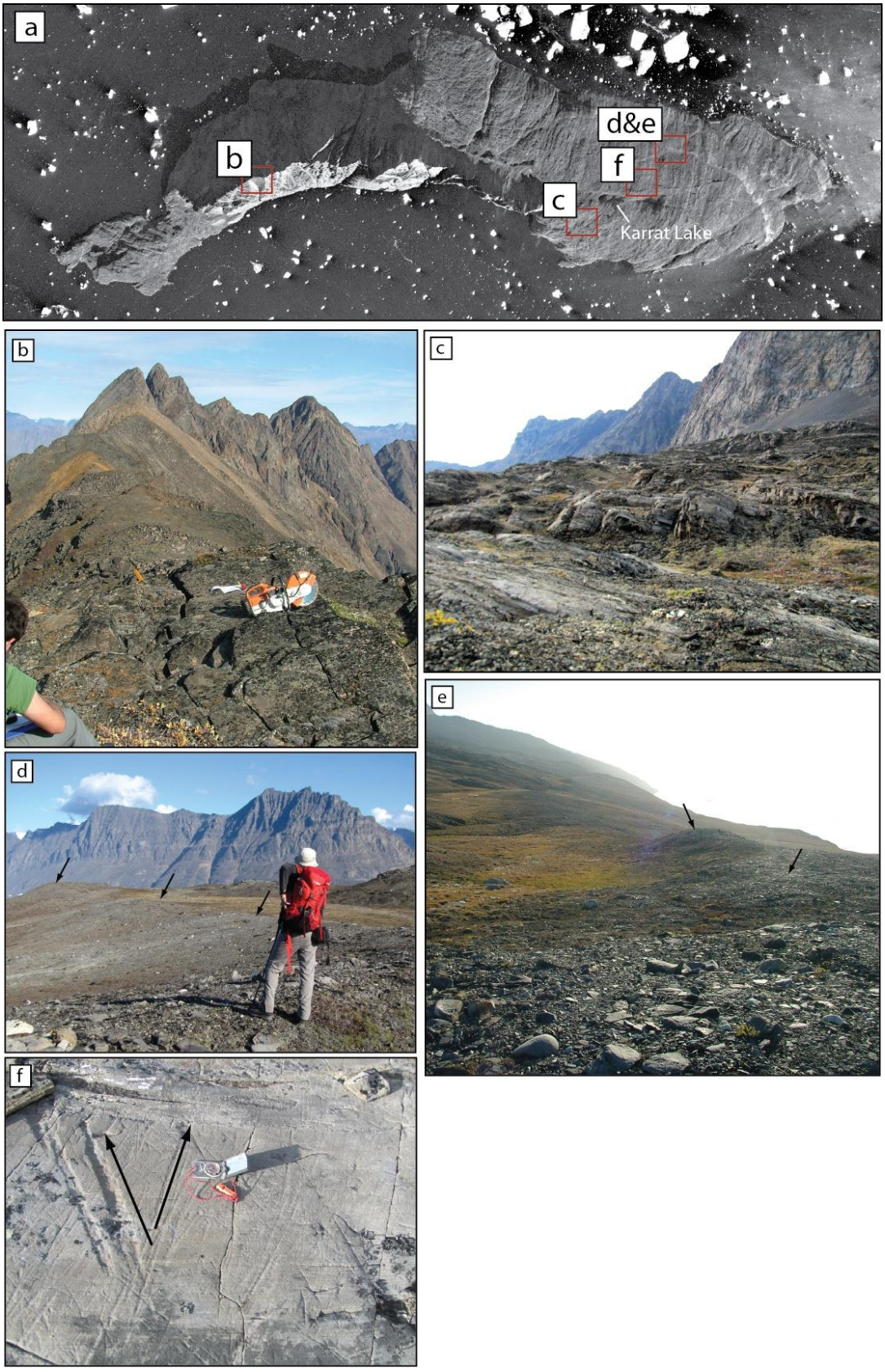

Figure 4.12. Plate of photographs from Karrat Island: (a) Aerial photograph of Karrat Island, showing the location of photographs. (b) *In situ* bedrock slab at 750 m a.s.l. (under saw); (c) Glacially polished roches moutonnées which are found ubiquitously across the east of the island at 200 m a.s.l.; (d and e) Views of K3, the outermost of the three moraines mapped on Karrat Island (210 m a.s.l.); (f) Bi-directional striae from eastern Karrat Island (~255 m a.s.l.).

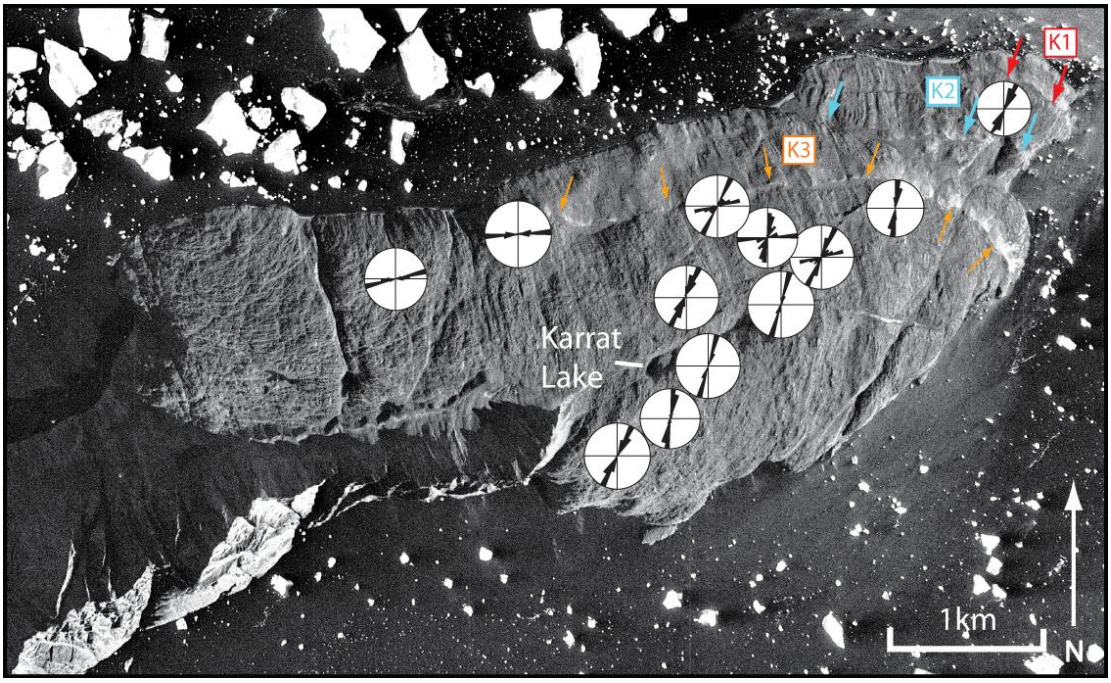

Figure 4.13. Aerial photograph of eastern Karrat Island, with Karrat moraines arrowed (K1-3). Superimposed rose diagrams show striae directions for locations across the island (n=50 for each location).

KA18, and KA19 are situated between moraines K3 and K2 (Figure 4.7), and returned ^{10}Be ages of 2.2±1.3 kyr, 3.4±0.3 kyr, and 6.5±0.5 kyr respectively (Table 4.3).

However KA15 and KA18 were not included in analysis of the results. Their ages (2.2±1.3 kyr and 3.4±0.3 kyr respectively) appear anomalously young, and are incompatible with a large number of other dates from Karrat Island, and Rink Fjord (KA16, KA17, KA19, KA20, KA23, and KA27). On the basis of their erroneously young ages they were excluded from the study. Both excluded samples were taken from slightly sloping bedrock surfaces, and it is therefore possible that they have been affected by sediment cover during their exposure history, leading to relatively recent exhumation, or intermittent burial (2.2±1.3 kyr, 3.4±0.3 kyr) (Putkonen and Swanson, 2003). Finally, sample KA17 was taken from glacially abraded bedrock between moraines K2 and K1 (Figure 4.7), and returned an age of 6.9±0.7 kyr (Table 4.3). Further constraint upon the deglacial chronology is provided by a ^{14}C age from Karrat Lake (KAL1). An age from the organic-minerogenic contact from lake sediment returned an age of 11196-11316 cal. yrs. BP (Table 4.5). This date represents a minimum age for deglaciation from this point, and is in agreement with the local TCN deglacial dates from this area (KA1, KA4, and KA6).

4.4.4. Ingia Fjord

4.4.4.1. Geomorphology

Fjord walls along Ingia Fjord are glacially smoothed up to 800-1000 m a.s.l. Above this, the terrain appears mantled by extensive scree, autochonous blockfield, and weathered bedrock surfaces. The boundary between these terrain types is marked by a faint trimline, which is most evident at the mouth of the fjord (arrowed in Figure 4.14a). Within the fjord, though present, the trimline is less distinct. The majority of work in Ingia Fjord was carried out on a small (24 km^2) peninsula, 15 km from the present ice margin. The low elevation peninsula is characterised by low relief, hilly topography, with ubiquitous roches moutonnées, whalebacks, and small lakes (Figure 4.14b). Bedform long axes are broadly concordant with striae directions and fjord topography, recording northeast to southwest ice flow (64°-244° see Figure 4.14b). A large (10-30m high), discontinuous moraine ridge was mapped at 420-446 m a.s.l., close to the break in slope at the steep fjord wall (Figure 4.14a). The ridge is composed of sub-angular to sub-rounded clasts from local lithologies, with some occasional erratic material. In places it appears to have undergone some post-depositional rock glacierisation.

4.4.4.2. Chronology

The surficial geology of this area is dominated by metagreywackes characterised by very thin bedding planes and high joint densities. However, these were very low in suitable quartz, and potentially dateable surfaces were unsuitable for dating. Some >20 cm wide quartz bands were found and sampled, but these were not processed in the lab. Chronological control for deglaciation through Ingia Fjord is reliant upon a single ^{14}C age from Ingia Lake (see Section 4.4.3.2), yielding an age of 9.7-9.9 cal. yrs BP. This provides a minimum age for the deglaciation of Ingia Isbræ to this mid-fjord position.

4.4.5. Lake sediments

Sediment cores were taken from two lakes in northern Uummannaq: Karrat Lake and Ingia Lake. Sediment cores were taken in order to: (i) provide samples for ^{14}C dating which would provide a minimum age for deglaciation at their location; and (ii) to investigate the palaeo-environmental history of the region, subsequent to deglaciation. Water depth in the centre

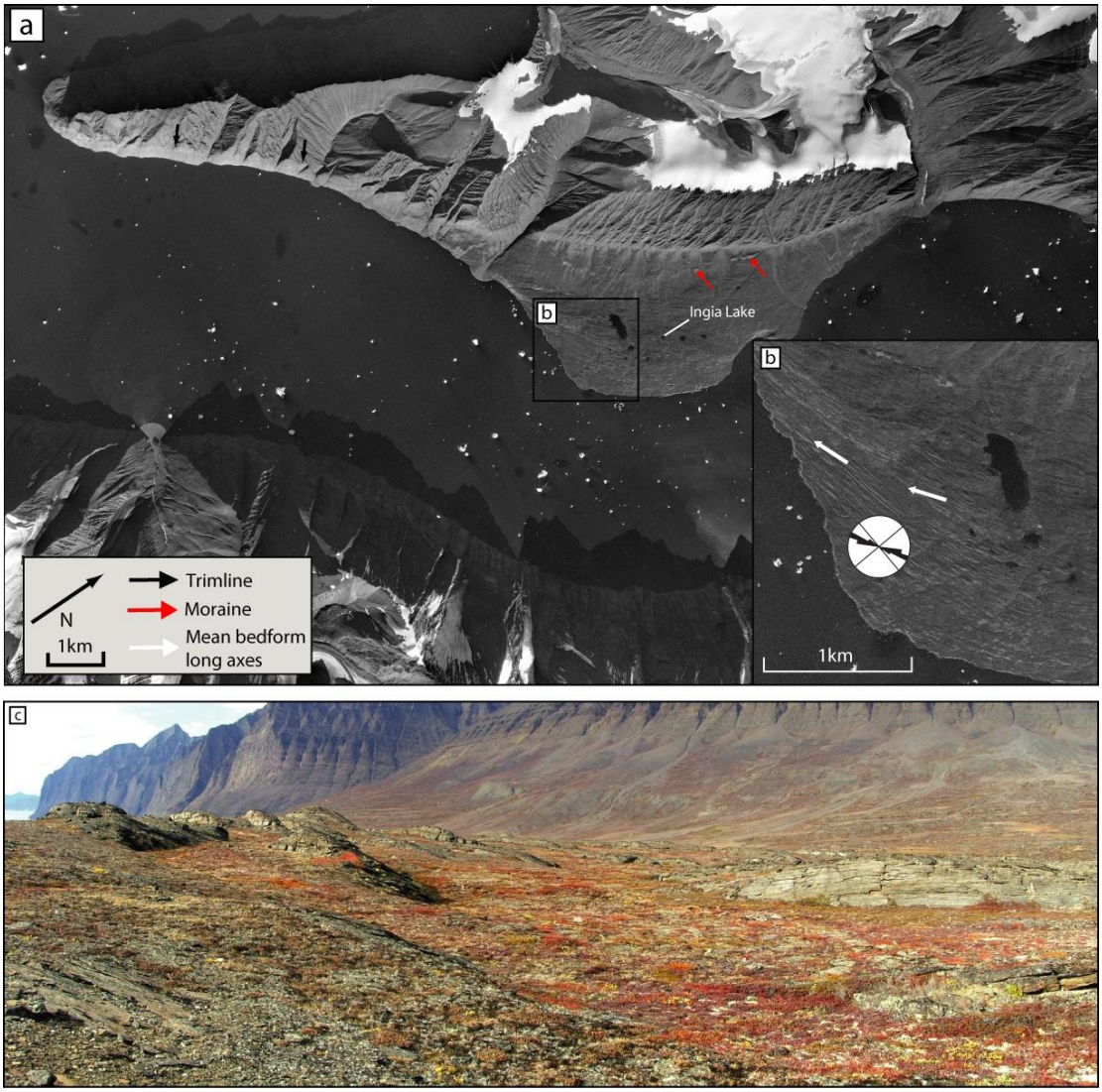

Figure 4.14. (a) Aerial photograph of Ingia Fjord (see Figure 4.4 for location). Black arrows mark a trimline separating abraded surfaces from weathered, debris-rich surfaces above. This is best developed in the outer fjord (left of photograph). Red arrows indicate the fragmentary, rock glacierised lateral moraine. (b) Enlargement of the southwest portion of the peninsula, showing the ubiquitous glacially eroded whaleback and roches moutonnées. Average bedform long axes are shown by the white arrow, and striae data are shown in a rose diagram (n=30). (c) Photograph of the landscape on the peninsula in Ingia Fjord. Photograph is taken looking west; south of the large lake visible in Figure 4.14b. Areally scoured terrain with large bedforms is visible in the fore- and mid-ground (ice-flow from right to left). Steep rock faces with gullies and associated talus cones are visible in the background. For scale, the bedform face to the right of picture is ~2 m high.

of both sampled lakes was >3 m. This depth was considered viable for coring and deep enough to have prevented sediment mixing via winter lake ice disturbance.

4.4.5.1. Karrat Lake

Karrat Lake (71.51399° N 52.94588° W) is a small lake on the low-level surface on eastern Karrat Island (Figure 4.13). It lies amongst widespread areally soured terrain, outside the K1-3 moraines. A 96 cm Eijkelkamp core (KAL1) was retrieved from the centre of this lake, following an exploratory gouge core transect across the lake. The core bottomed out in bedrock, or very rigid, consolidated sediment. The core contained two sediment lithofacies, a minerogenic sandy clay (KL1) and a highly organic gyttja (KL2) (Figure 4.15). The lowermost of these was made of three units: the first is a 4 cm thick unit of grey, silty coarse sand, with occasional granules (KL1i). This was sharply, but conformably overlain by 5 cm of grey silty clay, with a small (1 cm thick) sand lens (KL1ii). This grades into 4 cm of lighter grey clay, displaying some very faint laminations (KL1iii). Overlying this is the second lithofacies (KL2); 83 cm of organic, gelatinous lake gyttja, varying between black, brown, grey, and olive green. Detrital organic deposits were found throughout. Some faint laminations were present in the lower 71 cm of the gyttja, becoming less distinct towards the top of the core. In addition to the visual stratigraphy, the transition between KL1 and KL2 is marked by a very rapid decrease in magnetic susceptibility and porosity. This suggests a quick switch from dense, minerogenic material (KL1) to more porous, highly organic material (KL2). Initial total organic carbon (TOC) analysis was undertaken in order quantify the organic component of the sediment, however, the organic content of the carbon was >99% for all samples processed.

KL1 is a fining upwards sequence of sediments deposited into standing water. As such it is interpreted as glacio-lacustrine sequence, dominated by the input of glacially derived rock flour, deposited following ice retreat over the site. The upwards fining is a response to progressively increasing glacier distance. The overlying KL2 is high in organics and detrital plant remains. This facies represents lacustrine terrestrial deposition following ice retreat to the east. A bulk gyttja sample was taken from the base of KL2 for ^{14}C dating (KAL1), see section 4.4.3.2.

4.4.5.2. Ingia Lake

Ingia Lake (71.863° W 53.028° W) is a small, 2000 m^2 lake at 262 m a.s.l. on the Ingia Fjord peninsula (Figure 4.14b), amongst widespread areally soured terrain. Water depth in the centre of the lake was >3 m. A 97 cm Eijkelkamp core (InL1) was retrieved from the centre of this lake, following an exploratory gouge core transect across the lake.

The core bottomed out in either bedrock, or very rigid, consolidated sediment. The lowermost unit (IL1i) is 6 cm of unconsolidated grey to green gritty silt sand, with some clay component. Granules up to 15 mm in diameter were found, thought to be locally sourced metagreywacke. This was conformably overlain by 5 cm of grey silty clay (IL1ii), with some very faint laminations throughout. Sharply overlying this was 86 cm of organic gyttja, with common plant macros (IL2). In places the gyttja was interstratified with thin (<10 mm) bands of sand (e.g. at 85 and 87 cm). The lower 66 cm of the gyttja was moderately to faintly laminated and contained abundant detrital plant remains. The gyttja varied between dark and olive green, with grey laminae. The gyttja was generally elastic and gelatinous towards the base, becoming less consolidated towards the top of the facies. Sedimentological investigation shows a rapid drop in magnetic susceptibility and increase in porosity at the boundary between IL1 and IL2. This is in agreement with sedimentological properties, suggesting a change from dense, minerogenic material (IL1) to more porous, organic material (IL2). As in Karrat Lake, IL1 is interpreted as a fining upwards glacio-lacustrine deposit, formed following by sedimentation into a body of standing water, following local ice retreat. This is overlain by IL2, an organic unit which is thought to represent accumulation of organics through inwash and *in situ* organic production during the Holocene. A sample of macroscopic plant remains was taken for ^{14}C dating from the base of IL2. The sample yielded an age of 9685-9954 cal. yrs BP, providing a minimum age for the deglaciation of Ingia Isbræ to a mid-fjord position.

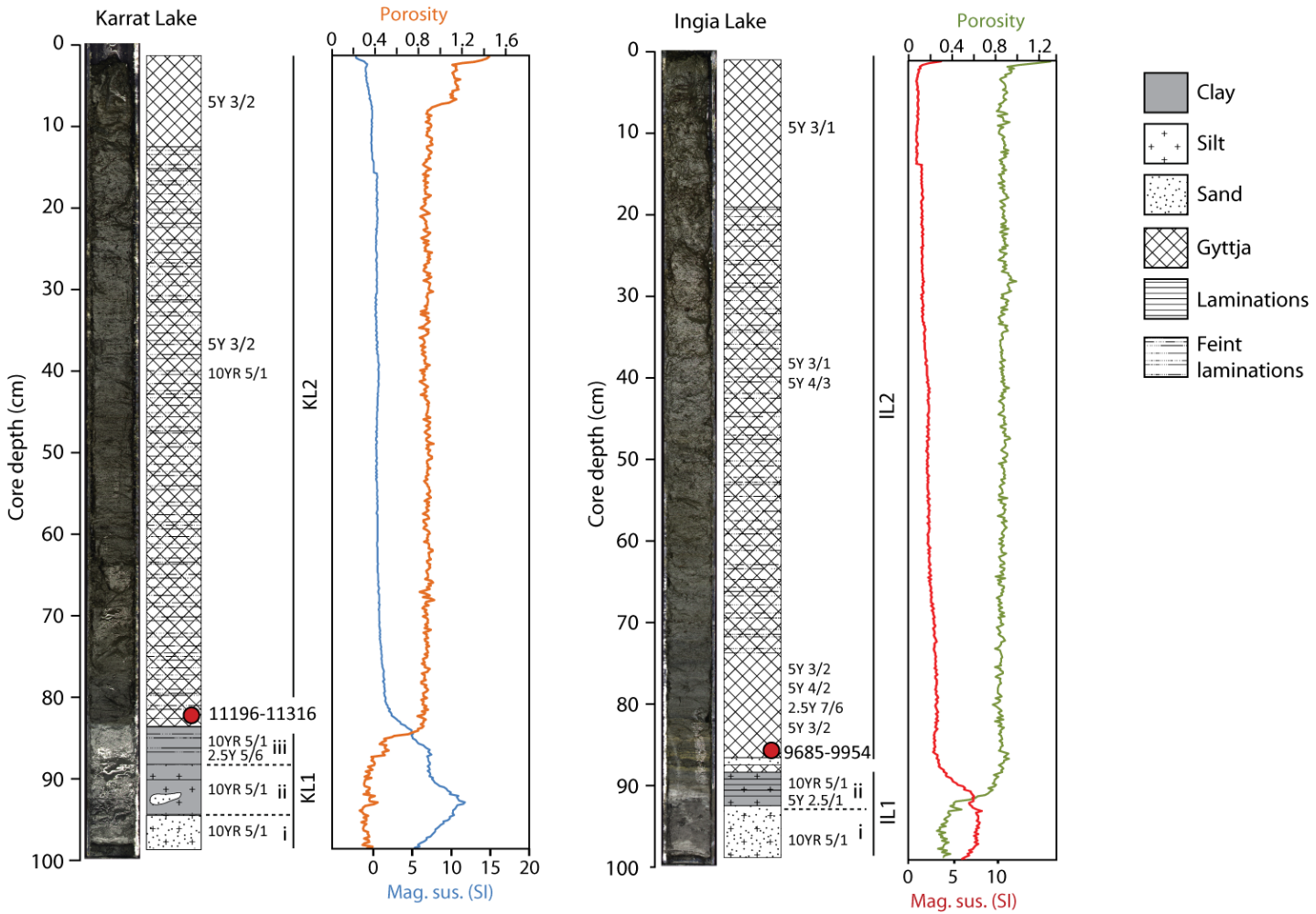

Figure 4.15. Photograph and sedimentological log of lake cores from Karrat and Ingia Lake. Sedimentology is show diagrammatically, as is the location of basal ^{14}C date taken (see Table 4.5 for results). Magnetic susceptibility and porosity measurements are shown to the right of each core (measured using a Geotek Multi Sensor Core Logger). Munsell codes indicate sediment colour throughout the cores.

4.5. Discussion

4.5.1. Configuration of the northern UISS during the LGM

Both geomorphological mapping/data and surface exposure ages provide compelling evidence for erosive warm-based ice throughout the inner fjords of Rink-Karrat, Umiámáko, and Ingia Fjords at the LGM. Warm-based ice thicknesses throughout the inner fjord region reached >1400 m a.s.l., but remained below 1968 m a.s.l., as constrained by KA5 and high-level geomorphology. Some overtopping of fjord topography occurred between 1000 and 1400 m a.s.l., but high-level plateaux between troughs (>2000 m a.s.l.) prevented the overwhelming of regional topography by unconfined, diffluent ice at the LGM. These high-level areas are presently covered by blockfields or small plateau icefields, and would have been exposed as nunataks, or more likely, covered by cold-based ice at the LGM. Concordance of ^{10}Be and ^{26}Al ages throughout samples below 1000 m a.s.l. suggests sufficient erosion of bedrock to prevent inheritance (Tables 4.3 and 4.4).

Based upon geomorphological and surface exposure data, ice thicknesses in the vicinity of Karrat Island were at least 720 m a.s.l., though ice is thought to have submerged Karrat Island (900 m a.s.l.). Ice from Rink and Umiámáko Isbræ would have become confluent to the east of Karrat Island, with Rink Isbræ forcing Umiámáko Isbræ over the centre and east of Qeqertarssuaq. Once ice from Rink-Karrat Fjord reached the east of Qeqertat Imát, it became confluent with ice from Ingia Fjord. Ocean floor bedforms provide evidence for highly convergent flow into the Uummannaq Trough from the east and north (latterly through Igdlorssuit Sund) (Ó Cofaigh et al., 2013b). This convergent flow of ice from the northern UISS into the Uummannaq Trough is due to intense ice drawdown. This drawdown is propagated through Igdlorssuit Sund, an over-deepened trough within the soft Cretaceous basin (Steenfelt et al., 1998). This trough presents the route of least resistance for ice flow from the north (Roberts *et al.*, 2013). This flow through Igdlorssuit Sund has been aided by a shallow sill between northern Ubekendt Ejland and southern Svartenhuk (Qeqertat Imât - <200m below sea-level). This would have aided this by acting as a topographic barrier to ice (Roberts *et al.*, 2013).

Although LGM ice thicknesses were comparable between the north and south UISS, outlet glaciers in the northern UISS remained within their fjord confines at the LGM, separated by high elevation plateaux (>2000 m a.s.l.) that would have remained as ice free nunataks or,

more likely, covered by cold-based ice caps. In contrast, plateaux elevations in the southern UISS (north of Nuussuaq) were <1000 m a.s.l., and not of sufficient altitude to keep outlet glaciers within their fjord confines at the LGM. As a result of this extensive diffluent flow, Roberts *et al*. (2013) proposed a progressive westward migration of the southern UISS onset zone through the last glacial cycle. This occurred as ice thicknesses increased and topographic controls within the inner fjord region became less influential on overall ice dynamics (Roberts *et al.*, 2013). As a result, larger-scale regional topography (e.g. Nuussuaq, Svartenhuk, and Ubekendt Ejland) would have become the principal topographic controls upon flow routing. In contrast, the outlet glaciers in the northern UISS appear to have remained within the confines of the local fjord topography and, hence, predicting any degree of onset zone migration during the LGM is difficult.

4.5.2. Deglaciation of the northern UISS; timing, retreat style, and controls

In combination with geomorphological and chronological data from the offshore and southern sectors of the UISS (Ó Cofaigh et al., 2013b, Roberts et al., 2013), this work provides the first complete reconstruction of the UISS' LGM geometry and the chronology of its subsequent deglaciation. The palaeo-UISS contains all diagnostic components of an ice-stream in both contemporary, and palaeo settings (Stokes and Clark, 1999): individual outlet glacier tributaries; a convergent onset zone; streamlined bedforms; and a trunk zone which feeds into a large trough mouth fan at its terminus A time-distance path for the retreat of ice through Rink-Karrat Fjord is presented in Figure 4.16c, constrained through Bayesian age modelling. The deglaciation of the region is therefore discussed with reference to this reconstruction. As with contemporary ice stream behaviour, the deglaciation of the UISS was influenced by climatic, oceanic, and topographic forcings (Figure 4.17). Their relative importance through the Uummannaq region is investigated here.

4.5.2.1. LGM limit to Ubekendt Ejland

The LGM deglaciation of the UISS from the shelf-edge is discussed by Ó Cofaigh et al. (2013b), with retreat from the continental break underway by 14.9 cal. kyr BP. Following this surface exposure dates from Ubekendt Ejland, record ice retreat and thinning to the south east of Ubekendt Ejland by 12.4 kyr (Roberts *et al.*, 2013). Moraines on the south coast of Ubekendt Ejland between 670 and 125 m a.s.l. represent a series of lowering

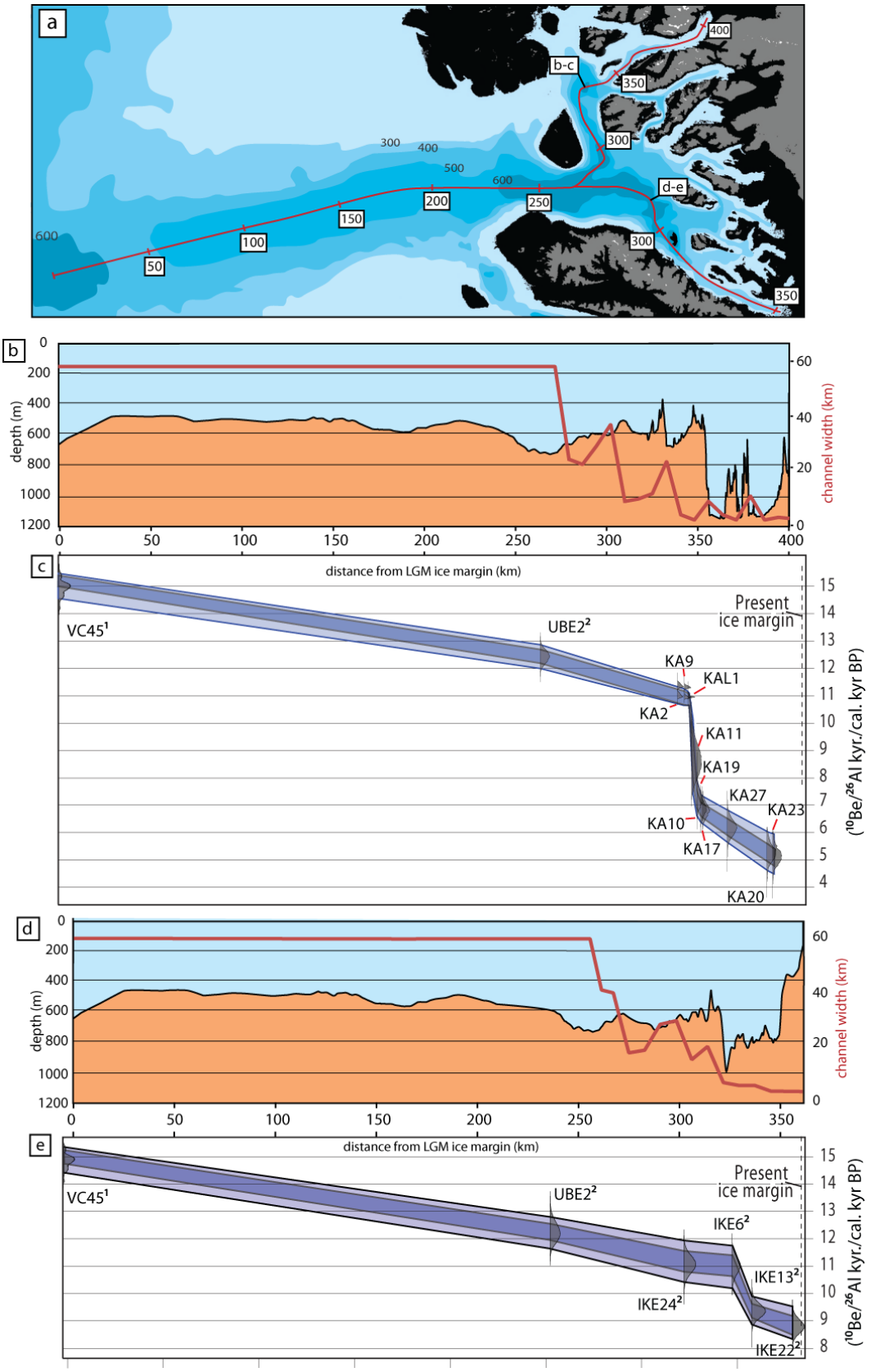

Figure 4.16. Sample locations, bathymetric profile, channel width, and dates from the northern UISS: (a) location of transects used in b and d, through the north and south of the Uummannaq region. Boxed numbers indicate distance in kilometres from the shelf (*cont.*)

edge LGM ice margin; (b) bathymetric profile through Uummannaq Trough, Igdlorssuit Sund, and Rink-Karrat Fjord using GEBCO and swath-bathymetry data (black line), and average channel width from the outer fjord to present margin (red line – measured manually); (c) Bayesian constrained age model of deglaciation through the northern Uummannaq region. Ages are from: [1]Ó Cofaigh et al., 2013b, [2]Roberts et al., 2013, and this study; (d) bathymetric profile through Uummannaq Trough, Igdlorssuit Sund, and the southern Uummannaq region using GEBCO and swath-bathymetry data (black line), and average channel width from the outer fjord to present margin (red line – measured manually); (e) Bayesian constrained age model of deglaciation through the southern Uummannaq region. Ages are from: [1]Ó Cofaigh et al., 2013b, [2]Roberts et al., 2013, and this study.

palaeo-ice surfaces, and are thought to related to thinning of the UISS from the mid-shelf during this period (Roberts *et al.*, 2013). This retreat from the shelf edge (14.9 cal. kyr BP) is coincidental with the onset of Greenland Interstadial 1e (Figure 4.17) (Lowe *et al.*, 2008), a period of increasing insolation (Huybers, 2006), and rising sea-level in West Greenland (Figure 4.17) (Long et al., 1999, Simpson et al., 2009, Roberts et al., 2013). Reconstructions of ocean temperature on the Uummannaq shelf suggest that the warm West Greenland Current (WGC) only entered the Uummannaq Trough after 8 cal. kyr BP (McCarthy, 2011). This initiation of the WGC onto the Uummannaq shelf is later than northwest Greenland and Baffin Bay (Levac et al., 2001, Knudsen et al., 2008). McCarthy suggest that anomalously late initiation of the WGC in the Uummannaq region may be a partial result of excess meltwater flux from the GIS as it retreated from the outer shelf (McCarthy, 2011). This would have diluted and cooled the basal water mass, or diverted the warm WGC water offshore (McCarthy, 2011). Thus, despite some uncertainties regarding warm water influx, it presently appears unlikely that this stage of early deglaciation was triggered by the influx of warm water.

Once retreat was underway, increased water depths of >600 m through the Uummannaq Trough would have led to increased ice discharge, and rapid thinning and retreat (Schoof, 2007). Enhancement of retreat rates by deep subglacial troughs is common, and has been reported in other studies from continental fjord margins (e.g. Briner et al., 2009). Once the UISS reached the southern coast of Ubekendt Ejland, the lateral confinement within the trough increased and the bed shallowed (Figure 4.16b). The topographic confinement is likely to have increased lateral resistive stresses, thickening the ice and increasing basal drag. This would have reduced ice flux and probably caused temporary retreat slowdown between Nuussuaq and Ubekendt Ejland.

4.5.2.2. Ubekendt Ejland to the fjord margins

Once ice retreated beyond south-eastern Ubekendt Ejland the north and south regions of the UISS separated, retreating north through Igdlorssuit Sund and east towards Uummannaq respectively. The timing of retreat through Igdlorssuit Sund is constrained by ages of 12.4 kyr on southern Ubekendt Ejland (122–233 m a.s.l.) (Roberts *et al.*, 2013) and 11.7 ^{10}Be kyr on Karrat Island. The ages are within 2σ errors, suggesting deglaciation could have been rapid, retreating ~65 km in 0.7 kyr. Though rapid, the lateral moraine staircase on western Qeqertarssuaq suggests a dynamic upstream response to calving at the grounding line during this stage of deglaciation. This period of deglaciation (12.4-11.7 kyr) occurs during the latter part of Greenland Stadial 1 (GS1 12.9 kyr to 11.7 kyr), and the early Holocene (Lowe *et al.*, 2008) (Figure 4.15), and is characterised by an increase in air temperature (~4 ‰ δ^{18}O increase in the GRIP and NGRIP record) and a regional peak in relative sea-level at ~12 kyr (Simpson *et al.*, 2009). In conjunction with the ice margin entering the deep (500 – 600 m b.s.l.) Igdlorssuit Sund (Figures 4.1 and 4.16b and 4.16d), this would have acted to enhance rapid retreat back to the fjord heads. The timing of retreat from Ubekendt Ejland to the fjord margins is similar between the northern and southern sectors of the UISS, occurring by 11.5 – 10.8 kyr (Roberts *et al.*, 2013).

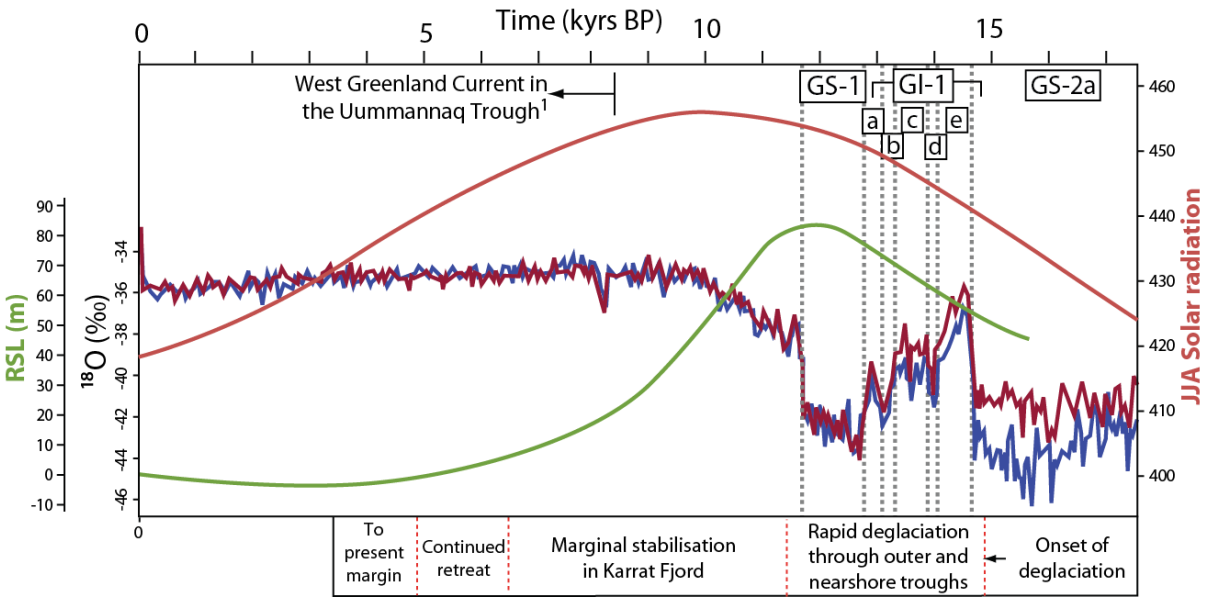

Figure 4.17. NGRIP (blue) and GRIP (dark red) δ18O record for the past 17 kyr (Lowe et al., 2008), relative sea-level curve from Arveprinsens Ejland (green) (Long et al., 1999, Simpson et al., 2009), and JJA radiation for 70°N (light red). Annotations below the figure show key events throughout the deglaciation of the north and south UISS.
[1] from McCarthy 2011.

4.5.2.3. Outer fjord to present ice margin

Following deglaciation through Igdlorssuit Sund the northern UISS progressively 'unzipped' as individual outlet glaciers retreated into their fjords. Dates from Rink-Karrat fjord suggest rapid retreat and thinning of ice across Karrat Island, with the exposure of Karrat Lake by ~11.2 cal. kyr BP, during a period of increasing air temperature (Figure 4.17). Following retreat to the present outer Rink-Karrat Fjord margin, geochronological data suggest that the ice margin underwent a dramatic decrease in retreat rate and temporary stagnation on eastern Karrat Island between ~11.2 and 6.5 kyr (Figure 4.16c). The chronological data are supported by moraines on Karrat Island (K1-3) and Nuugaatsiaq (N1-3), providing geomorphological evidence that retreat through Karrat Fjord was punctuated by a still-stand or slight re-advance.

Chronological results for moraine formation on Karrat Island constrain the formation of K3 to 9.1 - 6.9 kyr. Dates between K3 and K1 are within errors (6.5±0.5 kyr and 6.9±0.5 kyr), and suggest deposition of K3 by ~6.9 kyr. K3-N3 is a higher, larger volume, and less fragmentary moraine ridge than K2-N2 and K1-N1, suggesting that it formed over a longer period of time than K2-N2 and K1-N1. This is supported by the presence of >2 m thick sequence of glacio-lacustrine sediments southwest of N3 on Qeqertarssuaq. The similar, sub-parallel geomorphology and closely nested pattern of the moraines on Karrat Island suggest that they were not formed by a series of separate readvances. No evidence for a readvance was noted in the field, such as a second period of minerogenic input within the lake sediment cores, and an absence of bulldozed sediment within, or between, the moraines. As a result, the Karrat-Nuugaatsiaq moraine system is interpreted to have formed during a slow retreat across Karrat Island, punctuated by a lengthy marginal stabilisation. Similar latero-terminal moraines systems in other outer fjord localities (Fjord Stade moraines) have been identified throughout western Greenland (Weidick, 1968, Tenbrink and Weidick, 1974, Funder, 1989b, Long and Roberts, 2002, Briner et al., 2010, Young et al., 2011a, 2013). These moraines are thought to have formed as a variably ice sheet margin response to the GH-9.3 and GH-8.2 events (Long and Roberts, 2002, Briner et al., 2010, Young et al., 2011a, 2013). However, despite their widespread correlation with these climatic events, it has also been acknowledged that moraine formation could also be a dynamic response to, or enhanced by, topographic effects (Funder, 1989b, Warren and Hulton, 1990, Long et al., 2006). The Umivit-Keglen, and Ørkendalen moraines found further south in Greenland and have been dated to 8.4-7.4 cal. yr BP and 7.0-6.4 cal. kyr BP

respectively (recalibrated dates using Calib, and IntCal09) (Van Tatenhove and van der Meer, 1995, van Tatenhove et al., 1996). These moraines are also thought to relate to localised marginal re-advance, induced by short periods of climatic deterioration (Tenbrink and Weidick, 1974). Dates constrain the deposition of the Karrat-Nuugaatsiaq moraine system to between 9.1 and 6.9 kyr, therefore encompassing the period of Fjord Stade and Umivit-Keglen, /Ørkendalen moraine deposition (Long et al., 2006, Briner et al., 2010, Young et al., 2011a, 2011b, 2013). However, the present chronology shows that ice margin retreat resumed by ~6.9 kyr (see dates KA17 and KA19); making any correlation to other moraines is difficult. In addition, topographic control has clearly controlled this marginal stabilisation, rendering a correlation to disconnected moraines, based upon fjord position and broad chronology alone problematic.

The Rink-Karrat Fjord marginal still-stand occurred through the Early Holocene, and the Holocene Thermal Maximum (HTM), a period from 11 to 5 kyr, characterised by a warm climate (Wanner, 2008, Jansen, 2007, Renssen et al., 2009), most clearly recorded throughout the middle to high latitudes of the Northern Hemisphere (Jansen, 2007, Jansen, 2008). Within Greenland, the HTM was characterised by temperatures 2-3°C warmer than present, suppressed precipitation levels (Anderson and Leng, 2004, Bennike et al., 2010, Axford et al., 2013), a peak in summer insolation, and a drop in sea-level (Figure 4.17) (Long et al., 1999, Simpson et al., 2009). Though broadly constrained to 11-5 kyr, ocean-atmosphere-vegetation models have predicted that warming across central Greenland would have been greatest at 6-5 kyr (Renssen *et al.*, 2009). Palaeoecological data from the Kangerdlussuaq (Anderson and Leng, 2004, Bennike et al., 2010) and Jakobshavn (Axford *et al.*, 2013) regions report periods of maximum warmth at 7.2-5.6 kyr and 6-4 kyr respectively. In order to constrain the precise timing of maximum Holocene warmth in the Uummannaq region a local palaeoenvironmental reconstruction would be required. However, it appears likely that the margin stagnation within Rink-Karrat Fjord was maintained through a period of warm climate not conducive to ice margin stabilisation. Thus, the marginal stillstand is thought to have been controlled by non-climatic factors. Palaeo-ice stream channel width close to Karrat Island reduces to ~5 km, and bed topography shallows to ~400 m. Deeper topography exists to the east (>1000 m) and west (~700 m), making the area to the north of Karrat Island a prominent bathymetric high within the fjord. This is most pronounced directly north, offshore of the Karrat-Nuugaatsiaq moraines, where a narrow topographic high with steep up and downstream slopes is found. Bathymetric data from south of Karrat Island also shows evidence for a prominent bathymetric high close to the position of the

Karrat-Nuugaatsiaq moraines (Figure 4.16c). Though a continuation of the Karrat-Nuugaatsiaq moraines cannot be seen on fjord walls to the south of Karrat Island, it is glaciologically probably that the ice front to the south of Karrat Island stabilised at this point.

The narrowing and shallowing of the channel bed would have reduced the relative magnitude of ice flux necessary to maintain a stable grounding line (Mercer, 1961, Schoof, 2007, Jamieson et al., 2012). The narrowing of the channel further reduces this flux by increased lateral resistance (Mercer, 1961, Whillans and Van der Veen, 1997) and up-ice surface profile steepening (Jamieson *et al.*, 2012). These topographic effects would reduce calving rates and subsequently retreat rates. As a result, this topographic constriction would have facilitated the pinning of the ice margin during retreat. Such topographically controlled retreat dynamics have been reported elsewhere in Greenland (Warren and Hulton, 1990) and for Alaskan tidewater glaciers (O'Neel et al., 2005), and modelled for ice streams in Antarctica (Jamieson *et al.*, 2012).

Following moraine deposition on Karrat Island, ice retreat resumed at ~6.9 kyr, reaching the spur between Rink and Umiámáko Fjords by 6.5 kyr. Here, Rink and Umiámáko Isbræ separated, their detachment evidenced by lateral moraines on the spur between the fjords. Following this, retreat in Rink Fjord continued, reaching ~15 km from the present ice margin by 5 kyr. This final retreat from Karrat Island to Rink Isbræ's present margin is likely to have been forced by the persistence of warm air temperatures, and the possible influx of the warm WGC into the Uummannaq region, which occurred after 8 kyr (McCarthy, 2011). This perturbation was sufficient to detach the ice margin from its topographic pinning point at Karat Island and the over-deepening within inner Rink Fjord then further accelerated and sustained retreat to, or beyond, the present ice margin.

Retreat chronology in Ingia Fjord's is limited to a single date from south-east Svartenhuk, close to the fjord mouth (10.7 cal. kyr BP - Bennike, 2000), and a date from Ingia peninsula (9.9 cal. kyr BP - this study). As such, it is difficult to constrain retreat through Ingia Fjord in detail, other than to say ice had retreated beyond a mid-fjord position by 9.9 cal kyr BP which is consistent with the reconstructed retreat into Rink-Karat fjord.

4.5.3. Implications for LGM ice stream history of the West Greenland Ice Sheet

Results from the Greenlandic continental shelf have provided evidence for the asynchronous onset of ice stream deglaciation throughout Greenland (Evans et al., 2009, Funder et al., 2011, Ó Cofaigh et al., 2013b). This asynchronous behaviour continued through deglaciation, and is mirrored within individual outlet glaciers in the Uummannaq region. A schematic diagram of the reconstructed retreat behaviour is presented in Figure 4.18. As with other GIS ice streams, the retreat of the northern UISS from its shelf-edge terminus to its present margin has been driven by climatic, oceanic, and topographic forcings. Once within the inner fjord, the retreat behaviour was, however, strongly affected by channel topography and both bed depth and fjord width were the dominant control upon the rate of deglaciation. Similarly, a strong topographic control upon ice stream retreat is reported from the inner fjords of the southern UISS (Figure 4.14). Here, an ice margin stabilisation occurred in a similar topographically constricted inner fjord position as on Karrat Island. However, TCN dates from the southern UISS constrain the marginal pinning to between 11.4-9.3 kyr, again in a location characterised by channel narrowing and a shallowing in bed depth (Roberts *et al.*, 2013). This provides further evidence for the importance of topography on glacier retreat, and exemplifies the strongly asynchronous response of outlet glaciers within a single ice stream system.

Additionally, the lengthy period of margin stabilisation on Karrat Island occurred during the HTM (11-5 kyr). The HTM was characterised by high air temperatures, falling relative sea-level, and extensive moisture starvation across the GIS. Research has shown that this peak in air temperatures was accompanied by the widespread retreat of the GIS to an unknown position behind its present margin (Weidick et al., 1990, Weidick and Bennike, 2007, Roberts et al., 2010, Briner et al., 2010, Young et al., 2011b). Store Gletscher, the main outlet glacier of the southern UISS, reached its present margin by 8.7 kyr (Roberts *et al.*, 2013), and Jakobshavn Isbræ in Disko Bugt by 7 kyr (Long and Roberts, 2003, Young et al., 2011b, Ó Cofaigh et al., 2013b). Further south in the Sisimiut region a large ice stream occupied the offshore Holsteinsborg Dyb trough (Roberts et al., 2010), a region associated with the Umivit-Keglen and Ørkendalen moraines. Based upon radiocarbon dates from marine shells, retreat to (or beyond) its present margin occurred by 7.8 – 6.8 cal. kyr BP (Kelly, 1985). Thus, the hypothesised retreat of Rink Isbræ to its present margin after 5 kyr is later than deglaciation of most other ice streams in West Greenland. The Rink Isbræ margin was able to remain in a mid-fjord position throughout the HTM, displaying only a moderate

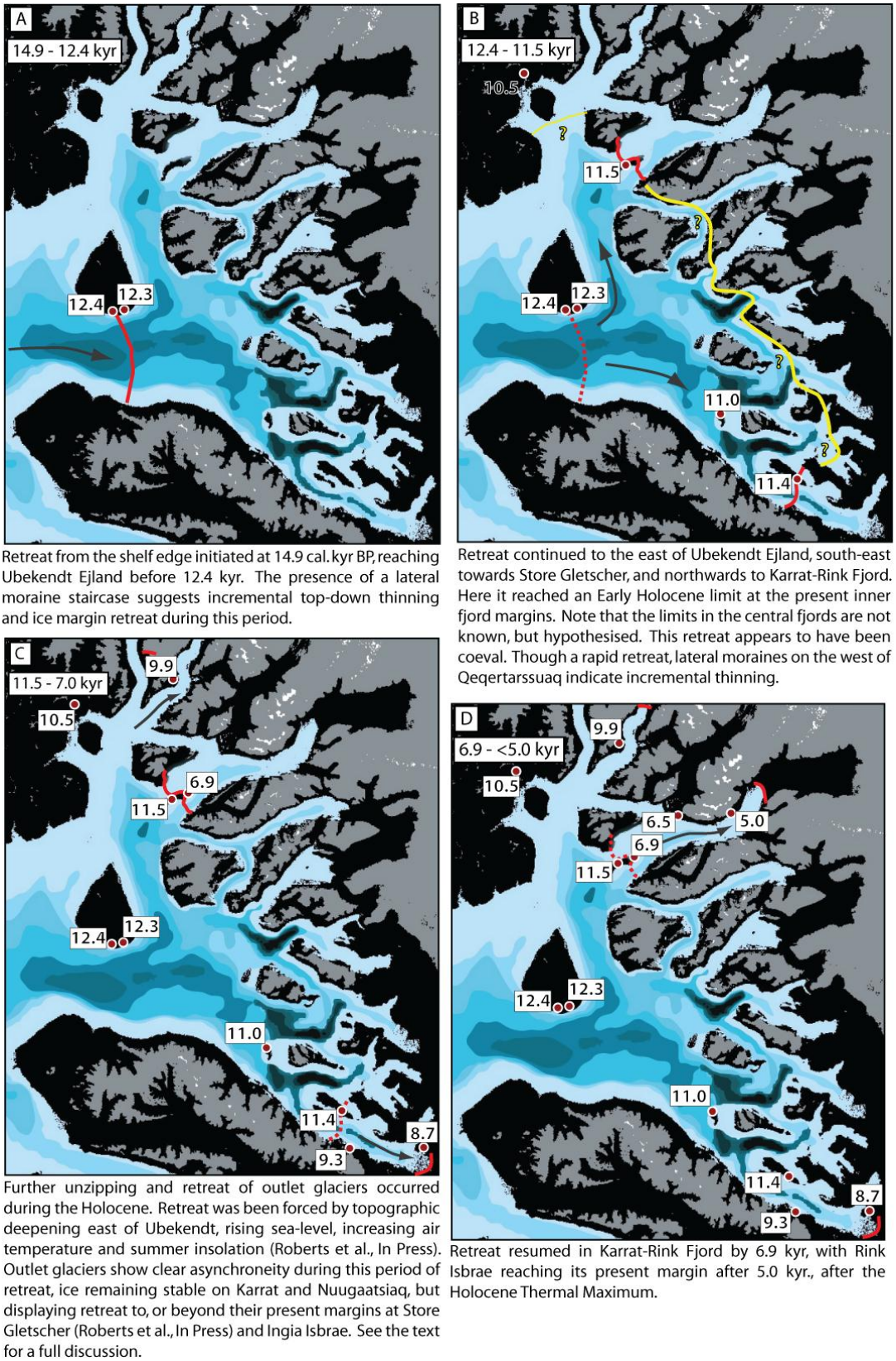

Figure 4.18. Schematic of the deglaciation of the UISS from its shelf-edge position at the LGM. Known margins, identified through geochronological and geomorphological data are in red, and hypothesised margins, with no geochronological control are in yellow. Arrows retreat in response to air temperature increase, instead appearing to retreat during the Neoglacial.show the predominant retreat directions during each phase of retreat. Data are from this study, Ó Cofaigh et al. (2013b) and Roberts et al. (2013).

4.6. Conclusion

The UISS existed as a large cross-shelf ice stream formed from multiple, confluent, outlet glaciers that terminated at the shelf-edge during the LGM. During the last glacial cycle, outlet glaciers in the northern Uummannaq region advanced through their fjord confines, and coalesced. Geomorphological and geochronological data provide evidence for warm-based ice between 1400 and 1900 m a.s.l. in the northern UISS during the LGM. These ice thicknesses are comparable to those in the southern UISS. High altitude terrain in the north of the region forced ice to remain topographically confined within 2000 m a.s.l. fjords, with intervening high-level areas likely to have been covered by cold-based plateau ice fields. Once coalescent, the majority of the ice was forced south by the geologically-controlled, over-deepened trough of Igdlorssuit Sund to the east of Ubekendt Ejland. Here it became confluent with ice from the southern UISS, draining west to the continental shelf edge. Deglaciation following the LGM took place in three stages: (1) Deglaciation from the shelf (underway by 14.9 cal. kyr BP) reached the southeast of Ubekendt Ejland by ~12.4 kyr BP; (2) Retreat through the confluent onset zone was accompanied by progressive separation of the individual outlet glaciers. Retreat was rapid and enhanced by trough over-deepening and widening, with ice reaching the northern outer fjords by 11.6 kyr; (3) Retreat through the present fjord system was interrupted by a period of topographically-controlled ice marginal stabilisation between ~9.1 and 6.9 kyr.

The first two stages of retreat were synchronous between the north and south of the UISS, reaching the present fjords by 11.5 kyr. This retreat was controlled by climatic and oceanographic forcings, enhanced by bathymetric depths. However, once within fjord confines, topographic constrictions became the dominant control upon individual outlet glacier dynamics, overriding climatic forcings, and causing early- to mid-Holocene ice marginal stabilisation in Rink-Karrat Fjord. A similar topographically controlled stabilisation also occurred in the southern UISS; with an earlier, shorter duration still stand (11-9.3 kyr). This topographic control forced the northern UISS to remain on Karrat Island until 6.9 kyr, during the onset of the Holocene Thermal Maximum. Thus, in fjord settings with high topography, care needs to be taken in correlating disconnected moraines simply on the basis of their position and their chronology. This could lead to erroneous correlations, and incorrect interpretation of controls upon moraine formation. Following this, Rink Isbræ retreated to a position at or beyond its present margin after 5.0 kyr. The ice within Rink-Karrat Fjord appears to have responded asynchronously with other West Greenland ice

streams. Additionally, ice retreat was clearly not responding in phase with the warm HTM and cooler Neoglacial. This ice stream therefore displays a unique dynamic within Greenland and provides compelling evidence for a first order topographical control on ice margin stabilisation in West Greenland. It also has major implications for our understanding and reconstructions of mid-Holocene ice sheet extent and Greenland Ice Sheet dynamics during the Neoglacial.

CHAPTER FIVE

Controls upon bedrock bedform development in the Uummannaq Ice Stream System, West Greenland

Abstract

A large body of work has used characteristics of bedrock bedforms in formerly glaciated regions to infer palaeo-ice flow conditions in areas of ice-sheet and ice-stream flow. This paper is an investigation of bedrock bedform evolution within the topographically confined upstream region of the palaeo-Uummannaq Ice Stream System (UISS), West Greenland. Bedform measurements were taken from four separate areas, and displayed high inter-area variability, despite similar palaeo-ice flow conditions. Bedforms included roches moutonnées and whalebacks, with elongation ratios (ELRs) varying from 0.8:1 to 8.4:1. Bedform long axes and plucked lee face orientations display a relationship to ice-flow conditions, responding to both uni- and bi-directional ice flow conditions. Joint and bedding plane frequency and orientation have controlled bedform width and length to varying degrees throughout the sub-areas. Lateral plucking, a mechanism previously only described for megagroove features, is invoked here for the formation of whaleback-type bedforms in Ingia Fjord. Bedding plane dip relative to palaeo-ice flow direction has been shown to be of vital importance for bedform morphology and ELR. Knowledge of dip relative to palaeo-ice flow allows predictions to be made about likely bedform shape, relative length, amplitude, and wavelength. These predictions have important ramifications for subglacial bed roughness and therefore cavity formation. The observations of this study demonstrate the direct link between bedding plane, joint structures, and bedrock bedform properties. They suggest that the use of bedrock bedform characteristics to directly infer palaeo-glaciological conditions must be approached with caution.

5.1. Introduction

5.1.1. Importance of glacial bedforms

Ice streams are zones of fast flowing ice which rapidly evacuate inland ice to the margin (Bennett, 2003). As a result, they are acknowledged to exert a considerable influence upon ice sheet dynamics and configuration (Stokes and Clark, 2001, Bennett, 2003). They are responsible for the majority of ice and sediment discharge from ice sheets, and their potential to expel much of this into the ocean has implications for ice sheet mass balance and ocean circulation (Bennett, 2003, Ó Cofaigh et al., 2003, Sejrup et al., 2003, Roberts et al., 2010). Our understanding of processes controlling ice stream behaviour is largely based upon the investigation and interpretation of landforms and sediments from palaeo-ice stream beds both onshore (Stokes and Clark, 1999, 2001, Roberts and Long, 2005, Stokes et al., 2009, Phillips et al., 2010) and offshore (Ó Cofaigh et al., 2002, 2013b, Canals et al., 2002, Sejrup et al., 2003, Evans et al., 2009, Hogan et al., 2010), remotely sensed observations of contemporary ice streams (e.g. Fahnestock et al., 1993, Goldstein et al., 1993, Bamber et al., 2000, Joughin et al., 2004, King et al., 2009), and *in situ* field studies of ice stream behaviour (Smith *et al.*, 2007).

Fast ice flow produces a suite of subglacial bedforms which display subglacial streamlining at varying levels. Ice streams have often been shown to display a marked downstream transition, which are manifest in bedform properties. Upstream regions are dominated by a rigid bedrock bed, often as a result of sediment deficiency and high erosive potential. Downstream regions are generally dominated by soft-beds of extensive sediment, generated once sufficient material has been eroded from upstream reaches (e.g. Graham et al., 2009, Evans et al., 2012). Here, soft-sediment bedforms are common, and elongation ratios (ELR) increase, and can be used to infer regions of ice streaming (Boyce and Eyles, 1991). These processes form a continuum of subglacial bedform development, from Rogen moraine and mega-scale glacial lineations (MSGL) (Stokes and Clark, 2001). Their form is thought to depend upon basal velocity, with highly attenuated bedforms (length to width ratios of >10:1) indicating fast ice flow (Stokes and Clark, 2002). Classification of these landforms based upon their elongation therefore allows for the reconstruction of palaeo-basal conditions during landform formation, including thermal regime, and basal velocity (Stokes and Clark, 2001). However, bedrock bedforms and the factors controlling their formation have received less attention.

A number of studies have reported bedrock bedforms in areas of palaeo-ice streaming. Offshore investigations have found bedrock dominated upstream portions of large palaeo-ice streams displaying landforms including rock drumlins and crudely streamlined bedforms with blunt stoss sides and tapered lee sides (Lowe and Anderson, 2002, Ó Cofaigh et al., 2002). Onshore studies have identified streamlined roches moutonnées and whalebacks (e.g. Gordon, 1981, Sugden et al., 1992b, Roberts and Long, 2005, Roberts et al., 2010, Krabbendam and Glasser, 2011), large bedrock ridges, mega-scale crag-and-tail forms (Jansson et al., 2003, Ottesen et al., 2008), and mega-grooves (Bradwell et al., 2008, Roberts et al., 2010). Despite this research, our understanding of bedrock bedform genesis and their relationship to ice flow dynamics remains limited.

5.1.2. Glacial erosion and bedrock bedforms

In glaciated regions devoid of sediment, the understanding bedrock bedforms and their relationship to ice flow is vital if palaeo-ice flow conditions are to be interpreted. Almost all features of glacial erosion are accounted for by processes of abrasion and plucking (Boulton, 1974a, Rea and Whalley, 1994), processes indicative of warm-based ice sliding across its bed (Rea, 2007). As defined by Rea (2007), abrasion is subglacial frictional wear at the bed, as debris-charged basal ice slides across it. This is enhanced as ice encounters a bedrock bump. Enhanced friction leads to increased basal melt and meltwater production, therefore moving particles held in the ice closer to the bed, increasing abrasive potential (Boulton, 1974a). Plucking occurs through bedrock fracture, bedrock block loosening, and block removal via entrainment (Boulton, 1974a, Rothlisberger and Iken, 1981, Rea and Whalley, 1994, Hallet, 1996). Bedrock fracturing occurs either through exploitation of pre-existing joint systems (Hooyer et al., 2012) or crack growth (Rea, 2007). The presence of ice-bed separation, and therefore subglacial cavity growth, is critical for block loosening as it encourages differential stresses across the bedrock obstacle (Rea, 2007, Krabbendam and Bradwell, 2011). Subsequent entrainment is thought to occur via bulldozing, freezing on of material to the glacier sole (Rea, 2007), and 'hydraulic jacking', when increased ice pressure expels water from the ice-bed interface, causing a sudden drop in ice pressure and refreezing of meltwater (Rothlisberger and Iken, 1981).

Work by Evans (1996a) suggested that variations in the presence or absence of whalebacks and roches moutonnées could be used to establish whether bed decoupling took place. It

was proposed that whalebacks formed as a result of continual ice-bed coupling across the bedform, preventing low-pressure cavity development (Evans, 1996a). In contrast, roches moutonnées form when ice-bed decoupling occurs, facilitating the development of low-pressure cavity formation, crack propagation, and block removal (Sugden et al., 1992b, Evans, 1996a, Benn and Evans, 2010). Evans (1996) therefore suggested that the preferential formation of whalebacks was indicative of thick ice, as large ice overburden pressures are able to suppress cavity formation, and encourage abrasion dominated erosion. This is supported by recent models which have shown that low effective pressures allow ice-bed separation, lowering glacier-induced stresses and the probability of erosion (Iverson, 2012). However, few extensive field studies have been able to show this relationship unequivocally.

One of the principle diagnostic characteristics of palaeo-ice streaming over soft sediment beds is subglacial landforms with a high elongation ratio (ELR) (>10:1) (Stokes and Clark, 2002). In contrast, in rigid bed settings, studies have reported low ELRs (<10:1) in areas of palaeo-ice streaming (Roberts and Long, 2005). This may be due to fixed basal perturbations and high levels of bed roughness which prevent flow stability at the ice-bed interface during subsequent glacial cycles (Roberts and Long, 2005). In addition, Roberts and Long (2005) proposed that roche moutonnée and whaleback development can occur during different phases of a single glacial advance and retreat, cycle as a response to changes in ice-bed coupling. Though plucking is a very effective erosive agent (Dühnforth et al., 2010), and can lead to rapid rock removal, bedrock bedforms are often more resistant to erosion than those formed of soft-sediment. This means that they can be formed and modified over multiple phases of glacial advance and retreat, often producing complex, double-plucked bedforms (Roberts and Long, 2005, Roberts et al., 2010). Thus, in contrast to soft sediment landforms, fast flow across a rigid bed results in high bedform densities and low ELRs (Roberts and Long, 2005).

In addition to controls imposed by ice flow, variability in bedrock structure can influence bedrock bedform morphology. Roberts *et al*., (2010) demonstrated that high ELRs (>10:1) in areas of palaeo-ice sheet flow were a result of repeated erosion sub-parallel to lines of geological weakness. Conversely, when dominant bedding structure was transverse to palaeo-ice flow, less elongate (ELRs = 3.7:1) bedforms were generated. In regions of constant inferred palaeo-ice flow direction and velocity, Krabbendam and Glasser (2011) proposed that bedform type (roche moutonnée vs. whaleback) and ELRs are controlled by

lithological variability. They found a direct link between the occurrence of plucking or abrasion, bedform morphology, bedrock hardness, and joint spacing. This is because an increase in bedrock hardness increases abrasion resistance, and low joint densities increase plucking resistance. Dühnforth *et al.* (2010) suggested that joint *spacing* governs the nature of erosion, and therefore the resultant bedform. Closely spaced fractures allow efficient plucking (and therefore roche moutonnée formation), whereas massive rock with few fractures is more susceptible to abrasion (and therefore whaleback formation). Others have discussed the role of joint density and orientation in bedrock bedform morphology. Hooyer *et al*. (2012) demonstrated that plucking preferentially occurs along pre-glacial joint systems, irrespective of sliding direction. This has been supported by a number of other studies (Gordon, 1981, Rea and Whalley, 1996, Krabbendam and Bradwell, 2011). A recent theory developed to describe glacial plucking suggested that bedrock of heterogeneous lithological strength, or with high joint density is likely to experience higher erosion rates, due to the increased probability of weakness exploitation (Iverson, 2012).

As a result of the current interest in ice stream activity in Greenland and their acknowledged importance to ice sheet dynamics (Velicogna, 2009, Holland, 2010, Box and Decker, 2011), our understanding of onshore ice stream behaviour from the LGM to present is developing quickly (Roberts et al., 2010, 2013, Weidick and Bennike, 2007, Briner et al., 2010, Young et al., 2011b). Knowledge of palaeo-ice stream behaviour in Greenland is important in order to predict future changes in ice stream activity, and appreciate the underlying processes. However, glacial activity in West Greenland produces relatively little sediment (Funder, 1989b), the majority of which is rapidly evacuated to ocean floor troughs and the continental shelf. These offshore troughs are often found to contain extensive soft sediment bedforms (Evans et al., 2009, Ó Cofaigh et al., 2013b). This lack of onshore sediment means that the majority of terrestrial glacial landforms in ice free areas of West Greenland are erosional, with regions of glacial scour dominating low elevation terrain (<1000 m a.s.l.) (Sugden, 1974; this study, Chapter Three, Glasser and Warren, 1990, Roberts and Long, 2005). In these areas, glacially eroded bedforms are ubiquitous, and it is from this evidence that palaeo-ice sheet basal conditions and velocities can be reconstructed.

This paper investigates bedrock bedform evolution within the onset zone of the Uummannaq Ice Stream System (UISS). Firstly, it explores the relationship between bedrock bedforms and basal ice flow conditions. Secondly, it considers the influence of local geology

on bedform formation, and finally, it considers the broader implications for our understanding of subglacial bedrock bedform genesis and evolution under ice streams.

5.2. Study site

5.2.1. Field sites

The study area lies within the Uummannaq region of Central West Greenland, between 71°21' and 71°57' N. The region covers ~25,000 km^2 and is delimited by two large peninsulas: Svartenhuk to the north; and Nuussuaq to the south (Figure 5.1). Repeated Quaternary glaciation through the Uummannaq region has formed a series of deep, coalescent fjords, running broadly east-west (Figure 5.1) (Roberts *et al.*, 2013). Topographic

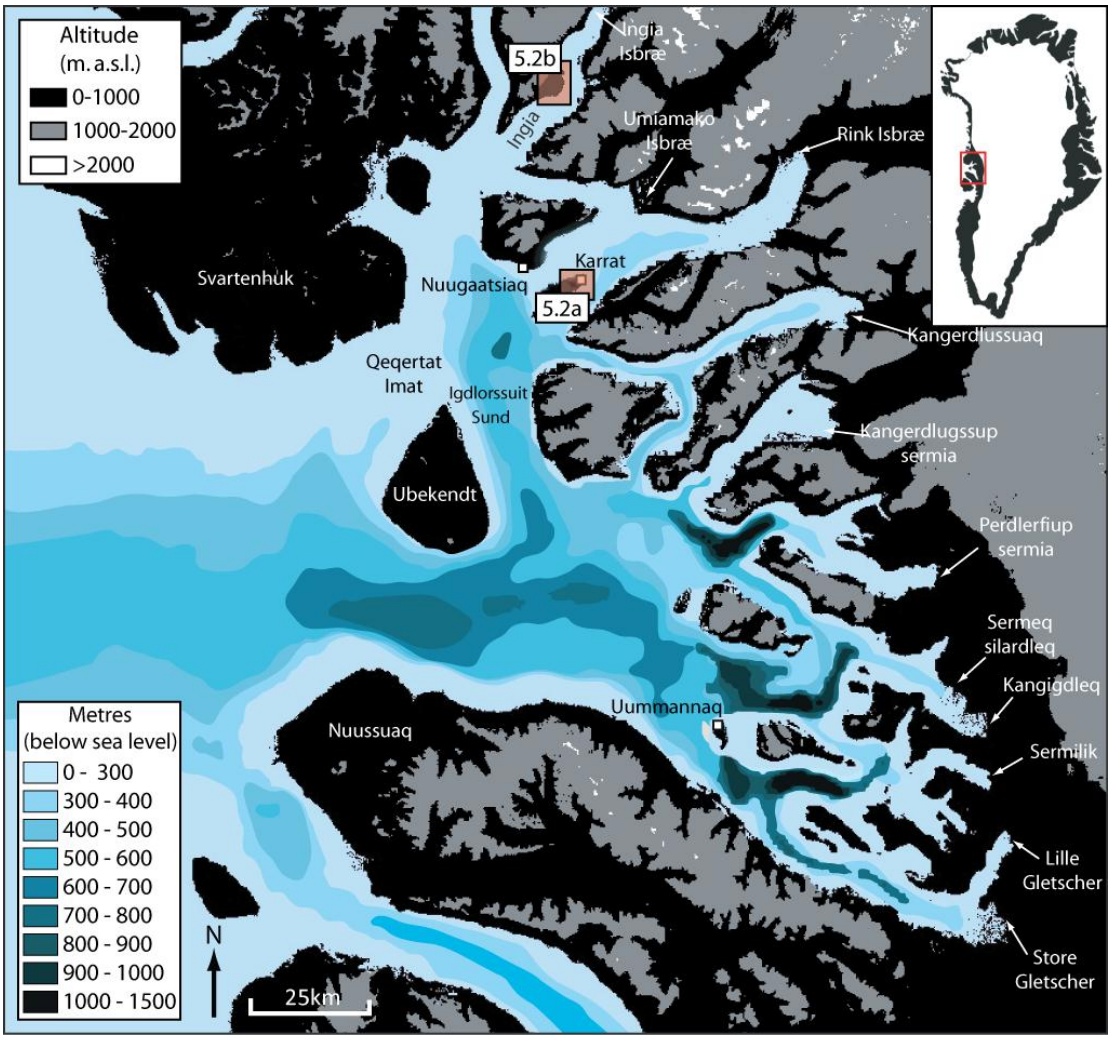

Figure 5.1. Overview topographic map of the Uummannaq region. Altitudes for contours have been extracted from ASTER GDEM2 data, and ocean floor bathymetry is from GEBCO. See Figure 5.2 (a and b) for enlargements.

dissection has created a highly mountainous landscape, with plateaux summits reaching 2000 m a.s.l., and fjords reaching 1300 m deep. The high-level terrain juxtaposed with these fjords fosters contemporary cold-based ice caps and regions of dissected plateaux. The two study sites are located within Rink-Karrat Fjord, and Ingia Fjord (Figure 5.1), 30 km and 18 km from current ice margins respectively. The sites are low in relief and elevation, in areas characterised by areal scouring, evidenced by ubiquitous glacially moulded bedrock. Sediment cover is sparse, evidenced only by a series of gravelly inset lateral moraines on Karrat Island, with little sediment between bedforms. In order to compare subglacial bedforms across settings of varying geological structure, two sub-areas have been selected in both Karrat and Ingia Fjords. Sub-areas KA1 and KA2 are in Rink-Karrat Fjord, and are both at similar elevations (200-260 m a.s.l.), on the eastern flank of the island (Figure 5.2). Sub-areas IN1 and IN2 are in Ingia Fjord, on the western side of a small peninsula at 100 m a.s.l. (Figure 5.2).

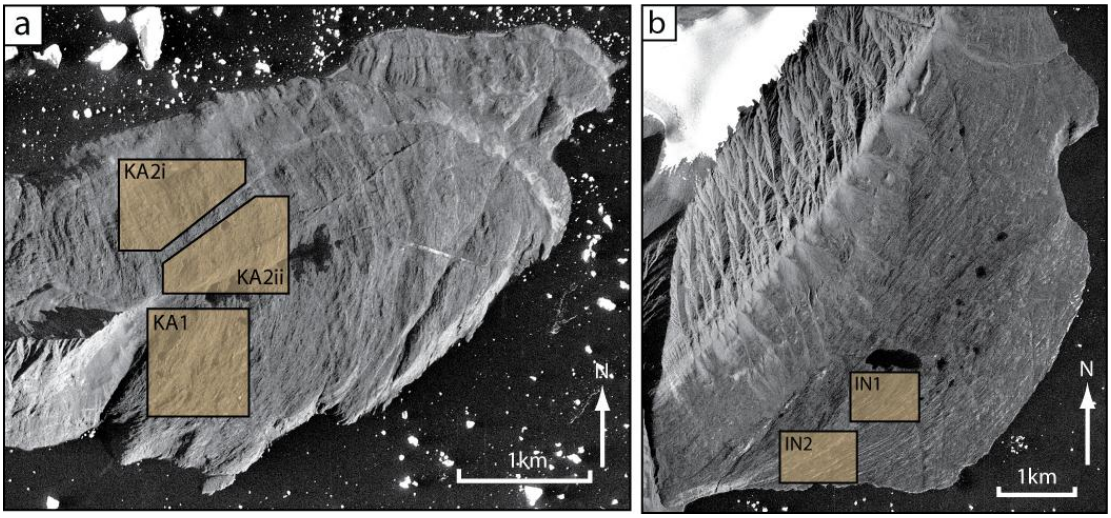

Figure 5.2. Aerial photographs showing the areas from which bedforms were analysed. Locations of each sub-area are labelled. Locations of Figure 5.2a and 5.2b are shown in Figure 5.1.

5.2.2. Geology

The geology of the Uummannaq region is characterised by Archaen basement rock in the East, overlain by Palaeozoic-Mesozoic sediments in the Igdlorssuit Sund region, and Palaeogene volcanic rocks offshore to the West (Figure 5.1 and 5.3) (Pedersen and Pulvertaft, 1992, Garde and Steenfelt, 1999, Henriksen et al., 2000). Exposed bedrock in Ingia and Karrat Fjord is from the Nûkavsak Formation, part of the extensive Rinkian belt

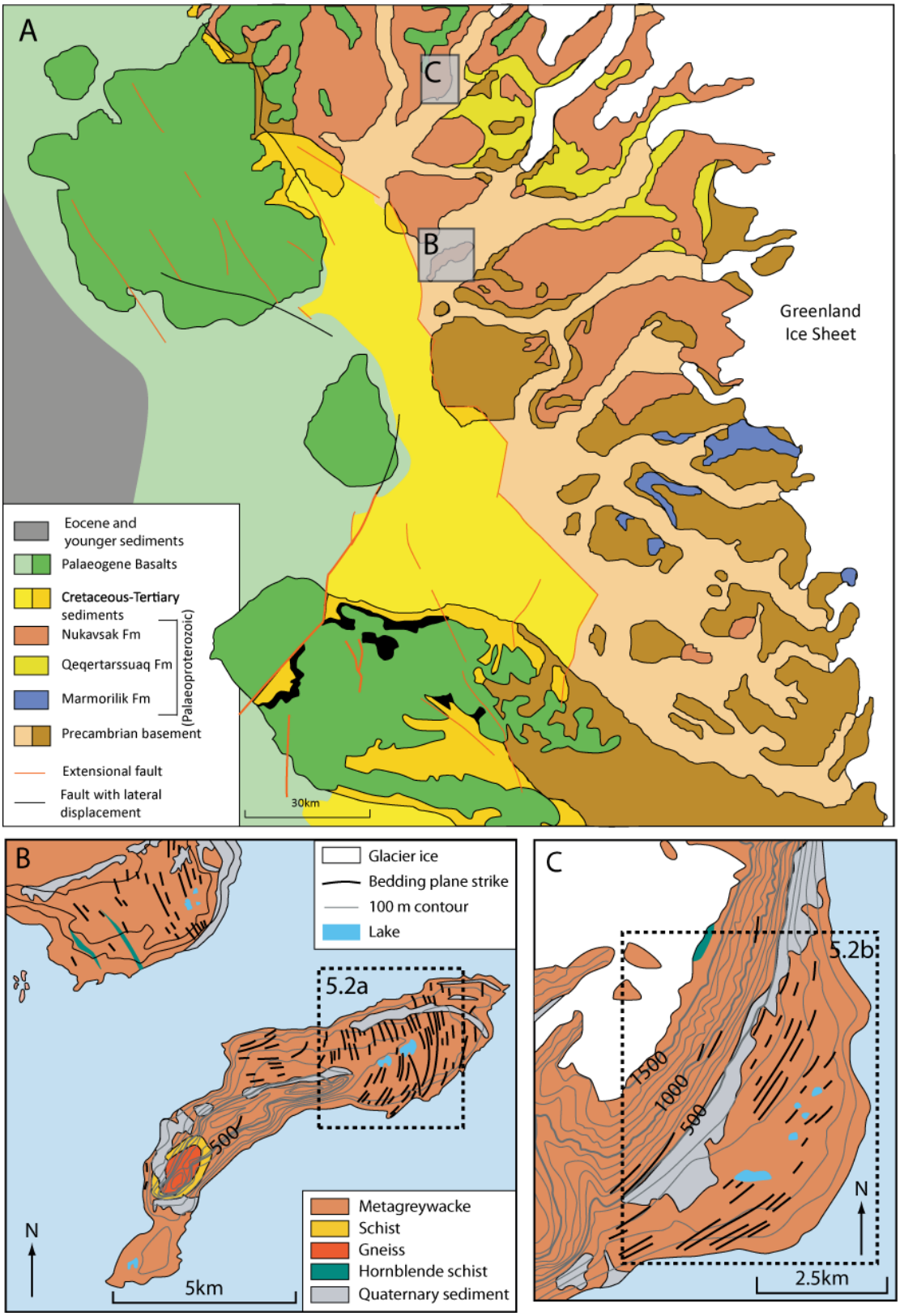

Figure 5.3. (a) Overview of the bedrock geology of the Uummannaq region (adapted from Christiansen et al., 1998). Note that the sites on Karrat Island and Ingia lie within the Precambrian basement; (b) enlargement of Karrat Island and Nuugaatsiaq Peninsula with dominant bedding structure indicated (adapted from Henderson, 1971); (c) enlargement of Ingia Peninsula, again with dominant bedding structure indicated (adapted from Henderson, 1971).

(Kalsbeek et al., 1998). As detailed extensively by Henderson and Pulvertaft (1987a) the Nûkavsak formation is composed of interlayered granular semipelite and pelitic schist, interpreted as turbidites. There is little lithological variation through their vertical and horizontal extent. This bedrock exhibits multiple sub-vertical and sub-horizontal joints, and beds of variable thickness (~5-20 cm). In the field, the metagreywacke was seen to be interbedded with infrequent veins of quartzite up to 50 cm thick. Though found in all sub-areas, their occurrence was most pronounced in IN1 and IN2.

5.2.3. Palaeo-glaciological background

During the Last Glacial Maximum (LGM), and potentially older glaciations, the entire Uummannaq region was dominated by a series of ice streams, which coalesced and extended ~200 km onto the continental shelf (Ó Cofaigh et al., 2013b), forming the Uummannaq Ice Stream System (UISS) (Roberts *et al.*, 2013). Recent field observations have shown that the upper limit of warm-based ice in the UISS was >1400 m a.s.l. during the LGM, with higher altitude areas either exposed as nunataks throughout the LGM, or covered by protective, cold-based ice (Roberts *et al.*, 2013; this study, Chapter Four). Palaeo-ice flow in the northern sector of the UISS (Ingia, Umiámáko and Rink Fjords) is thought to have coalesced and been deflected south, through Igdlorssuit Sund, an over-deepened Cretaceous bedrock basin (see Figure 5.3). Here it is thought to have coalesced with ice from the south of the system and flowed through the Uummannaq Trough onto the continental shelf (Roberts *et al.*, 2013). Therefore, all study areas sit in upstream branches of the palaeo-UISS within topographically constrained fjords. Based upon palaeo-glaciological reconstructions, ice would have remained topographically constrained within the fjord system at these points. These areas therefore represent unique locations in which to investigate the controls upon bedrock bedform structure in the upstream, topographically confined reaches of a large composite ice stream system.

5.3. Methods

Initial mapping was carried out using 1:50,000 topographic maps, geological maps (Henderson, 1971), 1:150,000 aerial photographs (3 m resolution) (Kort and Matrikelstyrelsen) and DEMs (created using ASTER GDEM2 imagery; ~15 m vertical resolution). This allowed for initial assessment of the broad-scale topography, and mapping of areas characterised by areal scour and bedrock bedforms. Regions of erosional glacial

landforms (e.g. roches moutonnées, whalebacks) were identified and mapped onto a topographic base map. Subsequently, four sub-areas were chosen for detailed analysis of subglacial bedforms in the field (Figure 5.2). These were chosen on the basis of accessibility and the ubiquity of bedrock bedforms throughout them. In these areas, glacial bedforms and their features (e.g. striae, plucked faces) were identified using previously identified criteria (Glasser and Warren, 1990, Roberts and Long, 2005), mapped, and classified as roches moutonnées or whalebacks, and by length as macro (100 m's), meso (100– 10 m's) or micro (<10 m's) (Roberts and Long, 2005). 50 or more bedforms were measured in each sub-area. Bedform long axis orientation and dimensions (length, width, and height) were measured, and elongation ratios (ELR) (the ratio of length to width) were calculated. Transverse wavelength (TW - transverse distance between bedform crests in metres) was measured in each sub-area, thereby allowing calculation of bedform density (km^2). Bedform density estimates were also made from aerial photographs to confirm these values. Bedrock structure was characterised within each study area, through measurement of bedding plane strike and dip, joint density, and joint strike and dip. Bedding planes, joint dip and dip direction were plotted using equal area lower hemisphere stereonets.

5.4. Results

5.4.1. Karrat sub-area 1 (KA1)

An overview of bedform data is presented in Table 5.1 and photographs from each study area are shown in Figure 5.4. Bedding planes in KA1 are tightly clustered, and strike WNW (Figures 5.3 and 5.5). Well-formed joint systems run NNE-SSW and SE-NW in KA1 (Figure 5.5), with 6-10 joints/m^2. Striae measurements are tightly clustered to 29°-209° (Figure 5.6 and 5.7) in broad accordance with average bedform long axis (220°). The majority of bedforms in KA1 are well-formed, meso-scale roches moutonnées, displaying some fragmentation. Abrasion is evident on stoss-sides, and plucking has occurred on mid- and lee-side slopes, dominantly on south-westerly faces (Figure 5.4a). Of the 50 measured bedforms, 6 are crudely formed whalebacks, with little plucking, and abundant abrasion. Average elongation ratio (ELR) is 2.52:1, and bedforms range from 1.9 – 23 m in length, 1.6 – 4 m in width, and 0.9 – 9 m in height. Bedform long axis becomes WSW (~250-260˚) to the south of the sample area. Bedform transverse wavelength is 20 m, with bedform densities of 190 – 250/km^2.

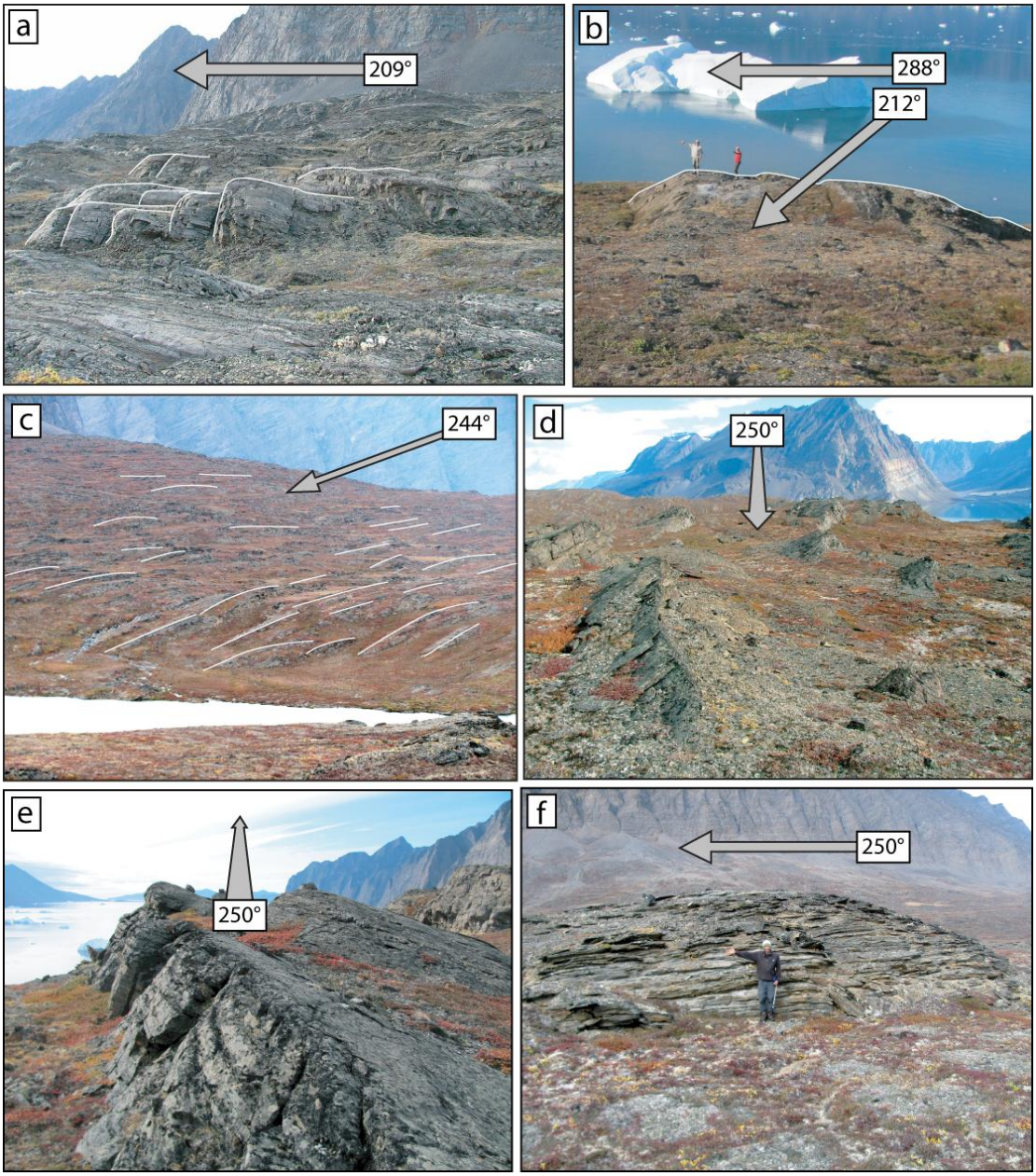

Figure 5.4. Photographs of bedforms from study sub-areas with long-axis orientations shown (grey arrows): (a) Roches moutonnées from KA1, with abraded stoss-sides and heavily plucked lee-sides. Frequent striae were found across upper faces. Palaeo-ice flow right to left; (b) Short, rectilinear roches moutonnées from KA2ii. Multidirectional striae and plucked faces suggest multiple palaeo-ice flow directions: right to left and obliquely towards the camera; (c) Field of whalebacks and occasional roches moutonnées in IN1: palaeo-ice flow right to left; (d) Asymmetrical whaleback forms from IN2 with palaeo-ice flow towards the camera. Little lee-side plucking is evident; (e) View looking down-ice of asymmetrical whalebacks in IN2 with steeply angled bedding planes apparent. Exposed ends of bedding planes can be seen to the left of the photo; (f) Side view of a whaleback from IN1, with palaeo-ice flow right to left. Sub-horizontal bedding planes are evident, and the lee-side morphology of the bedform conforms to bedding plane dip. See Figure 5.7 for photograph locations.

Area	Number (RM/WB)	Long axis (°)	Striae (°)	ELR	Height (m)	Density (bfms/km^{-2})	TW (m)	Joint density (m^2)
KA1	50 (44/6)	220	209	2.52	1.32	192-240	20	9
KA2	50 (50/0)	190	212/288	0.82	1.21	144-168	5	8
IN1	50 (9/41)	254	244	4.79	1.55	160-190	12	5
IN2	30 (5/25)	266	245	8.42	1.21	160-190	12	4

Table 5.1. Key features of bedforms mapped and characterised in this study.

5.4.2. Karrat sub-area 2 (KA2)

Bedding planes in KA2 are uniform and dip west (Figures 5.3 and 5.5). Well formed joint systems run N-S and E-W (Figure 5.5), with 6-10 joints/m^2. Bedforms are characterised by small, individual, rectilinear roches moutonnées. They display abraded stoss-sides, with ubiquitous lee-side plucking. No whalebacks or bedforms without lee-side plucking were recorded. Morphometric measurements from KA1 and KA2 demonstrate that KA2 represents population of bedform distinctly different to KA1 (Figure 5.5.b – 5.5d). Bedforms from KA2 were shorter, wider, and higher than those from KA1. The transverse wavelength of bedforms throughout KA2 is 40 m, and bedform densities are 170-190/km^2.

Ice flow direction, as indicated by striae and plucked face orientation, varied throughout KA2. As a result, sub-area KA2 was separated into KA2i and KA2ii (Figures 5.2a and 5.7). Bedforms in KA2i (n=40) displayed evidence for uni-directional ice flow (108° - 288°), and were found in the northwest of the KA2 region (Figures 5.2a and 5.7; Table 5.1). Bedform long axis (190°) is perpendicular to striae direction (108° - 288°). Bedforms are very short (0.80 - 13.20 m) and wide (1.50 - 15.00), with average ELRs of 0.80:1. Plucked faces in KA2i are westerly facing (varying between 275° and 285°), broadly concordant with striae direction. Westerly plucked faces are smooth, with a sloped, non-stepped appearance (Figure 5.4b), conformable to bedding plane strike and orientation.

Bedforms within KA2ii (n=10) displayed clear evidence for multi-directional ice flow (32° - 212° and 108° - 288°), and were found to the southeast of KA2i, further inland on Karrat Island (Figures 5.2a and 5.7a; Table 5.1). Within KA2ii, the striae show a cross-cutting relationship, with the 288° set superimposed upon the 212° set. As in KA2i, bedform long axis is 190°. This is oblique to the primary striae direction (212°), and perpendicular to secondary striae direction (288°). Bedforms were of similar length to those from KA2i (0.80

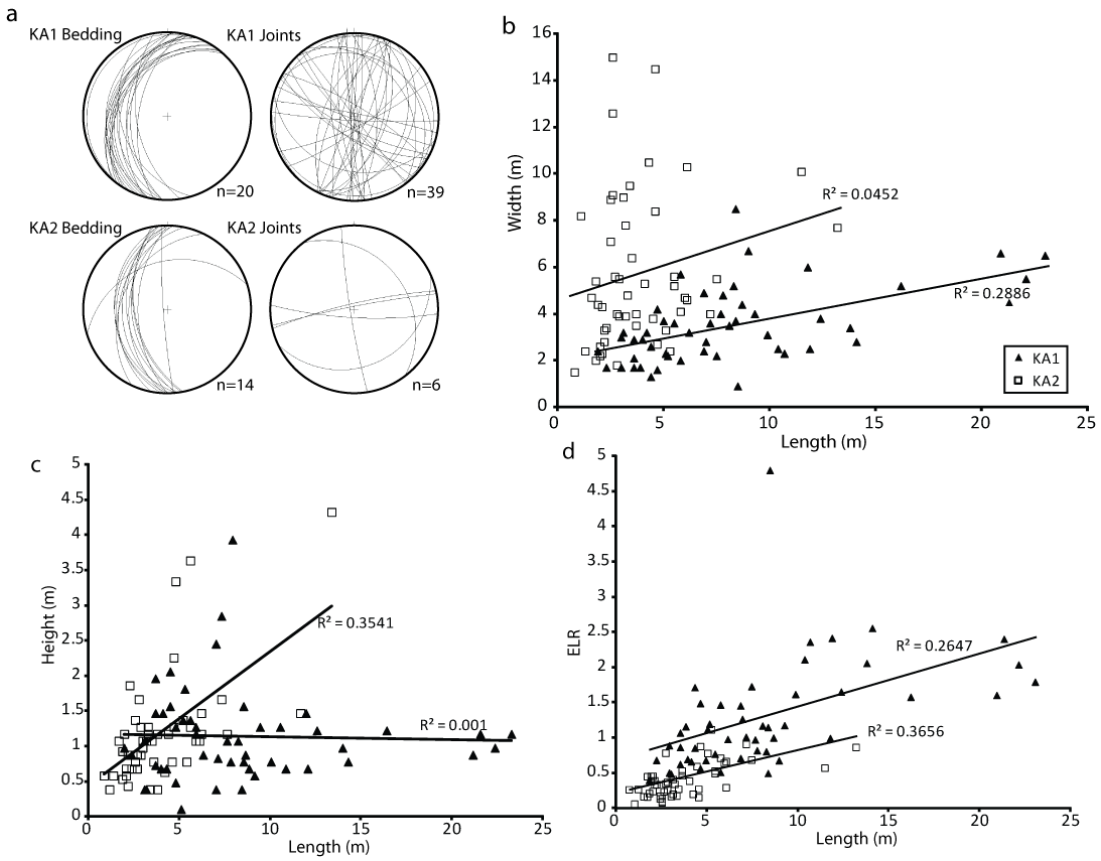

Figure 5.5. Bedform data from KA1 and KA2: (a) Bedding strike and joint dip orientation plotted in stereonets, (b) Scatter plot of width against length for KA1 and KA2 (c) Scatter plot of height against length for KA1 and KA2 (d) Scatter plot of elongation ratio (ELR) against length for KA1 and KA2.

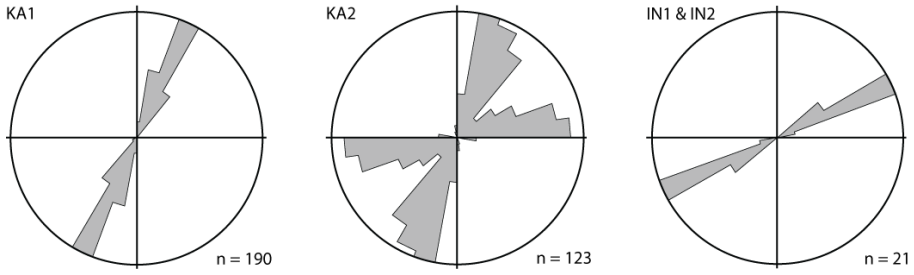

Figure 5.6. Striae data from the sub-areas studied, plotted in rose diagrams. Note that striae in IN1 and IN2 were very sparse, and poorly preserved. However, where present, identical striae directions were seen on bedforms in both IN1 and IN2

– 11.10 m), but slightly narrower (0.90 – 10.00 m), with ELRs of 0.88:1. Bedforms within KA2ii displayed two plucked faces, one smooth westerly face (as in KA2i) (~270°), and a second facing south-southwest (varying between 185° and 215°). These two plucked face orientations are broadly concordant with striae directions. Westerly plucked faces are

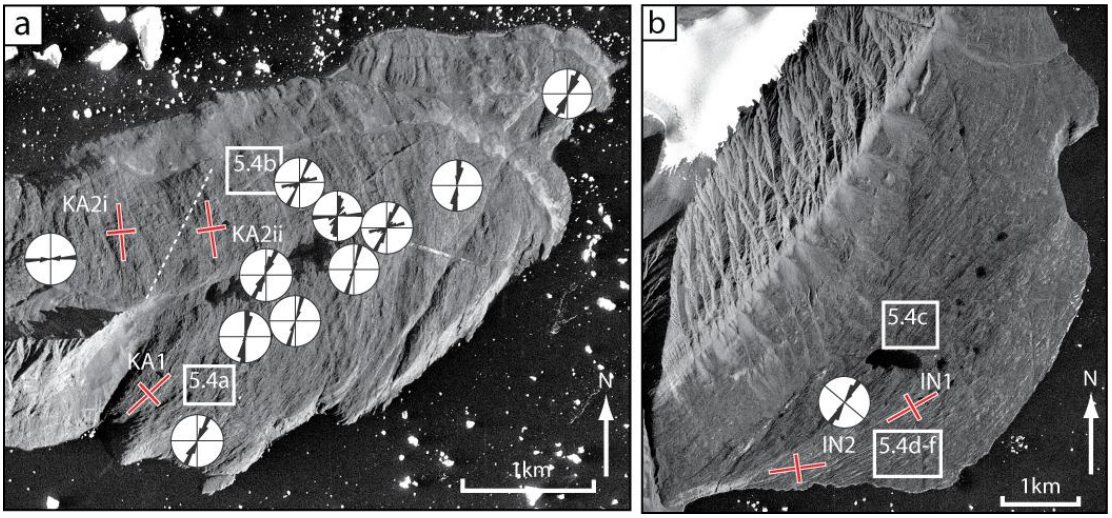

Figure 5.7. Aerial photograph with superimposed rose diagrams showing striae measurements across Karrat Island, and bedform long axes and secondary axes (red lines). Locations of photographs in Figure 5.4 are shown. The dashed white line in (a) delimits the boundary between KA2i and KA2ii.

smooth and conformable to bedding plane strike and orientation, similar to those in KA2i (Figure 5.4b). In contrast, south-southwest facing plucked faces are oblique to bedding plane and primary joint orientations.

5.4.3. Ingia sub-area 1 (IN1)

The metagreywacke in which the bedforms of IN1 and IN2 are formed is thinly bedded (5-15 cm), and strikes NW (Figure 5.8). Well-developed joint systems run NE-SW (dominant set) and NNW-SSE, with a joint density of 5-6 m^2. Based on striae evidence, palaeo-ice flow was NE-SW (244**°**), with bedform long axes in agreement (254**°;** see Table 5.1). Bedforms in this area are poorly formed meso-scale whalebacks (n=41) and roches moutonnées (n=9), with occasional superimposed micro-scale whaleback forms. Abrasion, as evidenced by striae and polished surfaces, is found on stoss-, mid- and lee-positions of bedforms, with some evidence of minor plucking. Where present, plucking is concentrated on the south-eastern lateral faces of bedforms, and some on the sloping lee-side faces. The bedforms are highly asymmetrical in transverse profile, with steep, stepped plucked SE faces and NW faces which slope with bedding (Figures 5.4d and 5.4e). Average elongation ratio (ELR) is 4.79:1, and bedforms range from 4.10 – 72.00 m in length, 0.70 - 18.90 m in width, and 0.20 - 7.60 m in height. Bedform transverse wavelength is 12 m, and bedform density is 160-190/km^2.

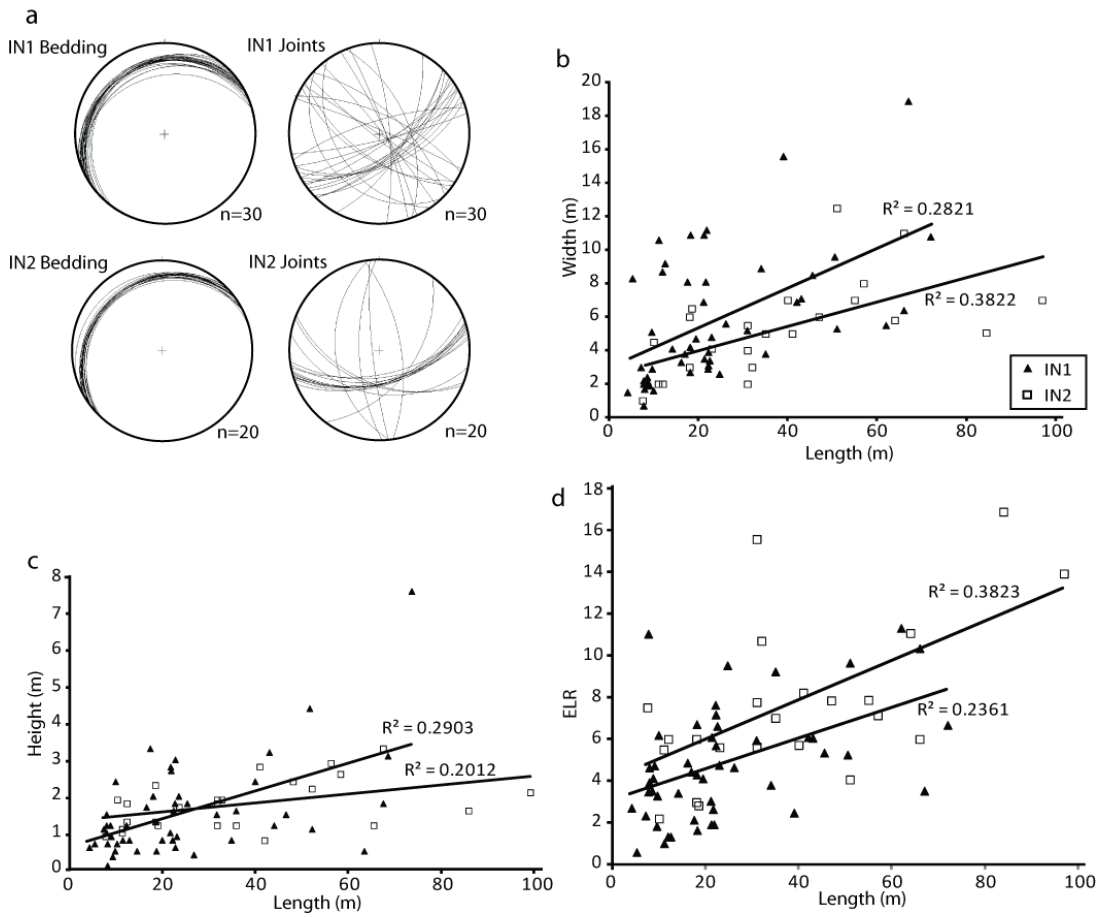

Figure 5.8. Bedform data from IN1 and IN2: (a) Bedding strike and joint dip orientation plotted as poles to planes in stereonets; (b) Scatter plot of width against length for IN1 and IN2; (c) Scatter plot of height against length for IN1 and IN2; (d) Scatter plot of elongation ratio (ELR) against length for IN1 and IN2.

5.4.4. Ingia sub-area 2 (IN2)

Bedrock in IN2 has similar properties to IN1, with thin, uniformly bedded bedding planes, striking NNW (Figure 5.8). Joint systems are well-developed and run NE-SW (dominant set) and N-S, with a joint density of 5-6/m^2. As in IN1, striae data show palaeo-ice flow to have been NE-SW (244**°**), with average bedform long axes of 266**°** (Table 5.1). Bedforms are characterised by poorly formed, meso-scale whalebacks (n=25), with occasional micro-scale whalebacks superimposed upon them. Rare roches moutonnées (n=5) were recorded. As in IN1, the cross-profile of the bedforms is highly asymmetrical. Abrasion has taken place on stoss-, mid- and lee-positions across bedforms. Where present, plucking is focused on the lateral, southern flanks of bedforms. Bedform ELRs are the highest in this area (8.42:1), and bedforms 7.50 – 96 m in length, 1 – 12 m in width, and 0.90 – 3.30 m high. The transverse wavelength of the meso-scale bedform ridges is 12 m, and bedform density is 160-190/km^2.

Morphometric measurements of bedforms from IN1 and IN2 demonstrate that, in contrast to KA1 and KA2, they represent very similar populations, with no major difference in width, height, length, or ELR (Figure 5.8.b – 5.8d).

5.5. Discussion

5.5.1. Bedform relationship to ice flow

The following section discusses the relationship of bedrock to the basal and glaciological conditions experienced during the last glacial cycle. Sites from both Karrat Island and Ingia sit in deeply incised fjords, upstream of the UISS onset zone. The UISS is known to have been active throughout the LGM and earlier glaciations (Roberts *et al.*, 2013). As a result of this deeply entrenched setting, all sub-areas would have been subject to focused selective linear erosion and areal scour by thick ice during multiple glacial cycles. It is likely that local ice flow velocities were high, induced through topographic drawdown into over-deepened troughs (Hall and Glasser, 2003, Roberts and Long, 2005, 2013). As demonstrated by striae and terrestrial cosmogenic nuclide evidence across Karrat Island and Ingia Fjords; warm-based, erosive UISS ice was present up to 1968 - 1400 m a.s.l. in the inner fjord, and >1040 m a.s.l. in the outer fjord (see Chapter Four). As both areas represent small, low elevation peninsulas (100-260 m a.s.l.), they would have been covered by >700 m of ice during the local LGM. This evidence, independent of bedform data, suggests that all study areas were subject to glacial erosion under thick, warm-based ice.

Thick ice leads to warmer basal conditions, lower ice viscosities, and increased subglacial meltwater production, encouraging higher basal erosion rates (Kessler et al., 2008, Iverson, 2012). The warm-based, low viscosity ice would have encouraged enhanced creep as bedrock basal perturbations were encountered (Benn and Evans, 2010). As bedform interpretation is typically used to assist in inferring palaeo-glaciological conditions, the bedform response to palaeo-glaciological conditions has to be approached with care. Although ice thicknesses throughout the region are known, and during glacial flow conditions the region would have been dominated by widespread, warm-based ice, accurate ice velocity estimates are difficult to make. However, as LGM ice thicknesses are thought to have been comparable between Ingia and Karrat Island, any regional bedform variation will therefore be accounted for by either changes in ice flow direction, velocity, or non-glacial factors.

Bedforms in KA1 show a clear relationship to palaeo-ice flow direction. Striae show evidence for uni-directional ice flow (209°), sub-parallel to average bedform long axis (Figure 5.7). Roches moutonnées show clear evidence of stoss-side abrasion, and extensive plucked southwest lee-side faces, consistent with the action of both abrasion and plucking across the bedform (Sugden et al., 1992b, Rea, 2007). Forces acting directly into the bed are greatest on the stoss-side, which encourages widespread abrasion. Conversely, lee-side block removal occurs through plucking, with reductions in normal stresses allowing fracture and consequent block entrainment (see section 5.1.2.) (Rea, 2007).

Bedforms within KA2 are a response to either: uni-directional (KA2i) or multidirectional (KA2ii) ice flow. In KA2i, uni-directional flow (288°) was perpendicular to bedding strike, creating short rectilinear bedforms with a single westerly lee-side plucked face, and an abraded stoss-side face. Bedforms from KA2ii display characteristics of multiple ice flow directions and are clustered to the southeast of KA2. Here, ice flow switching across Karrat Island has caused multiple phases of plucking, forming multiple plucked faces. Although only two phases of ice flow are recorded in the geomorphological evidence of KA2ii (212° and 288°), it is glaciologically implausible that they were not preceded by an initial phase of topographically constrained E-W ice flow. A geomorphological expression of this earlier flow phase is either not present due to erosion by subsequent ice flow, or is present, but cannot be differentiated from the latter E-W flow phase. Based upon this, a three stage ice flow model is predicted for the region:

(1) East-west, topographically constrained ice flow at ~288°. This phase would have occurred during ice build-up. This was transverse to bedding strike in KA2, causing abrasion of easterly stoss faces, and plucking of westerly lee-sides;

(2) As ice thicknesses increased they were sufficient to overwhelm west Karrat Island, and were probably sourced from Umiámáko Isbræ. As a result of the removal of this topographic constriction ice flow became northeast-south west at ~212°. This was oblique to bedding strike, abrading northeast faces and plucking south-southwest faces;

(3) Ice flow became topographically constrained, flowing east-west during deglaciation. Ice flow was transverse to bedding strike, causing further easterly stoss faces and westerly lee-side plucking. This would have reactivated plucked faces originally eroded in the first ice flow phase. In addition, plucked faces developed during the second stage of ice flow would have been smoothed.

Alternatively, the striae could solely represent the deglacial phase of LGM ice activity on Karrat Island. If so, it is likely that the cross-cutting striae are marking a response to increasing topographic control during deglaciation. This would mean only points 2 and 3 of the above model are represented in this striae set, explaining the possible absence of the earlier phase.

There are also large differences in ELR between KA1 and KA2i/KA2ii (2.52:1 and 0.80:1/0.88:1 respectively). However, due to their close proximity (<1.5 km), differences in palaeo-ice flow thicknesses and velocities are likely to have been negligible, suggesting that glaciological factors did not control bedform length and width in KA1, KA2i, and KA2ii.

As evidenced by striae and fjord orientations, ice flow across IN1 and IN2 was consistent (244°) and sub-parallel to bedding strike. As a result, bedforms in both IN1 and IN2 display a similar response to ice flow. This has produced elongate bedforms with long axes sub-parallel to ice flow (254° and 266°), abraded stoss- (NE) and lee-sides (SW), and plucked lateral faces (SSE). The fact that bedform long axes are sub-parallel to ice flow suggests that they represent a similar response to their palaeo-glaciological conditions as bedforms in KA1 – with abrasion and plucking creating bedforms with long axes conforming to palaeo-ice flow direction. However, as opposed to the dominance of roches moutonnées in KA1 and KA2 (94 out of 100), 66 of 80 bedforms in IN1 and IN2 are whalebacks. Although it has been previous suggested that fast ice preferentially produces whalebacks through suppression of cavity development (Evans, 1996a), all the areas in this study are thought to have experienced similar LGM ice velocities. This makes it unlikely that variability in bedform type is controlled by ice flow. There are differences in distance from the current ice margin and in topography between Karrat Island and Ingia, but both sites represent significant constrictions within the fjord, making it unlikely that the local topography controlled bedform morphology.

It is evident that bedform morphology in all sub-areas throughout this study is a result of a complex response to palaeo-ice flow conditions. Given the hypothesised consistency of other ice flow properties (thickness, basal conditions, and velocity), palaeo-ice flow direction has exerted an important control upon bedform characteristics in all sub-areas through plucking and abrasion (e.g. long axis, plucked face orientation). In areas of multi-directional ice flow (KA2ii), it has caused bedform shortening and the development of multiple plucked faces (Roberts and Long, 2005, 2010). In contrast, bedforms in areas of

unidirectional ice flow (KA1, KA2i, IN1, and IN2) would be hypothesised to display higher ELRs, due to a single flow direction, and therefore a consistent direction of erosion. Though applicable for most areas in this study (KA1, IN1, and IN2), this is not found in KA2i. Here bedforms are extremely short, with ELRs of <1:1, despite unidirectional ice flow and comparable palaeo-ice thicknesses to other sub-areas. It is therefore clear that variability in bedform morphology in this study (e.g. bedform type and ELR) it not explicable solely through ice flow properties.

5.5.2. Bedform relationship to geological structure

Although bedrock bedforms must develop as at least a partial response to the palaeo-glaciological characteristics they experience (thermal regime, thickness, velocity), only in KA1 does this response appear simple, with ice flow parallel bedding planes, and plucked lee-faces directly down ice of bedforms. In other areas long axis, orientation, ELR, plucked face orientation, and bedform type appear to be controlled by non-glaciological factors. Of these non-glacial factors, bedrock structure is well known to exert a direct control of varying impact upon bedform morphology and development. Initially explored by Gordon (1981), variations in bedding plane orientation, joint orientation, and rock hardness can influence the nature and morphology of resultant bedforms. These relationships have been investigated by a number of authors (Gordon, 1981, Rea and Whalley, 1994, Roberts and Long, 2005, Roberts et al., 2010, Dühnforth et al., 2010, Krabbendam and Bradwell, 2011, Krabbendam and Glasser, 2011, Hooyer et al., 2012). As described above, bedding plane strike, joint orientation and joint spacing vary greatly between Karrat Island and Ingia (Figures 5.5, 5.6 and 5.9), and it is possible that these differences have driven the bedform morphology variability.

In KA1, KA2i, and KA2ii, bedding plane and joint characteristics have had a demonstrable impact upon bedform properties. In KA1 the NW-SE joint set is transverse to palaeo-ice flow (Figure 5.5 and 5.7), which has facilitated widespread lee- and mid-slope plucking. Over time, block removal during glaciation has removed large volumes of material from lee-side slopes, resulting in bedform shortening (Roberts and Long, 2005). Bedform width has also been controlled by bedrock structure; joints running sub-parallel to palaeo-ice flow (NE-SW), and bedding planes dipping NW have acted as lines of weakness along which ice has been able to preferentially erode through both abrasion and plucking. The steep bedding plane

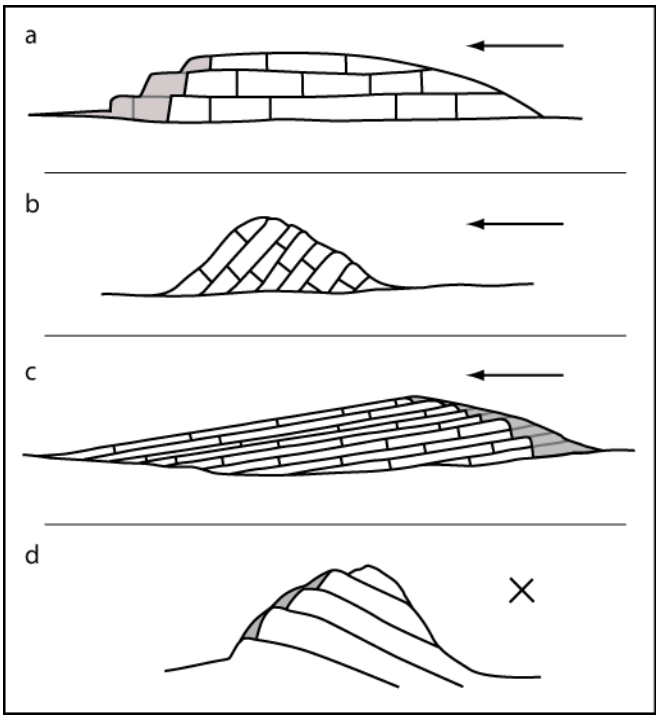

Figure 5.9. Idealised schematic diagrams of bedforms from: (a) KA1; (b) KA2i; (c & d) IN1 and IN2. Ice flow direction is indicated by arrows. (a, b and c) Long-sections through the bedforms, (d) short-section through the bedform displayed in c. Grey areas indicate zones which have experienced clear plucking. Note that ice flow in d is into the page.

dip (41°) has exposed more exploitable lines of weakness than shallow bedding would, encouraging the development of narrow bedforms in KA1.

As outlined above, bedforms in KA2i are a response to erosion from unidirectional ice flow during the LGM. Lee-side plucking of westerly bedform faces in KA2i has been facilitated by extensive, well-developed north to south striking bedding planes and joint systems (see Figures 5.5 and 5.9). These structures run perpendicular to palaeo-ice flow direction (288°), and dip down-ice. This orientation and angle of dip has encouraged block removal directly along bedding plane surfaces. Plucking of this nature has produced the low-relief, non-stepped plucked faces throughout KA2i, with faces parallel to bedding plane dip in three-dimensions. The steep average bedding plane dip has facilitated ice-bed separation across the lee-sides of the bedforms. This has caused the exploitation of bedding planes and sub-parallel joints, as lines of weakness, through plucking. It is this process and bedding plane configuration which has generated the smoothed, sloping lee-side plucked faces. Despite the non-stepped appearance of the faces, plucking was the dominant erosive agent during bedform development. The less extensive east to west joint system has exerted some control over bedform width, via joint propagation, block removal, and abrasion along them.

However, the low density of this joint set has meant width reduction has been minimal, allowing bedforms to maintain their large width and low ELRs. These low ELRs (~0.8:1) are therefore a direct result of bedrock structure, encouraging bedform shortening.

In contrast, bedforms within KA2ii are a result of erosion following multi-directional, multi-phase ice flow. Bedforms exhibit clear multiple plucked faces, recording an erosional response to east – west and northeast – southwest ice flow. In the model proposed in section 5.1.1., east – west ice flow caused plucking along north - south trending joints and bedding planes, forming westerly facing plucked faces, similar to those in KA2i. Subsequent north-east to south-west ice flow formed south-west and south facing plucked faces through block removal along east to west trending joints. This phase of ice flow was oblique to joint orientation, and resultant plucked faces are less distinct. A resumption of east to west ice flow led to plucking of westerly faces, causing further block removal and bedform shortening.

In IN1 and IN2, bedrock structure has exercised a strong control upon bedform type, length, width and orientation. Despite a stable ice flow direction between the two areas (244°), bedform long axis fluctuates between 254° (IN1) and 266° (IN2). This long axis variation closely mirrors a change in bedding plane strike from 317° and 325°, suggesting a formative relationship between the two. Though little lee-side plucking was documented, almost all bedforms in IN1 and IN2 show evidence of extensive block removal from their steep SE faces (Figure 5.4d). This plucking has been facilitated by exploitation of the exposed ends of NW striking bedding planes, with blocks removed along sub-vertical NE-SW joints, controlling bedform width.

Bedforms on Ingia are dominated by whaleback forms (66 out of 80). As discussed in section 5.1, their abundance (over roches moutonnées) is unlikely to be a function of ice flow characteristics, due to the similarity between Ingia and Karrat Island. They display ubiquitous stoss- and lee-side abrasion, and in general, little evidence of plucking or clear plucked faces on lee-sides, despite the presence of joints running transverse to palaeo-ice flow. This suppression of lee-side plucking is a result of three factors. Firstly, bedding planes and the majority of joints are sub-parallel to palaeo-ice flow, with few joints running transverse to palaeo-ice flow (1-5 m^2). This low joint density makes plucking difficult, as the ability of ice to exploit lines of weakness is reduced, and block loosening is hindered. Secondly, a number of bedforms display thick (30-50 cm) bands of quartzite, interbedded

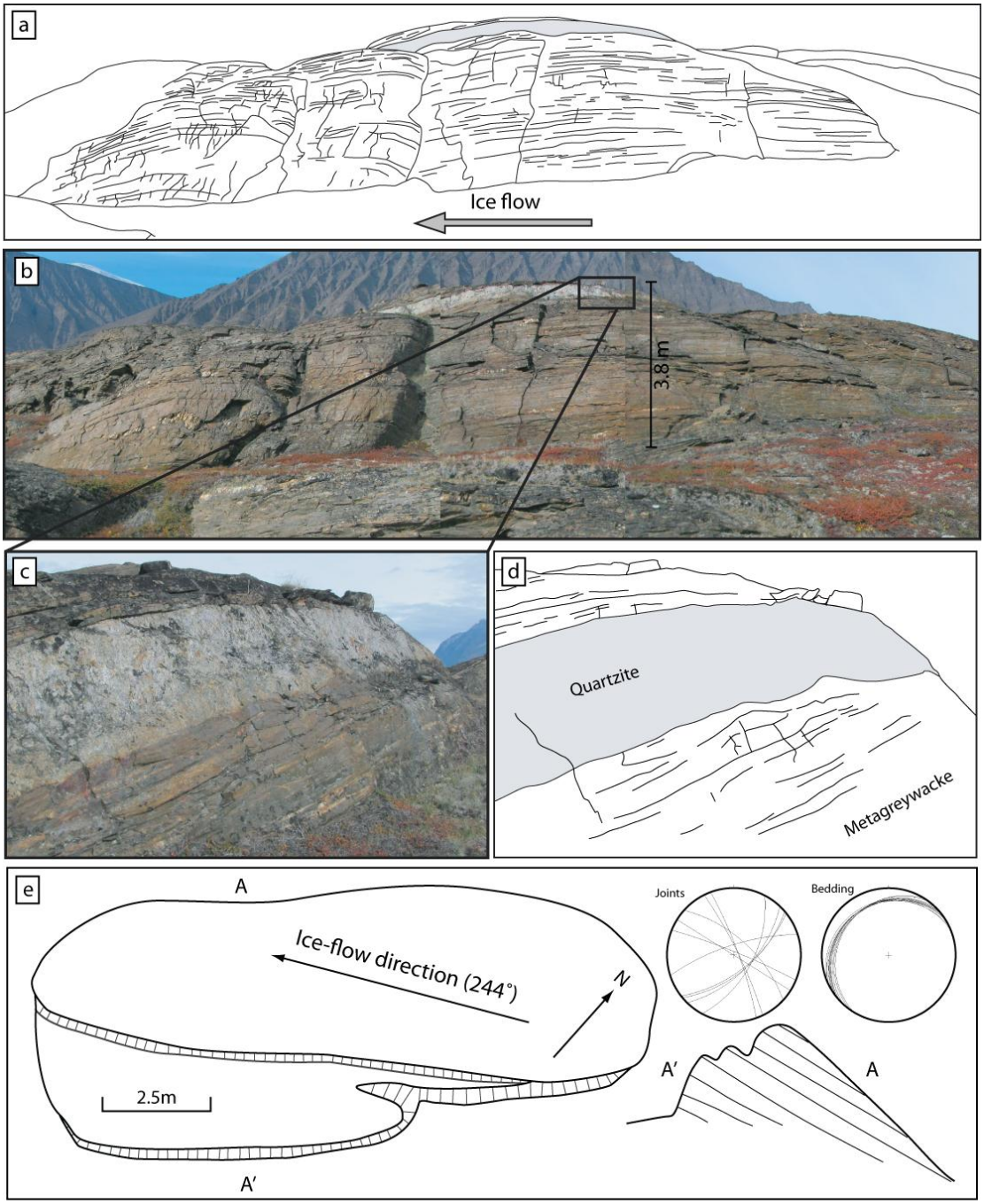

Figure 5.10. Photographs and sketches of a large, abraded whaleback bedform from IN1, representative of the bedforms found throughout the region. Palaeo-ice flow was right to left in a and b: (a) Sketch of the bedform, showing all major visible joints and bedding planes. The quartzite band towards the top of the bedform is marked by grey shading. Abrasion is evident on stoss- and lee-sides, with no demonstrable lee-side plucking; (b) Photograph of the whaleback. The southeast facing laterally plucked surface faces the camera; (c) and (d) Photograph and sketch of the upper half of the bedform, showing the noticeable difference in bedding and joint density between the metagreywacke and quartzite; (e) Plan and short cross-profile view of the bedform, with bedding and joint data.

with metagreywacke. In places these cap the bedforms, or outcrop at the bedform surface (Figure 5.10b and c). The crystalline quartzite is harder than metagreywacke, and also contains far fewer bedding planes and joints (~1-4 m^2) than the metagreywacke. These properties make the quartzite considerably more likely to experience abrasion than plucking (Krabbendam and Glasser, 2011). Therefore, where present, the quartzite has assisted in creating smooth stoss- or lee-side faces. Thirdly, bedding planes in IN1 and IN2 have a down-ice dip of 3° relative to ice flow. As the metagreywacke is thinly bedded (5-15 cm), ice on the lee-side of bedforms was able to easily abrade across the bedding plane surfaces; the most prominent lines of weakness. This again limits opportunities for block loosening and removal. Some erosion through plucking is likely to have taken place alongside the extensive abrasion. As the thin bedding planes dip down-ice, it is foreseen that plucking would occur through the removal of thin sheets, directly along the bedding planes. However, the available evidence cannot provide further detail on this process, and it forms an important impetus for further investigation.

Geological structure has played an important role in controlling the variability of a number of bedform properties that cannot be explained by spatial or temporal changes in ice flow characteristics. In particular, joint and bedding plane density and orientation have been shown to exert a strong control upon bedform type, length, width and orientation. In addition, the steepness of bedding plane dip *relative* to ice flow appears to have a strong effect upon both ELR and bedform type.

5.5.3. Relationship to other studies – importance of understanding bedrock structure

A number of studies have attempted to understand the complexities of interactions between bedrock bedforms, ice flow dynamics and bedrock structure. Results from KA1, KA2i, and KA2ii demonstrate the role that single and multiple flow directions, variations in bedding orientation, and joint characteristics play in bedform development. These findings reinforce some conclusions drawn by others. Roberts and Long (2005) reported bedforms from areas of ice streaming with low ELRs (2.8:1) but high densities (>200 km^2), as a result of abrasion, intense plucking, and consequent bedform shortening through advance and retreat cycles. Though joint structure is acknowledged to have had a role in bedform properties, it is concluded that ice velocity is the principal control upon bedform morphology. The bedforms from the Roberts and Long (2005) study appear directly comparable to those from KA1, displaying a similar response to palaeo-ice flow; low ELRs

and high densities. In the Sisimiut region, West Greenland, Roberts *et al*. (2010) demonstrated that strong bedding structure orientated sub-parallel to ice flow allowed slow flowing ice to produce elongate bedforms (ELRs >10:1) through repeated glacial inundation. In contrast, in an area of palaeo-ice streaming, bedforms with low ELRs (3.7:1) were reported (Roberts et al., 2010). High bedform densities were also reported (>200 bedforms km^2), similar to those in KA1 and KA2. These were formed by bi-directional ice flow, transverse and sub-parallel to the bedding plane direction, comparable to KA2ii. As in KA2ii, geological and glaciological conditions have produced short, wide bedforms with low ELRs and multiple plucked faces (Roberts et al., 2010). As plucking occurs through block removal, a reflection of palaeo-ice flow direction in plucked face orientation is expected. However, in KA2i, KA2ii, IN1 and IN2 there is an offset between plucked face orientation and palaeo-ice flow direction. This is because plucking has been facilitated by fracturing along pre-glacial joints, and does not always directly reflect palaeo-ice flow direction (Figure 5.11). This is supported by other studies (Gordon, 1981, Rea and Whalley, 1996, Krabbendam and Bradwell, 2011, Hooyer et al., 2012) and is in agreement with Hooyer et al.'s (2012) plucking model, in which block removal occurs when rock bridges between joint separated blocks fail, meaning plucked faced distribution preferentially follows joint orientation.

Recent work based on a small number of bedforms in northwest Scotland suggested that joint spacing is able to govern the amount of glacial erosion possible over a bedform surface (Krabbendam and Glasser, 2011). In combination with rock hardness, it can also control the switch between the plucking and abrasion as the dominant erosive mechanism. Though joint spacing is likely to have been an important control upon bedforms in the study area, there was not a sufficient sample size to analyse this relationship.

A similar type of bedrock plucking to that recorded on the lateral flanks of bedforms in IN1 and IN2 has been outlined by Krabbendam and Bradwell (2011), where it was termed "lateral plucking". In their description, this process formed a series of negative megagroove features, not positive bedforms as in this study (Krabbendam and Bradwell, 2011). Lateral plucking is described as a form of lee-side plucking, rotated by 90°, requiring a very particular orientation of joint and bedding planes in relation to ice flow. During lateral plucking, cavities form on steep walls with multiple protuberances, allowing block loosening and translocation about a vertical axis, causing erosion at right angles to ice flow (Krabbendam and Bradwell, 2011). In their discussion, erosion along the flat surfaces (i.e. megagroove floors) is dominated by abrasion due to a cited absence of protuberances in the

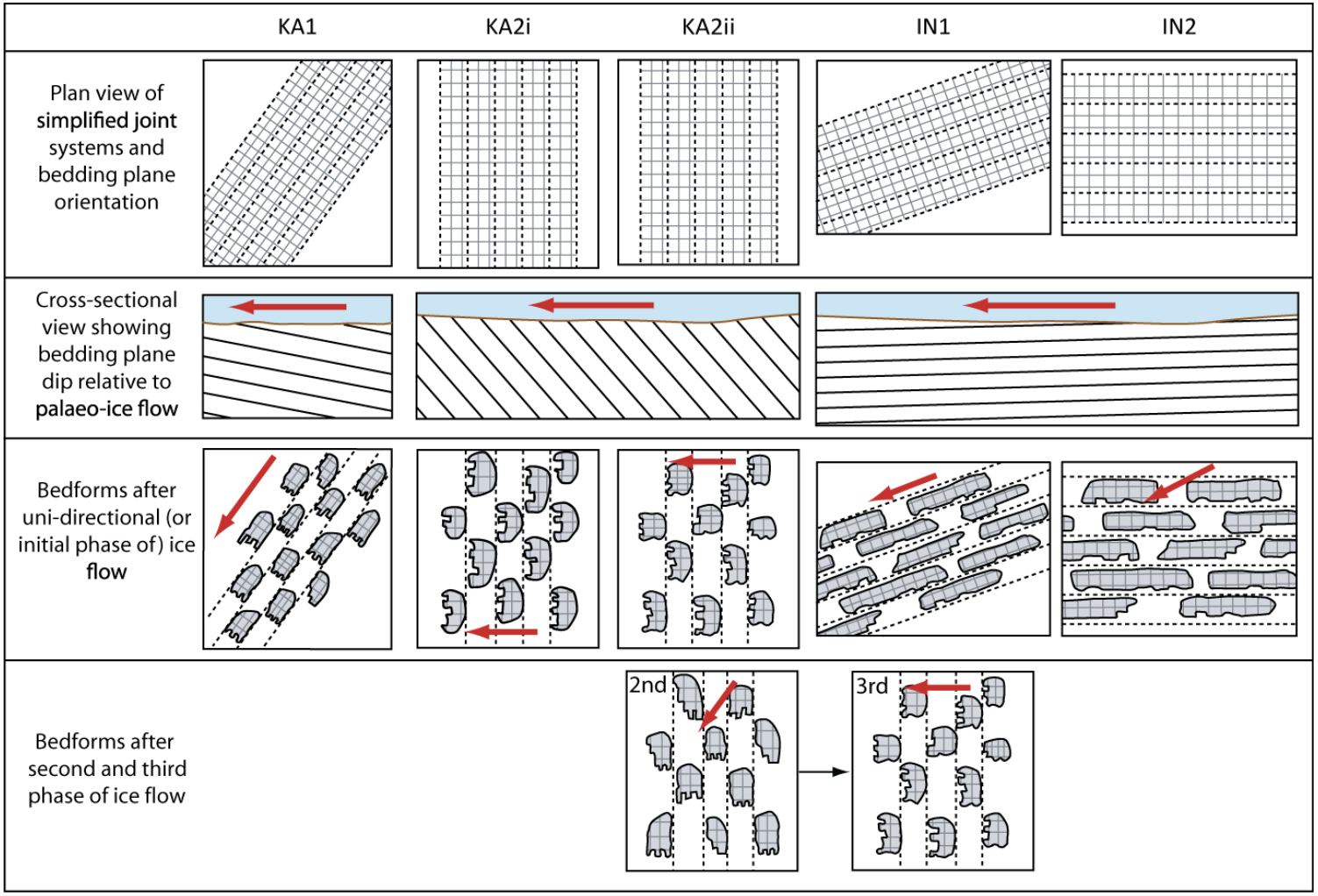

Figure 5.11. Schematic diagram showing the idealised development of bedforms in each sub-area, showing a simplified version of the joint and bedding systems. Idealised bedding planes are shown by the thicker lines, and joint systems are the thinner, more frequent lines.

surface, despite the variable bedding dip (5-40°) which is likely to have prepared bedding planes for plucking. In the examples from IN1 and IN2, this process of lateral plucking has acted to control bedform width. The nature of plucking processes (lee-side or lateral), and resultant landform (positive bedforms or negative grooves) depend upon highly local factors of geological structure, including bedding plane dip, bed thickness, joint orientation, joint spacing, and the land surface prior to glaciation.

The bedforms on Ingia appear very similar in morphology to those found in the Tyne Gap (Livingstone et al., 2010), an area between the Scottish Southern Uplands and the English Pennines. In addition to the similarity in bedform morphology, bedrock properties relative to palaeo-ice flow direction are similar between the two locations (bedding plane dip direction relative to ice flow, joint orientation). The bedforms from the Tyne Gap were first identified by Livingstone *et al*., (2010), and form a set of highly streamlined positive subglacial bedforms recording west to east ice stream flow. The southeast dipping, east-northeast to west-southwest striking bedrock (interbedded sandstone, mudstone and limestone) has helped promote the elongation of these bedforms. A study by Krabbendam and Bradwell (2011) investigated these bedforms, interpreting them as negative asymmetric megagrooves, formed through lateral plucking, as outlined above. Despite the variability in interpretation (i.e. positive vs. negative landforms), the bedforms are most likely to be a mixture of both positive and negative bedforms. However in this study only the positive bedforms are focused upon. The relationship between palaeo-ice flow direction, bedding orientation and bedding dip is identical to whaleback-type bedforms in sub-areas IN1 and IN2, although the Tyne Gap bedforms appear an order of magnitude larger. The bedforms in Ingia have also experienced a similar history of lateral plucking, controlling bedform width and promoting elongate bedforms. As a result, streamlined bedforms found in the Tyne Gap and whaleback type features found within Ingia Fjord are thought to be related features (forming under ice stream conditions), as a result of specific underlying bedrock structural properties. It is likely that asymmetrical megagrooves and the whaleback type landforms from IN1 and IN2 form part of a continuum of bedrock bedforms. The bedforms within this continuum are controlled by structural properties of the bedrock, and not glaciological properties, with bedding plane strike and dip angle being the dominant controls. However, their position within the continuum is not known at present, and requires further research in areas of similar glacial history, and similar structural bedrock configuration.

Evidence for abrasion and plucking was found in all sub-areas, yet in varying degrees of relative significance. A number of studies have concluded that plucking is the more efficient agent at rock removal (Briner and Swanson, 1998, Dühnforth et al., 2010). Others have argued that this is a generalisation (Krabbendam and Glasser, 2011), and that erosional efficiency is highly dependent on local bedrock properties and structure. Results from this study agree with this latter conclusion, and have shown that small variations in bedrock structure can result in large changes in erosive potential and erosional process. Despite the favourable conditions for intense abrasion throughout the study areas (thick, fast flowing ice promoting cavity suppression) plucking has been more efficient at removing rock than abrasion. This is due to the densely jointed, thinly bedded bedrock throughout the region, making it highly susceptible to plucking.

5.5.4. Importance of bedding plane dip relative to ice flow direction

Despite the work carried out concerning the influence of joint properties upon bedform characteristics, few have considered the role of bedding plane dip angle (Gordon, 1981). It was briefly described by Krabbendam and Bradwell (2011), though only in its impact upon lee-side plucking, and not considered more generally in bedform development. In addition to the strike and dip of bedding, bedding plane dip *relative* to palaeo-ice flow direction(s) is a significant controlling factor upon bedform relief and morphology in this study. When bedding plane dip relative to palaeo-ice flow is low (either up or down ice), resultant bedforms are low in relief and amplitude, with high transverse wavelengths and ELRs (e.g. IN1 and IN2) (Figure 5.12 a and b). In contrast, if bedding plane dip relative to palaeo-ice flow is high, bedforms are high in relief and amplitude, and display low transverse wavelengths and ELRs (e.g. KA2) (Figure 5.12 a and b). Based upon theoretical and field-based knowledge, it is therefore possible to make a number of predictions about the likely characteristics of bedforms under different bedding plane dip configurations (Figure 5.12).

A low bedding plane dip relative to ice flow allows ice to preferentially flow along bedding planes surfaces (Figure 5.12a-d). These planes offer a pathway of low resistance for basal ice, as they lie sub-parallel the ice sole in three dimensions. This forms a uniform surface, offering a stable subsole on either stoss (if dipping up ice) or lee (if dipping down ice) bedform slopes. This allows the maintenance of a low relief, low roughness bed, reducing stresses acting across the bed, and promoting the development of elongate bedforms. As erosion occurs across the bedding plane surface, its low relief suppresses cavity formation,

preventing the occurrence of conditions conducive to plucking. Therefore, in regions of down-ice bedding plane dip at a low angle, it is likely that resultant bedforms will be whaleback in form, with high ELRs and wavelengths (Figure 5.12a-d).

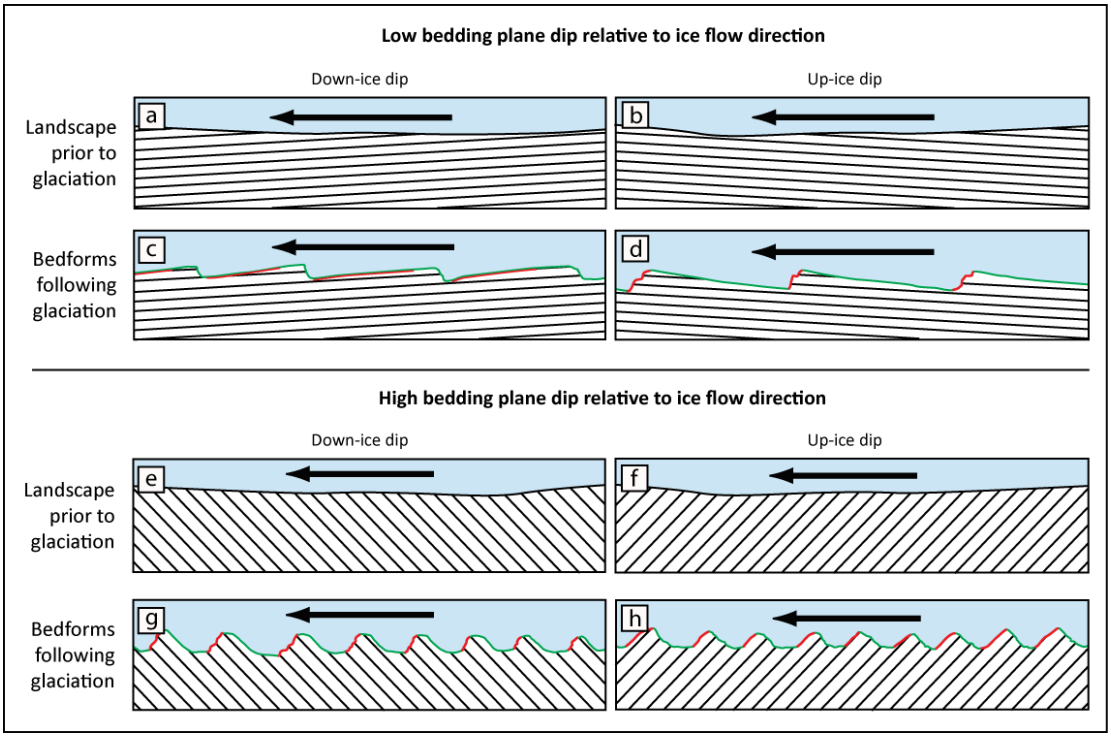

Figure 5.12. Model of bedform formation in regions of different relative up- or down-ice bedding plane dip, and hypothesised resultant bedforms. Black arrows represent ice flow direction. a, b, e, and f represent an idealised land surface, prior to glaciation and glaciation erosion. c, d, g, and h are idealised land surface cross-sections, following glaciation. Green areas indicate surfaces dominated by glacial abrasion; red areas indicate surfaces dominated by lee-side plucking.

Conversely, if the dip is up ice, bedforms will display high ELRs and wavelengths, but are likely to form low relief roches moutonnées, with lee-side plucking (Figure 5.12e-h). As bedding dip relative to ice flow increases (Figure 5.12e-h), the ice subsole cannot erode along bedding planes for long distances. Instead, ice flow was against bedding planes. This creates increased bed roughness across the bedforms, leading to higher basal stresses. If bedding plane dip is up ice, bed roughness is highest on lee-side slopes, encouraging lee-side cavity formation and plucking, producing classic roches moutonnées forms (Figure 4.12d) (Benn and Evans, 2010). If the dip is down ice, lee-side faces have low roughnesses, and allow ice to flow parallel to the bedding plane for short distances (Figure 5.12c). This produces roches moutonnées with smooth lee-side faces, reflecting block removal directly

along bedding planes (e.g. KA2i). In both instances, resultant bedforms are likely to have low ELRs and wavelength, and high amplitude.

5.6. Conclusion

This study has investigated the controls upon bedrock bedform development in the Uummannaq region, an area which experienced topographically constrained, fast ice flow during the LGM. Bedforms in four sub-areas from two neighbouring fjords were analysed from the upstream reached of the palaeo-UISS. Palaeo-glaciological conditions are thought to have been similar for all sites in the study, characterised by thick fast ice, flowing over a rigid bedrock bed. Palaeo-ice flow direction has exerted a broad control on bedform orientation, with the majority of areas displaying bedform long axes sub-parallel to ice flow. Bedforms in areas which experienced multiple ice flow directions (KA2ii) display multiple plucked faces and have experienced bedform shortening, as recorded in other studies. Most other sub-areas have experienced less bedform shortening, as a result of unidirectional ice flow (KA1, IN1, and IN2). However, much variability in bedform morphology (elongation ratio, bedform type, bedform length) cannot be accounted for by regional glaciological properties, with bedforms from some areas of unidirectional ice flow exhibiting intense bedform shortening (e.g. KA2i). Instead, structural characteristics of the host bedrock, predominantly pre-existing joint orientations, have been able to control bedform width and height, by encouraging plucking along these lines of weakness. Bedforms in Ingia displayed evidence for areally extensive abrasion and plucking. However, plucking has been focused upon the lateral flanks for bedforms. This process has been described elsewhere, though only in the formation of negative, megagroove features.

In this study, elongation ratios, often used as a measure of ice flow velocities in areas of differential ice flow, varied between 0.81:1 and 8.42:1. Due to the constant palaeo-glaciological conditions throughout the regions, this bedform property appears to bear no relationship to ice flow velocity. Instead, the bedding plane dip relative to palaeo-ice flow was found to be of great importance to the resultant bedform ELR. Shallow bedding plane angles promote high ELRs, whereas steep angles encourage low ELRs. Contrary to other studies, roches moutonnées and whalebacks were found in areas of similar ice dynamics, suggesting that their abundance is a direct result of bedrock structure, not palaeo-glaciological conditions. Whalebacks occur exclusively in areas of shallow, down-ice dipping bedrock, with low joint densities. This has resulted in bedding plane parallel plucking, with

some abrasion of lee-sides, creating whaleback forms. The results of this study echo those of other recent studies, highlighting the need to fully understand bedrock characteristics before using them to investigate palaeo-ice flow processes.

CHAPTER SIX

Last Glacial Maximum glaciation of the Svartenhuk Peninsula, an area peripheral to the Uummannaq Ice Stream System

Abstract

The Svartenhuk Peninsula is a large, relatively low-altitude (<1000 m a.s.l.) landmass which forms the northern border of the Uummannaq region. Previous research on this peninsula has provided biostratigraphic, chronological and sedimentological studies evidence for the 'Svartenhuk Marine Event'. This was a period of deposition into a higher than present relative sea-level. Based upon a series of infinite radiocarbon ages, U/Th ages, and shell amino acid racemization results this marine event was dated to 115 – 55 kyr, thought to record deposition during an interstadial.

This chapter provides detailed geomorphological and sedimentological results from three valleys across the southern Svartenhuk coast, reporting ice-contact and glacier-fed deltas, striated bedrock, moraines, kettled outwash, and subglacial till. Together these present a compelling argument for the glaciation of the Svartenhuk coastline in the past. In conjunction with ice directional indicators, clast lithological results demonstrate that ice was sourced from the higher altitude interior of the Svartenhuk Peninsula and expanded to the present coastline. The presence of two subglacial tills in bother Arfertuarssuk and Tasiussaq suggests that deposits record at least two glacial advances, separated by a period of proglacial delta development. New shell radiocarbon dates from both subglacial tills overlap, and provide 49.8 cal. kyr BP as a maximum age for glaciation. This suggests that both glacial advances occurred during the last glacial cycle. Sedimentological evidence of deglaciation is predominately of raised marine origin, and is therefore likely to have occurred during the early phases of deglaciation, in association with a glacio-isostatically higher sea-level.

These results are in direct contrast with previous results, and question the tenability of the age and characteristics of the 'Svartenhuk Marine Event'. The correlation of the 'Svartenhuk Marine Event' to highly localised evidence for a number of other Greenlandic marine events or interstadials must also now be questioned.

6.1. Introduction

Ice sheets are well known to exert major impacts upon landscape evolution at local, regional and continental scales, and have done throughout the Quaternary (Sugden, 1974, Whillans, 1978). The ice-free periphery of the Greenland Ice Sheet (GIS) is a unique region in which to interrogate landscape evolution resulting from repeated ice sheet erosion during the Pleistocene. The present ice free landscape of Greenland is dominated by areas resulting from ice sheet activity (areal scour, selective linear erosion, and little to no glacial modification), and those formed through the action of independent valley and mountain glacier systems (Sugden, 1974) (see Chapter Three). During full glacial conditions, the majority of land surrounding Greenland would have been inundated and covered by thick, ice stream and inter-stream ice as it moved offshore (Funder *et al.*, 2011). The extent of the GIS during the Last Glacial Maximum (LGM) and preceding glacial periods remains poorly constrained. However, knowledge of the influence ice streams had upon ice sheet dynamics is increasing (Ó Cofaigh et al., 2004, 2013b, Weidick and Bennike, 2007, Evans et al., 2009, Roberts et al., 2008, 2009, 2013, Funder et al., 2011), and their effect upon long-term landscape dynamics is becoming better understood (Swift et al., 2008, Jamieson et al., 2008, Kessler et al., 2008). At the LGM, the GIS in West Greenland was drained by a series of large, cross-shelf ice streams which terminated at, or close to, the shelf-edge, and produced large trough mouth fans (Roberts et al., 2010, 2013, Ó Cofaigh et al., 2013a, 2013b). The location and longevity of these systems is likely to have had an important impact upon landscape evolution and modification (Swift et al., 2008, Roberts et al., 2009, 2010).

Despite the extensive glacial activity which has eroded much of the land surrounding the GIS, a number of lowland regions were thought to have remained ice free throughout glacial cycles. Based upon botanical evidence, these were hypothesised to have acted as refugia for plants during glacial periods (McCarthy, unpublished). Although a number of these were disproved, other regions were identified by (Sugden, 1974) as areas displaying 'little or no evidence of glacial erosion' (Figure 6.1). Areas classified as such by Sugden (1974) are highly localised in their distribution, and it was suggested that a highly local combination of favourable factors are required to generate and then preserve these landscapes (Sugden, 1974). It is possible that the intense focusing of ice flow which occurs in ice streams could have starved peripheral

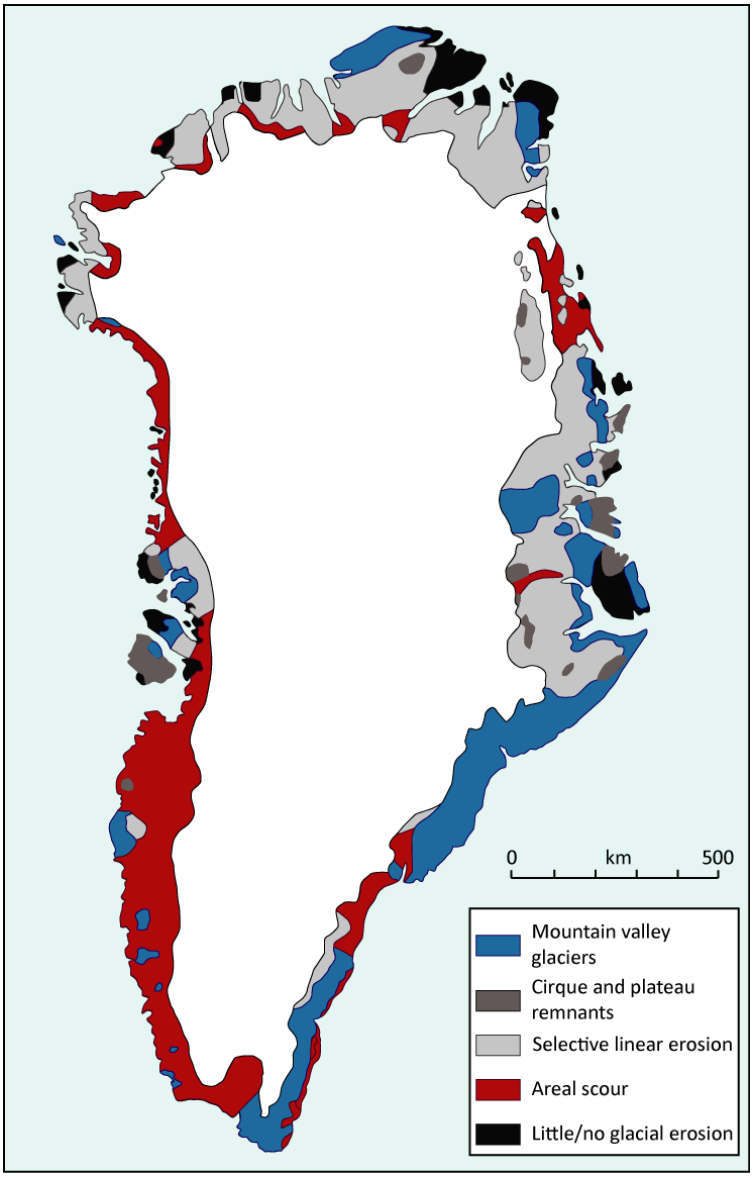

Figure 6.1. Map of the landscapes of glacial erosion on the ice-free rim of Greenland, as mapped by Sugden (1974).

inter-stream areas of warm-based ice, leaving them stranded as fields of cold-based ice, a phenomenon outlined by Kleman and Glasser (2007) in discussing the subglacial thermal organisation of an ice sheet. This would produce large ice sheet proximal regions exhibiting very restricted evidence for glacial activity, although it is probable that higher altitude terrain was colonised by small warm-based valley glaciers, cold-based plateau ice-fields, or inter-stream areas. Western Svartenhuk is hypothesised to be one such region (Sugden, 1974; Chapter Three, this study).

It is thought to have been minimally effected by the nearby Uummannaq Ice Stream System (UISS) (Roberts *et al.*, 2013) during glacial conditions, and was instead occupied by local mountain and plateau glaciers. However, the extent and timing of glacier growth remains

unknown. This chapter therefore aims to: (i) evaluate the pre-LGM and LGM glacial history of the Svartenhuk landscape, understanding the contributions of both GrIS ice and independent mountain valley glaciers and ice caps; (ii) investigate the morphology and sedimentology of landforms throughout the southern Svartenhuk region; (iii) create a chronological framework for the landforms and deposits in this region, in order to allow re-evaluation of the overall glacial history of the peninsula.

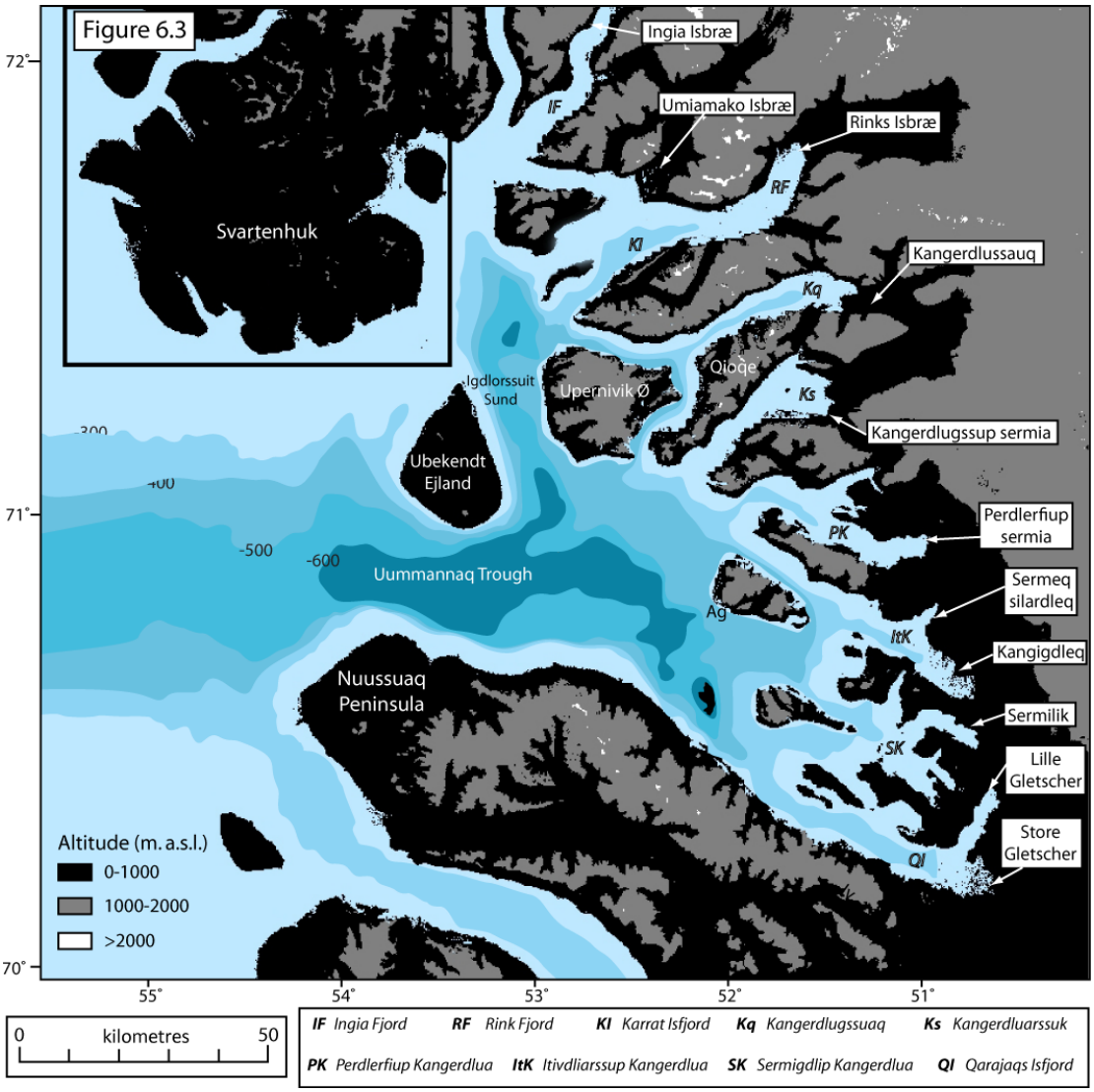

Figure 6.2. Topographic overview map of Uummannaq region. Altitudes are taken from ASTER imagery, and bathymetry from GEBCO.

6.2. Previous work on the glacial history of the Svartenhuk Peninsula

6.2.1 Geomorphological context

The Uummannaq region covers an area of ~25,000 km^2 (70.33°N to 72.00°N, 50.00°W to 55.00°W) (Figure 6.2), and is one of the most mountainous areas of West Greenland, with summits reaching >2000 m a.s.l. It is bounded to the north and south by large peninsulas. These landmasses form large topographic barriers, confining the flux of ice and water from the Uummannaq region to the narrow passages north and south of Ubekendt. The regional-scale topography of the area is characterised by a series of deep coalescent fjords, running

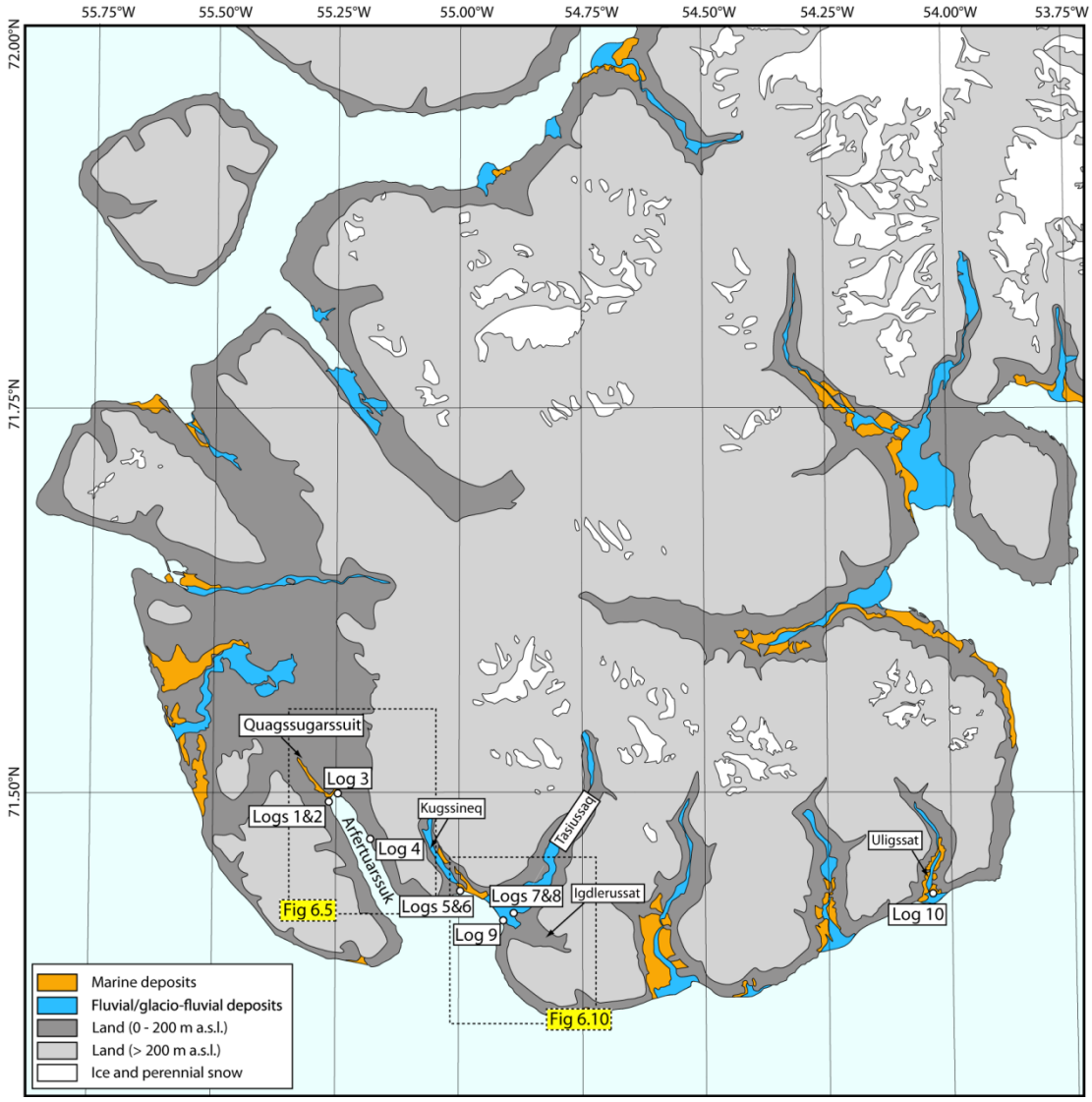

Figure 6.3. Enlargement of the Svartenhuk Peninsula, with investigated sites and valleys discussed in the text labelled. In addition, surficial deposits of glaciofluvial/fluvial and marine sediment are shown (Henderson and Pulvertaft, 1987a, 1987b).

broadly east-west (Figure 6.2). These are occupied by marine terminating outlet glaciers - which drain the central West Greenland Ice Sheet.

The Svartenhuk Peninsula is a large (~ 4,000 km^2) peninsula bordering the northern edge of the Uummannaq region (Figure 6.2 and 6.3). It is formed of Tertiary basalts, and within the Uummannaq region, is an area of relatively low altitude (Figure 6.4). Summit heights in the west are all <1000 m a.s.l., increasing in the east to 1100 – 1200 m a.s.l. Several small (<5 km^2) mountain valley glaciers exist in the central and west portions of the peninsula. The southern coast is dominated by four large valley systems which drain the interior of the peninsula. During the LGM, areas to the east and south of Svartenhuk were occupied by the Uummannaq Ice Stream System (UISS) (Ó Cofaigh et al., 2013b, Roberts et al., 2013). Within the inner fjord confines in this region, mapping, model output, and terrestrial cosmogenic nuclide (TCN) ages constrain LGM ice surface elevation to ~ 1400 m a.s.l., with ice thickness exceeding 1600 m in the Uummannaq Trough (Roberts *et al.*, 2013; This Study, Chapter Five). Regional mapping has identified an onset zone in the north of the system, as ice is deflected south into Igdlorssuit Sund, coalescing with southern outlet glaciers (Roberts *et al.*, 2013; This Study, Chapter Five) (Figure 6.2). This regional flow pattern triggered the formation of the UISS, and would have enhanced regional southward drawdown of outlet glaciers from the north. This is thought to have effectively starved Svartenhuk of any significant GIS inundation, in particular the west, which would have been isolated from UISS ice, and GIS ice from the north (Roberts *et al.*, 2013).

The geomorphology of the Svartenhuk Peninsula has received little attention. Early study reported that the region is dominated by a fluvial system and widespread, thin sediment cover (Laursen, 1944). Mineralogical analysis of samples from fluvial, deltaic, and beach settings has shown a composition almost exclusively derived from local basaltic material, with only a small number of erratic boulders reported (Laursen, 1944). From aerial imagery and field studies, Sugden (1974) classified the south and west of Svartenhuk as displaying little or no glacial erosion, with the north and east classified as landscapes of cirque glaciers and plateau remnants. Recent regional mapping (see Chapter Three) reclassified a larger proportion of the peninsula as landscapes of mountain valley and cirque glaciers, with a more restricted area to the west mapped as showing little evidence of glacial erosion. In addition, a series of large valleys displaying glacial lowland depositional landsystems occur along the southern coast. A number of the mountain valley glaciers in the interior of the

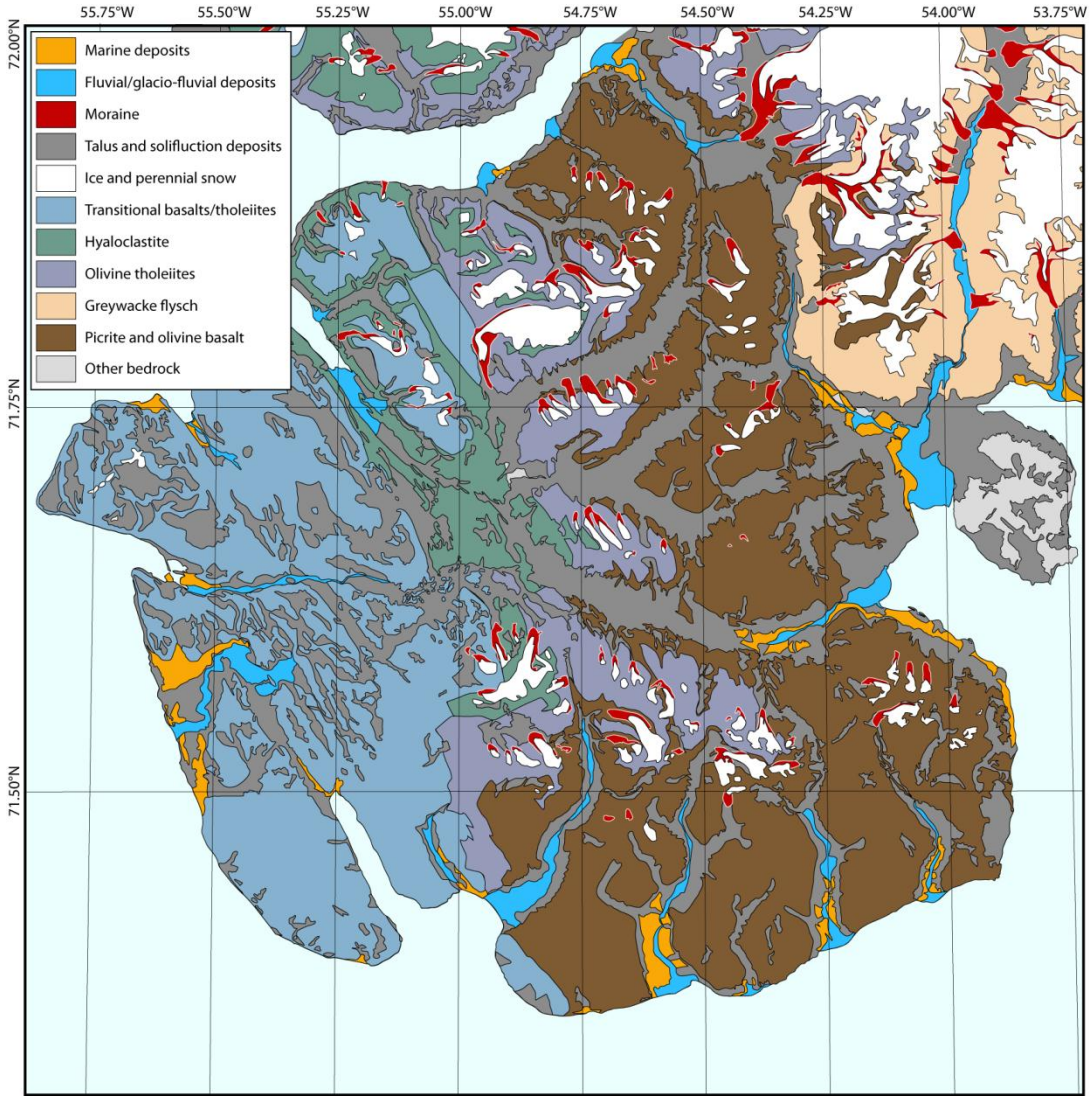

Figure 6.4. Geology map of the Svartenhuk peninsula showing bedrock geology, and surficial deposits (Henderson and Pulvertaft, 1987b).

peninsula display marginal moraines indicative of previous periods of more spatially extensive ice cover (Laursen, 1944). Beyond this, little intensive geomorphological investigation of the region has been carried out.

6.2.2 Sedimentology and biostratigraphy

The Svartenhuk region has been subject to a long history of sedimentological and palaeoecological investigation (Rink, 1853, Steenstrup, 1883, Laursen, 1944, Funder, 1989b, Bennike et al., 1994). Initial sedimentological studies in Svartenhuk reported the presence of deltaic deposits with in-situ marine molluscs thought to relate to glacioisostatically uplifted sediments (Funder, 1989a), with no direct glacial deposits reported. A thin cover of morainic material was reported across the interior of the peninsula, with infrequent erratic

Log #	Site Name	Lat. (°N)	Long. (°W)	References (Site #)
1	Arfertuarssuk fjord head 1	71.495	55.256	Bennike *et al*., 1994 (6); Kelly, 1986 (15)
2	Arfertuarssuk fjord head 1	71.495	55.256	Bennike *et al*., 1994 (6); Kelly, 1986 (15)
3	Arfertuarssuk fjord head 2	71.500	55.217	Bennike *et al*., 1994 (8)
4	Arfertuarssuk fjord side 1	71.468	55.168	Bennike *et al*., 1994 (9)
5	Kugssineq Coast	71.450	55.001	Bennike *et al*., 1994 (10); Kelly, 1986 (16); Laursen, 1944
6	Kugssineq Coast	71.450	55.001	Bennike *et al*., 1994 (10); Kelly, 1986 (16); Laursen, 1944
7	Igdlerussat	71.422	54.882	*New location*
8	Igdlerussat	71.422	54.882	*New location*
9	Tasiussaq	71.415	54.905	Bennike *et al*., 1994 (12)
10	Uligssat qôruat	71.436	54.031	*New location*
11	Tasingortarssuit	71.633	55.583	Bennike *et al*., 1994 (1)
12	Maligissap kûa	71.633	55.517	Bennike *et al*., 1994 (2)
13	Iluliángûp qáqâ	71.485	55.509	Bennike *et al*., 1994 (3)
14	Umiarssuaussarssuaq	71.383	55.033	Bennike *et al*., 1994 (4)
15	Quagssugârssuit	71.505	55.297	Bennike *et al*., 1994 (7)
16	Kugssineq Valley	71.450	55.033	Bennike *et al*., 1994 (11)

Table 6.1. List of locations discussed or recorded in this study, their log number, and a reference if they have been studied by previous authors. Note that analysis of sites 11-16 was not carried out in this study.

Log #	Material	Elevation (m a.s.l.)	Age (^{14}C yrs BP)	δ^{13}C‰	Reference
1	T. borealis	-	>40000	-	Kelly 1986
3	Shells of *M. truncata, H. arctica*	22	>40000	0.1	Bennike et al 1994
5/6	Shells of *M. truncata, H. arctica*	7	>36600	-0.3	Bennike et al 1994
11	Shells of *P. arctica*	0-2	37570±2570/1890	-	Bennike et al 1994
12	Shells of *M. truncata, H. arctica*	8-10	>32530	1.4	Bennike et al 1994
14	Shells of *M. truncata, H. arctica*	14	>30400	0.9	Bennike et al 1994
16	Shells of *Astarte borealis*	35	>347100	0.2	Bennike et al 1994

Table 6.2. Table of present chronological control from the southern and western Svartenhuk Peninsula. All ^{14}C except one returned non-finite ages.

Species	Site Number											
	1	2	3	4	6	8	10	11	12	13	14	15
BIVALVIA												
Nucoloma belloti												
Portlandia arctica												
Portlandia intermedia												
Yoldiella fraterna												
Yoldiella lenticula												
Muscculus sp.												
Actinula greenlanica												
Chlamys islandica												
Astarte borealis												
Astarte elliptica												
Astarte montagui												
Astarte montagui var. *striata*												
Astarte montagui var. *warhami*												
Clinocardium ciliatum												
Macoma calcarea												
Mya truncata												
Hiatella arctica												
Nuculatenuis												
Modiolarianigra												
Tridonta borealis												
Tridonta elliptica												
Tridonta montagui												
Strongylocentrotusdroebach.												
CIRRIPEDIA												
*Balanus*sp.												
ECHINODERMATA												
Strongylocentrousdroebachiensis												
POLYCHAETA												
*Caulostrepsis*isp.												
*Spirobis*cf. *verruca*												
S. vitreus												
GASTROPODA												
Natica sp./Lunatia sp.												
Buccinum sp.												

rare *common* *abundant*

Table **6.3**.Summary of macrofossil biostratigaphic results (Kelly, 1986, Bennike et al., 1994).

boulders across land surfaces (not restricted to fluvial channels) (Laursen, 1944). More recent studies of 17 sites along the southern and western coasts of Svartenhuk reported widespread raised marine deposits, characterised by shell-bearing littoral gravel and sub-littoral muds, with a single exposure of diamicton (Bennike *et al.*, 1994; Kelly, pers. comms.).

These sites are thought to represent palaeo- spits, cuspate forelands, alluvial cones, and deltas, which extend up to 35 m a.s.l., and are not covered by diamicton or affected by glaciotectonic disturbance (Bennike *et al.*, 1994). Bennike *et al*., (1994) reported twenty-three macrofaunal taxa from 12 sites (See Figure 6.3 and Tables 6.1 and 6.2). These assemblages were dominated by *Hiatella arctica* and *Mya truncata* (Table 3). In addition, macrofossils at two sites (also studied by Bennike *et al.*, 1994) were analysed by Laursen (1944) and Kelly (1986). The marine macrofaunal assemblages found were analogous to Holocene faunas from North Greenland, but with some additional species. This indicated that palaeo-environmental conditions in Svartenhuk during the deposition of these sediments were warmer than present day North Greenland (Kelly, 1986, Bennike et al., 1994). In contrast, ostracod assemblages found in Arfertuarssuk (Figure 6.3) represented a quiet, shallow marine environment, far from meltwater sources, analogous to present day environments in Disko Bugt (Bennike *et al.*, 1994). Foraminiferal assemblages have been investigated from one site in Arfertuarssuk (Site 1, Figure 6.3). These displayed high species diversity, suggestive of glacier-distal to sub-arctic conditions (Bennike *et al.*, 1994). Therefore, investigation of the biostratigraphy from sediments correlated to the same single period of elevated sea-level returned a wide range of palaeo-environmental reconstructions. However, authors were still able to infer ocean temperatures analogous to present day Disko Bugt and North Greenland (Bennike, 1994). In addition to the difficulties of a highly mixed assemblage, a lack of site specific sedimentological process interpretations makes it difficult to place the local biostratigraphy within a robust depositional context.

6.2.3. Chronology

Previous work has developed a preliminary chronology for the Quaternary deposits of southern and western Svartenhuk, through ^{14}C dating, amino acid racemization (AAR), and U/Th age determinations of shell material (Kelly, 1986, Bennike et al., 1994). The majority of radiocarbon dates from shells across Svartenhuk returned pre-AMS, non-finite ages of >40,000 ^{14}C yrs BP (six dates), with one finite age of 37,970 +2470/-1890 ^{14}C yrs BP (Table 2) (Kelly, 1986, Bennike et al., 1994). These age determinations are from single shells at each

site. Amino acid determinations from marine shells taken from sites throughout Svartenhuk returned alle/Ile ratios of F = 0.182 and T = 0.0236 (12 samples) (Kelly, 1986), and F = 0.173 and T = 0.032 (8 samples) (Bennike *et al.*, 1994), suggesting an age of >55 kyr (Kelly, 1986). Finally, two U/Th dates from marine shells returned ages of >89 kyr and 115 kyr (no errors given) (quoted in Funder et al., 1994 as from Kelly, 1986).

On the basis of this chronology, sediments found across the Svartenhuk coastal zone were proposed to represent a period of elevated sea-level (~35 m a.s.l.) in MIS 5e-a, between ~115 and 55 kyr, named the 'Svartenhuk Marine Event' (Kelly, 1986, Funder et al., 1991, Bennike et al., 1994), and correlated with the Thule aminozone in north-west Greenland (Bates, 1953). The nature of 'Svartenhuk Marine Event' sediments, their potential age range, and their extensive preservation supports the hypothesis that ice from the GrIS and UISS had minimal impact upon Svartenhuk during the LGM, causing little erosion.

However despite these interpretations, a complete understanding of Svartenhuk's late-Quaternary history is lacking for a number of reasons:

- (1) palaeo-environmental indicators taken from stratigraphic evidence are conflicting, with foraminifera, ostracods, and bivalves producing variable palaeo-environmental reconstructions for sediments.
- (2) detailed sedimentological work has not yet been undertaken through the region, and a comprehensive understanding of the depositional environments of the 'Svartenhuk Marine Event' sediments is lacking;
- (3) the Svartenhuk landscape upon which these sediments are deposited has not been geomorphologically assessed in detail. Instead the region is simply characterised as non-glaciated/affected by little glacial activity.
- (4) the current chronological framework is based on relatively few dates, which are sparsely distributed across region.

The only known Holocene sediments on the peninsula are found on the north-eastern coast of Svartenhuk, close to the outer limit Ingia Fjord (Figure 6.3) (Bennike, 2000). There, small raised deltas formed of shell bearing marine sediment were recorded up to 6.5 m a.s.l., dated to (10.4 – 10.2 cal. kyr BP). These are thought to relate to the local Holocene maximum marine limit (Bennike, 2000), and to the Holocene deglaciation of the UISS from its offshore LGM position into its present fjord confines.

6.3. Methods

6.3.1. Geomorphological mapping

Regional geomorphological mapping was carried out using 1:50,000 topographic maps, geological maps (Henderson and Pulvertaft, 1987a, Henderson and Pulvertaft, 1987b), 1:150,000 aerial photographs (Kort and Matrikelstyrelsen) and ASTER GDEMs, focusing upon the southern coast of Svartenhuk. These were ground truthed in the field. Glacial, glaciofluvial, and fluvial landforms were identified and mapped, using a Garmin GPS 60 in order to record their location.

6.3.2. Sedimentology

Sediment exposures were logged and sketched, noting any lateral sediment variability and macroscale sediment structure. Sediment description adopted a lithofacies approach (Edwards, 1986, Evans and Benn, 2004) and included description of: grain size; depositional and deformation structures; thickness; geometry; colour; clast size; sediment texture; and contact between lithofacies (Evans and Benn, 2004). Clast form analysis was performed upon clasts from gravel and diamicton units (n=50 per unit), measuring the length of the A, B and C axes, and recording each clast's roundness on the Powers' roundness scale (Benn and Ballantyne, 1994). Follow collection, clast form was presented using ternary diagrams, a clear way in which to display clast shape free of any bias (Sneed and Folk, 1958, Benn and Ballantyne, 1994, Lukas et al., 2013). Ternary diagrams use c:a and b:a axis ratios to distinguish equant/blocky ($a \approx b \approx c$), elongate ($a >> b \approx c$), and oblate/platy ($a \approx b > c$) shaped clasts (Benn and Ballantyne, 1994). Ternary plots used in this chapter were created using a custom made Microsoft Excel spreadsheet. Clast C40 index (percentage of clasts with a c:a ratio of ≤ 0.4) was used to further characterise the data set, distinguishing blocky from elongated clasts, an important factor in glaciated environments (Ballantyne, 1982, Benn, 1994, Benn and Ballantyne, 1994). Totals for the clast roundness categories were converted to percentages for each sample and presented as a series of frequency distributions. RA indexes were calculated by adding the percentages of very angular and angular clasts (Figure 6.19).

Clast fabric data were collected units of diamicton (Evans and Benn, 2004). The orientation and dip of fifty selected clasts within a 1 m^2 exposure was measured for each sample.

Eigenvalues were calculated for samples, and results were plotted as stereonets and rose diagrams using the RockWare RockWorks software package.

In addition to these field methods, samples of sediment were taken from each sedimentary unit for laboratory particle size measurement. The size of particle >2 mm were described in the field, with samples of sediment <2 mm taken for particle size analysis. Laboratory based particle size was determined for the <2mm fraction using laser diffraction, widely regarded as providing the greatest reproducibility (Sperazza et al., 2004, Goossens, 2008). In this study a Malvern Mastersizer 2000 was used, running a standard operating procedure developed for this study:

1. System alignment and measurement of background obscuration/residual noise.
2. Manual introduction of the sample in solution and application of 25 seconds of pretreatment ultrasound to disaggregate the sample.
3. Samples passed through the detection lens. Three repeat measurements are taken and a mean value calculated. Values are reported as percentage volume concentrations.
4. The system is cleaned and refilled between sample runs to minimise cross contamination.

6.3.2. Radiocarbon dating

Shells were collected for radiocarbon dating from sediments at all sites, where found. Where visible, shells were picked from sediment exposures with care using a trowel. In addition, bulk sediment samples were taken in the field. These were sieved and residual shells were retained for radiocarbon dating. In order to ensure that dated shells were *in situ* only paired, articulated bivalves were sampled. Shells were lightly cleaned to remove surficial dirt. Samples were processed at the NERC Radiocarbon Facility, East Kilbride. Here, samples were cleaned in an ultrasonic bath in deionised H_2O for two minutes and then rinsed in deionised H_2O. Once cleaned the outer 20% by weight of shell was removed by controlled hydrolysis with dilute HCl. The samples were then rinsed in deionised water, dried and homogenised. A known weight of the pre-treated sample was hydrolysed to CO2 using 85% orthophosphoric acid at room temperature. The CO2 was converted to graphite by Fe/Zn reduction. Results in this study have been corrected to $\delta^{13}C_{VPDB}$‰ -25 using the $\delta^{13}C$ values provided in the report. The $\delta^{13}C$ values were measured on a dual inlet stable isotope mass spectrometer (Thermo Scientific Delta V Plus) and are representative of $\delta^{13}C$ in the original, pre-treated sample material.

The marine radiocarbon reservoir effect is a difference in ^{14}C age between organisms which derive their carbon from the terrestrial environment, and those which live in the marine environment, or incorporate marine-derived carbon into their systems through ingestion (Ascough et al., 2005). As the oceans can only take in atmospheric carbon at their surface, deep water is far removed from its source of carbon. The slow mixing of these water masses means that marine flora and fauna are depleted in ^{14}C relative to their terrestrial counterparts (Ascough et al., 2005). In the North Atlantic region, the reservoir effect is +400-800 ^{14}C years (Ascough et al., 2005), and thus this range was used in new dates from this study.

6.4. Results

In order to successfully study and characterise the sediments of southern Svartenhuk, geomorphological and sedimentological investigation was undertaken in three distinct valleys: Arfertuarssuk (1); Kugssineq and Tasiussaq (2); and Uligssat (3) (See Figure 6.3). A series of logs were taken from each of the three valley sites, and the sedimentary sequences recorded through these have been sub-divided into five lithofacies associations (see Table 6.4 for a summary of the lithofacies associations recorded). Geomorphological results are presented by each of these three areas, and sedimentological results and interpretations are presented by lithofacies association. Clast form data are shown in ternary plots, clast roundness data are presented in histograms, and clast fabric data are presented in rose diagram stereonets.

6.4.1. Geomorphological descriptions

6.4.1.1. Arfertuarssuk and Quagssugarssuit (Logs 1 - 4)

Arfertuarssuk is a sheltered, northwest to southeast trending, steep-sided fjord in western Svartenhuk (Figures 6.3 and 6.5). It is bounded by ground which rises rapidly to higher altitude terrain (>600 m a.s.l.) to the east and west. The fjord head region, and the hinterland to the north rises more gently, characterised by smooth, rolling topography, reaching up to 300 m a.s.l. in altitude. The steep walls to the east and west, and the more gently sloping terrain in the north of the fjord are overprinted by a series of palaeoshorelines, alluvial fans, and deltas (Figures 6.5 and 6.6).

A series of erosional benches are found incised into the fjord walls, up to a height of 68 m a.s.l. These vary in their size and preservation, and are discontinuous, with individual sections reaching up to 500 m in length, with tread depths up to 11 m. In places their surfaces displayed a thin gravel cap, formed of coarse gravels held in a sandy matrix. The depth of these sediment caps could not be ascertained in the field, but was >30 cm. The benches are most clearly formed on the east side of the fjord, close to the fjord head (Figures 6.3 and 6.5b). The most prominent of these benches is at 32 m a.s.l., and backed by a distinct, frost shattered, fossil cliff line. To the southeast, this ridge grades into a flat topped alluvial fan (32 m a.s.l.), towards the base of a contemporary fluvial channel (Figure 6.6a).

Raised, alluvial fans are found throughout Arfertuarssuk, formed on terrain to the east, west and north of the fjord. Alluvial fans are sediment accumulations which form when channels emerge from an upland areas (Bull, 1977). Their surfaces are smooth, displaying a gentle apex to toe slope. Although elevated above present sea-level (12 – 32 m a.s.l.), the fans are found in conjunction with a clearly definable palaeo-fluvial source (i.e. formed at the base of a fluvial channel) (Figure 6.5). These are interpreted as coastal fan deltas which formed through sediment aggradation to sea-level, and have been subsequently raised by glacioisostatic rebound. The largest coastal alluvial fan complex in Arfertuarssuk is found on the western side of the fjord, opposite Log 4 (Figures 6.5 and 6.6b). It emanates from a deeply incised fluvial channel sourced from high altitude terrain to the west. The fan extends ~500 m up valley and its surface is flat, graded to ~32-20 m a.s.l. (apex to toe). The fan surface is composed of angular to sub-rounded local basaltic material held within a silty matrix, and has experienced extensive frost heaving. A 1-2 m deep bench is incised into the eastern and southern faces of the fan, at 13 m a.s.l. (Figure 6.6b).

In addition to the fluvially deposited deltas, a number of raised deltas were found throughout Arfertuarssuk Fjord, at the fjord head (Logs 1-3) and in the mid-fjord (Log 4), with no clear source channel. These are spatially extensive features with flat-topped surfaces. The deltas upper surfaces are graded to between 12 and 16 m a.s.l. At the head of the valley, an extensive delta appears to infill the southern Quagssugarssuit valley. Logs 1-3 are coastal exposures through this delta (Figure 6.6d). Log 4 is taken from a delta on the eastern side of Arfertuarssuk, mid-way up the fjord (Figure 6.5). The delta has a flat top with a gentle south-west dip, and is graded to 16-14 m a.s.l. An exposure of *in-situ* bedrock was found at the base of the delta section, exposed by coastal processes. This was heavily

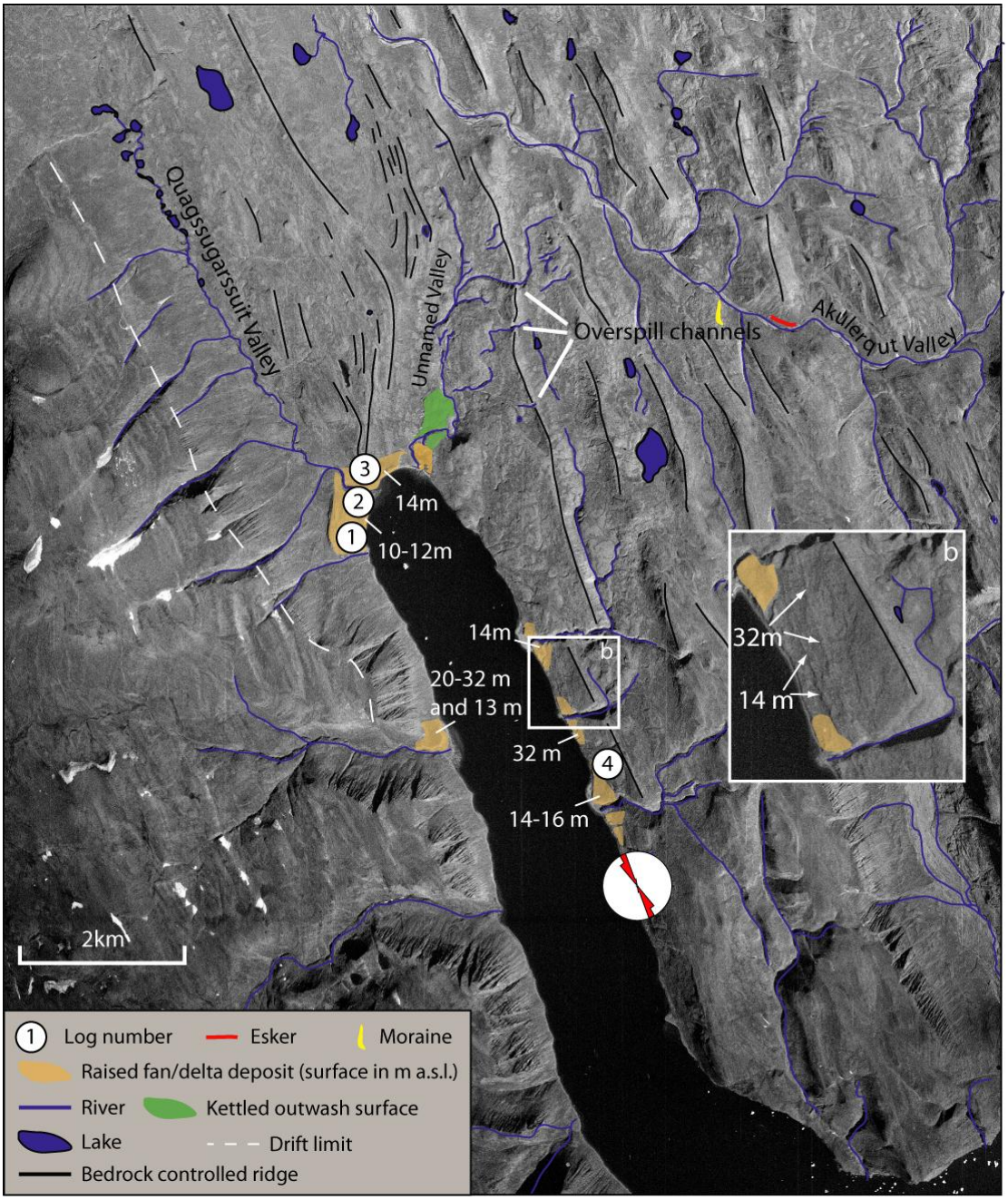

Figure 6.5. Geomorphological map of the Arfertuarssuk Fjord and Quagssugarssuit valley region, showing log numbers referred to in the text. Rose diagrams show bedrock striae measurements (n = 25).

striated, with a dominant 160° - 340° direction, sub-parallel to fjord long axis (see rose diagram in Figure 6.5). The narrow, low lying "Unnamed Valley" to the northeast of Logs 1-3 (Figure 6.5) contains a thick sediment infill which continues inland from the coast for ~800 m. It has a smooth surface which dips downstream towards Arfertuarssuk, at a height of 32 to 16 m a.s.l. The surface has been heavily dissected by contemporary fluvial channels, and grades directly into the upper surfaces of deltas at Sites 1 and 2. There are a series of 1 m

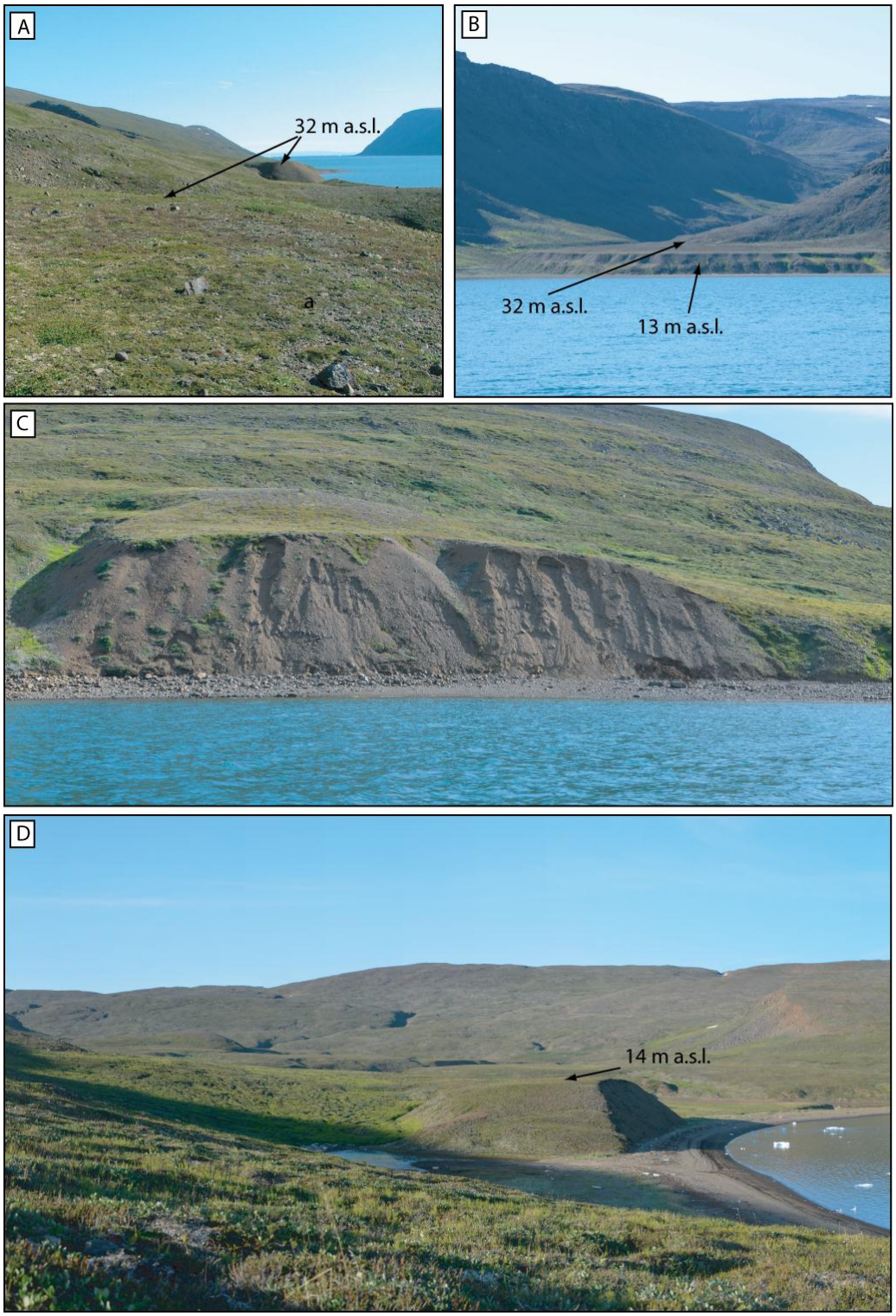

Figure 6.6. Photographs from Arfertuarssuk Fjord: (a) view south from the 32 m a.s.l. ridge north of Log 4 (see Figure 6.5) with alluvial fan graded to the same height in the distance; (b) view southwest from Log 4 to an alluvial fan on the west side of the fjord (32-20 m a.s.l.). The fan's dipping surface can be seen, with an incised step at 13 m a.s.l.; (c) view eastwards, looking east at Log 4 - delta bedding visibly dipping to the bottom right; (d) view from the surface of the Log 1 and 2 delta, looking northeast to Log 3. Log 3 was recorded from the 14 m a.s.l. high mound in the centre of the photo. The valley in the background beyond this is the location in which extensive glaciofluvial sediment, an esker, and pitted outwash were found (see text).

deep, ~100 m long channels incised into the bedrock topography at the eastern margin of the surface.

Although the surface was generally smooth, a series of circular depressions, up to 4 m in depth and 10 m in diameter were found formed across its surface, with no obvious pattern of distribution. Based upon the morphology of this area it is interpreted as a region of kettled outwash, with an extensive outwash surface cratered by circular kettle holes (Benn and Evans, 2010, Maizels, 1977). This is probably a result of the melt out of blocks detached from the snout of a glacier (Rich, 1943, Price, 1970, Gustavson and Boothroyd, 1987), or through the melt of icebergs deposited on the outwash surface through a flood event (Maizels, 1992). In addition, an 80 m long, 1 m high ridge was found grading into the upper limit of the flat-topped surface, from the north. This sinuous, low relief ridge was formed of coarse, unsorted sand and gravel, with locally sourced basaltic pebbles and cobbles. Based upon the form, valley position, and internal sedimentology of the ridge, it is interpreted as a small esker, formed of glaciofluvial sand and gravel (Warren and Ashley, 1994, Benn and Evans, 2010).

The terrain north of Arfertuarssuk is rolling and hilly, dominated by the low-lying, NNW – SSE running Quagssugarssuit valley (Figure 6.3, 6.5, and 6.7). The area is characterised by a series of NNW – SSE trending bedrock ridges, elevated up to 100 m above the surrounding terrain, with a transverse wavelength of ~500 m. The presence of these ridges is strongly controlled by the inclined bedding of the basaltic bedrock which has allowed preferential erosion along exposed lines of weakness. This erosion has produced parallel ridges controlled by large-scale geological bedding continuity. The summit surfaces of these ridges display either: exposed heavily weathered bedrock (with weathering pits up to 10 cm deep and frequent tors and micro-tors), or a thin cover of weathered regolith (generally angular autochonous blockfield with some abraded, sub-rounded erratic clasts). Where present, the regolith has been subjected to extended periods of periglacial processes including frost shattering and stone sorting (Figure 6.7). Very occasionally weathered bedrock surfaces display fragments of glacially polished and striated faces. Infrequent sub-rounded boulders of local basaltic and far-travelled gneissic lithologies are present up to 400 m a.s.l., perched upon the present land surface. Above this elevation sub-rounded boulders become less common. Low lying regions between the bedrock ridges contain well-developed fluvial systems, draining to the NNW and SSE. The majority of clasts found within these channels are local basaltic lithologies, though infrequent gneissic erratics were found, increasing in

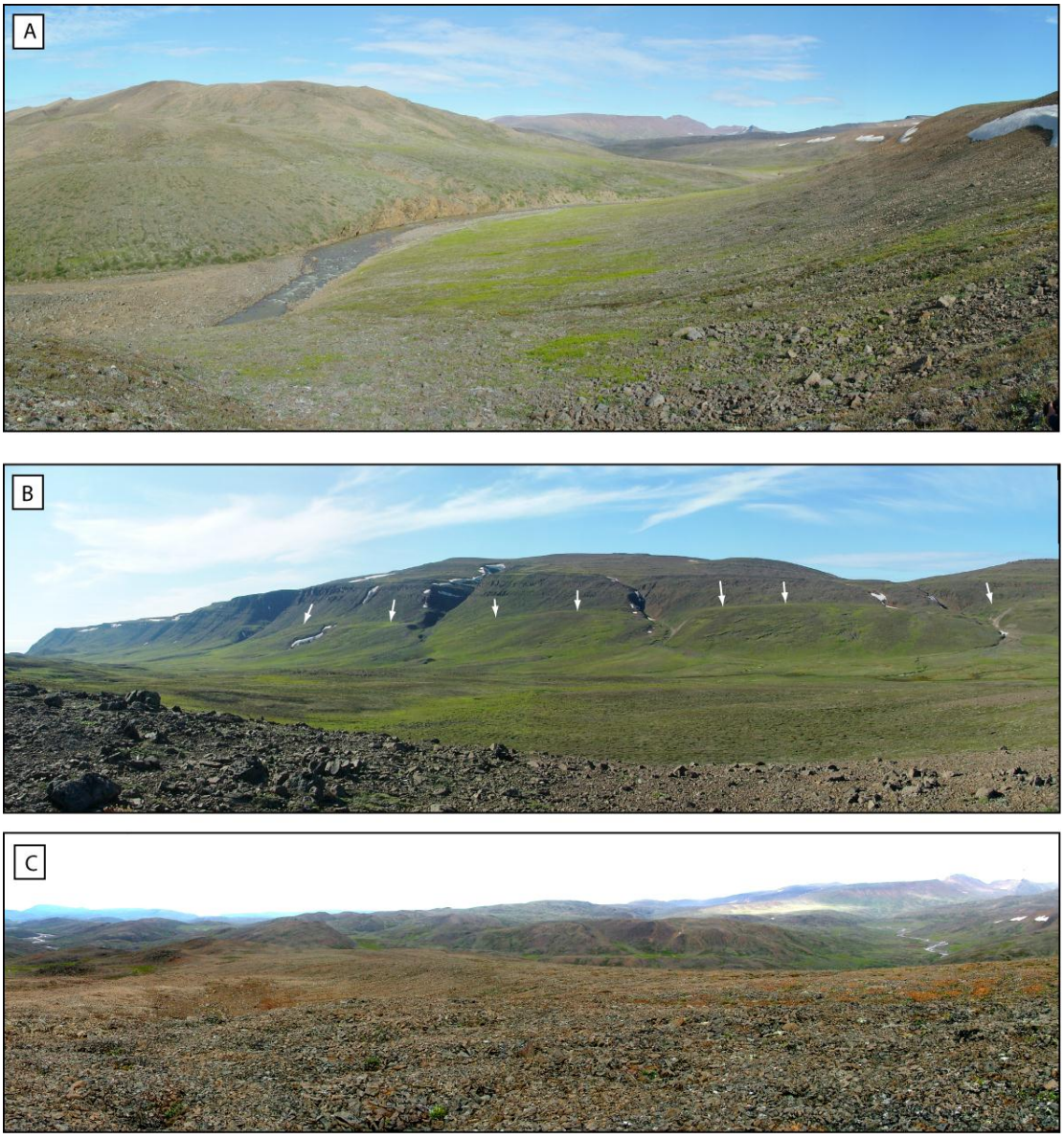

Figure 6.7. Photographs of the general morphology of the Quagssugarssuit region. (a) photograph looking east, to the higher ground of the Akulerqut Valley – taken from the crest of a small moraine; (b) photograph looking west across the low-lying Quagssugarssuit valley. The higher ground in the background rises steeply to ~400 m a.s.l., and has distinct drift limit halfway up its face (arrowed). Arfertuarssuk fjord head is to the far left of the photograph; (c) heavily weathered and frost shattered terrain which characterises the region >300 m a.s.l., with a well-developed fluvial system in the lowland to the left and right of the photograph.

abundance to the north east of the valley. A series of small (<100 m in length), relict channels containing clasts up to boulder size were mapped across this landscape. They broadly trend N-S, and run obliquely to slope angle. A number of the NNW – SSE bedrock ridges within the Quagssugarssuit valley contain deeply incised meltwater channels at their summit ridges. The channels are short but deep features (up to 10 m), and have not incised

to valley floor. They appear to cut across local watersheds and in places appear to form at ridge interfluves, with no clear meltwater source area (Figure 6.8).

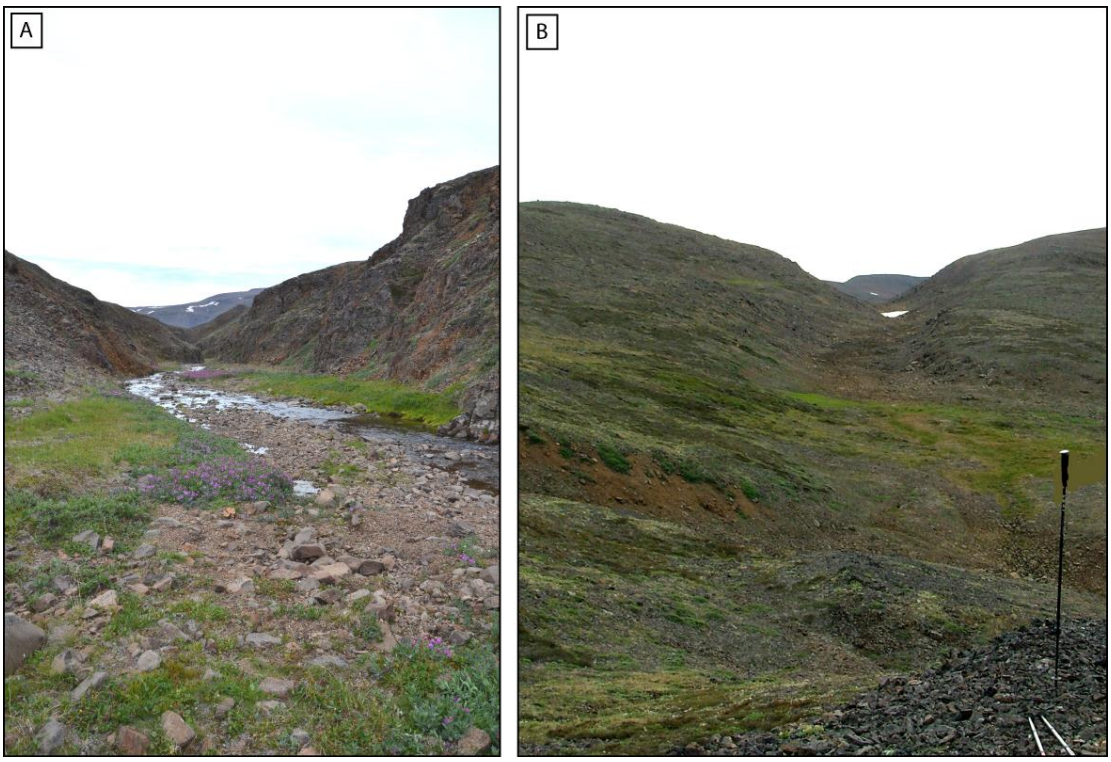

Figure 6.8. Two examples of the deeply incised overspill channels described in the text, close to the Unknown Valley (Figure 6.5). Note that the channel in B originates at an interfluve, with no obvious upslope meltwater source.

A small lobate ridge was mapped on the east of Quagssugarssuit, close to the mouth of the Akulerqut Valley (Figure 6.7a). It is ~2-3 m high, 5 m wide, and only present on the southern side of the valley. Based upon its morphology and position upon the flank of the valley, the ridge is interpreted as a partial remnant of a lateral moraine. A small (0.5 – 1 m high), discontinuous ridge was mapped 500 m up-valley of the moraine, close to the present fluvial channel. It was formed of sub-rounded cobble-sized, locally derived basaltic clasts. On the basis of its mid-valley position, internal sediments, and morphology, this is interpreted as an esker, as defined above (Warren and Ashley, 1994, Benn and Evans, 2010). Up valley of the moraine valley morphology is wide, with a clear U-shaped profile. In contrast, down-valley of the moraine, the valley is narrower with a clear V-shaped cross-profile. This valley is sourced from the interior of Svartenhuk and currently hosts a number of small, independent valley glaciers in its upper reaches. In addition, a number of the small valleys between basalt ridges to the north east of Sites 1 and 2 contain arcuate poorly formed, discontinuous lateral moraines.

6.4.1.2. Kugssineq and Tasiussaq (Logs 5 - 9)

The south coast of Svartenhuk contains five north-south trending valleys, sourced in the high-level (>1000 m a.s.l.) interior of Svartenhuk. These valleys are fed by a number of individual, small (<3 km^2) valley glaciers. The valleys have large, U-shaped cross-profiles up to 5km in width. Valley floors are currently characterised by contemporary tidal flats, salt marshes, and misfit fluvial streams. The low gradient floors of the valleys continue for up to 10 km inland, with steeply rising walls either side. Other than the Tasiussaq valley, little evidence of glacial activity is visible in any of the valley systems (e.g. moraines, eskers, striated bedrock surfaces). From mapping by Henderson and Pulvertaft (1987b) and this study, all five valley systems were seen to contain thick sequences of sediment close to the valley mouths, extending up to 3 km inland. These sediments are found deposited in flat-topped fans and deltas, graded to various heights between 14 and 43 m a.s.l. These are bisected by contemporary fluvial systems which appear to misfit valley morphology. The two most westerly of these valleys are Kugssineq and Tasiussaq (Figure 6.3). The Kugssineq valley is a 0.8 km wide, flat-bottomed valley, the floor of which contains a contemporary salt-marsh system. A series of sediments were preserved at the mouth of the valley in a large, flat-topped delta, reaching 18 m a.s.l. Sections of this are exposed by current fluvial and coastal processes (Figure 6.9a). A possible higher bedrock incised terrace was seen up valley (at ~80m a.s.l.), but was not investigated further.

The floor of the Tasiussaq valley is characterised by contemporary salt marsh, with a number of large circular pools (Figure 6.9c). Two discontinuous ridges were mapped on the south side of the valley, between Tasiussaq and Igdlerussat valleys (Figure 6.10), above the valley-floor deltas. They are orientated NE-SW, sub-parallel to Tasiussaq valley long axis (Figure 6.9b and 6.10), and run down-slope at a gentle gradient. They are wide and low in relief (<10 m wide, <4 m high) and formed of angular to sub-rounded clasts between pebble and boulder size. Based upon these criteria, these features are interpreted as a series of inset lateral moraines (Boulton and Eyles, 1979, Benn and Evans, 2010), relating to the presence of ice within the Tasiussaq valley. High-level terrain south of the Tasiussaq valley, outside of these moraines, is characterized by frost shattered bedrock, with a thin, patchy cover of weathered regolith (Figure 6.11b). Where bedrock remains intact and exposed, outcrops displayed weathering pits up to 6 cm deep and very occasional abraded and striated surfaces (173-353^o). No exotic (i.e. non-basaltic) erratics were found throughout this high-level terrain. The mapped extent of this weathered surface is shown in Figure

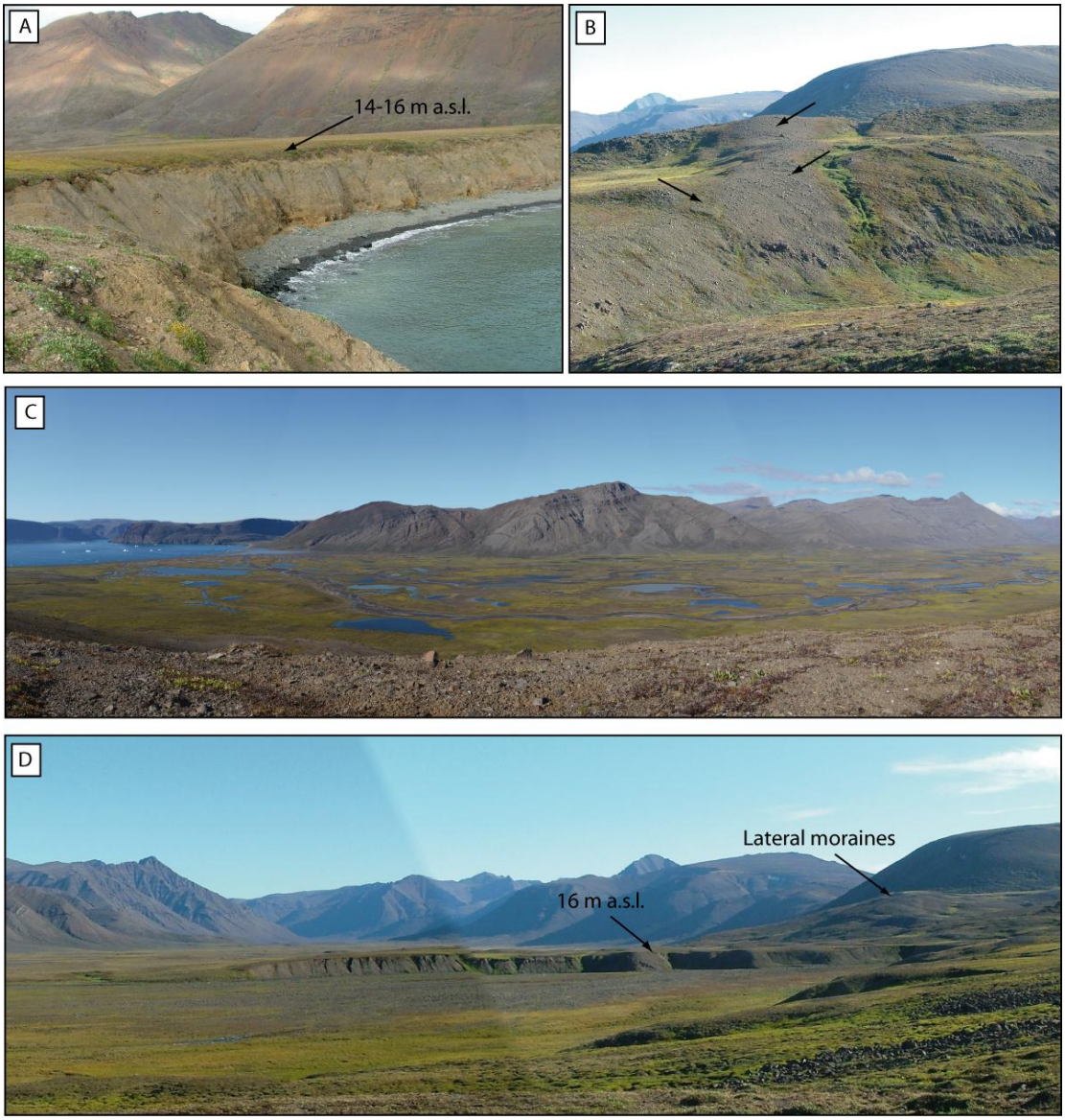

Figure 6.9. Photographs from the Kugssineq and Tasiussaq valleys (see Figure 6.3). (a) View east to the cliff exposure of the delta to the north west of Tasiussaq, the surface of which is graded to 14-16 m a.s.l. Logs 5 and 6 were taken from this exposure; (b) view northeast from close to Logs 7 and 8, with the largest inset lateral moraines on the southern border of the Tasiussaq valley arrowed; (c) oblique view of the Tasiussaq valley looking northwest. Note the well-developed sediment filled valley floor with circular pools, and steeply rising terrain to the north; (d) view of the Tasiussaq valley, looking northeast, up valley. The obvious flat topped feature in the centre is a delta, graded to 16 m a.s.l. Logs 7 and 8 were taken from the exposure facing the camera. In addition, inset lateral moraines (as in Figure 6.9a) can be seen to the right of the image.

6.10. However, based upon field observations, it is likely that this type of surface covers the majority of high-altitude (>500 m a.s.l.) areas. In contrast, lower altitude terrain inside of the lateral moraine complex is dominated by fluvial and salt marsh environments. Where present, bedrock surfaces appear less weathered that terrain outside of the moraines, with weathering pits commonly 1-2 cm in depth.

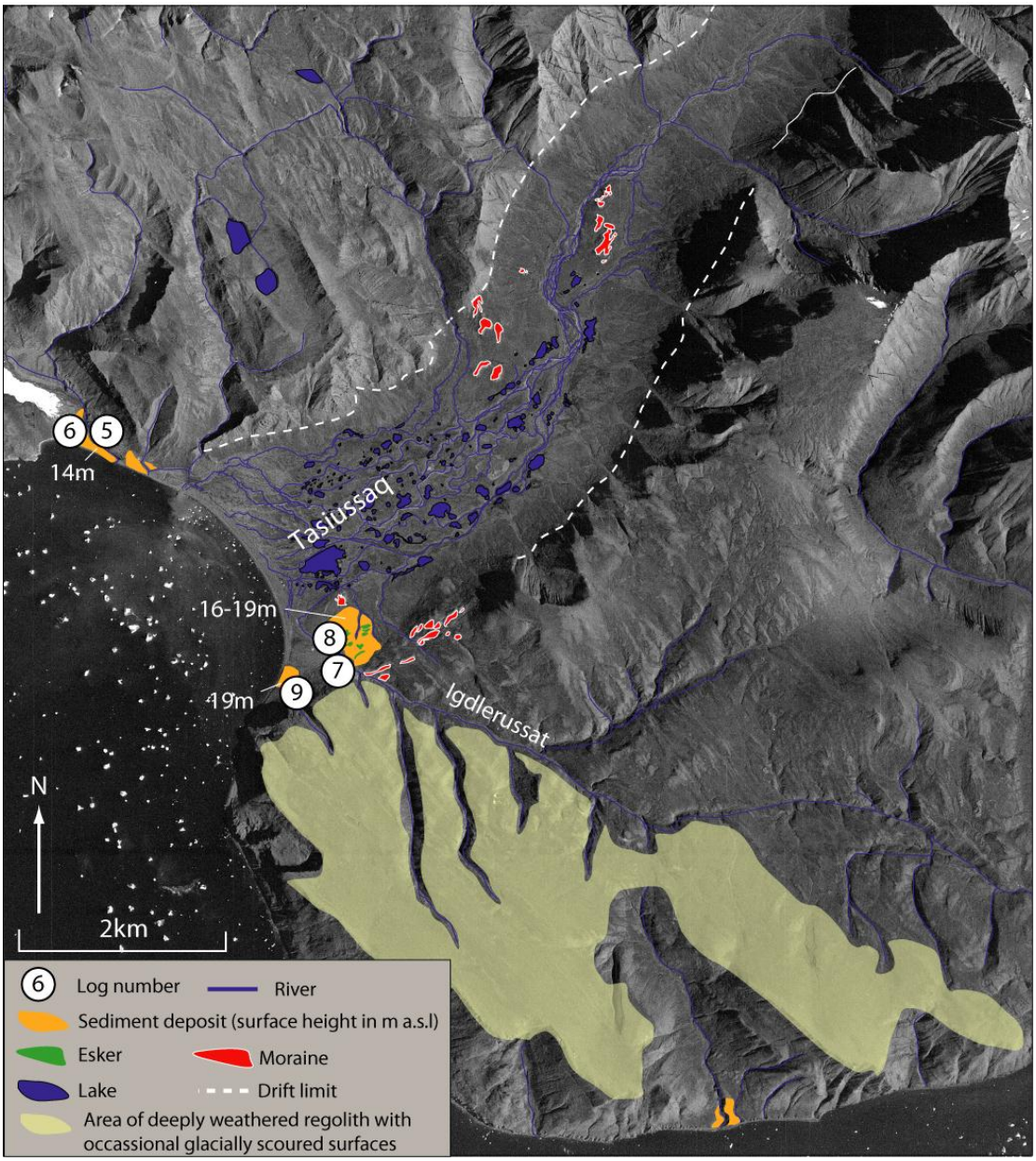

Figure 6.10. Geomorphological map of the Kugssineq valley and Tasiussaq region showing deposits and landforms mapped during this study. Logs are labelled with numbers referred to in the text.

Sediments at the mouth of Tasiussaq valley (Figure 6.9d) are best preserved on the southern side of the valley, close to the neighbouring Igdlerussat, in a flat topped delta sequence graded to 16 m a.s.l. (Figure 6.10 and 6.11a). The sediments are dissected by contemporary fluvial channels from both Tasiussaq and Igdlerussat. A series of low relief, sinuous, ridges were found deposited upon these flat topped deposits, orientated sub-parallel to both the Tasiussaq valley and lateral moraines found on higher ground to the south (Figures 6.11a and 6.11b). On the basis of their sinuous form and internal sediments, these ridges were interpreted as eskers (Warren and Ashley, 1994, Benn and Evans, 2010). These are deemed

indicative of a subglacial environment, and suggest that the delta surface has been overrun by ice subsequent to its formation. Delta top eskers could have 'emerged' following melt-out of an ice-cored delta, however the sedimentological context of the delta demonstrates this is not the case. A large sedimentary 'feature' was found in south-west Tasiussaq, south-west of the delta (Log 9), measuring 120 m long by 20 m high. The feature has been eroded by contemporary coastal processes, and lies below a small valley sourced from high ground to the southeast, close to Igdlerussat (Figure 6.10). The feature appears to have been

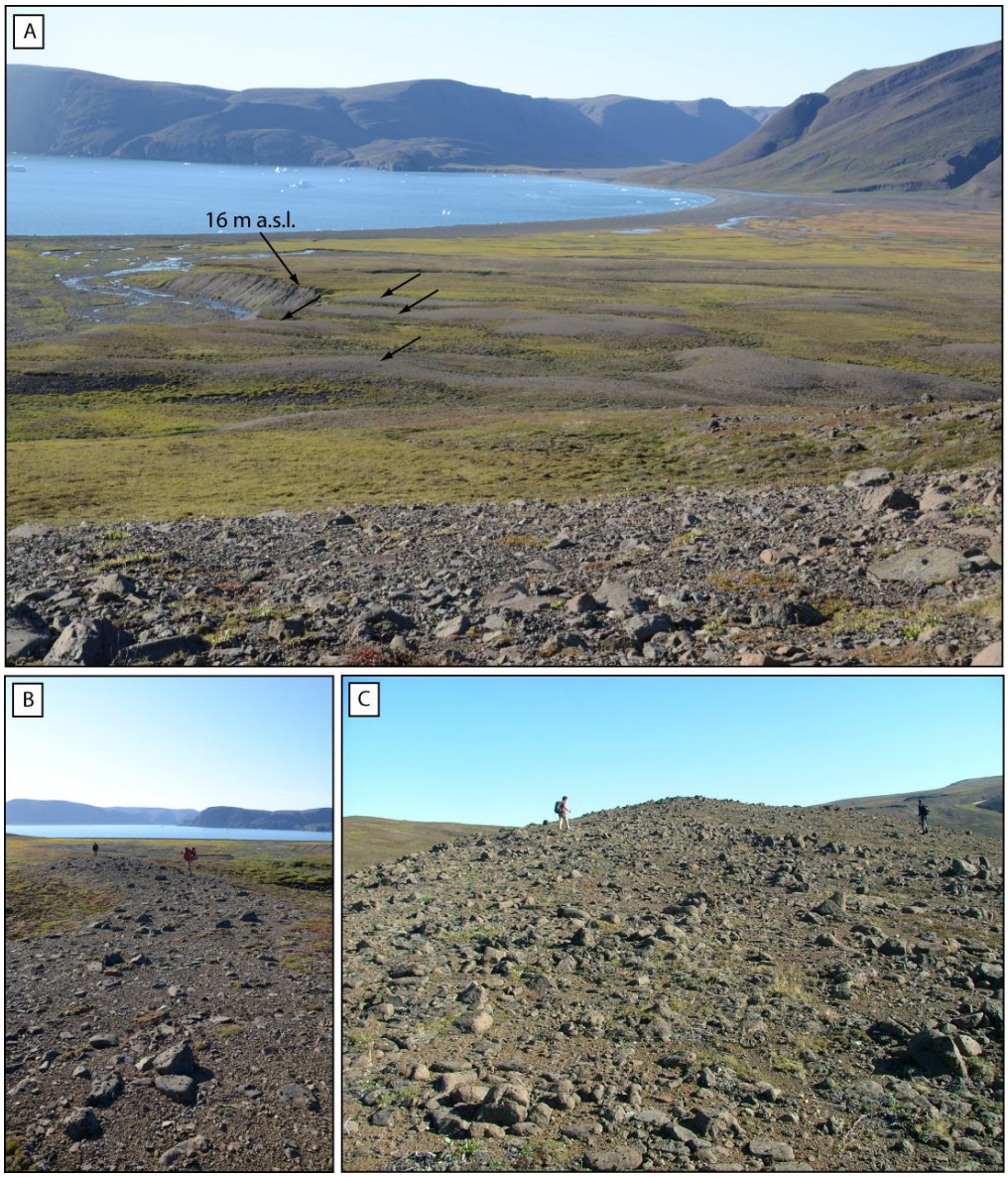

Figure 6.11. Photographs from Tasiussaq valley (a) oblique view looking northwest over the delta surface from which Logs 7 and 8 were recorded. Small sinuous gravelly ridges are indicated by black arrows, trending from right to left across the photo. These are interpreted as eskers (see text for details); (b) view along a sinuous, low relief gravel esker overlying Site 7; (c) typical terrain outside the Tasiussaq lateral moraine limit - extensive heavily weathered bedrock and regolith, with occasionally ice scoured surfaces.

glacially streamlined, its internal sedimentary structure showing clear evidence of erosion following deposition. The deposit's south western face also displays evidence of later bisection by contemporary coastal processes.

6.4.1.3. Uligssat (Log 10)

Uligssat is the easternmost of the Svartenhuk valleys (Figure 6.3). The valley trends north – south, and is sourced by high altitude terrain in the central-east of the Svartenhuk Peninsula. Extensive sediments are preserved close to the valley mouth and further up-valley, in a series of inset deltas and up-valley alluvial fans, the surfaces of which are graded to between 20 and 75 m a.s.l. This is the highest evidence for marine activity throughout the Svartenhuk area, and therefore is thought to represent the marine limit. A large delta complex is found close to the mouth of the valley, dissected by post-depositional fluvial and coastal erosion, with a series of sub-angular to sub-rounded erratic quartzite boulders resting upon its surface (Figures 6.12 and 6.13). This delta is flat-topped, with a gentle surface slope, and steeply dipping up-valley face (Figure 6.13c). The surface of this delta reaches 36 m a.s.l. at its highest point, dropping to ~24 m a.s.l. at its down-valley edge (Figure 6.13c and d). Smaller deltaic deposits were found up to 43 m a.s.l., though these could not be associated with the larger delta in the valley. The highest altitude feature in the valley is found at 75 m a.s.l., and appears as an alluvial fan, emanating from a small (0.25 km^2) bench incised into the bedrock valley wall. The fluvial system in the centre of the valley is a clear misfit to the large U-shaped valley in which is flows.

Figure 6.12. Erratic boulders found resting upon the upper surface of the 36-24 m a.s.l. delta. Boulder location is between the yellow star and closest white arrow in Figure 6.13c.

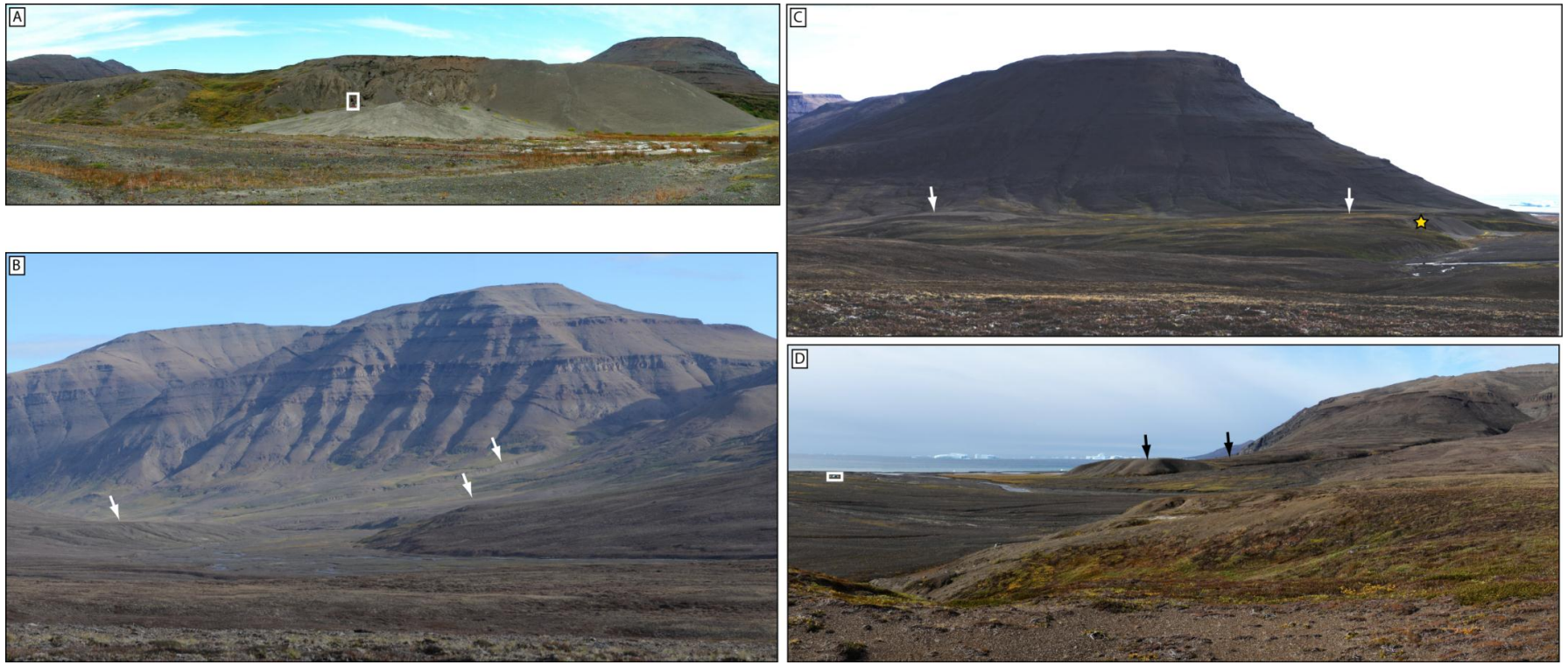

Figure 6.13. Plate of photographs from the Uligssat Valley (see Figure 6.3 for valley location). (a) Photograph looking up-valley at the face of the delta, including the section logged in Log 10. A person can be seen surrounded by a box in the centre of the photograph for scale; (b) view northeast looking up-valley. A series of raised deposits are arrowed, not investigated in the field; (c) view looking east towards a raised delta (arrowed) in the mouth of the Uligssat valley. Location of Log 10 is shown by a star; (d) view westward from the delta surface seen in photograph C. A continuation of the logged delta surface is seen arrowed in the background. The area between the two surfaces is dissected by contemporary fluvial activity. Tents identified by a white box can be seen on the flat fluvial surface to the left for scale.

A series of ridges were found on valley flanks at higher altitudes, but are believed to be bedrock controlled, formed through preferential weathering along lines of local geological weakness, and do not reflect raised shorelines. Tributary fluvial channels up-valley feed into a series of alluvial fans (Figure 6.13b). In addition, kame terraces, poorly formed discontinuous lateral moraines, and a trimline are found on valley walls. A section was logged from the large delta at the mouth of the valley (Log 10 - Figure 6.13a and c). The front edge of this delta was 24 m a.s.l. with the up-valley apex reaching 36 m a.s.l.

6.4.2. Sedimentological descriptions

As outlined in Section 6.3.1., a lithofacies approach was adopted for sediment description and interpretation (Edwards, 1986, Evans and Benn, 2004). The sediments from the sites of southern Svartenhuk have been sub-divided into a series of distinct lithofacies, which were then grouped as lithofacies associations where deemed suitable (Table 6.4). As a result, sedimentological logs are presented first, followed by clast form and fabric data. These are followed by sedimentological descriptions and interpretations. Sediment logs are presented in Figures 6.14-6.17, clast form data is presented in Figures 6.18 and 6.19, particle size analysis data in Figure 6.20, and clast fabric data in Figure 6.21.

Lithofacies		Sediment description	Lithofacies codes	Logs pres. in	Sediment interp.
LFA5	LF5b	Matrix-supported gravels	Gmm	7, 8	Esker gravel
	LF5a	Upper matrix-supported diamicton	Dmm	1, 2, 7, 8	Upper subglacial diamicton
LFA4		Massive to horizontally bedded gravel and fines	Gmm, Ghm, Fm, Shf, Ghf	3, 9	Slope deposits
LFA3	LF3c	Horizontally bedded gravels interstratified with fines	Glt, Ghc, Gmc, Sm, Fm, Shf, Fm, GRh	6, 10	Ice marginal glacio/fluviodeltaic topsets
	LF3b	Dipping planar stratified to massive coarse gravels	Gmm, GRm, Sm, Ghc, Shf, Ghf, Fm, Gmc, Ghm, Fs, Gfu	1, 2, 3, 4, 7, 8, 10	Ice marginal glacio/fluviodeltaic foresets
	LF3a	Massive to horizontally bedded fines and fine gravel	Sm, Fs, Ghf, Gmc, Fm, Gcu, Gmm, Ghc	7, 8, 9, 10	Ice marginal glacio/fluviodeltaic bottomsets
LFA2		Lower matrix-supported diamicton	Dmm	1, 2, 5, 6, 9	Lower subglacial diamicton
LFA1		Shattered bedrock to diamicton	Dcm	5	Periglacially reworked bedrock

Table 6.4. Table of lithofacies associations, lithofacies, a short description of each lithofacies, and the facies from each logged section correlated to each lithofacies association.

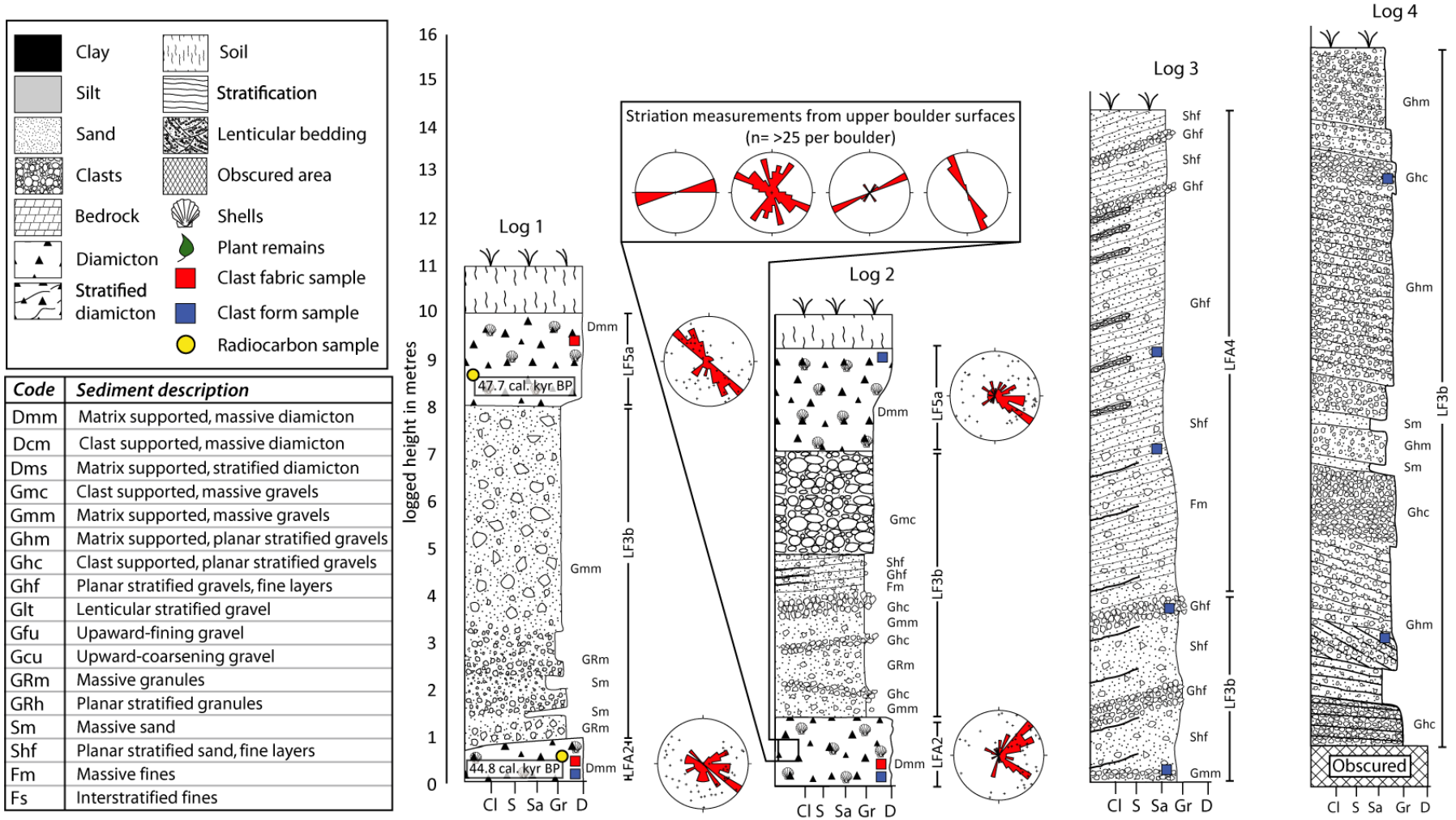

Code	Sediment description
Dmm	Matrix supported, massive diamicton
Dcm	Clast supported, massive diamicton
Dms	Matrix supported, stratified diamicton
Gmc	Clast supported, massive gravels
Gmm	Matrix supported, massive gravels
Ghm	Matrix supported, planar stratified gravels
Ghc	Clast supported, planar stratified gravels
Ghf	Planar stratified gravels, fine layers
Glt	Lenticular stratified gravel
Gfu	Upaward-fining gravel
Gcu	Upward-coarsening gravel
GRm	Massive granules
GRh	Planar stratified granules
Sm	Massive sand
Shf	Planar stratified sand, fine layers
Fm	Massive fines
Fs	Interstratified fines

Figure 6.14. Sedimentary Logs 1-4, recorded from Arfertuarssuk Fjord. Facies codes and sediment symbols outlined to the left are used throughout the chapter. Clast fabric directional data are shown in red stereonets. The inset box for Log 2 shows results of striae found on boulder from LFA2.

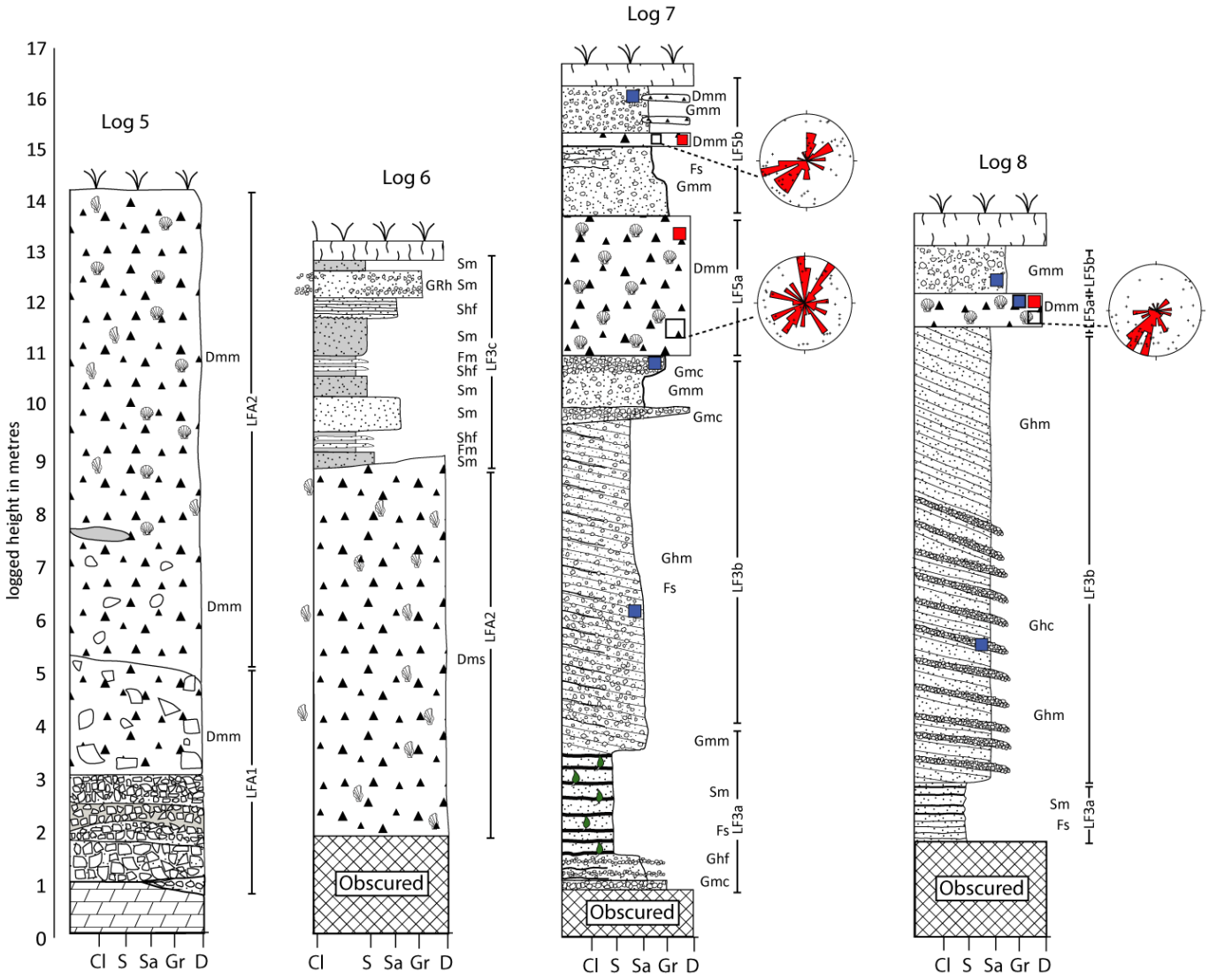

Figure 6.15. Sedimentary Logs 5-8 from Tasiussaq Valley. Clast fabric directional data are shown in red stereonets

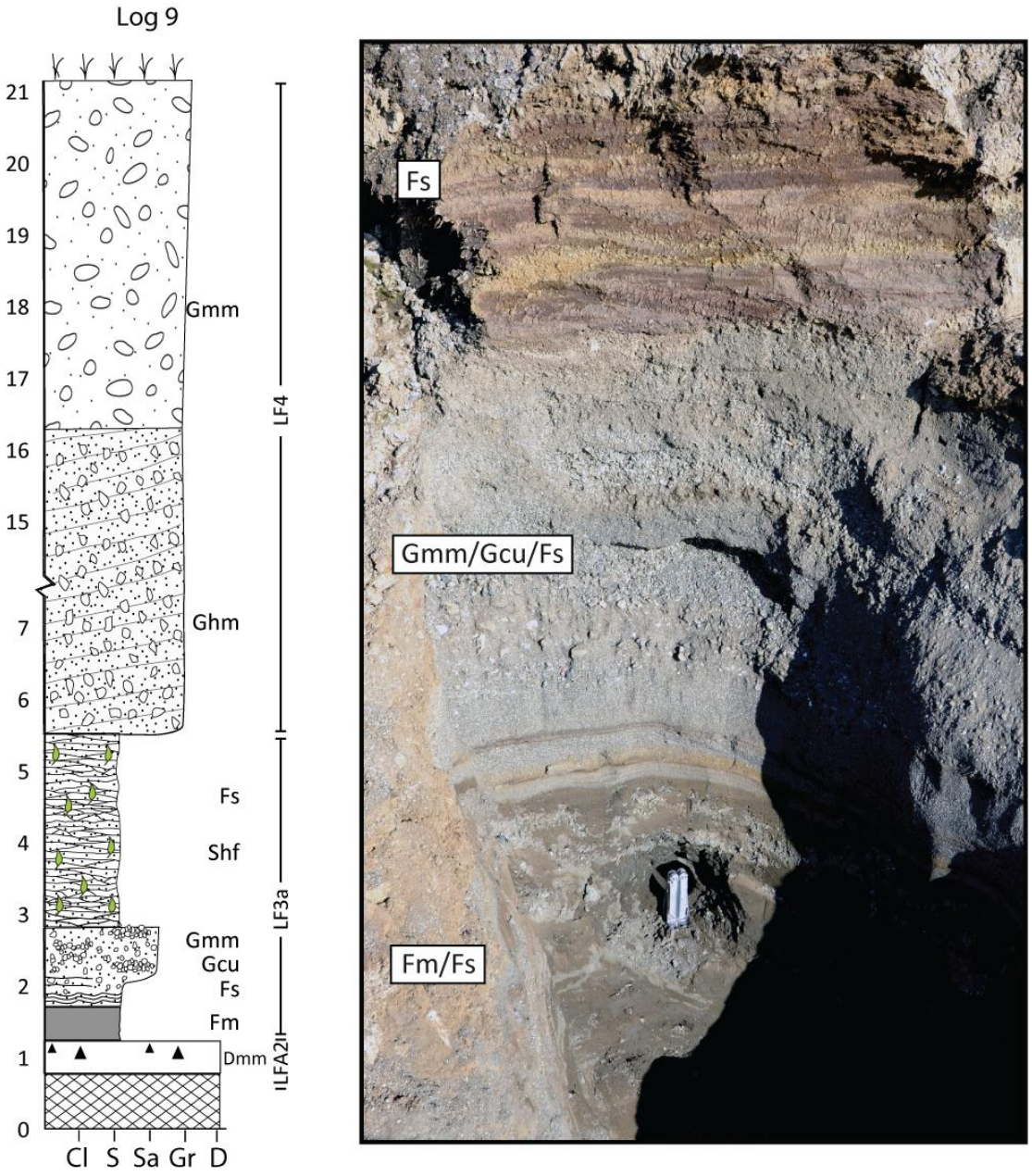

Figure 6.16. Log 9, from the mouth of Tasiussaq (see Figures 6.3 and 6.10 for location). Photograph to the right displays the variability within LF3a; varying from Fm/Fs, to Fs/Gcu/Gmm, to Shf interbedded with Fs. Note the extreme colour change at the top of the photograph, representing an increased organic content.

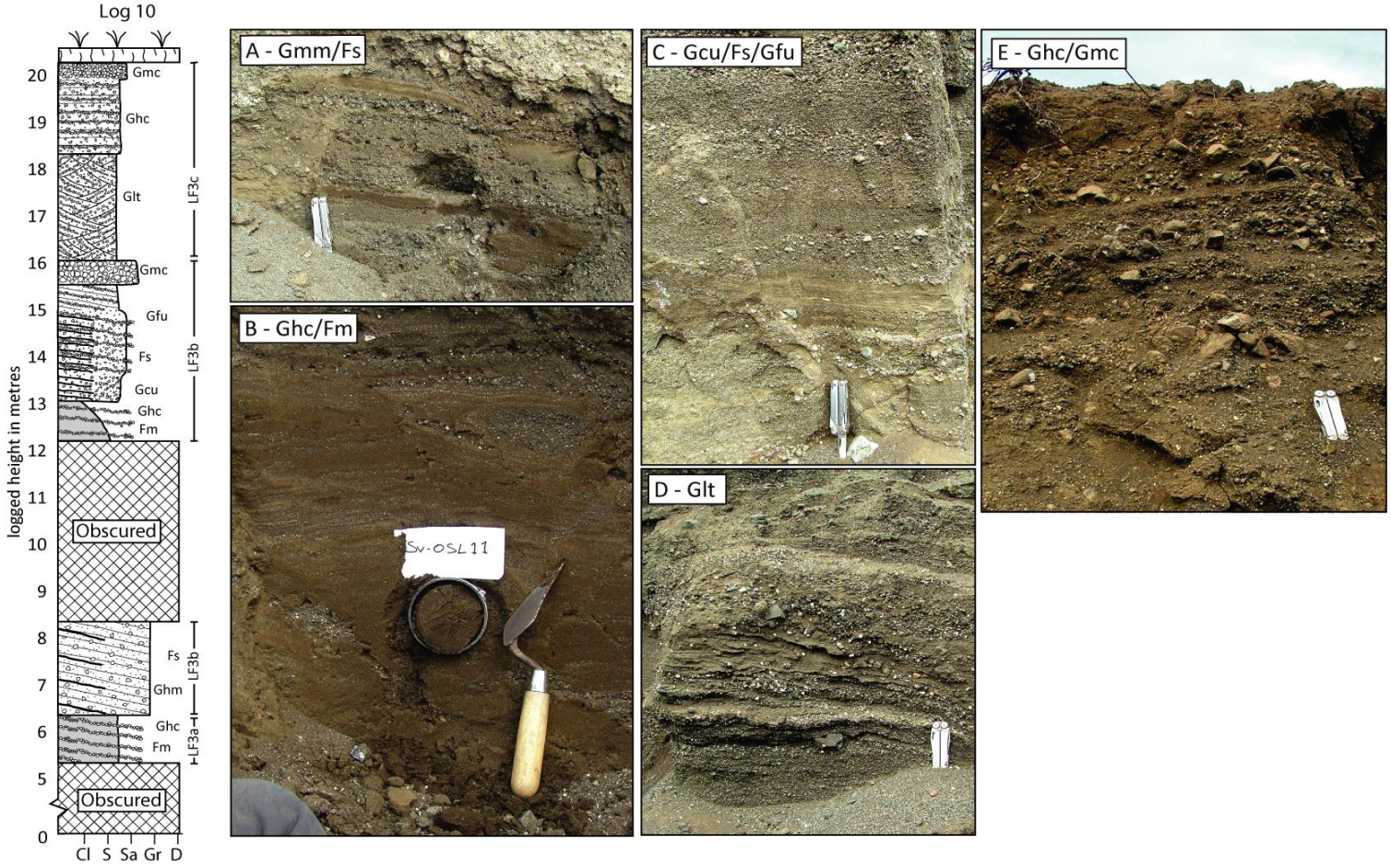

Figure 6.17. Sedimentary log and sediment photographs from Log 10. Photos show the variability in grain size and structure through the section. (a) dipping, interstratified silts, fine sands, and granules; (b) similar facies with less coarse units; (c) coarse deposits of sands and matrix supported gravels, still showing planar stratification and both normal and inverse grading; (d) coarse gravels, in places clast supported. Some planar stratification and lenticular bedding; (e) horizontal, planar stratified gravels, with larger clasts than lower facies.

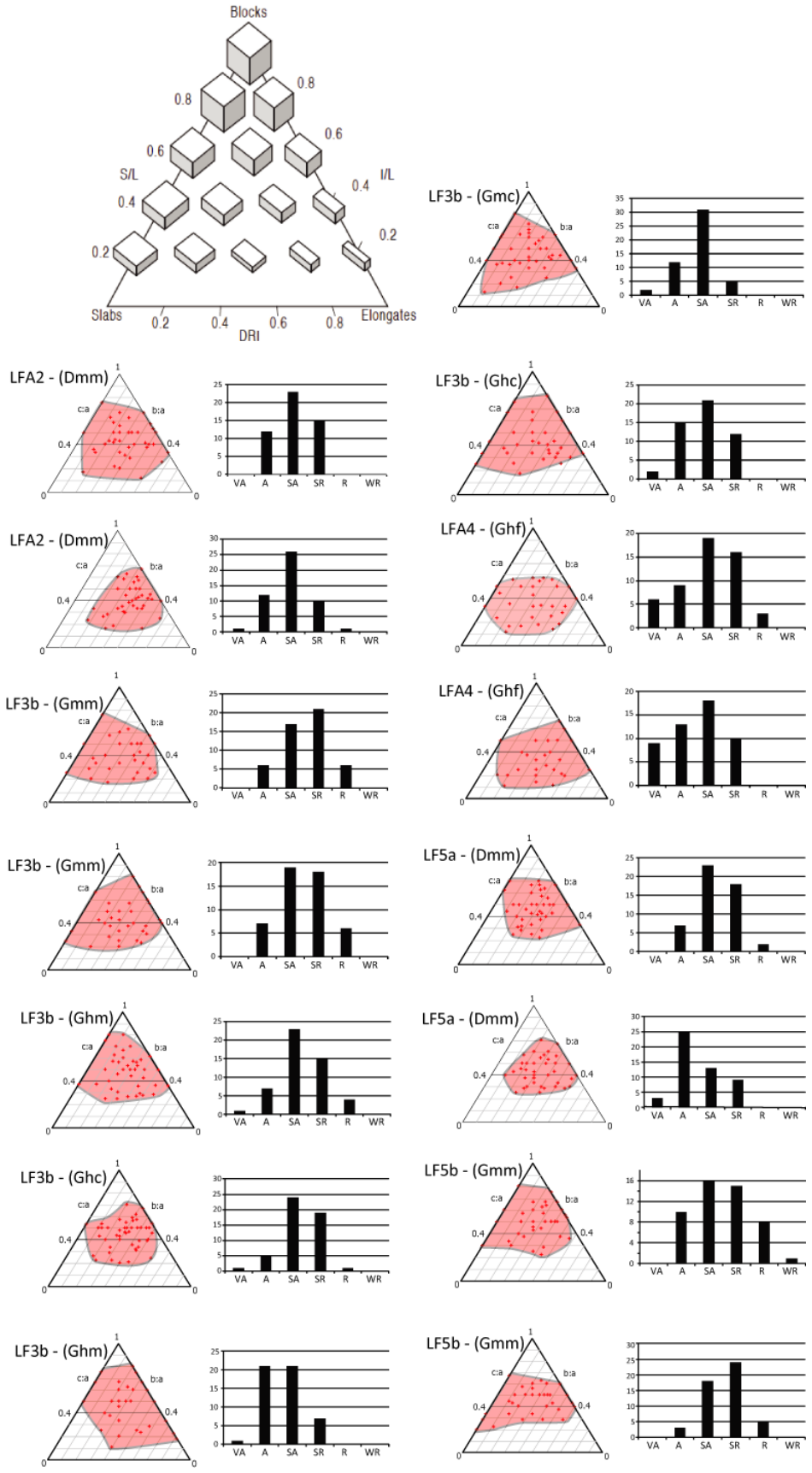

Figure 6.18. Clast form (triangle plots) and clast roundness (histograms) from a number of sites in the study. The specific facies of each sample location is marked, with the facies code.

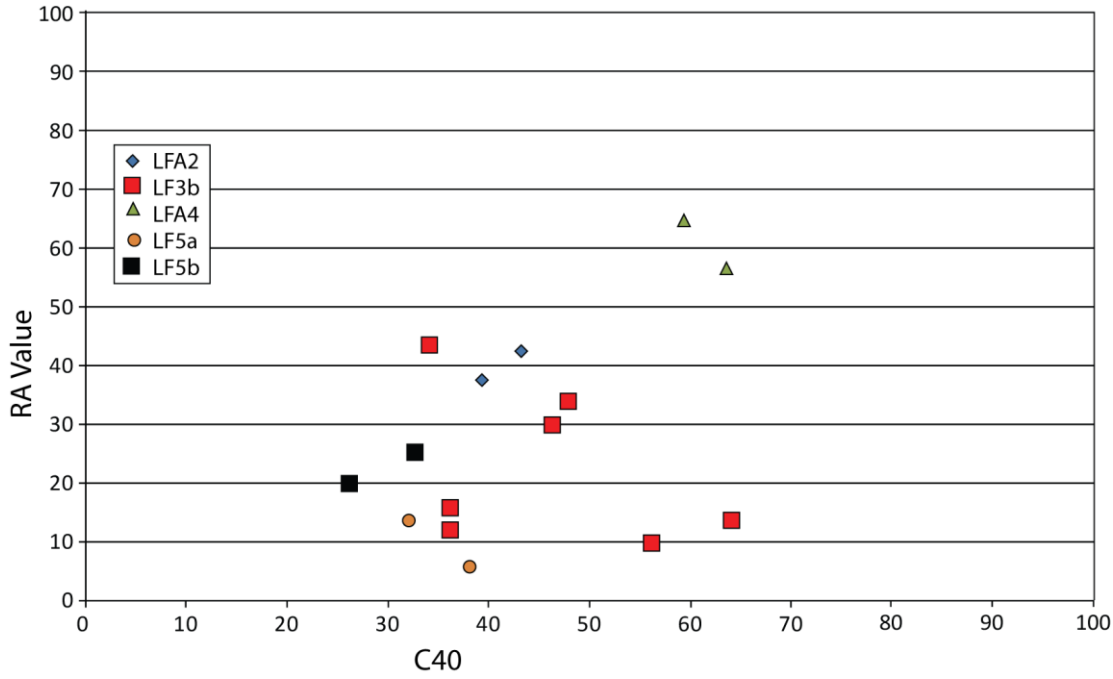

Figure 6.19. Plot of clast form data from this study, showing RA values against C40 values for all samples, with lithofacies codes labelled.

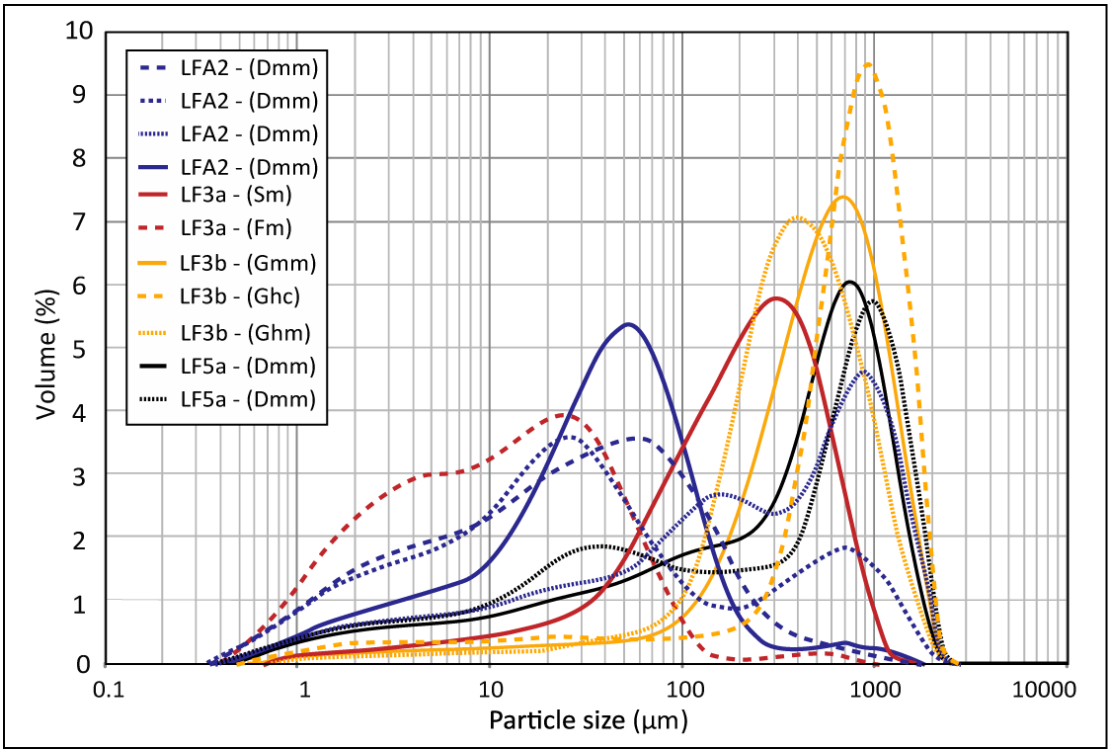

Figure 6.20.Cumulative distribution graphs showing the particle size of matrix samples taken from this study.

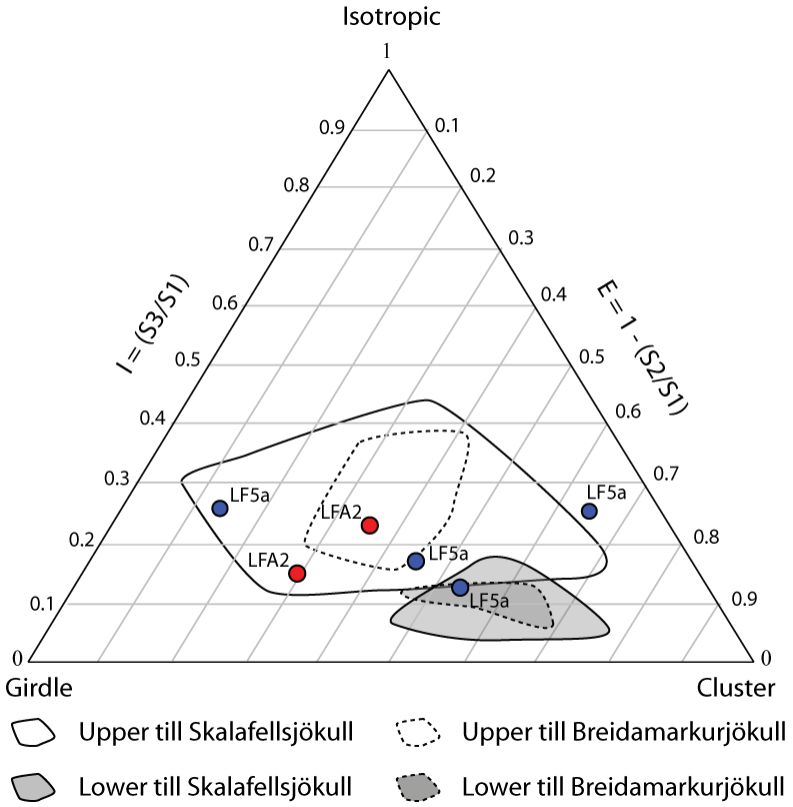

Figure 6.21. (a) clast fabric triangle of samples from LFA2 and LF5a taken during this study (red circles), superimposed upon known subglacial till fabric data from previous studies (Benn, 1994)

6.4.2.1. LFA1 results

LFA1 was found at one location throughout the sites studied, cropping out extensively at the base of Log 5 (Figure 6.15). It consists of diamictic sediment with variable clast content, characterised by angular to very angular, locally-derived basaltic clasts held within a clay to silty sand matrix. The diamicton appeared in bands of altering colour, varying between layers of red, brown, yellow, and purple. Clast density throughout this lithofacies is variable, and in places the diamict is clast-supported. The majority of clasts show a high degree of weathering and extensive brecciation. In places LFA1 was seen to be transitional into, or interstratified with, *in-situ* bedrock breccias, evidenced by a higher clast density, in places displaying primary bedrock structure (Figure 6.22b). In places the *in-situ* bedrock appears to have been displaced/thrust, with the coarse, angular, diamict found between areas of heavily brecciated bedrock.

6.4.2.2. LFA1 interpretation

The brecciated bedrock of lithofacies association LFA1 is interpreted as heavily weathered, tectonised *in-situ* bedrock. The amount of weathering varies throughout the lithofacies association, between areas of brecciated bedrock and clast-rich diamict. This modification occurred during an extended period of periglacial, cold-climate conditions. Initial bedrock brecciation is likely to have been caused by ground ice development during prolonged periglacial conditions (Murton, 1996). However, the interfingering of zones of brecciated bedrock with bedrock-rich diamicton (Figure 6.22b) suggests formation and bedrock disturbance through glaciotectonism under a warm-based ice mass (Harris, 1991, Phillips et al., In Press). Periglaciation and glaciotectonism is a precursor to full glacial erosion (Croot and Sims, 1996), and would have acted to deform and crush both underlying bedrock and sediment (Aber et al., 1989), before the subglacial processes of erosion and deposition dominated. The presence of a marked transition from undeformed bedrock (via heavily brecciated bedrock) to a clast- to matrix-supported diamict is a result of this change in process through time. These are therefore genetically linked lithofacies, and their occurrence has been reported elsewhere (Croot and Sims, 1996, Benn and Evans, 1996, Hiemstra et al., 2007). The lowermost bedrock which varies between intact and brecciated is the result of minor glaciotectonic activity. The diamictic lithofacies both above this bedrock (and in places interstratified with it) is formed through more intense glaciotectonic processes, including bedrock crushing and mixing with fine rock flour (Goldthwait and Matsch, 1989, Hiemstra et al., 2007). It is also possible that the overlying LFA2 is a glaciotectonite, forming the final facies within this transitional sequence from glaciotectonic action to subglacial erosion.

6.4.2.3. LFA2 results

LFA2 was found as a basal unit in Logs 1 and 2 in Arfertuarssuk. It is a grey, poor to well-consolidated, generally structureless matrix-supported diamicton (Dmm), with occasional discontinuous lenses of well-sorted sandy silt (~10 cm thick, ~30 cm wide). Some very crude stratification was visible in section (e.g. facies 5c). Clast abundance throughout the LFA2 was highly variable, though the diamict remained matrix supported throughout. The matrix is composed of silt to silty-sand, with particle size peaks at 1000 µm, 150 µm, and 60 µm (Figure 6.20). It contains abundant marine shell fragments, dominated by *Hiatella arctica* and occasional single valves, although very rare paired valves were found. Clasts within

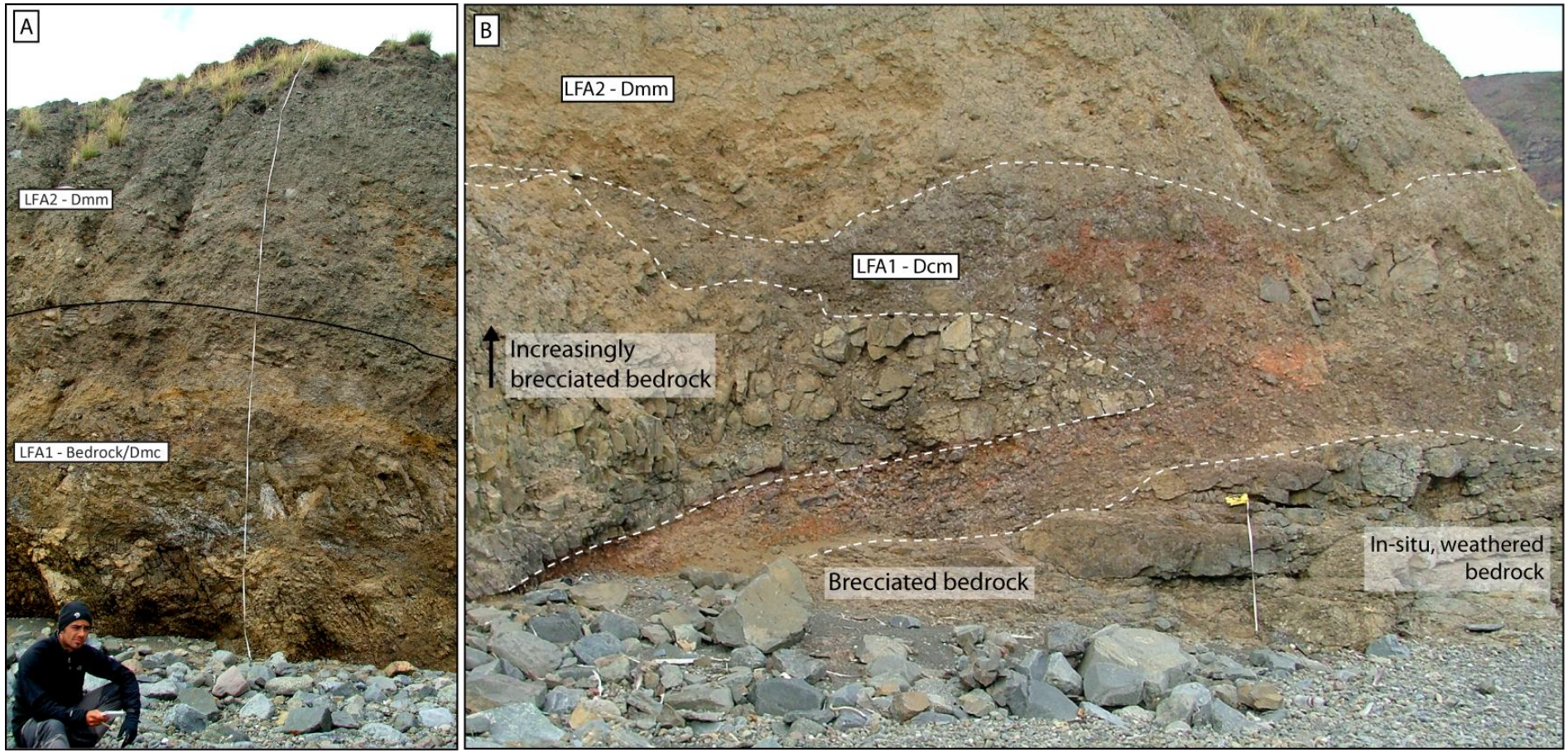

Figure 6.22. Photograph from Logs 5, showing the only exposure of LFA1. (a) Overview of the section logged in Log 5; (b) enlargement of LFA1 and its contact with bedrock below, and LFA2 above. The interstratified/injected LFA1 can be seen. Tape measure is ~60 cm in length.

LFA2 are up to 50 cm in diameter, angular to sub-rounded, often striated, and dominated by local basaltic lithologies and occasional gneissic erratics. Clast form data reveal a preference toward blocky to elongate clasts, with C40 values between 38 and 44%, and RA values of 37-42. Clast macro fabrics were only taken from Arfertuarssuk, and display NW-SE orientated a-axes, with a less important perpendicular, NE-SW component (Figure 6.14). S1 values are 0.54, suggesting moderate a-axis clustering, and fabric shapes plot as girdles to moderate clusters (Figure 6.21). Striae were measured on boulders found emplaced within LFA2, ~100 m to the southwest of Site 1. Results showed highly uniform intra-boulder striae, but high inter-boulder variability, suggesting some boulder rotation subsequent to striation, and during diamicton emplacement (Figure 6.14). A paired valve was sampled from the sediment for radiocarbon dating, and returned a finite age of 47.7 cal. kyr BP (Table 6.5).

6.4.2.4. LFA2 interpretation

LFA2 displays many sedimentological, structural and clast properties of subglacial till, formed through deformation and lodgement (Evans *et al.*, 2006). These include a poor to well-consolidated diamictic matrix, with sub-rounded, lodged, striated clasts. Clasts are dominated by local basaltic lithologies, suggesting that ice eroded and incorporated basaltic bedrock from the Svartenhuk interior into LFA2, prior to emplacement. The thick nature of LFA2 (thicknesses reaching 5 m) may be due to lodgement and reworking of pre-existing sediment, including till (Dowdeswell and Sharp, 1986, Evans et al., 2006), or due to ice-marginal processes (folding, thrusting and stacking), which lead to till thickening (Evans and Hiemstra, 2005, Ó Cofaigh et al., 2011). It is possible that the massive, structureless nature of LFA2 is due to sediment homogenisation through high levels of strain and sediment mixing (Boulton and Jones, 1979, van der Wateren, 1995), or is partially inherited from a pre-existing sediment. Rare interbedded stratified diamicton could relate to part of the continuum from a stratified to massive diamict, which would be indicative of progressive homogenisation through mixing (Evans et al., 2006, Ó Cofaigh et al., 2011). The presence of abundant shell fragments throughout the facies suggests the glacier was also able to rework local pre-existing marine sediment during till genesis.

Clast fabric data support the interpretation of LFA2 as a subglacial till. The data show low isotropy and variable elongation, lying between girdles and moderate clusters. These fall within known envelopes of upper till fabric, suggesting clast emplacement through lodgement and non-solid state deformation (Figure 6.21) (Benn, 1994; Bennett *et al*., 1999).

Pub. code	Sample code	Lat. (°N)	Long (°W)	Sample type	$\delta^{13}C_{VPDB}$‰ ± 0.1	Carbon content (% by wt.)	14C Enrichment (% modern)	+/- 1σ (% modern)	14C Age (years BP)	cal. Min (yr)	cal. Max (yr)	cal. mid (yr)
SUERC-37526	SV_1a (LFA2)	71.51	55.24	*Astarte montagui*	-0.265	11.5	0.41	0.06	44097 ±1177	*45604*	*49808*	*47706*
SUERC-37530	SV_1c (LF5a)	71.51	52.95	*Astarte montagui*	0.796	11.7	0.6	0.06	41106 ±810	*43552*	*46085*	*44819*

Table 6.5. Table of two new radiocarbon ages produced during this study, from Log 1, Arfertuarssuk. The results have been corrected to δ13CVPDB‰ -25 using the δ13C values seen above. Both samples from paired *Astarte montagui* bivalves.

In places, clast fabric data are highly bimodal (See Log 2; Figure 6.14), with a secondary modal peak transverse to the direction of ice-flow reconstructed from bedrock striae evidence. This bimodality could be the result of a localised increase in lodgement, aligning clasts transverse to flow (Andrews and Shimizu, 1966, Lindsay, 1970), or could be the result of weakly constrained deformation (Hicock, 1992, Hicock and Fuller, 1995). Given the multimodal fabric from Log 1, the latter appears more likely. Directional clast fabric data suggest ice flow from the north-northwest within Arfertuarssuk; in agreement with striae from bedrock within the fjord (see Section 6.4.1.1.). The relatively weakly clustered clast fabrics suggest ductile deformation similar to the upper A horizons of tills in Iceland (Evans *et al.*, 2006). In places clast fabric show no preferential orientation. This is likely to be a result of a localised drop in the strain experienced by the sediment (Benn, 1995), or a function of the thick deforming layer (Hart, 1994). Though measured clasts are blocky and elongate, clast form covariance data reveal a relatively angular clast assemblage (Figures 6.18 and 6.19), although it should be noted that clast form was only sampled from Arfertuarssuk. This suggests a short transport distance for the clasts, with rapid erosion and subsequent deposition. Thus, LFA2 displays characteristics of a subglacial till, with variable deformation and lodgement components. This is likely to result from the heterogeneous properties of subglacial beds, and the variability between deforming and stable areas (Piotrowski et al., 2004, Evans et al., 2006).

6.4.2.5. LFA3

6.4.2.5.1. LF3a Results

Based upon their sedimentological properties, deposits from LFA3 have been subdivided into three lithofacies (LF3a, LF3b, and LF3c). As a lithofacies association, the sediments relate to ice marginal deposition in a deltaic setting. LF3a is the lowest lithofacies within LFA3, and is found either at the base of the logged sequences (Log 7 and 8), or sharply, but conformably overlying LFA2 (Log 9). It is characterised by planar bedded, interstratified silty-clay, silt, and medium sand (Figure 24), with a fine gravel content (average grain size 300 µm - Figure 6.20). Planar stratification was horizontal, except for 9b, where bedding dips west at 2°. Where present, gravelly horizons were clast supported and lensate, held within a medium sand (Gcu – Gmc). These interstratified units vary from ~1 mm to 60 cm in thickness. LF3a shows evidence of variable grading, displaying normal grading (e.g. Log 7), inverse grading (e.g. Log 9), and no grading (e.g. Log 8). In places the finer beds display

distinct evidence of post-depositional loading deformation including convolutions, flames, and pipes. The silty-clay and silt beds often contained ubiquitous detrital plant remains. Abundant marine shell fragments and rare whole marine valves were retrieved from finer layers. In Log 9 the abundance of macroscopic plant remains increases dramatically between towards the top of LF3a. Here planar stratified minerogenic silty sand is interstratified with layers of dense mats of plant remains, up to 15 mm thick. The organic remains were dominated by aquatic reed species, and in places small twigs thought to be *Salix herbacea* and *Betula nana*.

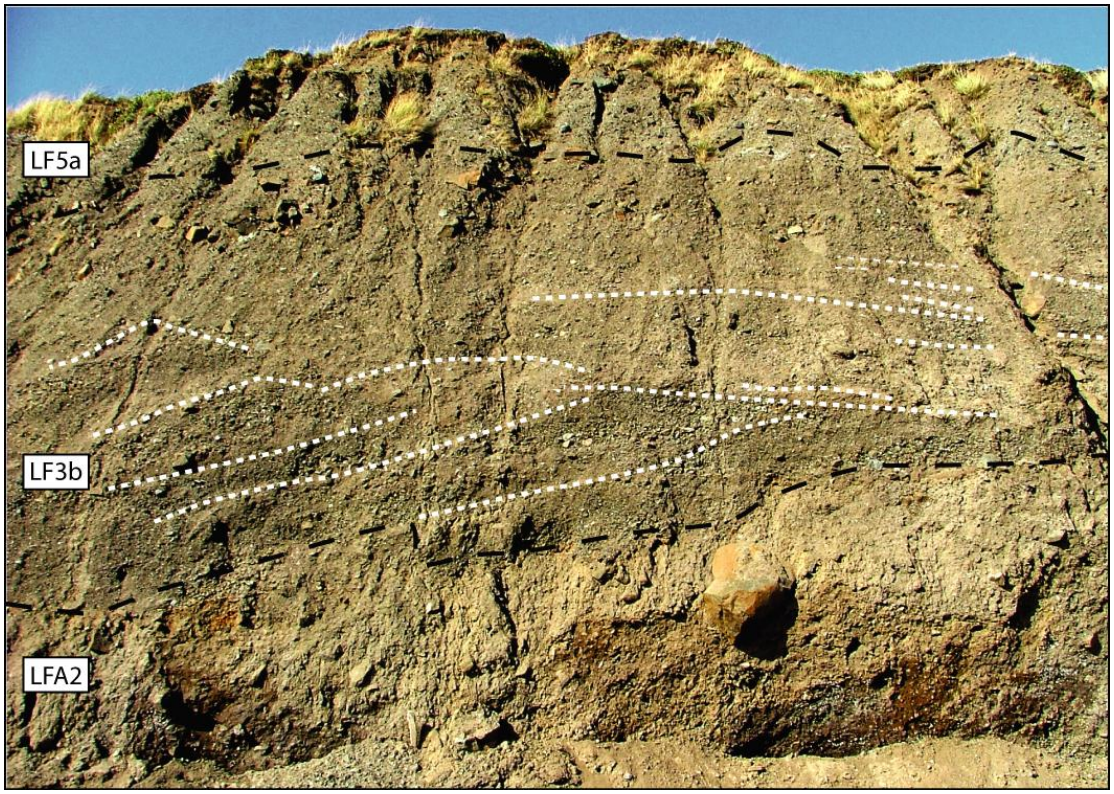

Figure 6.23. Photograph of the sedimentary exposure 10 m to the north of Log 2. The two diamictic lithofacies (LFA2 and LF5a) can be seen at the base and top of the sequence. Between these is the horizontal to planar stratification of LF3b.

6.4.2.5.2. LF3a Interpretations

The very fine-grained planar stratified deposits are interpreted as bottomsets of a delta, and represent low-energy fluviodeltaic sedimentation (Gilbert, 1885, Lønne, 1995). These sediments are deposited by suspended-load sediment settling in front of an advancing delta (Gilbert, 1885, Kenyon and Turcotte, 1985, Lønne, 1995). The ubiquitous macroscopic plant remains found throughout the lithofacies are suggestive of a low energy depositional

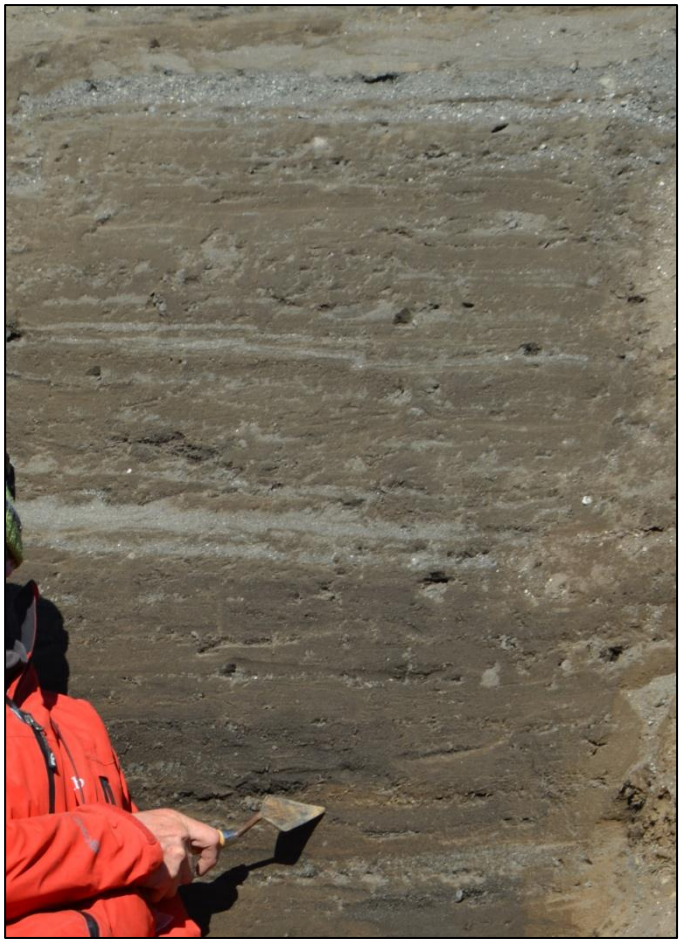

Figure 6.24. Photograph of horizontally stratified silty-clay, silt, and sand, characteristic of LF3a from Log 7. Trowel is pointing at a ~5 cm thick layer of dense organic remains.

environment, with slow flowing water allowing the settling of terrestrial plant remains. It is likely that these were introduced from higher altitude upstream regions. The variability in both the frequency and relative density of macroscopic organic remains throughout LF3a is a result of variability in vegetation availability and its delivery into the delta. This lithofacies displaying high organic component is indicative of either: a period of ice-free conditions sufficient to allow vegetation growth and inwash; or reworking of pre-existing vegetation through glacial advance. The transitions between LF3a and the overlying LF3b are sharp but conformable, suggesting a rapid, but continuous transition. The coarsening upwards sequence noted within LF3a suggests a progressive increase in the proximity of the of the ice margin to the location of deposition.

6.4.2.5.3. LF3b Results

The lithofacies is characterised by orange-brown crudely to well-stratified medium sand and gravel. The gravel is matrix-supported and interstratified with thin (~2 cm thick) facies of coarse, clast-supported gravel, massive medium to coarse sand, and silt. The gravels are predominantly planar stratified, offlapping to the south-southeast at 6-37°, and in places display a lensate, channel-like morphology (Figure 6.17, 6.23, and 6.25). Interstratified fine grained units (clayey silt and silt) often show distinct loading structures; convolution, flames, and pipes. Occasional facies of clast supported (Gmc), open framework gravel were logged. Facies thickness varies widely, often with areas of thin (~5 cm) silty sand facies interstratified with thick (>30 cm) facies of gravel. Matrix grain size shows a strongly unimodal distribution, with a matrix dominated by coarse to medium sand (~700-900 µm in Tasiussaq and 400 µm in Arfertuarssuk) (Figure 6.20). Clasts throughout are pebble to cobble sized sub-angular to sub-rounded local basaltic lithologies, reaching 60 cm in diameter, with variable C40 values of 36-64%, and RA values of 10-44 (Figures 6.18 and 6.19). These are suggestive of generally blocky, compact, sub-rounded clasts (Figure 6.18). Very infrequent shell fragments were found throughout LF3b, but no whole shells were retrieved. In Log 10 (Uligssat), a 2.5 m section of matrix supported gravel contained large-scale cross-cutting lenticular geometry. In Log 8, LF3b displayed a distinct fining upwards sequence, with a marked reduction in clast size and density, accompanied by an increase in bedding dip.

6.4.2.5.4. LF3b Interpretation

On the basis of its geomorphic context (flat topped raised deltaic features) and sedimentology (dipping, planar stratified sand and gravel), LF3b is interpreted as a sequence of gravelly delta forests (Gilbert, 1885, Edwards, 1986, Nemec and Steel, 1984). Based upon the deltaic setting and the presence of frequent marine shell fragments, LF3b was deposited in a marine environment. The poor sorting and weak imbrications of clasts within foreset beds reflects deposition through avalanching, highly concentrated debris flows, and bedload deposition down the delta face, forming dipping, planar stratified deposits (Postma and Roep, 1985, Kenyon and Turcotte, 1985). The upward fining sequence recorded in LF3b exposures from Tasiussaq are common sedimentological characteristics of delta foresets (Clemmensen and Houmark-Nielsen, 1981), likely to represent a retreat of the ice margin. In contrast, the exposure of LF3b found at the head of Arfertuarssuk (Log 1 and 2) is

characterised by a coarsening upwards sequence. It is possible that this is due to the development of deposition proximal to a glacier meltwater efflux (Bannerjee and McDonald, 1975, Cheel and Rust, 1982). The inferred direction of delta formation from foreset dip varies between logged sections, with deposition from the north in Arfertuarssuk, the east in Tasiussaq, and the north in Uligssat. The orientation of dipping planar stratified lithofacies provides further evidence for the interpretation of sediments and belonging to a Gilbert-type delta. In addition, dip orientation assists in precluding a fluvial source for the sediments (e.g. Logs 4, 7, and 8). Clast form data are variable throughout logged exposures of the lithofacies, but suggest active transport. C40 and RA values are higher than those reported from other deltaic deposits (Benn and Evans, 1993), suggesting a short transport history, and therefore limited clast rounding.

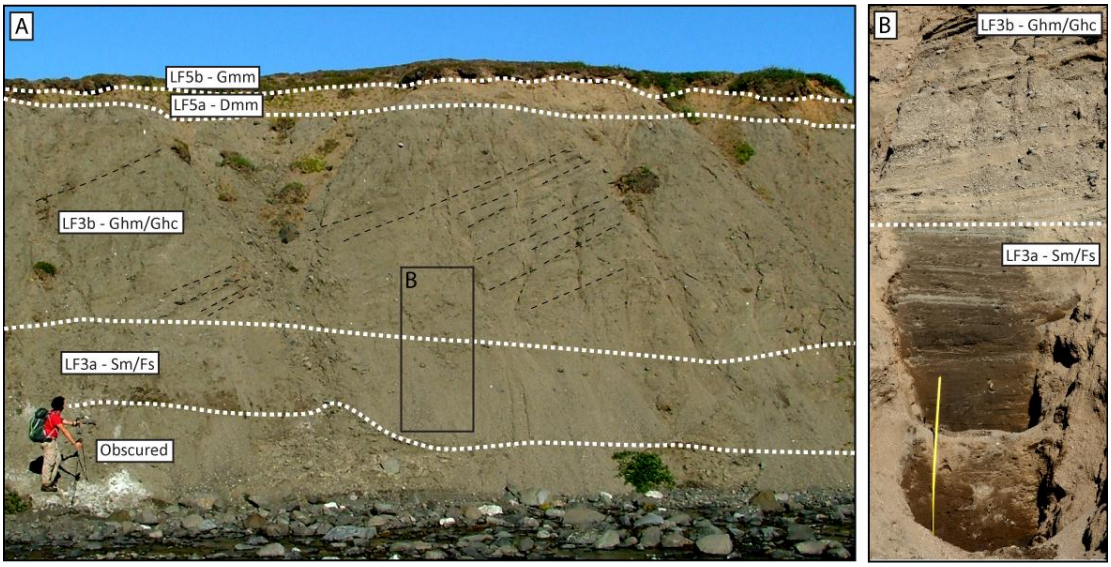

Figure 6.25. Photographs from the delta section recorded in Log 8. (a) Overview photograph of the section described in Log 8, dominated by the dipping, planar stratified LF3b; (b) enlargement, showing the sharp switch from LF3a to LF3b.

6.4.2.5.5. LF3c Results

LF3c is composed of well to very-well sorted interstratified clayey silts, fine to coarse sand, and fine sand and gravel. Units are horizontally planar stratified, with no clear grain size grading, and are up to 50 cm thick (Figure 6.26). Granule sized clasts are dominated by local basaltic material, and appear sub-angular to sub-rounded. No clast form data was taken from this lithofacies. In Log 10 (Uligssat), a 2.5 m section of matrix supported gravel contained well-developed, large-scale cross-cutting lenticular geometry (Figures 17 and 26).

6.4.2.5.6. LF3c Interpretation

The facies of massive to planar interstratified silt to gravel is interpreted as low energy glaciolacustrine and glaciofluvial deposits, formed in the proglacial zone as delta topsets. Sediment variability is thought to be a function of variability in water depth (Fyfe, 1990), and local glacier proximity. The fine grain size, and low energy nature of the sediments suggest that this deposition occurred in an ice-distal setting. Though LFA3 is found extensively throughout Arfertuarssuk, Tasiussaq, exposure of LF3c is very restricted, only found in Logs 6 and 10. The well-developed lenticular geometry of sediments in Log 10 records the development of palaeochannels, a common feature of topset deposits (Fyfe, 1990, Lønne and Nemec, 2004). This provides evidence for the development of well-defined, channelised flow across the surface of the delta.

Figure 6.26. Photograph of horizontally stratified medium sands characteristic of LF3c. Photograph is from Log 6.

6.4.2.5.7. LFA3 Interpretation

Based upon both their sedimentology (bottomsets, foresets, and topsets) and geomorphology (flat topped features with sloping front and rear faces - see Section 6.4.1.)

they are interpreted as partial sequences from Gilbert-type deltas (Gilbert, 1885, Bates, 1953, Benn and Evans, 2010).

Gilbert-type deltas form in both glacier-fed and ice-contact settings (Benn and Evans, 2010), and often display very similar sedimentological properties (Lønne, 1993). The raised deltas from which Logs 4 (centre of the Arfertuarssuk Fjord) and 10 (Uligssat valley) were recorded display steeply sloping upstream flanks, and lower angle downstream slopes. These upstream slopes are interpreted as ice-contact slopes, providing evidence that the delta was ice-contact during its formation (Figures 6.6c and 6.13c). In addition, there is limited continuation of the raised deltas, providing evidence that it was formed through deposition in an ice-contact, and not glacier-fed setting. In contrast, the delta from which Logs 1-3 were recorded, at the head of Arfertuarssuk Fjord, does not display a clear ice-contact slope. It is possible that this too represents an ice-contact delta, although evidence is inconclusive, and is tentatively interpreted as glacier-fed. Similarly, the deltas from which Logs 6-9 were recorded do not display clear ice-contact slopes, and as a result can only be classified as Gilbert-type deltas, and not as glacier-fed or ice-contact.

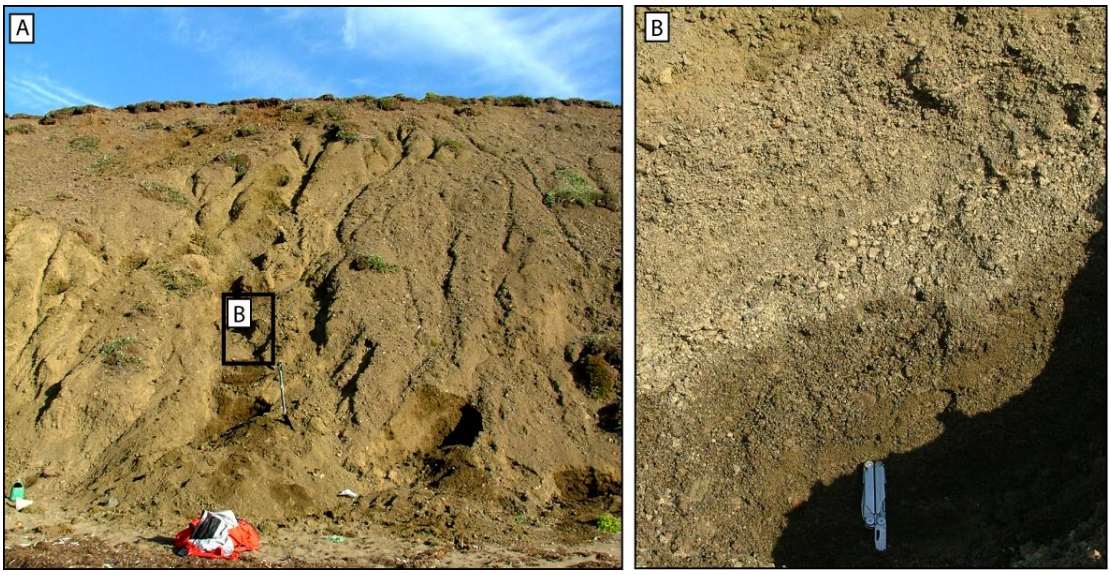

Figure 6.27. (a) Photograph of section from Log 3, displaying dipping, planar bedded gravels (LF3b), overlain by LFA4; (b) sedimentary detail of LFA4 – with dipping bedding evident.

6.4.2.6. LFA4 Results

LFA4 is found in Arfertuarssuk and Tasiussaq, and composed of extensive moderately to poorly stratified, medium to coarse dipping planar stratified sand and gravel (Figure 6.27).

The bulk of LFA4 is matrix supported, though infrequent facies of clast supported gravels were logged. Clasts throughout the lithofacies association are pebble to cobble sized, angular to rounded, and dominated by local basaltic lithologies. The clast assemblage returned C40 values of 60-64% and RA values of 55-65 (Figures 6.18 and 6.19). Gravelly facies in Log 3 are interstratified with fine grained facies of beige sandy silt, and discontinuous lenses of brown silty clay. These contain angular basaltic granules up to 3 cm in diameter. Facies from LFA4 dip variably throughout Svartenhuk: south-southeast at 20-38° in Arfertuarssuk, and west at 8-20° in Tasiussaq.

6.4.2.7. LFA4 Interpretation

Based upon the dipping stratification, and frequent sharp switches between matrix and clast supported facies, LFA4 is interpreted as a stratified slope deposit (DeWolf, 1988, Francou, 1990). Though impossible to comprehensively separate and understand the depositional processes responsible for deposition, these kind of deposits are likely to have formed through gravitationally driven slope wash, debris flow, and solifluction (Bertran *et al.*, 1997), sourced from steep terrain backing a number of delta sites. The presence of stratification and a clear sorted structure are indicative of an overland flow component (Bertran and Texier, 1999). The fine gravelly facies of LFA4 at Log 3 are indicative of a relatively short transport distance along the flow distance (Van Steijn *et al.*, 2002). The repeatable pattern of switches between matrix rich gravel and layers of coarser clast rich gravels is characteristic of stratified slope deposits, formed through multiple stacked grain flows (Van Steijn *et al.*, 2002). Clast form data support this interpretation, with the highest C40 and RA values reported from this study. The C40 – RA plot places the LFA4 samples in a similar region to previously reported scree and supraglacial material (Benn and Ballantyne, 1994) (Figure 6.19). The high angularity is characteristic of slope deposits, with a relatively short, passive transport pathway (Ballantyne, 1982, van Steijn, 1996, Van Steijn et al., 2002). These data suggest a preference to slabby, elongate forms, also indicative of unmodified, frost-weathered clast (Ballantyne, 1982). Though difficult to fully interpret the sediment based upon this exposure, the presence of interstratified fines throughout LFA4 suggests some input through slope wash. Though periglacial conditions are likely to have enhanced slope deposition through increased frost action, they are not necessary; slope deposits can form under a wide range of conditions (Van Steijn *et al.*, 2002).

6.4.2.8. LFA5

LFA5 was subdivided into two distinct lithofacies. LF5a is a diamicton found capping Logs 1 and 2 in Arfertuarssuk, and is also found in Tasiussaq. Within Tasiussaq, LF5a appears below, or in places interbedded with LF5b, a facies of sand and gravel. Due to their dissimilar sedimentology they have been analysed and interpreted separately.

6.4.2.8.1. LF5a results

LF5a is a grey to pink-grey, massive, matrix-supported diamicton (Dmm). It is moderately to well consolidated, with a bimodal matrix distribution, with modes at 1000 µm (coarse sand) and 45 µm (coarse silt) (Figure 6.20). A lesser component of clay to silt was also found. The matrix is rich in marine shells, with common fragments and rare intact *in-situ* single valves. In places the shells are held in distinct horizons within the matrix. The contact between LFA5 and underlying lithofacies is very sharp in all exposures, with no evidence of sediment mixing. Clasts in LF5a are dominated by local basaltic lithologies, up to 20 cm in diameter and sub-angular to sub-rounded, with ~14% striated. Clast fabrics are moderately to strongly clustered, displaying low isotropy (Figures 6.21). The macrofabric data return an S1 eigenvalue of 0.59, suggesting moderate to high a-axis clustering, and a girdle to moderate cluster clast form shape (Figure 6.21). Clast form analysis is clustered toward blocky and elongate, and data show C40 values of 38-48%, and a highly variable RA of 6-56 (Figures 6.18 and 6.19). As with LFA2, the lithofacies contained abundant marine shell fragments, with very rare paired valves. A paired valve was sampled from the sediment for radiocarbon dating, and returned a finite age of 44.8 cal. kyr BP (Table 6.5).

6.4.2.8.2. LF5a interpretation

Based upon its diamictic nature, moderate to strong clustering of clast fabric coincident with independent indicators of ice flow direction, and the presence of striated clasts, LF5a is interpreted as a moderately to well-consolidated subglacial till. The presence of local basaltic clasts and shell fragments throughout LF5a suggests extensive erosion of the underlying basaltic bedrock, and cannibalisation of pre-existing localised marine sediments. Clast form data display a higher C40 value than previously reported subglacial tills (Benn and Ballantyne, 1994), though the low RA values are similar. The high angularity of clasts in comparison to other studies could be due to short transport distance, as discussed in LFA2.

Clast fabric data support the interpretation of LFA2 as a subglacial till, showing low isotropy and moderate to high elongation; falling within known envelopes of upper till fabric (Benn, 1994; Bennett *et al*., 1999). Although the strength and direction of preferential clast orientation varies between logged diamicton facies, orientation is in agreement with independent ice flow indicators, inferring north-northwest to south east ice flow in Arfertuarssuk, and northeast to southwest ice flow in Tasiussaq (see Figures 6.14 and 6.15). When LF5a is found in association with LFA2, clast macrofabrics from both lithofacies are in agreement, suggesting multiple ice advances overriding the sites from similar directions. Fabric from the lower portion of LF5a in Log 7 is multimodal, with no preferential orientation. This could be a result of a localised decrease in the strain experienced by the sediment (Benn, 1995), or a function of a thick deforming bed, allowing free rotation of clasts (Hart, 1994, Hicock, 1992, Evans et al., 2006). The absence of any bedding or deformation structures could suggest sediment homogenisation through mixing (van der Wateren, 1995), or simply be a primary sedimentary characteristic of a partially reworked deposit. As argued for LFA2 above, this therefore suggests that LF5a contains both lodgement and deformation components. In summary, the sedimentological and clast macro fabric data suggest that LF5a is a subglacial till, dominated by lodgement emplaced by glacier movement from the north-northwest in Arfertuarssuk, and northeast in Tasiussaq.

6.4.2.8.3. LF5b Results

LF5b was recorded capping Logs 7 and 8 in Tasiussaq. This lithofacies is characterised by up to 1 m of yellow, clast supported sandy gravel, in places held within a friable open framework. The facies is generally structureless, with some very crude sub-horizontal stratification. In Log 7, the gravel is interstratified with occasional lenses (~3 cm thick) of well-consolidated pink diamicton, similar in colour, texture, and grain size to LF5a. Clasts are local basaltic lithologies, up to ~14 cm in diameter. Clasts are local basalt, and dominated sub-rounded and rounded clasts. Clast form data show C40 values of 26-32%, and RA values 14-20 (Figures 6.18 and 6.19).

6.4.2.8.4. LF5b Interpretation

Exposures of LF5b are only found in locations where eskers were found on the land surface (see Section 6.4.1.2.). As a result, the LF5b sand and gravel is interpreted as esker fill gravel (Warren and Ashley, 1994, Benn and Evans, 2010). Clasts are locally derived from the

Svartenhuk Peninsula interior, and the low C40 (26-32%) and RA (14-20) values reflect an active transport history, either through subglacial or englacial pathways (Benn and Evans, 2010).

6.5. Discussion

6.5.1. Geomorphological evidence for glaciation of southern Svartenhuk

Previous research has proposed LGM glacial extent on Svartenhuk was very restricted (Laursen, 1944). Although never comprehensively mapped, ice is thought to have been restricted to high-altitude mountain massifs in the interior of the peninsula, forming individual mountain valley glaciers and small cold-based ice fields. This restricted LGM glaciation is hypothesised to have allowed preservation of extensive coastal deposits of non-glacial MIS 5e-a sediments, deposited during periods of elevated sea-level. Results from this study directly contradict this interpretation. Geomorphological evaluation of sites from the Arfertuarssuk, Tasiussaq, and Uligssat valleys in southern Svartenhuk provide ubiquitous evidence for warm-based glaciers extending down to the present coastline. Glacially striated bedrock found at a mid-fjord position within Arfertuarssuk provides evidence for grounded warm-based ice. Evidence constrains this to at least the mid fjord, though its terminal position is not known. Inset lateral moraines in Tasiussaq provide direct evidence for occupation of the valley by a large, warm-based glacier. Within Tasiussaq, terminal position of valley glacier is very poorly constrained. However, based upon the altitude of the valley-side lateral moraines, it must have extended offshore.

As discussed in section 6.4, a series of ice-contact and glacier-fed deltas were recorded throughout Arfertuarssuk, Tasiussaq, and Uligssat, and regions of kettled outwash found at the head of Arfertuarssuk and throughout Tasiussaq. Together these provide further convincing evidence for the extensive, warm-based glaciation of the region. In particular, the preservation of the deltas and kettled outwash surfaces record the last deglaciation of southern Svartenhuk, from the coast toward the interior. The presence of glaciogenic deltas is suggestive of a retreating glacier front, punctuated with a series of stabilisations, allowing the formation of large-scale, high-energy deltas. The preservation of kettled outwash geomorphology and its stratigraphic position above the glaciogenic deltas in Arfertuarssuk and Tasiussaq suggests that the kettled surfaces represent the final stages of the last deglaciation from southern Svartenhuk, likely to be of outlet glaciers with debris charged

snouts (Benn and Evans, 2010). This caused snout burial and stagnation during withdrawal, creating an ice-proximal, kettled outwash surface through ice block melt-out (Benn and Evans, 2010). The small esker which runs into and across the outwash surface is likely to have formed either englacially or subglacially.

Although the coastal valleys and fjords contain ubiquitous evidence of glacial activity, evidence further inland is limited. Within the interior region to the north and east of Arfertuarssuk only discrete, small-scale evidence of ice activity was found. These included small, subdued lateral moraines, small fragmentary eskers, and occasional edge-rounded boulders, perched upon the landsurface (e.g. occasional edge-rounded erratic boulders, small subdued moraines). The series of overspill channels found incised into bedrock ridges to the northeast of Arfertuarssuk also provide evidence of glaciation within the interior of Svartenhuk. As outlined in section 6.4.1.1, these overspill channels would have formed following damming and overtopping of the topography by pooled water. Damming of this magnitude is not feasible with the present regional topographic configuration, and it is therefore believed that damming was caused by glacier ice. Meltwater would have become dammed between the retreating ice-front, lateral basaltic ridges, and higher terrain to the southeast (Figure 6.3). This would have formed large, topographically bound basins which then filled with meltwater. Once filled, water escape through overspill would have occurred along lines of weakness on the ridges, forming gorges and channels flowing into neighbouring valleys.

Evidence for glacial alteration on high-level land surfaces to the east of Arfertuarssuk and north and southeast of Tasiussaq is minor, with erratics and rare striated surfaces above 300 m a.s.l. Heavily weathered, high-altitude surfaces display evidence of a long-term surface exposure history, with some evidence for non-erosive glacial activity. This suggests that the area has been covered by thin, protective, cold-based ice (Rea and Evans, 2003), likely to have been sourced from these high-level plateaux. This protective ice cover is likely to have developed during both the LGM and previous glacial periods, though there is presently no chronological control on the exposure history of the surface. However, it is likely that surface would have a complex exposure history, showing multiple periods of burial (by cold-based ice) and exposure.

The large sub-angular to sub-rounded boulders found upon lower fan surfaces in Uligssat are clearly erratic in nature, and not sourced from the Svartenhuk Peninsula. There are no

other erratic boulders in the valley, either upon fan surfaces, or within deltaic sediments, suggested that they were deposited on top of the fan surface subsequent to deposition, perhaps by stranded ice bergs sourced from outlets to the east (e.g. Rink and Ingia Isbræ). However, these boulders remain enigmatic, and their source and depositional history are not fully understood.

6.5.2. Sedimentological evidence for glaciation of southern Svartenhuk

Geomorphological evidence for the warm-based glaciation of southern Svartenhuk is supported by sedimentological evidence from Arfertuarssuk, Tasiussaq and Uligssat.

6.5.2.1. Subglacial sediment

Subglacial till (LFa2 and LF5a) is found extensively throughout both Arfertuarssuk (Logs 1 and 2) and Tasiussaq (Logs 5, 6, and 9). As outlined in sections 6.4.2.3., 6.4.2.4., 6.4.2.8.1., and 6.4.2.8.2., these deposits are glacial in origin, and provide direct evidence for grounded, warm-based ice flowing through Arfertuarssuk and Tasiussaq valleys. In places, both bedrock and sedimentary deposits displayed clear evidence of deformation through glaciotectonism (LFA1 – Log 5), providing further evidence for the overrunning of the region by mobile, warm-based ice. In conjunction with their geomorphology, the esker gravels (LF5b) recorded in Logs 7 and 8 present additional sedimentological evidence for subglacial deposition during a second ice advance. Clast fabric data from subglacial tills within Arfertuarssuk and Tasiussaq are in agreement with bedrock striae, moraine and delta orientation, and fjord/valley morphology. These suggest north-northwest to south-south east ice flow in Arfertuarssuk, northeast to southwest ice flow in Tasiussaq, and north to south ice flow in Uligssat. In conjunction with the results of clast lithological analysis (a clast assemblage of close to 100% locally derived clasts) this ice directional data suggests ice in all three valleys was sourced from the high-altitude centre of the Svartenhuk Peninsula, with no input from the GIS. In Arfertuarssuk, both LFA2 and LF5a were visible within a single section. These exposures provide unequivocal evidence for two distinct ice advances within Arfertuarssuk. In contrast, only LFA2 *or* LF5a were visible in section in Tasiussaq. However, Log 9 (in which LFA2 is present) is in close proximity to Logs 7 and 8 (in which LF5a is present). LFA2 is the basal facies in Log 9, and lies below the ground surface of Logs 7 and 8. It is therefore hypothesised that LFA2 is present in Logs 7 and 8, though remains below the present land surface, and was not excavated.

The presence of whole and fragmentary marine shells throughout LFA2 and LF5a suggests that the sediments were either originally deposited under marine conditions (i.e. a higher than present sea-level), or consist of reworked marine sediments. The latter is most likely for subglacial deposition, as discussed below (Section 6.5.3.).

6.5.2.2. Proglacial sediment

LFA3 is found between the subglacial tills, and broadly records a period of proglacial delta formation under marine conditions. These provide evidence for the retreat of ice through Arfertuarssuk, Tasiussaq, and Uligssat. During retreat, it is likely that ice became temporarily pinned a number of times, allowing for delta development. No direct glacial sediments were found in Uligssat, and as a result the exposures of LFA3 (found within ice contact deltas), provide indirect evidence for glaciation. The presence of whole and fragmentary marine shells throughout LFA3 suggests that the sediments were deposited during marine conditions, as the sediments are *in situ*. This is supported by delta and alluvial fan geomorphology from the Svartenhuk coast, which is graded to a series of heights above sea-level (16 – 75 m a.s.l.), inferring formation during a higher than present relative sea-level.

6.5.3. Chronology of southern Svartenhuk deposits

The existing chronology constraining the deposits analysed in this study is based upon a number of infinite (>40 kyr) radiocarbon ages from locations at Logs 1, 3, and 5/6 (Table 6.2), amino acid racemisation determinations, and U-series ages (>89 and 115 kyr BP (no errors quoted) - Funder et al., 1994 as from Kelly, 1986). As discussed, these have been used to suggest pre-LGM sediment deposition. Despite the stark disagreement in the sedimentological interpretations presented by this study and the studies from which the dates originate, the chronological control remains valid. This study has provided an additional two dates from Arfertuarssuk (Log 1 - Table 6.5), which returned finite ages of 47.7 cal. kyr BP and 44.8 cal. kyr BP (MIS3).

Together, these new and old chronological data present a number of possibilities for the age of the sediment deposition throughout southern Svartenhuk, and thus, the age of glacial inundation. The newly produced ages from shells in Log 1 are overlapping within 2σ error, despite appearing inverted within the sequence. There is a possibility that the ages are

underestimates, and the use of an inorganic carbonate standard to correct the samples (Iceland Spar Calcite) has artificially lowered the background from accurate levels. If so, the shells would have returned measurements indistinguishable from background. However, based upon the chronology presented, shell ages and their associated geomorphological and sedimentological setting presents a number of possible interpretations:

(1) Shell ages represent the age of subglacial till deposition demonstrating deposition of two tills rapidly after one another at ~49.8 – 43.5 cal. kyr BP. This would correlate to MIS 3, within the last glacial cycle.

(2) Shells formed during the period ~49.8 – 43.5 cal. kyr BP, but their age does not represent the age of the sediment deposition (LFA2 and LF5a). Instead shells have been post-depositionally reworked from pre-existing marine sediment by glacial activity, and included within the subglacial diamict. This interpretation could place the deposition of sediments within the LGM (24 – 16 cal. kyr BP (Clark et al., 2009, Funder et al., 2011)).

The small number of new ages and infinite values of older ages makes the robust validation of any one of these interpretations very difficult. However, a number of observations can be drawn from the data. Unless these dates represent large underestimates of shell age, they are in disagreement with the proposed age of deposition for the sediments (115 – 55 cal. kyr BP - Kelly, 1986, Funder et al., 1991, Bennike et al., 1994). The majority of published radiocarbon ages which have been used to constrain the age of deposits (n=6) produced non-finite ages of >30.4 to >40 cal. kyr BP (Table 6.2), in which the shell signal was not discernable from background. However, recent progress in the precision of measurements and the use of AMS makes it possible that rerunning of these samples would now return a finite measurement. The new shell ages, taken from a subglacial till of a possibly reworked assemblage therefore provide a *maximum* age for the emplacement of the subglacial till, and consequently the glacier advance. On this basis of this reasoning it can be tentatively argued that the deposits within Arfertuarssuk (as no new dates exist from Tasiussaq or Uligssat) represent deposition during the last glacial cycle, after 43.5 cal. kyr BP. The highly crushed nature of the shell assemblage within LFA2 and LF5a (other than the two shell samples used for dating), and the mixed macrofossil assemblage (Bennike *et al.*, 1994) provide some evidence of post-depositional sediment reworking during later glacial activity. This makes it possible that the shells dated from Svartenhuk, though dating shell formation, are not dating sediment genesis.

The sparse chronology of sediments throughout southern Svartenhuk makes correlation between sites, and indeed individual valley systems difficult. As no new dates were produced for Tasiussaq or Uligssat, they remain undated. Further chronological control from all three valleys would assist in correlation, however the similar geomorphology, sedimentology, stratigraphy, and hypothesised source region (the high-altitude Svartenhuk interior) suggests that lithofacies found at multiple sites *were* deposited during the same phase of glacial activity (i.e. the LGM). The present chronology also makes understanding the outcropping of multiple subglacial tills difficult. Where found, they are consistently separated by LFA3, suggesting a distinct period of ice retreat before the second phase of overrunning and deposition of LF5a. Further constraint upon age of deposition could be provided by the relative height of deposits throughout southern Svartenhuk. The deposits are graded to a number of distinct levels above present sea-level, and the presence marine fauna within the deposits indicates their deposition in a marine setting at a time with a higher than present sea-level, or the reworking of previously deposited marine sediment by subsequent glacial advance. The *in situ* LFA3 were clearly deposited during a period of ice retreat, into a higher than present relative sea-level. As an LGM age is assigned for these deposits, delta formation is likely to have been during the early stages of deglaciation, prior to outpacing of eustatic sea-level rise by glacioisostatic adjustment (Long et al., 1999).

Samples for surface exposure dating (^{36}Cl), optically stimulated luminescence, and radiocarbon dating (from macroscopic plant remains) have been submitted to dating laboratories, and results are forthcoming. It is hoped that the results from this multiple-method dating approach will help to further constrain the glacial activity of ice across southern Svartenhuk.

6.5.4. Implications for regional ice sheet history

Both geomorphological and sedimentological data demonstrate glaciation of the peninsula to the present coastline, characterised by large warm-based valley glaciers. The findings provide compelling evidence for glacier expansion to the present coastline, and its subsequent retreat to the Svartenhuk interior. Based upon ice flow indicators and clast lithological composition, these glaciers are thought to have been sourced from high altitude plateaux in central Svartenhuk. Very little evidence exists for the presence of any widespread ice sheet or ice stream activity within any of the valleys studied. This suggests that the large UISS did not move on-shore in southern Svartenhuk either during or following

the deposition of the sediments throughout southern Svartenhuk. This absence of ice stream impact upon a very low-lying coastal area, in close proximity is due to a number of reasons. Firstly, during glacial condition, the onset zone of the UISS (to the southeast of Ubekendt Ejland) would have caused intense ice stream drawdown through Igdlorssuit Sund and into the Uummannaq Trough (see Chapter Four). In conjunction with the shallow bathymetry to the north of Ubekendt Ejland, this is likely to have prevented the majority of ice from the northern Uummannaq region flowing directly west, towards the Svartenhuk coastline. However, although this topographic diversion and powerful drawdown is likely to have prevented some ice flow, it remains likely that some ice (up to 800 m a.s.l. in thickness) still flowed through Qeqertat Imat, just south of Svartenhuk. If true, a secondary factor must have prevented ice stream ice from moving onshore. In this case, it appears that ice from the Svartenhuk Peninsula was able to expand sufficiently to reach the coast and prevent ice from the northern Uummannaq region from moving onshore. Thus, the tentative correlation of deposits to the last glacial cycle is supported by the hypothesised configuration of the UISS during the LGM (Ó Cofaigh et al., 2013b, Roberts et al., 2013) as it is unlikely that pre-LGM sediments would have survived through the LGM within large, low elevation valleys. Though a systematic analysis of the entire peninsula was not undertaken, glacial activity across Svartenhuk is likely to have been characterised by a patchwork of mountain valley glaciers and protective cold-based plateaux. The presence of this large system of ice caps and mountain valley systems is not uncommon throughout Greenland, many of which can be seen today. However, their expansion to the present coastline at a time thought to represent full-glacial conditions is unusual in Greenland, and appears to be a unique result of the topographic configuration of the Uummannaq region.

These results clearly present a different interpretation of the sediments found throughout the Svartenhuk coast. As argued above, a number of the deposits are clearly glacial in origin, in disagreement with previous studies (Kelly, 1986, Bennike et al., 1994). This discrepancy in process-interpretation, in combination with new shell ages from subglacial diamicton has implications for the 'Svartenhuk Marine Event', originally interpreted from these sediments and dated to 115-55 cal. kyr BP. This event, thought to be associated with warm temperatures and an elevated relative sea-level during the last interglacial, is clearly untenable when viewed in light of the newly presented glacial history of the coastline, based upon geomorphological and sedimentological evidence. This has further repercussions for a number of previously identified sequences which have been correlated to the 'Svartenhuk Marine Event', including the 'Qarmat Interstade' (Funder, 1990b),

'Petersbugt Interstade'(Funder et al., 1991), 'Jameson Land Marine Episode'(Funder, 1990a), 'Kaffehavn Marine Event' (Kelly, 1986), and 'Thule Aminozone' (Kelly, 1986, Funder, 1990b). These can now no longer be correlated to the 'Svartenhuk Marine Event'. Although this work has provided a solid sedimentological and geomorphological context for the sediments, further chronological control upon the deposits is needed in order to fully understand the depositional history of the coastline, and to robustly correlate between the three valleys studied.

6.6. Conclusions

Morphosedimentary investigation of deposits from three valleys in southern Svartenhuk has produced compelling evidence for the expansion of warm-based glaciers to the present coastline in the past. These findings are in direct disagreement with sedimentological results from previous research in the Svartenhuk region. These studies investigated some of the same sediments to this study, and interpreted them as pre-LGM, littoral marine sediments, with little/no evidence of glacial activity. As a result the 'Svartenhuk Marine Event' was proposed (Kelly, 1986, Funder et al., 1991, Bennike et al., 1994). Although evidence was found for marine depositional environments, sedimentological results provide evidence for deposition within fluvial, glaciofluvial, and subglacial environments, close to present sea-level. These deposits have formed a series of ice-contact and glacier-fed deltas, alluvial fans, and kettled outwash surfaces which, in places, appear to have been graded to a high relative sea-level.

The chronological control from Arfertuarssuk Fjord is also contrary to previous work, which constrained the deposition of the 'Svartenhuk Marine Event' to 115 – 55 cal. kyr BP. Two new shell dates from the lower and upper subglacial tills in Arfertuarssuk returned ages which provide a maximum age of 49.8 cal. kyr BP for till emplacement, and therefore glacial advance. This places maximum age of the most recent glaciation of Arfertuarrsuk, and potentially the entire southern Svartenhuk coast, within MIS 3. It is possible that the marine fauna within the subglacial tills could represent a heavily reworked assemblage, and therefore the dates presented here represent an age over-estimation. As a result, the glaciation of Arfertuarssuk is tentatively correlated to the last glacial cycle, though it may represent an advance prior to the LGM in Greenland. No new chronological control could be provided for Tasiussaq or Uligssat, and as a result they remain undated within this framework. However, further radiocarbon, surface exposure (^{36}Cl), and OSL dates are

forthcoming. These will provide a more rigorous age control upon the glaciation of the southern Svartenhuk coast. Deposits and landforms record widespread glacier retreat and a series of marginal oscillations during deglaciation. This area is therefore unique in West Greenland, where due to ice sheet cover; few areas contain evidence for independent valley glaciation. Further detailed investigation of other valleys and areas across Svartenhuk could provide important information about the way in which glaciers not coupled with the main ice sheet responded to changes in climate, ocean temperature, and neighbouring ice sheet and ice stream extent.

CHAPTER SEVEN

Thesis conclusions and wider implications

The findings of this thesis have a number of wider implications for our understanding of long-term ice stream development and onset; ice stream geometry and controls upon deglacial behaviour; bedrock bedform development beneath an ice stream; and landscape development in areas peripheral to large ice streams. These are outlined below.

7.1. Long-term development of the Uummannaq Ice Stream System

The long-term history of the UISS has been investigated using glacial landsystem investigation (cf. Evans, 2003), and integrated with the previously devloped uplift history and geological properties of the region. This assimilation of Pliocene-Pleistocene tectonic uplift, bedrock geology, and glacial landsystem distribution has significantly enhanced our understanding of the factors controlling the development and distribution of large ice streams.

This research has demonstrated that the Uummannaq region is dominated by areas of long-term selective linear erosion and areal scour. The onset of glaciation in West Greenland is thought to have occurred at ~4-3 Ma (Maslin *et al.*, 1998), and in the Uummannaq region this would have been accompanied by erosion along pre-existing fluvial valleys. During the intensification of glaciation throughout the Pleistocene, erosion would have remained confined within these valleys which, over multiple glacial cycles, would have developed into a series of recognisably glaciated, over-deepened fjords. As is common in areas of selective linear erosion (1974, Sugden, 1968, Sugden and John, 1976, Hall and Glasser, 2003), inter-fjord areas within northern Uummannaq have been removed from the impact of intense ice sheet erosion through the development of over-deepened troughs. They instead form high-elevation plateaux which have been colonised by cold-based plateaux ice fields and small mountain valley glaciers. During the LGM and previous glacial phases, these areas would have remained as cold-based ice fields or nunataks. This focusing of ice through the fjord system, and latterly across the continental shelf, has isolated areas to the north and south of the system, namely the Svartenhuk and Nuussuaq Peninsulas. The isolation of peripheral areas is thought to have become increasingly pronounced though time, as fjord incision encouraged more efficient ice flow.

The uplift history of West Greenland is relatively well studied, and has been shown to be complex, characterised by four major uplift 'events' (2007, Green et al., 2011, 2009, Japsen et al., 2005), and this thesis has integrated this knowledge with our newly developed high resolution regional landsystem classifications. Following this, it is suggested that the persistent uplift of land surfaces since the onset of glaciation (~4-3 Ma) has had a fundamental impact upon glacial erosion at a regional scale throughout the Uummannaq region. This uplift, and subsequent fluvial and glacial erosion to a new base-level, has further encouraged selective linear erosion, beyond what would be expected in a less tectonically active region.

Further to the over-deepened fjords which run through the Uummannaq region, the confluent nature of the fjord system, governed by pre-glacial fluvial topography, is responsible for the development of the UISS. The confluence of the fjord network to the east of Ubekendt Ejland has been promoted by a switch in first order geology from hard Archaen gneiss to soft Cretaceous sediment. This encouraged glacial erosion, coalescence, and a subsequent increase in trough cross-sectional area, leading to the development an efficient fast flowing ice stream channel (Swift et al., 2008). Such geological control upon the glaciological process of ice stream onset is not unique to the Uummannaq system (Swift et al., 2008), and could be a feature indicative of areas of large-scale palaeo-ice streaming.

7.2. The geometry and behaviour of the northern Uummannaq Ice Stream System during the Last Glacial Maximum

7.2.1. Northern Uummannaq Ice Stream System geometry during the Last Glacial Maximum

Geomorphological and surface exposure ages (Chapter 4) have demonstrated that ice thicknesses within the northern UISS reached 1400 – 1900 m a.s.l., which are comparable to the southern UISS. Data have shown that ice from the northern fjords expanded during the LGM, becoming confluent in Igdlorssuit Sund. Diffluent flow, unconfined by topography, was recorded on low elevation surfaces within fjords (e.g. Karrat Island, east Qeqertarssuaq), but not at elevations higher than 1040 m a.s.l. In contrast to the southern UISS, ice thicknesses in the northern UISS were not sufficient to overtop plateaux between individual fjords. Once ice expanded beyond the fjord system, the over-deepened Igdlorssuit Sund (formed of soft Cretaceous sediments) acted to drawdown ice from the

northern UISS into the UISS onset zone. This work has therefore filled a gap in the previous knowledge of the UISS and provided evidence for the expansion and coalescence of ice from the northern Uummannaq region.

7.2.2. Bedrock bedform development within the Uummannaq Ice Stream System

As observed throughout much of Greenland, onshore areas in the northern Uummannaq region are devoid of extensive sediment cover which is, instead, concentrated offshore. Work presented in Chapter 5 analysed the response of a rigid bedrock bed to thick, fast flowing ice beneath an outlet glacier during the LGM, and provides an important insight into the controls upon bedrock bedform development. Data from both Rink-Karrat and Ingia Fjord indicate that bedrock bedform response to similar hypothesised subglacial conditions demonstrates considerable inter-site variability. Elongation ratios, a measure often used to differentiate between fast and slow flowing ice, varied widely between the study areas, from 0.8:1 to 8.4:1, suggesting that ice flow properties were not the governing factor in bedform development. Thus, bedforms appear to have developed as a complex response to subglacial conditions *and* underlying bedrock properties. As reported in other studies (Hooyer et al., 2012, Gordon, 1981, Roberts and Long, 2005, Roberts et al., 2010, Krabbendam and Bradwell, 2011, Krabbendam and Glasser, 2011), joint and bedding plane properties (e.g. their frequency, thickness and orientation) have exerted a strong control upon bedform development. For the bedforms considered in this study, the bedding plane dip *relative* to palaeo-ice flow directions was shown to be the most important factor in resultant bedform properties. Where the bedding plane dip relative to ice flow was low, bedforms displaying high ELRs developed. In contrast, when bedding plane dip was high, short, wide bedforms developed, with ELRs up to an order of magnitude lower. These variations can then have consequences for bed roughness, and therefore cavity formation. This has provided further evidence that the sole use of bedrock bedform characteristics to infer palaeo-glaciological properties is problematic and should be supported by a thorough understanding of the bedrock properties in which bedforms have developed.

Further study of bedrock bedforms within palaeo-ice stream areas, and from regions of differing geology would enhance the present dataset, and allow further hypothesis development.

7.2.3. Behaviour of the northern Uummannaq Ice Stream System during the Last Glacial Maximum

Prior to this research, the timing and nature of LGM deglaciation though the northern Uummannaq Fjords was very poorly constrained. Results from this study (Chapter 4) have created a robust chronological dataset constraining the retreat of ice through Rink-Karrat Fjord. Outlet glacier retreat is known to be driven by a number of climatic and aclimatic factors including: air temperature; ocean temperature; relative sea-level; and topography. Controls upon UISS retreat speed and style appear to have changed during the ice stream's deglaciation. Initial retreat was forced by an increase in air temperature and rising sea level, and accelerated through the Uummannaq Trough by calving into an over-deepened channel. Subsequently, retreat to the east and north of the UISS onset zone forced outlet glaciers from the UISS to separate. Following this unzipping, surface exposure and radiocarbon dates have revealed that ice streams within the Uummannaq region experienced a strongly asynchronous retreat response throughout the Holocene. Results from the southern UISS have shown the ice margin experienced a temporary marginal stabilisation at 11.0 to 9.3 kyr in response to an increase in topographic confinement (Roberts *et al.*, 2013). Following this, ice stream retreat continued, and ice reached its present margin by 8.7 kyr (Roberts *et al.*, 2013). This is in agreement with a number of reconstructions of LGM deglaciation, with reports generally placing the ice margin at, or beyond, its present location by 7 kyr (Weidick et al., 1990, Long and Roberts, 2003, Young et al., 2011b, Briner et al., 2010). However, the chronology from the northern UISS is in stark contrast to this data, with evidence for ice remaining topographically pinned within the inner fjord system into the Holocene Thermal Maximum. This demonstrates the extreme asynchroneity of West Greenland ice stream response to forcings during deglaciation, and the ability of topographic forcing to override climatic controls. This has clear implications for predictions of future ice stream response in a warming climate.

7.3. Geomorphological and sedimentological evidence for the glaciation of the Svartenhuk Peninsula

The Svartenhuk Peninsula is a large, relatively low elevation land mass in very close proximity to the route of the palaeo-UISS. Previous research has, however, suggested that the entire peninsula remained ice free during the LGM, instead containing extensive MIS 5 deposits. Both geomorphological and sedimentological evidence from three valleys from

the southern Svartenhuk coastline have provided convincing support for the presence of warm-based glaciation in the past. Results provide evidence for the expansion of ice sourced from the Svartenhuk interior to the present coastline or beyond. Results also record the deglaciation of these ice masses, with widespread raised deltas indicating deglaciation into a higher than present sea-level.

This evidence contrasts with previous conclusions drawn from the region, which reported widespread marine sediments, and no evidence for glacial activity (Kelly, 1986, Funder, 1989b, Bennike et al., 1994). This evidence also renders the 'Svartenhuk Marine Event', a period of extensive marine deposition into a relative sea-level higher than present (at 115-55 kyr) (Kelly, 1986), untenable. Initial chronological results instead allow a tentative suggestion that the glaciation recorded through the southern Svartenhuk valleys is LGM in age, and previous chronological controls have largely overestimated the age of deposition.

The local ice caps and mountain glaciers on Svartenhuk are therefore thought to have extended to the present coastline during the LGM. In conjunction with the drawdown of northern UISS ice through Igdlorssuit Sund, the presence of a large ice mass over Svartenhuk would have prevented UISS ice from encroaching upon it. The Svartenhuk area therefore represents a relatively unique area within Greenland in which large glaciers independent of the Greenland Ice Sheet have been able to grow during the LGM, and potentially earlier glaciations.

Future work will focus on the generation of a more robust chronology for the glaciation of Svartenhuk, with surface exposure, OSL, and further radiocarbon dating planned. This will constrain the glacial activity throughout all three valleys, and provide a more solid basis upon which the LGM history of the Svartenhuk Peninsula can be established.

References

ABDALATI, W., KRABILL, W., FREDERICK, E., MANIZADE, S., MARTIN, C., SONNTAG, J., SWIFT, R., THOMAS, R., WRIGHT, W. & YUNGEL, J. 2001. Outlet glacier and margin elevation changes: Near-coastal thinning of the Greenland ice sheet. *Journal of Geophysical Research-Atmospheres,* 106**,** 33729-33741.

ABER, J. S., CROOT, D. G. & FENTON, M. M. 1989. *Glaciotectonic landforms and structures*, Kluwer Academic Publishers.

AMANTOV, A., FJELDSKAAR, W. & CATHLES, L. 2011. Glacial erosion/sedimentation of the Baltic region and the effect on the postglacial uplift. *In:* HARFF, J., BJÖRCK, S. & HOTH, P. (eds.) *The Baltic Sea Basin.* Berlin: Springer.

ANDERSEN, M. L., NETTLES, M., ELOSEGUI, P., LARSEN, T. B., HAMILTON, G. S. & STEARNS, L. A. 2011. Quantitative estimates of velocity sensitivity to surface melt variations at a large Greenland outlet glacier. *Journal of Glaciology,* 57**,** 609-620.

ANDERSON, N. J. & LENG, M. J. 2004. Increased aridity during the early Holocene in West Greenland inferred from stable isotopes in laminated-lake sediments. *Quaternary Science Reviews,* 23**,** 841-849.

ANDREWS, J. T. & SHIMIZU, K. 1966. Threedimensional vector technique for analyzing till fabrics: Discussion and FORTRAN program. *Geological Bulletin,* 8**,** 151-165.

ANGELIS, H. D. & KLEMAN, J. 2008. Palaeo-ice-stream onsets: examples from the north-eastern Laurentide Ice Sheet. *Earth Surface Processes and Landforms,* 33**,** 560-572.

AUGUSTINUS, P. C. 1992. The influence of rock mass strength on glacial valley cross-profile morphometry: A case study from the Southern Alps, New Zealand. *Earth Surface Processes and Landforms,* 17**,** 39-51.

AXFORD, Y., LOSEE, S., BRINER, J. P., FRANCIS, D. R., LANGDON, P. G. & WALKER, I. R. 2013. Holocene temperature history at the western Greenland Ice Sheet margin reconstructed from lake sediments. *Quaternary Science Reviews,* 59**,** 87-100.

BALCO, G., BRINER, J., FINKEL, R. C., RAYBURN, J. A., RIDGE, J. C. & SCHAEFER, J. M. 2009. Regional beryllium-10 production rate calibration for late-glacial northeastern North America. *Quaternary Geochronology,* 4**,** 93-107.

BALCO, G., STONE, J. O., LIFTON, N. A. & DUNAI, T. J. 2008. A complete and easily accessible means of calculating surface exposure ages or erosion rates from 10Be and 26739 Al measurements. *Quaternary Geochronology,* 3**,** 22.

BALLANTYNE, C. K. 1982. Aggregate clast form characteristics of deposits near the margins of four glaciers in the Jotunheimen Massif, Norway. 103-113.

BALLANTYNE, C. K. 1997. Periglacial trimlines in the Scottish Highlands. *Quaternary International,* 38-39**,** 18.

BALLANTYNE, C. K., SCHNABEL, C. & XU, S. 2009. Exposure dating and reinterpretation of coarse debris accumulations ('rock glaciers') in the Cairngorm Mountains, Scotland. *Journal of Quaternary Science,* 24**,** 19-31.

BAMBER, J. L., ALLEY, R. B. & JOUGHIN, I. 2007. Rapid response of modern day ice sheets to external forcing. *Earth and Planetary Science Letters,* 257**,** 1-13.

BAMBER, J. L., LAYBERRY, R. L. & GOGINENI, S. P. 2001. A new ice thickness and bed data set for the Greenland ice sheet 1. Measurement, data reduction, and errors. *J. Geophys. Res.,* 106**,** 33773-33780.

BAMBER, J. L., VAUGHAN, D. G. & JOUGHIN, I. 2000. Widespread Complex Flow in the Interior of the Antarctic Ice Sheet. *Science,* 287**,** 1248-1250.

BANNERJEE, I. & MCDONALD, B. C. 1975. Nature of esker sedimentation. *In:* JOPLING, A. V. & MCDONALD, B. C. (eds.) *Glaciofluvial and Glaciolacustrine Sedimentation. .* SEPM Special Publications 23.

BATES, C. C. 1953. Rational theory of delta formation. *American Association of Petroleum Geologists Bulletin,* 37**,** 2119-2161.

BAUER, A. 1968. Missions Aériennes de reconnaissance au Groenland 1957-1958. *Meddeleser om Grønland, Kommissionen for widenskabelige Undersøgelser i Grønland,* 173.

BAUER, A., BAUSSART, M., CARBONNELL, M., KASSER, P., PERROUD, P. & RENAUD, A. 1968. Missions aériennes de reconnaissance au Groenland 1957–1958. Observations aériennes et terrestres, exploitation des photographies aériennes, détermination des vitesses des glaciers vêlant dans Disko Bugt et Umanak Fjord. *Meddelelser om Grønland,* 173**,** 116.

BENN, D. & EVANS, D. J. A. 2010. *Glaciers and Glaciation.,* London, Hodder Education.

BENN, D. I. 1994. Fabric Shape and the Interpretation of Sedimentary Fabric Data *Journal of Sedimentary Research, Section A: Sedimentary Petrology and Processes,* 64A**,** 910-915.

BENN, D. I. 1995. Fabric signature of till deformation, Breiðamerkurjökull, Iceland. *Sedimentology* 42**,** 735-747.

BENN, D. I. & BALLANTYNE, C. K. 1994. Reconstructing the transport history of glacigenic sediments: a new approach based on the co-variance of clast form indices. *Sedimentary Geology,* 91**,** 215-227.

BENN, D. I. & EVANS, D. J. A. 1993. Glaciomarine deltaic deposition and ice-marginal tectonics: The 'Loch Don Sand Moraine', Isle of Mull, Scotland. *Journal of Quaternary Science,* 8**,** 279-291.

BENN, D. I. & EVANS, D. J. A. 1996. The interpretation and classification of subglacially-deformed materials. *Quaternary Science Reviews,* 15**,** 23-52.

BENN, D. I., KIRKBRIDE, M. P., OWEN, L. A. & V, B. 2003. Glaciated valley landsystems. *In:* EVANS, D. J. A. (ed.) *Glacial Landsystems.* London: Arnold.

BENN, D. I., WARREN, C. R. & MOTTRAM, R. H. 2007. Calving processes and the dynamics of calving glaciers. *Earth-Science Reviews,* 82**,** 143-179.

BENNETT, M. R. 2003. Ice streams as the arteries of an ice sheet: their mechanics, stability and significance. *Earth-Science Reviews,* 61**,** 31.

BENNIKE, O. 1995. Palaeoecology of two lake basins from Disko, West Greenland. *Journal of Quaternary Science,* 10**,** 149-155.

BENNIKE, O. 2000. Palaeoecological studies of Holocene lake sediments from west Greenland. *Palaeogeography, Palaeoclimatology, Palaeoecology,* 155**,** 285-304.

BENNIKE, O., ANDERSON, N. J. & MCGOWAN, S. 2010. Holocene palaeoecology of southwest Greenland inferred from macrofossils in sediments of an oligosaline lake. *Journal of Paleolimnology,* 43**,** 787-798.

BENNIKE, O. & BJORCK, S. 2002. Chronology of the last recession of the Greenland Ice Sheet. *Journal of Quaternary Science,* 17**,** 211-219.
BENNIKE, O., BJORCK, S. & LAMBECK, K. 2002. Estimates of South Greenland late-glacial ice limits from a new relative sea level curve. *Earth and Planetary Science Letters,* 197**,** 171-186.
BENNIKE, O., HANSEN, K. B., KNUDSEN, K. L., PENNEY, D. N. & RASMUSSEN, K. L. 1994. Quaternary Marine Stratigraphy and Geochronology in Central West Greenland. *Boreas,* 23**,** 194-215.
BENTLEY, C. R. 1987. Antarctic ice streams: a review. *Journal of Geophysical Research,* 92**,** 15.
BERTRAN, P., HÉTU, B., TEXIER, J.-P. & VAN STEIJN, H. 1997. Fabric characteristics of subaerial slope deposits. *Sedimentology,* 44**,** 1-16.
BERTRAN, P. & TEXIER, J.-P. 1999. Facies and microfacies of slope deposits. *CATENA,* 35**,** 99-121.
BINDSCHADLER, R. 2006. Climate change - Hitting the ice sheets where it hurts. *Science,* 311**,** 1720-1721.
BJORCK, A., KJÆR, K. H., KORSGAARD, N. J., KHAN, S. A., KJELDSEN, K. K., ANDRESEN, C. S., BOX, J. E., LARSEN, N., FUNDER, S., -, J., 2012/05/27/ONLINE, P.-. & PUBLICATION, V.-A. O. 2012. An aerial view of 80 years of climate-related glacier fluctuations in southeast Greenland. *Nature Geoscience*.
BLOCK, A. & BELL, R. 2011. Geophysical evidence for soft bed sliding at Jakobshavn Isbrae, West Greenland. *The Cryosphere Discussions,* 5**,** 339-366.
BONOW, J. M., JAPSEN, P., LIDMAR-BERGSTRÖM, K., CHALMERS, J. A. & PEDERSEN, A. K. 2006a. Cenozoic uplift of Nuussuaq and Disko, West Greenland—elevated erosion surfaces as uplift markers of a passive margin. *Geomorphology,* 80**,** 325-337.
BONOW, J. M., LIDMAR-BERGSTROM, K. & JAPSEN, P. 2006b. Palaeosurfaces in central West Greenland as reference for identification of tectonic movements and estimation of erosion. *Global and Planetary Change,* 50**,** 161-182.
BONOW, J. M., LIDMAR-BERGSTRÖM, K., JAPSEN, P., CHALMERS, J. A. & GREEN, P. F. 2007. Elevated erosion surfaces in central West Greenland and southern Norway: their significance in integrated studies of passive margin development. *NORWEGIAN JOURNAL OF GEOLOGY,* 87**,** 197-206.
BOULTON, G. & EYLES, N. 1979. Sedimentation by valley glaciers: a model and genetic classification. *Moraines and varves,* 33**,** 11-23.
BOULTON, G. S. 1974a. Processes and patterns of glacial erosion. *In:* COATES, D. R. (ed.) *Glacial Geomorphology.* New York: State University of New York.
BOULTON, G. S. 1974b. Processes and patterns of glacial erosion. *In:* COATES, D. R. (ed.) *Glacial Geomorphology.* New York: State University of New York.
BOULTON, G. S. & JONES, A. S. 1979. Stability of temperate ice caps and ice sheets resting on beds of deformable sediment. *Journal of Glaciology,* 24**,** 29-43.
BOX, J. 2006. Greenland Ice Sheet surface mass balance variability (1988-2004) from calibrated polar MM5 output. *J. Clim.,* 19**,** 2783-2800.
BOX, J., FETTWEIS, X., STROEVE, J., TEDESCO, M., HAL, D. & STEFFEN, K. 2012. Greenland ice sheet albedo feedback: thermodynamics and atmospheric drivers. *The Cryosphere,* 6**,** 21.

BOX, J. E., BROMWICH, D. H. & BAI, L. S. 2004. Greenland ice sheet surface mass balance 1991–2000: Application of Polar MM5 mesoscale model and in situ data. *Journal of Geophysical Research: Atmospheres (1984–2012),* 109.

BOX, J. E. & DECKER, D. T. 2011. Analysis of Greenland marine-terminating glacier area changes: 2000-2010. *Annals of Glaciology,* 52**,** 8.

BOYCE, J. I. & EYLES, N. 1991. Drumlins carved by deforming till streams below the Laurentide ice sheet. *Geology,* 19**,** 787-790.

BRADWELL, T., STOKER, M. & KRABBENDAM, M. 2008. Megagrooves and streamlined bedrock in NW Scotland: The role of ice streams in landscape evolution. *Geomorphology,* 97**,** 22.

BRETT, C. P. & ZARUDZKI, E. F. K. 1979. Project Westmar. A shallow marine geophysical survey on the West Greenland continental shelf. . *Rapport Grønlands Geologiske Undersøgelse,* 87**,** 27.

BRINER, J. P., BINI, A. C. & ANDERSON, R. S. 2009. Rapid early Holocene retreat of a Laurentide outlet glacier through an Arctic fjord. *Nature Geosci,* 2**,** 496-499.

BRINER, J. P., STEWART, H. A. M., YOUNG, N. E., PHILIPPS, W. & LOSEE, S. 2010. Using proglacial-threshold lakes to constrain fluctuations of the Jakobshavn Isbræ ice margin, western Greenland, during the Holocene. *Quaternary Science Reviews,* 29**,** 3861-3874.

BRINER, J. P. & SWANSON, T. W. 1998. Using inherited cosmogenic Cl-36 to constrain glacial erosion rates of the Cordilleran ice sheet. *Geology,* 26**,** 3-6.

BRINER, J. P., YOUNG, N. E., GOEHRING, B. M. & SCHAEFER, J. M. 2012. Constraining Holocene 10Be production rates in Greenland. *Journal of Quaternary Science,* 27**,** 2-6.

BRONK RAMSEY, C. 2008. Deposition models for chronological records. *Quaternary Science Reviews,* 27**,** 42-60.

BRONK RAMSEY, C. 2009. Bayesian Analysis of Radiocarbon Dates. *Radiocarbon,* 51**,** 24.

BROOK, M. S., KIRKBRIDE, M. P. & BROCK, B. W. 2004. Rock Strength and Development of Glacial Valley Morphology in the Scottish Highlands and Northwest Iceland. *Geografiska Annaler: Series A, Physical Geography,* 86**,** 225-234.

BULL, W. 1977. The alluvial fan environment. *Progress in Physical Geography,* 1**,** 49.

CANALS, M., CASAMOR, J. L., URGELES, R., CALAFAT, A. M., DOMACK, E. W., BARAZA, J., FARRAN, M. & DE BATIST, M. 2002. Seafloor evidence of a subglacial sedimentary system off the northern Antarctic Peninsula. *Geology,* 30**,** 603-606.

CARBONELL, M. & BAUER, A. 1968. Exploitation des couvertures photographiques aériennes répétées du front des glaciers vélant dans Disko Bugt et Umanak Fjord, juin-juillet 1964. *Meddeleser om Grønland, Kommissionen for widenskabelige Undersøgelser i Grønland,* 173.

CARBONNELL, M. & BAUER, A. 1968. Exploitation des couvertures photographiques aériennes répétées du front des glaciers vélant dans Disko Bugt et Umanak Fjord, juin-juillet 1964. *Meddelelser om Grønland,* 173**,** 78

CHEEL, R. J. & RUST, B. R. 1982. Coarse grained facies of glaciomarine depositis near Ottawa, Canada. *In:* DAVIDSON-ARNOTT, R., W., N. & FAHEY, B. D. (eds.) *Research in Glaciofluvial and Glaciolacustrine Systems.* Norwich: Geobooks.

CHEN, J. L., WILSON, C. R. & TAPLEY, B. D. 2006. Satellite gravity measurements confirm accelerated melting of Greenland ice sheet. *Science,* 313**,** 1958-1960.
CHIVERRELL, R. C., THRASHER, I. M., THOMAS, G. S. P., LANG, A., SCOURSE, J. D., VAN LANDEGHEM, K. J. J., MCCARROLL, D., CLARK, C. D., COFAIGH, C. Ó., EVANS, D. J. A. & BALLANTYNE, C. K. 2013. Bayesian modelling the retreat of the Irish Sea Ice Stream. *Journal of Quaternary Science,* 28**,** 200-209.
CHRISTOFFERSEN, P., MUGFORD, R., HEYWOOD, K., JOUGHIN, I., DOWDESWELL, J., SYVITSKI, J., LUCKMAN, A. & BENHAM, T. 2011. Warming of waters in an East Greenland fjord prior to glacier retreat: mechanisms and connection to large-scale atmospheric conditions. *The Cryosphere,* 5**,** 701-714.
CLARK, P. U., DYKE, A. S., SHAKUN, J. D., CARLSON, A. E., CLARK, J., WOHLFARTH, B., MITROVICA, J. X., HOSTETLER, S. W. & MCCABE, A. M. 2009. The Last Glacial Maximum. *Science,* 325**,** 6.
CLARKE, D. B. & PEDERSEN, A. K. 1976. Tertiary volcanic province of West Greenland. *In:* ESCHER, A. & WATT, W. S. (eds.) *Geology of Greenland.* Copenhagen: Geological Survey of Greenland.
CLEMMENSEN, L. B. & HOUMARK-NIELSEN, M. 1981. Sedimentary features of a Weichselian glaciolacustrine delta. *Boreas,* 10**,** 229-245.
CORBETT, L. B., BIERMAN, P., GRALY, J. A., NEUMANN, T. A., ROOD, D. & FINKEL, R. C. 2009. In situ cosmogenic 10Be estimates of deglaciation timing and glacial erosion efficiency, Western Greenland. *Geological Society of America Abstracts with Programs,* 41**,** 1.
CROOT, D. G. & SIMS, P. C. 1996. Early stages of till genesis: an example from Fanore, County Clare, Ireland. *Boreas,* 25**,** 37-46.
DAHL, R. 1965. Plastically sculptured detail forms on rock surfaces in northern Nordland, Norway. *Geografiska Annaler. Series A. Physical Geography***,** 83-140.
DAM, G., NØHR-HANSEN, H., PEDERSEN, G. K. & SØNDERHOLM, M. 2000. Sedimentary and structural evidence of a new early Campanian rift phase in the Nuussuaq Basin, West Greenland. *Cretaceous Research,* 21**,** 127-154.
DAS, S. B., JOUGHIN, I., BEHN, M. D., HOWAT, I. M., KING, M. A., LIZARRALDE, D. & BHATIA, M. P. 2008. Fracture Propagation to the Base of the Greenland Ice Sheet During Supraglacial Lake Drainage. *Science,* 320**,** 778-781.
DEWOLF, Y. 1988. Stratified slope deposits. *In:* CLARK, M. J. (ed.) *Advances in Periglacial Geomorphology.* Chichester: Wiley.
DI NICOLA, L., STRASKY, S., SCHLÜCHTER, C., SALVATORE, M. C., AKÇAR, N., KUBIK, P. W., CHRISTL, M., KASPER, H. U., WIELER, R. & BARONI, C. 2009. Multiple cosmogenic nuclides document complex Pleistocene exposure history of glacial drifts in Terra Nova Bay (northern Victoria Land, Antarctica). *Quaternary Research,* 71**,** 83-92.
DONNER, J. & JUNGNER, H. 1975. Radiocarbon dating of shells from marine Holocene deposits in the Disko Bugt area, West Greenland. *Boreas,* 4**,** 25-45.
DOWDESWELL, J. A. & SHARP, M. J. 1986. Characterization of pebble fabrics in modern terrestrial glacigenic sediments. *Sedimentology,* 33**,** 699-710.
DÜHNFORTH, M., ANDERSON, R. S., WARD, D. & STOCK, G. M. 2010. Bedrock fracture control of glacial erosion processes and rates. *Gelogy,* 38**,** 423-427.

DUNAI, T. J. & STUART, F. M. 2009. Reporting of cosmogenic nuclide data for exposure age and erosion rate determinations. *Quaternary Geochronology,* 4**,** 437-440.
EDWARDS, M. B. 1986. Glacial Environments. *In:* H.G., R. (ed.) *Sedimentary Environments and Facies.* Oxford: Blackwell.
EGHOLM, D. L., NIELSEN, S. B., PEDERSEN, V. K. & LESEMANN, J. E. 2009. Glacial effects limiting mountain height. *Nature,* 460**,** 884-887.
ENGLAND, J. 1999. Coalescent Greenland and Innuitian ice during the Last Glacial Maximum: revising the Quaternary of the Canadian High Arctic. *Quaternary Science Reviews,* 18**,** 421-456.
ETTEMA, J. 2009. Higher surface mass balance of the Greenland ice sheet revealed by high-resolution climate modelling. *Geophys. Res. Lett.,* 36**,** L12501.
EVANS, D. J., HIEMSTRA, J. F., BOSTON, C. M., LEIGHTON, I., COFAIGH, C. Ó. & REA, B. R. 2012. Till stratigraphy and sedimentology at the margins of terrestrially terminating ice streams: case study of the western Canadian prairies and high plains. *Quaternary Science Reviews,* 46**,** 80-125.
EVANS, D. J. A. (ed.) 2003. *Glacial Landsystems,* London: Hodder Arnold.
EVANS, D. J. A. 2009. Controlled moraines: origins, characteristics and palaeoglaciological implications. *Quaternary Science Reviews,* 28**,** 183-208.
EVANS, D. J. A. & BENN, D. I. 2004. *A practical guide to the study of glacial sediments,* London, Arnold.
EVANS, D. J. A. & HIEMSTRA, J. F. 2005. Till deposition by glacier submarginal, incremental thickening. *Earth Surface Processes and Landforms,* 30**,** 1633-1662.
EVANS, D. J. A., PHILLIPS, E. R., HIEMSTRA, J. F. & AUTON, C. A. 2006. Subglacial till: Formation, sedimentary characteristics and classification. *Earth-Science Reviews,* 78**,** 115-176.
EVANS, I. S. 1996a. Abraded rock landforms (whalebacks) developed under ice streams in mountain areas. *Annals of Glaciology,* 22**,** 9-15.
EVANS, I. S. 1996b. Abraded rock landforms (whalebacks) developed under ice streams in mountain areas. *Annals of Glaciology,* 22**,** 8.
EVANS, J., Ó COFAIGH, C., DOWDESWELL, J. A. & WADHAMS, P. 2009. Marine geophysical evidence for former expansion and flow of the Greenland Ice Sheet across the north-east Greenland continental shelf. *Journal of Quaternary Science,* 24**,** 279-293.
EYLES, N. 2012. Rock drumlins and megaflutes of the Niagara Escarpment, Ontario, Canada: a hard bed landform assemblage cut by the Saginaw–Huron Ice Stream. *Quaternary Science Reviews,* 55**,** 34-49.
FABEL, D., BALLANTYNE, C. K. & XU, S. 2012. Trimlines, blockfields, mountain-top erratics and the vertical dimensions of the last British–Irish Ice Sheet in NW Scotland. *Quaternary Science Reviews,* 55**,** 91-102.
FAHNESTOCK, M., BINDSCHADLER, R., KWOK, R. & JEZEK, K. 1993. Greenland Ice Sheet Surface Properties and Ice Dynamics from ERS-1 SAR Imagery. *Science,* 262**,** 1530-1534.
FETTWEIS, X., TEDESCO, M., VAN DE BROEKE, M. R. & ETTEMA, J. 2011. Melting trends over the Greenland ice sheet (1958–2009) from spaceborne microwave data and regional climate models. *The Cryosphere,* 5**,** 359-375.

FOGED, N. 1977. *The diatoms in four postglacial deposits at Godthåbsfjord, West Greenland*, Nyt Nordisk Forlag.
FRANCOU, B. 1990. Stratification mechanisms in slope deposits in high subequatorial mountains. *Permafrost and Periglacial Processes,* 1**,** 249-263.
FUNDER, S. 1989a. The Baffin-Bay Region during the Last Interglaciation - Evidence from Northwest Greenland. *Geographie Physique Et Quaternaire, Vol 43, No 3***,** 255-262.
FUNDER, S. 1989b. Quaternary geology of the ice-free areas and adjacent shelves of Greenland. *In:* FULTON, R. J. (ed.) *Quaternary Geology of Canada and Greenland.* Geological Survey of Canada and Greenland.
FUNDER, S. 1990a. *Descriptive text to Quaternary map of Greenland 1:500,000, Scoresby Sund, Sheet 12,* Copenhagen.
FUNDER, S. 1990b. Late Quaternary stratigraphy and glaciology in the Thule area, Northwest Greenland. *Meddelelser om Grønland, Geoscience,* 22**,** 1-63.
FUNDER, S. & HANSEN, L. 1996. The Greenland ice sheet - a model for its culmination and decay during and after the last glacial maximum. *Bulletin of the Geological Society of Denmark,* 42**,** 137-152.
FUNDER, S., HJORT, C. & KELLY, M. 1991. Isotope stage 5 (130-74 ka) in Greenland, a review. *Quaternary International,* 10–12**,** 107-122.
FUNDER, S., HJORT, C. & LANDVIK, J. Y. 1994. The Last Glacial Cycles in East Greenland, an Overview. *Boreas,* 23**,** 283-293.
FUNDER, S., KJELDSEN, K. K., KJÆR, K. H. & Ó COFAIGH, C. 2011. The Greenland Ice Sheet During the Past 300,000 Years: A Review. *In:* EHLERS, J., GIBBARD, P. L. & HUGHES, P. D. (eds.) *Quaternary Glaciations - Extent and Chronology: A Closer Look.* Oxford: Elsevier.
FYFE, G. F. 1990. The effect of water depth on ice-proximal glaciolacustrine sedimentation: Salpausselka I, southern Finland. *Boreas,* 19**,** 18.
GARDE, A. A. & STEENFELT, A. 1999. Precambrian geology of Nuussuaq and the area north-east of Disko Bugt, West Greenland. *In:* KALSBEEK, F. (ed.) *Precambrian geology of the Disko Bugt region, West Greenland.* Copenhagen: GEUS.
GILBERT, G. K. 1885. The topographic features of lake shores. *U.S. Geological Survey Annual Report,* 5**,** 49.
GILKS, W. R., RICHARDSON, S. & SPIEGELHALTER, D. 1995. *Markov Chain Monte Carlo in practice: interdisciplinary statistics*, Chapman & Hall/CRC.
GLASSER, N. F. & WARREN, C. R. 1990. Medium Scale Landforms of Glacial Erosion in South Greenland; Process and Form *Geografiska Annaler Series a-Physical Geography,* 72**,** 5.
GOLDSTEIN, R. M., ENGELHARDT, H., KAMB, B. & FROLICH, R. M. 1993. Satellite Radar Interferometry for Monitoring Ice Sheet Motion: Application to an Antarctic Ice Stream. *Science,* 262**,** 1525-1530.
GOLDTHWAIT, R. P. & MATSCH, C. L. 1989. Genetic classification of glacigenic deposits.
GOOSSENS, D. 2008. Techniques to measure grain-size distributions of loamy sediments: a comparative study of ten instruments for wet analysis. *Sedimentology,* 55**,** 65-96.
GORDON, J. E. 1981. Ice-Scoured Topography and Its Relationships to Bedrock Structure and Ice Movement in Parts of Northern Scotland and West Greenland. *Geografiska Annaler. Series A, Physical Geography,* 63**,** 55-65.

GOSSE, J. C. & PHILLIPS, F. M. 2001. Terrestrial in situ cosmogenic nuclides: theory and application. *Quaternary Science Reviews,* 20**,** 1475-1560.

GRAHAM, A. G. C., LARTER, R. D., GOHL, K., HILLENBRAND, C.-D., SMITH, J. A. & KUHN, G. 2009. Bedform signature of a West Antarctic palaeo-ice stream reveals a multi-temporal record of flow and substrate control. *Quaternary Science Reviews,* 28**,** 2774-2793.

GREEN, P. F., JAPSEN, P., CHALMERS, J. A. & BONOW, J. M. 2011. Thermochronology, erosion surfaces and missing section in West Greenland. *Journal of the Geological Society,* 168**,** 817-830.

GUSTAVSON, T. C. & BOOTHROYD, J. C. 1987. A depositional model for outwash, sediment sources, and hydrologic characteristics, Malaspina Glacier, Alaska: A modern analog of the southeastern margin of the Laurentide ice sheet. *Geological Society of America Bulletin,* 99**,** 187-200.

HAKANSSON, L., ALEXANDERSON, H., HJORT, C., MOLLER, P., BRINER, J. P., ALDAHAN, A. & POSSNERT, G. 2009. Late Pleistocene glacial history of Jameson Land, central East Greenland, derived from cosmogenic Be-10 and Al-26 exposure dating. *Boreas,* 38**,** 244-260.

HAKANSSON, L., BRINER, J., ALEXANDERSON, H., ALDAHAN, A. & POSSNERT, G. 2007a. Be-10 ages from central east Greenland constrain the extent of the Greenland ice sheet during the Last Glacial Maximum. *Quaternary Science Reviews,* 26**,** 2316-2321.

HAKANSSON, L., GRAF, A., STRASKY, S., IVY-OCHS, S., KUBIK, P. W., HJORT, C. & SCHLUCHTER 2007b. Cosmogenic Be-10-ages from the Store Koldewey island, NE Greenland. *Geografiska Annaler Series a-Physical Geography,* 89A**,** 195-202.

HALL, A. & GLASSER, N. F. 2003. Reconstructing the basal thermal regime of an ice stream in a landscape of selective linear erosion: Glen Avon, Cairngorm Mountains, Scotland. *Boreas,* 32**,** 18.

HALLET, B. 1996. Glacial quarrying: A simple rheoretical model. *Annals of Glaciology,* 22**,** 1-8.

HANNA, E., HUYBRECHTS, P., JANSSENS, I., CAPPELEN, J., STEFFEN, K. & STEPHENS, A. 2005. Runoff and mass balance of the Greenland ice sheet: 1958-2003. *Journal of Geophysical Research-Atmospheres,* 110**,** -.

HARFF, J. E. 2007. *Deglaciation history, coastal development, and environmental change during the Holocene in western Greenland, Cruise Report R/V Maria S. Merian, Cruise MSM 05/03*.

HARRIS, C. 1991. Glacial deposits at Wylfa Head, Anglesey, North Wales: Evidence for Late Devensian deposition in a non-marine environment. *Journal of Quaternary Science,* 6**,** 67-77.

HARRIS JR, S. E. 1943. Friction cracks and the direction of glacial movement. *The Journal of Geology***,** 244-258.

HART, J. K. 1994. Till fabric associated with deformable beds. *Earth Surface Processes and Landforms,* 19**,** 18.

HATTESTRAND, C. & STROEVEN, A. J. 2002. A relict landscape in the centre of Fennoscandian glaciation: Geomorphological evidence of minimal Quaternary glacial erosion. *Geomorphology,* 44**,** 127-143.

HENDERSON, G. & PULVERTAFT, T. C. R. 1987a. *Descriptive text to geological map of Greenland 1:100 000, Marmorilik 71 V.2 Agnete Syd, Nugatsiaq 71 V.2 Nord and Pangnertoˆq 72 V.2 Syd,* Copenhagen,, Geol. Survey Greenland.

HENDERSON, G. & PULVERTAFT, T. C. R. 1987b. *Geological map of Greenland, 1:100 000, Mârmorilik 71 V.2 Syd, Nûgâtsiaq 71 V.2 Nord, Pangnertôq 72 V.2 Syd.* Copenhagen.

HENRIKSEN, N., HIGGINS, A. K. & KALSBEEK, F. 2000. *Greenland from Archaean to Quaternary Descriptive text to the Geological map of Greenland,1:2 500 000,* Copenhagen, GEUS.

HENRIKSEN, N., HIGGINS, A. K., KALSBEEK, F. & PULVERTAFT, T. C. R. 2009. Greenland from Archaean to Quaternary. Descriptive text to the 1995 Geological map of Greenland, 1:2 500 000. 2nd edition. *Geological Survey of Denmark and Greenland Bulletin,* 18**,** 126.

HICOCK, S. R. 1992. Lobal interactions and rheologic superposition in subglacial till near Bradtville, Ontario, Canada. *Boreas* 21**,** 73-88.

HICOCK, S. R. & FULLER, E. A. 1995. Lobal interactions, rheologic superposition, and implications for a Pleistocene ice stream on the continental shelf of British Columbia. *Geomorphology* 167-184.

HIEMSTRA, J. F., EVANS, D. J. A. & COFAIGH, C. O. 2007. The role of glacitectonic rafting and comminution in the production of subglacial tills: examples from southwest Ireland and Antarctica. *Boreas,* 36**,** 386-399.

HOGAN, K. A., DOWDESWELL, J. A., NOORMETS, R., EVANS, J., Ó COFAIGH, C. & JAKOBSSON, M. 2010. Submarine landforms and ice-sheet flow in the Kvitøya Trough, northwestern Barents Sea. *Quaternary Science Reviews,* 29**,** 3545-3562.

HOLLAND, D., THOMAS, R. H., DE YOUNG, B. & RIBERGAARD, M. H. 2008a. Acceleration of Jakobshavn Isbrae triggered by warm subsurface ocean waters. *Nature Geosci.,* 1**,** 659-664.

HOLLAND, D. M., THOMAS, R. H., DE YOUNG, B., RIBERGAARD, M. H. & LYBERTH, B. 2008b. Acceleration of Jakobshavn Isbrae triggered by warm subsurface ocean waters. *Nature Geoscience,* 1**,** 659-664.

HOLLAND, P. 2010. Warm bath for an ice sheet. *Nature Geoscience,* 3**,** 147-148.

HOOYER, T. S., COHEN, D. & IVERSON, N. R. 2012. Control of glacial quarrying by bedrock joints. *Geomorphology,* 153**,** 91-101.

HOWAT, I. M., AHN, Y., JOUGHIN, I., VAN DEN BROEKE, M. R., LENAERTS, J. T. M. & SMITH, B. 2011. Mass balance of Greenland's three largest outlet glaciers, 2000–2010. *Geophys. Res. Lett.,* 38**,** L12501.

HOWAT, I. M., JOUGHIN, I., FAHNESTOCK, M., SMITH, B. E. & SCAMBOS, T. A. 2008. Synchronous retreat and acceleration of southeast Greenland outlet glaciers 2000-06: ice dynamics and coupling to climate. *Journal of Glaciology,* 54**,** 646-660.

HOWAT, I. M., JOUGHIN, I. & SCAMBOS, T. A. 2007. Rapid changes in ice discharge from Greenland outlet glaciers. *Science,* 315**,** 1559-1561.

HOWAT, I. M., JOUGHIN, I., TULACZYK, S. & GOGINENI, S. 2005. Rapid retreat and acceleration of Helheim Glacier, east Greenland. *Geophysical Research Letters,* 32**,** L22502.

HUGHES, T. J. 1995. Ice sheet modelling and the reconstruction of former ice sheets from geo(morpho)logical field data. *In:* MENZIES, J. (ed.) *Modern Glacial*

Environments-Processes, Dynamics and Sediments. Oxford: Butterworth-Heinemann Ltd.
HUYBERS, P. 2006. Early Pleistocene Glacial Cycles and the Integrated Summer Insolation Forcing. *Science,* 313**,** 508-511.
IVERSON, N. R. 1991. Morphology of glacial striae: implications for abrasion of glacier beds and fault surfaces. *Geological Society of America Bulletin,* 103**,** 1308-1316.
IVERSON, N. R. 2012. A theory of glacial quarrying for landscape evolution models. *Geology,* 40**,** 679-682.
JAMIESON, S. S. R., HULTON, N. R. J. & HAGDORN, M. 2008. Modelling landscape evolution under ice sheets. *Geomorphology,* 97**,** 91-108.
JAMIESON, S. S. R., VIELI, A., LIVINGSTONE, S. J., COFAIGH, C. O., STOKES, C., HILLENBRAND, C.-D. & DOWDESWELL, J. A. 2012. Ice-stream stability on a reverse bed slope. *Nature Geosci,* advance online publication.
JANSEN, E. 2007. Climate Change 2007: The Physical Science Basis. 4th Assessment Report IPCC. Nature Publishing Group.
JANSEN, E. 2008. Natural Climate Variability and Global Warming: A Holocene Perspective. Nature Publishing Group.
JANSSON, K. N., STOEVEN, A. P. & KLEMAN, J. 2003. Configuration and timing of Ungava Bay ice streams, Labrador-Ungava, Canada. *Boreas,* 32**,** 256-263.
JAPSEN, P., BONOW, J. M., GREEN, P. F., CHALMERS, J. A. & LIDMAR-BERGSTRÖM, K. 2006. Elevated, passive continental margins: Long-term highs or Neogene uplifts? New evidence from West Greenland. *Earth and Planetary Science Letters,* 248**,** 330-339.
JAPSEN, P., BONOW, J. M., GREEN, P. F., CHALMERS, J. A. & LIDMAR-BERGSTRÖM, K. 2009. Formation, uplift and dissection of planation surfaces at passive continental margins – a new approach. *Earth Surface Processes and Landforms,* 34**,** 683-699.
JAPSEN, P., GREEN, P. F. & CHALMERS, J. A. 2005. Separation of Palaeogene and Neogene uplift on Nuussuaq, West Greenland. *Journal of the Geological Society,* 162**,** 299-314.
JOHANSSON, M., OLVMO, M. & LIDMAR-BERGSTRÖM, K. 2001. Inherited landforms and glacial impact of different palaeosurfaces in Southwest Sweden. *Geografiska Annaler, Series A: Physical Geography,* 83**,** 67-89.
JOUGHIN, I. 2008. Seasonal speedup along the western flank of the Greenland Ice Sheet. *Science,* 320**,** 781-783.
JOUGHIN, I., ABDALATI, W. & FAHNESTOCK, M. 2004. Large fluctuations in speed on Greenland's Jakobshavn Isbrae glacier. *Nature,* 432**,** 608-611.
JOUGHIN, I., DAS, S. B., KING, M. A., SMITH, B. E., HOWAT, I. M. & MOON, T. 2008a. Seasonal Speedup Along the Western Flank of the Greenland Ice Sheet. *Science,* 320**,** 781-783.
JOUGHIN, I., HOWAT, I., ALLEY, R. B., EKSTROM, G., FAHNESTOCK, M., MOON, T., NETTLES, M., TRUFFER, M. & TSAI, V. C. 2008b. Ice-front variation and tidewater behavior on Helheim and Kangerdlugssuaq Glaciers, Greenland. *Journal of Geophysical Research-Earth Surface,* 113**,** -.
JOUGHIN, I., HOWAT, I. M., FAHNESTOCK, M., SMITH, B., KRABILL, W., ALLEY, R. B., STERN, H. & TRUFFER, M. 2008c. Continued evolution of Jakobshavn Isbrae

following its rapid speedup. *Journal of Geophysical Research-Earth Surface,* 113**,** -.

JOUGHIN, I., SMITH, B. E., HOWAT, I. M., FLORICIOIU, D., ALLEY, R. B., TRUFFER, M. & FAHNESTOCK, M. 2012. Seasonal to decadal scale variations in the surface velocity of Jakobshavn Isbrae, Greenland: Observation and model-based analysis. *J. Geophys. Res.,* 117**,** F02030.

JOUGHIN, I., SMITH, B. E., HOWAT, I. M., SCAMBOS, T. & MOON, T. 2010. Greenland flow variability from ice-sheet-wide velocity mapping. *Journal of Glaciology,* 56**,** 415-430.

KALSBEEK, F., PULVERTAFT, T. C. R. & NUTMAN, A. P. 1998. Geochemistry, age and origin of metagreywackes from the Palaeoproterozoic Karrat Group, Rinkian Belt, West Greenland. *Precambrian Research,* 91**,** 383-399.

KELLY, M. 1980. *The status of the Neoglacial in western Greenland*, Grønlands geologiske undersøgelse.

KELLY, M. 1985. A review of the Quaternary geology of western Greenland. *In:* ANDREWS, J. T. (ed.) *Quaternary Environments in Eastern Canadian Arctic, Baffin Bay and Western Greenland.* Boston: Allen and Unwin.

KELLY, M. 1986. Quaternary, pre-Holocene, marine events of western Greenland. *Grønlands geologiske Undersøgelse,* 131**,** 23.

KELLY, M., FUNDER, S., HOUMARK-NIELSEN, M., KNUDSEN, K. L., KRONBORG, C., LANDVIK, J. & SORBY, L. 1999. Quaternary glacial and marine environmental history of northwest Greenland: a review and reappraisal. *Quaternary Science Reviews,* 18**,** 373-392.

KENYON, P. M. & TURCOTTE, D. L. 1985. Morphology of a delta prograding by bulk sediment transport. *Geological Society of America Bulletin,* 96**,** 1457-1465.

KESSLER, M. A., ANDERSON, R. S. & BRINER, J. P. 2008. Fjord insertion into continental margins driven by topographic steering of ice. *Nature Geosci,* 1**,** 365-369.

KHAN, S. A., WAHR, J., BEVIS, M., VELICOGNA, I. & KENDRICK, E. 2010. Spread of ice mass loss into northwest Greenland observed by GRACE and GPS. *Geophys. Res. Lett.,* 37**,** L06501.

KING, E. C., HINDMARSH, R. C. A. & STOKES, C. R. 2009. Formation of mega-scale glacial lineations observed beneath a West Antarctic ice stream. *Nature Geosci,* 2**,** 585-588.

KJÆR, K. H., KHAN, S. A., KORSGAARD, N. J., WAHR, J., BAMBER, J. L., HURKMANS, R., VAN DEN BROEKE, M., TIMM, L. H., KJELDSEN, K. K., BJØRK, A. A., LARSEN, N. K., JØRGENSEN, L. T., FÆRCH-JENSEN, A. & WILLERSLEV, E. 2012. Aerial Photographs Reveal Late–20th-Century Dynamic Ice Loss in Northwestern Greenland. *Science,* 337**,** 569-573.

KLEMAN, J. 1994. Preservation of landforms under ice sheets and ice caps. *Geomorphology,* 9**,** 19-32.

KLEMAN, J. & BORGSTRÖM, I. 1994. Glacial land forms indicative of a partly frozen bed. *Journal of Glaciology,* 40**,** 255-264.

KLEMAN, J. & BORGSTRÖM, I. 1996. Reconstruction of palaeo-ice sheets: the use of geomorphological data. *Earth Surface Processes and Landforms,* 21**,** 893-909.

KLEMAN, J. & GLASSER, N. F. 2007. The subglacial thermal organisation (STO) of ice sheets. *Quaternary Science Reviews,* 26**,** 585-597.

KLEMAN, J. & STROEVEN, A. P. 1997. Preglacial surface remnants and Quaternary glacial regimes in northwestern Sweden. *Geomorphology,* 19**,** 35-54.
KLEMAN, J., STROEVEN, A. P. & LUNDQVIST, J. 2008. Patterns of Quaternary ice sheet erosion and deposition in Fennoscandia and a theoretical framework for explanation. *Geomorphology,* 97**,** 73-90.
KNUDSEN, K. L., STABELL, B., SEIDENKRANTZ, M. S., EIRIKSSON, J. & BLAKE JR, W. 2008. Deglacial and Holocene conditions in northernmost Baffin Bay: sediments, foraminifera, diatoms and stable isotopes. *Boreas,* 37**,** 346-376.
KRABBENDAM, M. & BRADWELL, T. 2011. Lateral plucking as a mechanism for elongate erosional glacial bedforms: explaining megagrooves in Britain and Canada. *Earth Surface Processes and Landforms,* 36**,** 1335-1349.
KRABBENDAM, M. & GLASSER, N. 2011. Glacial erosion and bedrock properties in NW Scotland: Abrasion and plucking, hardness and joint spacing. *Geomorphology,* 130**,** 10.
KRABILL, W., FREDERICK, E., MANIZADE, S., MARTIN, C., SONNTAG, J., SWIFT, R., THOMAS, R., WRIGHT, W. & YUNGEL, J. 1999. Rapid thinning of parts of the southern Greenland ice sheet. *Science,* 283**,** 1522-1524.
KRABILL, W., HANNA, E., HUYBRECHTS, P., ABDALATI, W., CAPPELEN, J., CSATHO, B., FREDERICK, E., MANIZADE, S., MARTIN, C., SONNTAG, J., SWIFT, R., THOMAS, R. & YUNGEL, J. 2004. Greenland Ice Sheet: Increased coastal thinning. *Geophysical Research Letters,* 31**,** -.
LAL, D. 1991. Cosmic-Ray Labeling of Erosion Surfaces - Insitu Nuclide Production-Rates and Erosion Models. *Earth and Planetary Science Letters,* 104**,** 424-439.
LAMBECK, K. & CHAPPELL, J. 2001. Sea level change through the last glacial cycle. *Science,* 292**,** 679-686.
LAURSEN, D. 1944. Contributions to the Quaternary geology of northern West Greenland especially the raised marine deposits. *Meddelelser om Gronland,* 135**,** 125.
LEVAC, E., VERNAL, A. D. & BLAKE JR, W. 2001. Sea-surface conditions in northernmost Baffin Bay during the Holocene: palynological evidence. *Journal of Quaternary Science,* 16**,** 353-363.
LIDMAR-BERGSTRÖM, K. 1997. A Long-Term Perspective on Glacial Erosion. *Earth Surface Processes and Landforms,* 22**,** 297-306.
LINDSAY, J. F. 1970. Clast Fabric of Till and its Development. *Journal of Sedimentary Research (SEPM),* 40**,** 629-641.
LINDSTROM, E. 1988. Are roches moutonnees mainly preglacial forms? *Geografiska Annaler: Series A, Physical Geography,* 70A**,** 323-322.
LINTON, D. L. 1963. The forms of glacial erosion. *Transactions of the Institute of British Geographers,* 33**,** 1-28.
LIVINGSTONE, S. J., COFAIGH, C. Ó. & EVANS, D. J. A. 2010. A major ice drainage pathway of the last British–Irish Ice Sheet: the Tyne Gap, northern England. *Journal of Quaternary Science,* 25**,** 354-370.
LLOYD, J. M., PARK, L. A., KUIJPERS, A. & MOROS, M. 2005. Early Holocene palaeoceanography and deglacial chronology of Disko Bugt, West Greenland. *Quaternary Science Reviews,* 24**,** 1741-1755.
LONG, A. J. & ROBERTS, D. H. 2002. A revised chronology for the 'Fjord Stade' moraine in Disko Bugt, west Greenland. *Journal of Quaternary Science,* 17**,** 561-579.

LONG, A. J. & ROBERTS, D. H. 2003. Late Weichselian deglacial history of Disko Bugt, West Greenland, and the dynamics of the Jakobshavns Isbrae ice stream. *Boreas,* 32**,** 208-226.

LONG, A. J., ROBERTS, D. H. & DAWSON, S. 2006. Early Holocene history of the west Greenland Ice Sheet and the GH-8.2 event. *Quaternary Science Reviews,* 25**,** 904-922.

LONG, A. J., ROBERTS, D. H. & WRIGHT, M. R. 1999. Isolation basin stratigraphy and Holocene relative sea-level change on Arveprinsen Ejland, Disko Bugt, West Greenland. *Journal of Quaternary Science,* 14**,** 323-345.

LØNNE, I. 1993. Physical signatures of ice advance in a Younger Dryas ice-contact delta, Tromso, northern Norway: implications for glacier-terminus history. . *Boreas,* 22**,** 12.

LØNNE, I. 1995. Sedimentary facies and depositional architecture of ice-contact glaciomarine systems. *Sedimentary Geology,* 98**,** 13-43.

LØNNE, I. & NEMEC, W. 2004. High-arctic fan delta recording deglaciation and environment disequilibrium. *Sedimentology,* 51**,** 553-589.

LOWE, A. L. & ANDERSON, J. 2002. Reconstruction of the West Antarctic ice sheet in Pine Island Bay during the Last Glacial Maximum and its subsequent retreat history. *Quaternary Science Reviews,* 21**,** 1879-1897.

LOWE, J. J., RASMUSSEN, S. O., BJÖRCK, S., HOEK, W. Z., STEFFENSEN, J. P., WALKER, M. J. C. & YU, Z. C. 2008. Synchronisation of palaeoenvironmental events in the North Atlantic region during the Last Termination: a revised protocol recommended by the INTIMATE group. *Quaternary Science Reviews,* 27**,** 6-17.

LUCKMAN, A., MURRAY, T., DE LANGE, R. & HANNA, E. 2006. Rapid and synchronous ice-dynamic changes in East Greenland. *Geophysical Research Letters,* 33**,** L03503.

LUKAS, S., BENN, D. I., BOSTON, C. M., BROOK, M., CORAY, S., EVANS, D. J., GRAF, A., KELLERER-PIRKLBAUER, A., KIRKBRIDE, M. P. & KRABBENDAM, M. 2013. Clast shape analysis and clast transport paths in glacial environments: A critical review of methods and the role of lithology. *Earth-Science Reviews*.

LYKKE-ANDERSEN, H. 1998. NEOGENE–QUATERNARY DEPOSITIONAL HISTORY OF THE EAST GREENLAND SHELF IN THE VICINITY OF LEG 152 SHELF SITES. *Proceedings of the Ocean Drilling Program, Scientific Results,* 152**,** 29-38.

MADEN, C., ANASTASI, P. A. F., DOUGANS, A., FREEMAN, S. P. H. T., KITCHEN, R., KLODY, G., SCHNABEL, C., SUNDQUIST, M., VANNER, K. & XU, S. 2007. SUERC AMS ion detection. *Nuclear Instruments and Methods in Physics Research Section B: Beam Interactions with Materials and Atoms,* 259**,** 131-139.

MAIZELS, J. 1992. Boulder Ring Structures Produced during Jökulhlaup Flows. Origin and Hydraulic Significance. *Geografiska Annaler. Series A. Physical Geography***,** 21-33.

MAIZELS, J. K. 1977. Experiments on the origin of kettle-holes. *Journal of Glaciology,* 18**,** 291-303.

MASLIN, M. A., LI, X. S., LOUTRE, M. F. & BERGER, A. 1998. THE CONTRIBUTION OF ORBITAL FORCING TO THE PROGRESSIVE INTENSIFICATION OF NORTHERN HEMISPHERE GLACIATION. *Quaternary Science Reviews,* 17**,** 411-426.

MCCARTHY, D. unpublished. Unpublished Thesis.

MCCARTHY, D. J. 2011. *Late Quaternary ice-ocean interactions in central West Greenland.* PhD, Durham University.
MCFADDEN, E. M., HOWAT, I. M., JOUGHIN, I., SMITH, B. E. & AHN, Y. 2011. Changes in the dynamics of marine terminating outlet glaciers in west Greenland (2000–2009). *J. Geophys. Res.,* 116**,** F02022.
MEIER, M. F. & POST, A. 1987. Fast Tidewater Glaciers. *J. Geophys. Res.,* 92**,** 9051-9058.
MERCER, J. H. 1961. The Response of Fjord Glaciers to changes in the Firn Limit. *Journal of Glaciology,* 3**,** 850-858.
MOON, T. & JOUGHIN, I. 2008. Changes in ice front position on Greenland's outlet glaciers from 1992 to 2007. *J. Geophys. Res.,* 113**,** F02022.
MOON, T., JOUGHIN, I., SMITH, B. & HOWAT, I. 2012. 21st-Century Evolution of Greenland Outlet Glacier Velocities. *Science,* 336**,** 576-578.
MOTE, T. L. 2007. Greenland surface melt trends 1973-2007: Evidence of a large increase in 2007. *Geophys. Res. Lett.,* 34**,** L22507.
MURTON, J. B. 1996. Near-surface brecciation of chalk, isle of thanet, south-east England: a comparison with ice-rich brecciated bedrocks in Canada and Spitsbergen. *Permafrost and Periglacial Processes,* 7**,** 153-164.
NEMEC, W. & STEEL, R. J. 1984. Alluvial and coastal conglomerates : Their significant features and some comments on gravelly mass-flow deposits. *In:* KOSTER, E. H. & STEEL, R. J. (eds.) *Sedimentology of Gravels and Conglomerates: Canadian Society of Petroleum Geologists.*
NESJE, A. & DAHL, S. O. 1990. Autochthonous block fields in southern Norway: implications for the geometry, thickness, and isostatic loading of the Late Weichselian Scandinavian ice sheet. *Journal of Quaternary Science,* 5**,** 225-234.
NESJE, A. & SEJRUP, H. P. 1988. Late Weichselian/Devensian ice sheets in the North Sea and adjacent land areas. *Boreas,* 17**,** 371-384.
NICK, F. M., VIELI, A., HOWAT, I. M. & JOUGHIN, I. 2009. Large-scale changes in Greenland outlet glacier dynamics triggered at the terminus. *Nature Geoscience,* 2**,** 110-114.
NIELSEN, S. B., GALLAGHER, K., LEIGHTON, C., BALLING, N., SVENNINGSEN, L., JACOBSEN, B. H., THOMSEN, E., NIELSEN, O. B., HEILMANN-CLAUSEN, C., EGHOLM, D. L., SUMMERFIELD, M. A., CLAUSEN, O. R., PIOTROWSKI, J. A., THORSEN, M. R., HUUSE, M., ABRAHAMSEN, N., KING, C. & LYKKE-ANDERSEN, H. 2009. The evolution of western Scandinavian topography: A review of Neogene uplift versus the ICE (isostasy–climate–erosion) hypothesis. *Journal of Geodynamics,* 47**,** 72-95.
NISHIIZUMI, K., WINTERER, E. L., KOHL, C. P., KLEIN, J., MIDDLETON, R., LAL, D. & ARNOLD, J. R. 1989. Cosmic ray production rates of 10Be and 26Al in quartz from glacially polished rocks. *Journal of Geophysical Research: Solid Earth,* 94**,** 17907-17915.
O'NEEL, S., PFEFFER, W. T., KRIMMEL, R. & MEIER, M. 2005. Evolving force balance at Columbia Glacier, Alaska, during its rapid retreat. *Journal of Geophysical Research: Earth Surface,* 110**,** F03012.
Ó COFAIGH, C., ANDREWS, J. T., JENNINGS, A. E., DOWDESWELL, J. A., HOGAN, K. A., KILFEATHER, A. A. & SHELDON, C. 2013a. Glacimarine lithofacies,

provenance, and depositional processes on a West Greenland trough-mouth fan. *Journal of Quaternary Science,* 28**,** 13-26.
Ó COFAIGH, C., DOWDESWELL, J., EVANS, J., KENYON, N. H., TAYLOR, J., MIENERT, J. & WILKEN, M. 2004. Timing and significance of glacially influenced mass-wasting in the submarine channels of the Greenland Basin. *Marine Geology,* 207**,** 39-54.
Ó COFAIGH, C., DOWDESWELL, J. A., JENNINGS, A. E., HOGAN, K. A., KILFEATHER, A., HIEMSTRA, J. F., NOORMETS, R., EVANS, J., MCCARTHY, D. J., ANDREWS, J. T., LLOYD, J. M. & MOROS, M. 2013b. An extensive and dynamic ice sheet on the West Greenland shelf during the last glacial cycle. *Geology,* 41**,** 219-222.
Ó COFAIGH, C., EVANS, D. J. A. & HIEMSTRA, J. F. 2011. Formation of a stratified subglacial 'till' assemblage by ice-marginal thrusting and glacier overriding. *Boreas,* 40**,** 1-14.
Ó COFAIGH, C., PUDSEY, C. J., DOWDESWELL, J. A. & MORRIS, P. 2002. Evolution of subglacial bedforms along a paleo-ice stream, Antarctic Peninsula continental shelf. *Geophys. Res. Lett.,* 29**,** 1199.
Ó COFAIGH, C., TAYLOR, J., DOWDESWELL, J. A. & PUDSEY, C. J. 2003. Palaeo-ice streams, trough mouth fans and high-latitude continental slope sedimentation. *Boreas,* 32**,** 37-55.
Ó COFAIGH, C. E. 2009. Marine geophysical and geological investigations of past flow and stability and stability of a major Greenland ice stream in the late Quaternary, RRS Cruise Report RRS James Clark Ross, Cruise JR175 West Greenland and Baffin Bay. 29.
OSKIN, M. & BURBANK, D. W. 2005. Alpine landscape evolution dominated by cirque retreat. *Geology,* 33**,** 933-936.
OTTESEN, D., STOKES, C. R., RISE, L. & OLSEN, L. 2008. Quaternary ice-sheet dynamics and ice streaming along the coastal parts of northern Norway. *Quaternary Science Reviews,* 27**,** 19.
PARIZEK, B. R. & ALLEY, R. B. 2004. Implications of increased Greenland surface melt under global-warming scenarios: ice-sheet simulations. *Quaternary Science Reviews,* 23**,** 1013-1027.
PEDERSEN, G. K. & PULVERTAFT, T. C. R. 1992. The nonmarine Cretaceous of the West Greenland Basin, onshore West Greenland. *Cretaceous Research,* 13**,** 263-272.
PFEFFER, W. T., HARPER, J. T. & O'NEEL, S. 2008. Kinematic constraints on lacier contributions to 21st-century sea-level rise. *Science,* 321**,** 4.
PHILLIPS, E., EVEREST, J. & DIAZ-DOCE, D. 2010. Bedrock controls on subglacial landform distribution and geomorphological processes: Evidence from the Late Devensian Irish Sea Ice Stream. *Sedimentary Geology,* 232**,** 98-118.
PHILLIPS, E., LEE, J. R., RIDING, J. B., KENDALL, R. & HUGHES, L. In Press. Periglacial disruption and subsequent glacitectonic deformation of bedrock: an example from Anglesey, North Wales, UK. *Proceedings of the Geologists' Association*.
PIOTROWSKI, J. A., LARSEN, N. K. & JUNGE, F. W. 2004. Reflections on soft subglacial beds as a mosaic of deforming and stable spots. *Quaternary Science Reviews,* 23**,** 993-1000.
POSTMA, G. & ROEP, T. B. 1985. Resedimented Conglomerates in the Bottomsets of Gilbert-type Gravel Deltas. *Journal of Sedimentary Research (SEPM),* 55**,** 12.
PRICE, R. 1970. Moraines at fjallsjökull, Iceland. *Arctic and Alpine Research***,** 27-42.

PRITCHARD, H., ARTHERN, R. J., VAUGHAN, D. G. & EDWARDS, L. A. 2009. Extensive dynamic thinning on the margins of the Greenland and Antarctic ice sheets. *Nature,* 461**,** 5.

PUTKONEN, J. & SWANSON, T. 2003. Accuracy of cosmogenic ages for moraines. *Quaternary Research,* 59**,** 255-261.

RASCH, M. & JENSEN, J. F. 1997. Ancient Eskimo dwelling sites and Holocene relative sea-level changes in southern Disko Bugt, central West Greenland. *Polar Research,* 16**,** 101-115.

RASCH, M. & NIELSEN, N. 1994. Holocene relative sea-level changes indicated by morphostratigraphic sequences; Sinigfik, Disko Island, West Greenland. *Geografisk Tidsskrift***,** 37-45.

RASCH, M. & NIELSEN, N. 1995. Coastal morpho-stratigraphy and Holocene relative sea level changes at Tuapaat, southeastern Disko Island, central West Greenland. *Polar Research,* 14**,** 277-290.

RASCH, M., NIELSEN, N. & JAKOBSEN, B. H. 1997. Geomorphology and sedimentary record of three guspate forelands as indicators of Late Holocene relative sea-level changes, Disko, west Greenland. *Geografisk Tidsskrift***,** 33-46.

RASMUSSEN, S. O., ANDERSEN, K. K. & SVENSSON, A. M. 2006. A new Greenland ice core chronology for the last glacial termination. *Journal of Geophysical Research,* 111**,** D06102.

REA, B. 2007. Glacial landforms, erosional features: Micro to macro-scale forms. *In:* ELIAS, S. (ed.) *Encyclopedia of Quaternary Science.* Oxford: Elsevier.

REA, B. & EVANS, D. J. A. 2003. Plateau Icefield Landsystem. *In:* EVANS, D. J. A. (ed.) *Glacial Landsystems.* London: Arnold.

REA, B. R. & EVANS, D. J. A. 1996. Landscapes of areal scouring in NW Scotland. *The Scottish Geographical Magazine,* 112**,** 47-50.

REA, B. R. & WHALLEY, B. W. 1994. Subglacial observations from øksfjordjøkelen, North Norway. *Earth Surface Processes and Landforms,* 19**,** 659-673.

REA, B. R. & WHALLEY, W. B. 1996. The role of bedrock topography, structure, ice dynamics and preglacial weathering in controlling subglacialerosion beneath a high-latitude, maritime ice field. *Annals of Glaciology,* 22**,** 5.

REDFIELD, T. F. 2010. On apatite fission track dating and the Tertiary evolution of West Greenland topography. *Journal of the Geological Society,* 167**,** 261-271.

REEH, N. 1985. Was the Greenland ice sheet thinner in the late Wisconsinan than now? *Nature,* 317**,** 797-799.

RENSSEN, H., SEPPA, H., HEIRI, O., ROCHE, D. M., GOOSSE, H. & FICHEFET, T. 2009. The spatial and temporal complexity of the Holocene thermal maximum. *Nature Geosci,* 2**,** 411-414.

RICH, J. L. 1943. Buried stagnant ice as a normal product of a progressively retreating glacier in a hilly region. *American Journal of Science,* 241**,** 95-100.

RIGNOT, E. & KANAGARATNAM, P. 2006. Changes in the velocity structure of the Greenland Ice Sheet. *Science,* 311**,** 986-990.

RIGNOT, E., KOPPES, M. & VELICOGNA, I. 2010. Rapid submarine melting of the calving faces of West Greenland glaciers. *Nature Geoscience,* 3**,** 5.

RIGNOT, E., VELICOGNA, I., VAN DEN BROEKE, M. R., MONAGHAN, A. & LENAERTS, J. 2011. Acceleration of the contribution of the Greenland and Antarctic ice sheets to sea level rise. *Geophys. Res. Lett.,* 38**,** L05503.

RINK, H. 1853. Udsigt over Nordgronlands Geognosie. *Kongelige danske Videnskabernes Selskabs Skrifter* 5**,** 23.

RINTERKNECHT, V., GOROKHOVICH, Y., SCHAEFER, J. & CAFFEE, M. 2009. Preliminary Be-10 chronology for the last deglaciation of the western margin of the Greenland Ice Sheet. *Journal of Quaternary Science,* 24**,** 270-278.

ROBERTS, D. H. & LONG, A. J. 2005. Streamlined bedrock terrain and fast ice flow, Jakobshavns Isbrae, West Greenland: implications for ice stream and ice sheet dynamics. *Boreas,* 34**,** 25-42.

ROBERTS, D. H., LONG, A. J., DAVIES, B. J., SIMPSON, M. J. R. & SCHNABEL, C. 2010. Ice stream influence on West Greenland Ice Sheet dynamics during the Last Glacial Maximum. *Journal of Quaternary Science,* 25**,** 850-864.

ROBERTS, D. H., LONG, A. J., SCHNABEL, C., DAVIES, B. J., XU, S., SIMPSON, M. J. R. & HUYBRECHTS, P. 2009. Ice sheet extent and early deglacial history of the southwestern sector of the Greenland Ice Sheet. *Quaternary Science Reviews,* 28**,** 2760-2773.

ROBERTS, D. H., LONG, A. J., SCHNABEL, C., FREEMAN, S. & SIMPSON, M. J. R. 2008. The deglacial history of southeast sector of the Greenland Ice Sheet during the Last Glacial Maximum. *Quaternary Science Reviews,* 27**,** 1505-1516.

ROBERTS, D. H., REA, B. R., LANE, T. P., SCHNABEL, C. & RODES, A. 2013. New constraints on Greenland ice sheet dynamics during the last glacial cycle: evidence from the Uummannaq ice stream system. *Journal of Geophysical Research (Earth Surface)*.

ROTHLISBERGER, H. & IKEN, A. 1981. Plucking as an effect of water-pressure variations at the glacier bed. *Annals of Glaciology,* 2**,** 57-62.

SCHOOF, C. 2007. Ice sheet grounding line dynamics: Steady states, stability, and hysteresis. *Journal of Geophysical Research,* 112**,** F03S28.

SEALE, A., CHRISTOFFERSEN, P., MUGFORD, R. I. & O'LEARY, M. 2011. Ocean forcing of the Greenland Ice Sheet: Calving fronts and patterns of retreat identified by automatic satellite monitoring of eastern outlet glaciers. *J. Geophys. Res.,* 116**,** F03013.

SEJRUP, H. P., LARSEN, E., HAFLIDASON, H., BERSTAD, I. M., HJELSTUEN, B. O., JONSDOTTIR, H. E., KING, E. L., LANDVIK, J., LONGVA, O., NYGARD, A., OTTESEN, D., RAUNHOLM, S., RISE, L. & STALSBERG, K. 2003. Configuration, history and impact of the Norwegian Channel Ice Stream. *Boreas,* 32**,** 18-36.

SHEPHERD, A., HUBBARD, A., NIENOW, P., KING, M., MCMILLAN, M. & JOUGHIN, I. 2009. Greenland ice sheet motion coupled with daily melting in late summer. *Geophys. Res. Lett.,* 36**,** L01501.

SHEPHERD, A. & WINGHAM, D. 2007. Recent Sea-Level Contributions of the Antarctic and Greenland Ice Sheets. *Science,* 315**,** 1529-1532.

SIMONARSON, L. A. 1981. Upper Pleistocene and Holocene marine deposits and faunas on the north coast of Nugssuaq, west Greenland. *Gronlands Geologiske Undersogelse Bulletin***,** 1-107.

SIMPSON, M. J. R., MILNE, G. A., HUYBRECHTS, P. & LONG, A. J. 2009. Calibrating a glaciological model of the Greenland ice sheet from the Last Glacial Maximum to present-day using field observations of relative sea level and ice extent. *Quaternary Science Reviews,* 28**,** 1631-1657.

SMALL, E. E. & ANDERSON, R. S. 1998. Pleistocene relief production in Laramide Mountain Ranges, western U.S. *Geology,* 26**,** 123-126.

SMITH, A., MURRAY, T., NICHOLLS, K., MAKINSON, K., AÐALGEIRSDÓTTIR, G., BEHAR, A. & VAUGHAN, D. 2007. Rapid erosion, drumlin formation, and changing hydrology beneath an Antarctic ice stream. *Geology,* 35**,** 127-130.

SNEED, E. D. & FOLK, R. L. 1958. Pebbles in the lower Colorado River, Texas a study in particle morphogenesis. *The Journal of Geology***,** 114-150.

SOLE, A., PAYNE, T., BAMBER, J., NIENOW, P. & KRABILL, W. 2008. Testing hypotheses of the cause of peripheral thinning of the Greenland Ice Sheet: is land-terminating ice thinning at anomalously high rates? *The Cryosphere,* 2**,** 673-710.

SOLLID, J. L. & SØRBEL, L. 1979. Deglaciation of western central Norway. *Boreas,* 8**,** 233-239.

SPERAZZA, M., MOORE, J. N. & HENDRIX, M. S. 2004. High-resolution particle size analysis of naturally occurring very fine-grained sediment through laser diffractometry. *Journal of Sedimentary Research,* 74**,** 736-743.

STEENFELT, A., THOMASSEN, B., LIND, M. & KYED, J. 1998. Karrat 97: reconnaissance mineral exploration in central West Greenland. *Geology of Greenland Survey Bulletin,* 180**,** 73-80.

STEENSTRUP, K. V. J. 1883. Om Forekomsten af Forsteninger i de kulførende Dannelser i Nord-Grønland. *Meddelelser om Grønland,* 5**,** 43-67.

STEER, P., HUISMANS, R. S., VALLA, P. G., GAC, S. & HERMAN, F. 2012. Bimodal Plio-Quaternary glacial erosion of fjords and low-relief surfaces in Scandinavia. *Nature Geoscience,* 5**,** 635-639.

STOKES, C. R. & CLARK, C. D. 1999. Geomorphological criteria for identifying Pleistocene ice streams. *Annals of Glaciology,* 28**,** 67-79.

STOKES, C. R. & CLARK, C. D. 2001. Palaeo-ice streams. *Quaternary Science Reviews,* 20**,** 1437-1456.

STOKES, C. R. & CLARK, C. D. 2002. Are long subglacial bedforms indicative of fast ice flow? *Boreas,* 31**,** 239-249.

STOKES, C. R., CLARK, C. D. & STORRAR, R. 2009. Major changes in ice stream dynamics during deglaciation of the north-western margin of the Laurentide Ice Sheet. *Quaternary Science Reviews,* 28**,** 721-738.

STONE, J. O. 2000. Air pressure and cosmogenic isotope production. *Journal of Geophysical Research-Solid Earth,* 105**,** 23753-23759.

STRANEO, F., HAMILTON, G. S., SUTHERLAND, D. A., STEARNS, L. A., DAVIDSON, F., HAMMIL, M. O., STENSON, G. B. & ROSING-ASVID, A. 2010. Rapid curculation of warm subtropical waters in a major glacial fjord in East Greenland. *Nature Geoscience,* 3**,** 182-186.

STRASKY, S., DI NICOLA, L., BARONI, C., SALVATORE, M. C., BAUR, H., KUBIK, P. W., SCHLUCHTER, C. & WIELER, R. 2009. Surface exposure ages imply multiple low-amplitude Pleistocene variations in East Antarctic Ice Sheet, Ricker Hills, Victoria Land. *Antarctic Science,* 21**,** 59-69.

STROEVEN, A. P., FABEL, D., HATTESTRAND, C. & HARBOR, J. 2002. A relict landscape in the centre of Fennoscandian glaciation: cosmogenic radionuclide evidence of tors preserved through multiple glacial cycles. *Geomorphology,* 44**,** 145-154.

STROEVEN, A. P. & SWIFT, D. A. 2008. Glacial landscape evolution — Implications for glacial processes, patterns and reconstructions. *Geomorphology,* 97**,** 1-4.

SUGDEN, D. 1978. Glacial erosion by the Laurentide ice sheet. *Journal of Glaciology,* 20**,** 367-391.
SUGDEN, D. E. 1968. The Selectivity of Glacial Erosion in the Cairngorm Mountains, Scotland. *Transactions of the Institute of British Geographers,* 45**,** 79-92.
SUGDEN, D. E. 1974. Landscapes of glacial erosion in Greenland and their relationship to ice, topographic and bedrock conditions. *In:* BROWN, E. H. & WATERS, R. S. (eds.) *Progress in Geomorphology: Papers in honour of David L. Linton. Institute of British Geographers Special Publication. No. 7.* London: Institute of British Geographers.
SUGDEN, D. E., GLASSER, N. & CLAPPERTON, C. M. 1992a. Evolution of large roche moutonnees. *Geografiska Annaler: Series A, Physical Geography,* 74 (A)**,** 12.
SUGDEN, D. E., GLASSER, N. & CLAPPERTON, C. M. 1992b. Evolution of large roche moutonnees. *Geografiska Annaler: Series A, Physical Geography,* 74 (A)**,** 253-264.
SUGDEN, D. E. & JOHN, B. S. 1976. *Glaciers and Landscape,* London Arnold.
SWIFT, D. A., PERSANO, C., STUART, F. M., GALLAGHER, K. & WHITHAM, A. 2008. A reassessment of the role of ice sheet glaciation in the long-term evolution of the East Greenland fjord region. *Geomorphology,* 97**,** 109-125.
SWITHINBANK, C. W. M. 1954. Ice Streams. *Polar Record,* 7**,** 185-186.
TARASOV, L. & PELTIER, W. R. 2002. Greenland glacial history and local geodynamic consequences. *Geophysical Journal International,* 150**,** 198-229.
TENBRINK, N. W. & WEIDICK, A. 1974. Greenland Ice Sheet History since Last Glaciation. *Quaternary Research,* 4**,** 429-&.
THOMAS, R., FREDERICK, E., KRABILL, W., MANIZADE, S. & MARTIN, C. 2009. Recent changes on Greenland outlet glaciers. *Journal of Glaciology,* 55**,** 147-162.
THOMAS, R., FREDERICK, E., LI, J., KRABILL, W., MANIZADE, S., PADEN, J., SONNTAG, J., SWIFT, R. & YUNGEL, J. 2011. Accelerating ice loss from the fastest Greenland and Antarctic glaciers. *Geophys. Res. Lett.,* 38**,** L10502.
THOMAS, R. H. 2004. Force-perturbation analysis of recent thinning and acceleration of Jakobshavn Isbrae, Greenland. *Journal of Glaciology,* 50**,** 57-66.
THORP, P. 1981. A trimline method for defining the upper limit of Loch Lomond Advance glaciers: examples from the Loch Leven and Glen Coe areas. *Scottish Journal of Geology,* 17**,** 49-64.
TRUFFER, M. & ECHELMEYER, K. 2003. Of Isbrae and Ice Streams. *Annals of Glaciology,* 36**,** 66-72.
TRUFFER, M. & FAHNESTOCK, M. 2007. Rethinking Ice Sheet Time Scales. *Science,* 315**,** 1508-1510.
VAN DE WAL, R. S. W., BOOT, W., VAN DE BROEKE, M. R., SMEETS, C. J. P. P., REIJMER, C. H., DONKER, J. J. A. & OERLEMANS, J. 2008. Large and Rapid Melt-Induced Velocity Changes in the Ablation Zone of the Greenland Ice Sheet. *Science,* 321**,** 111-114.
VAN DEN BROEKE, M., BAMBER, J., ETTEMA, J., RIGNOT, E., SCHRAMA, E., VAN DE BERG, W. J., VAN MEIJGAARD, E., VELICOGNA, I. & WOUTERS, B. 2009. Partitioning Recent Greenland Mass Loss. *Science,* 326**,** 984-986.
VAN DER WATEREN, F. M. 1995. Processes of glaciotectonism. *In:* MENZIES, J. (ed.) *Modern Glacial Environments: Processes, Dynamics and Sediments.* Oxford: Butterworth-Heinemann.

VAN STEIJN, H. 1996. Debris-flow magnitude—frequency relationships for mountainous regions of Central and Northwest Europe. *Geomorphology,* 15**,** 259-273.
VAN STEIJN, H., BOELHOUWERS, J., HARRIS, S. & HÉTU, B. 2002. Recent research on the nature, origin and climatic relations of blocky and stratified slope deposits. *Progress in physical geography,* 26**,** 551-575.
VAN TATENHOVE, F. G. M. & VAN DER MEER, J. J. M. 1995. Glacial-Geological/Geomorphological Research in West Greenland used to test an Ice-Sheet model. *Quaternary Research,* 44**,** 317-327.
VAN TATENHOVE, F. G. M., VAN DER MEER, J. J. M. & KOSTER, E. A. 1996. Implications for Deglaciation Chronology from New AMS Age Determinations in Central West Greenland. *Quaternary Research,* 45**,** 245-253.
VELICOGNA, I. 2009. Increasing rates of ice mass loss from the Greenland and Antarctic ice sheets revealed by GRACE. *Geophysical Research Letters,* 36**,** L19503.
VELICOGNA, I. & WAHR, J. 2006. Acceleration of Greenland ice mass loss in spring 2004. *Nature,* 443**,** 329-331.
VIELI, A. & NICK, F. 2011. Understanding and Modelling Rapid Dynamic Changes of Tidewater Outlet Glaciers: Issues and Implications. *Surveys in Geophysics,* 32**,** 437-458.
WANNER, H. 2008. Mid- to late Holocene climate change: An overview. *Quat. Sci. Rev.,* 27**,** 1791-1828.
WARREN, C. R. & HULTON, N. R. J. 1990. Topographic and glaciological controls on Holocene ice-sheet margin dynamics, central West Greenland. *Annals of Glaciology,* 14**,** 307-310.
WARREN, W. P. & ASHLEY, G. M. 1994. Origins of the ice-contact stratified ridges (eskers) of Ireland. *Journal of Sedimentary Research,* 64**,** 433-449.
WEIDICK, A. 1968. Observations on some Holocene glacier fluctuations in west Greenland. *Meddelelsser om Grønland,* 165.
WEIDICK, A. 1972. *Holocene shore-lines and glacial stages in Greenland: an attempt at correlation*, Grønlands Geologiske Undersøgelse.
WEIDICK, A. 1976. Glaciation and the Quaternary of Greenland. *Geology of Greenland***,** 430-458.
WEIDICK, A. 1993. Neoglacial change of ice cover and the related response of the Earth's crust in West Greenland.
WEIDICK, A. 1996. Neoglacial changes of ice cover and sea level in Greenland - a classical enigma. *In:* GRONNOW, B. (ed.) *The Paleo-Eskimo Cultures of Greenland.* Copenhagen: Danish Polar Centre.
WEIDICK, A. & BENNIKE, O. 2007. Quaternary glaciation history and glaciology of Jakobshavn Isbrae and the Disko Bugt region, West Greenland: A review. *Geological Survey of Denmark and Greenland Bulletin,* 14**,** 1-78.
WEIDICK, A., KELLY, M. & BENNIKE, O. 2004. Late Quaternary development of the southern sector of the Greenland Ice Sheet, with particular reference to the Qassimiut lobe. *Boreas,* 33**,** 284-299.
WEIDICK, A., OERTER, H., REEH, N., THOMSEN, H. H. & THORNING, L. 1990. The Recession of the Inland Ice Margin during the Holocene Climatic Optimum in the Jakobshavn-Isfjord Area of West Greenland. *Global and Planetary Change,* 82**,** 389-399.

WHILLANS, I. M. 1978. Erosion by Continental Ice Sheets. *The Journal of Geology,* 86**,** 9.

WHILLANS, I. M. & VAN DER VEEN, C. J. 1997. The role of lateral drag in the dynamics of Ice Stream B,Antarctica. *Journal of Glaciology,* 43**,** 231-237.

WILSON, P., BENTLEY, M. J., SCHNABEL, C., CLARK, R. & XU, S. 2008. Stone run (block stream) formation in the Falkland Islands over several cold stages, deduced from cosmogenic isotope (10Be and 26Al) surface exposure dating. *Journal of Quaternary Science,* 23**,** 461-473.

WINSBORROW, M. C. M., ANDREASSEN, K., CORNER, G. D. & LABERG, J. S. 2010. Deglaciation of a marine-based ice sheet: Late Weichselian palaeo-ice dynamics and retreat in the southern Barents Sea reconstructed from onshore and offshore glacial geomorphology. *Quaternary Science Reviews,* 29**,** 424-442.

WOLF-WELLING, T. C. W., THIEDE, J. & MYHRE, A. M. 1995. Bulk sediment parameter and coarse fraction analysis: Paleoceanographic implications of Fram Strait Sites 908 and 909, ODP Leg 151 (NAAG). *Eos Transactions,* 76**,** 1-165.

YOUNG, N. E., BRINER, J., ROOD, D., FINK, D., CORBETT, L. B. & BIERMAN, P. 2013. Age of the Fjord Stade moraines in the Disko Bugt region, western Greenland, and the 9.3 and 8.2 ka cooling events. *Quaternary Science Reviews,* 60**,** 76-90.

YOUNG, N. E., BRINER, J. P., AXFORD, Y., CSATHO, B., BABONIS, G. S., ROOD, D. H. & FINKEL, R. C. 2011a. Response of a marine-terminating Greenland outlet glacier to abrupt cooling 8200 and 9300 years ago. *Geophys. Res. Lett.,* 38**,** L24701.

YOUNG, N. E., BRINER, J. P., STEWART, H. A. M., AXFORD, Y., CSATHOS, B., ROOD, D. H. & FINKEL, R. C. 2011b. Response of Jakobshavn Isbræ, Greenland, to Holocene climate change. *Geology,* 39**,** 131-145.

ZARUDZKI, E. F. K. 1979. Interpretation of shallow seismic profiles over the continental shelf in West Greenland between latitudes 64 degrees and 69 degrees 30'N. *Rapport Grønlands Geologiske Undersøgelse,* 100**,** 4.

ZWALLY, H. J., ABDALATI, W., HERRING, T., LARSON, K., SABA, J. & STEFFEN, K. 2002. Surface melt-induced acceleration of Greenland ice-sheet flow. *Science,* 297**,** 218-222.